The effect of cell-based therapy on LASIK-like corneal wounds

Thesis Submitted to Cardiff University for the degree of Doctor of Philosophy

December 2018

Camilla Phillips

Structural Biophysics Research Group

School of Optometry and Vision Sciences

Cardiff University

Abstract

The aim of this study was to determine if oral mucosal lamina propria progenitor cell (OMLP-PC)-based therapy to the stromal beds of LASIK-like wounded corneas could improve wound healing.

After epithelial and/or stromal injury, a wound healing cascade is triggered that includes keratocyte apoptosis and proliferation in the underlying stroma. Activation of keratocytes leads to their transformation into myofibroblasts, which are responsible for matrix remodelling. Unfortunately, LASIK-like wound healing can result in incomplete closure at the flap interface, reduced biomechanical strength and decreased transparency.

The hypothesis of this study was that a therapeutic application of OMLP-PCs, known to facilitate non-scarring healing, to the corneal wound bed, would reduce keratocyte activation and consequent myofibroblastic transformation to augment matrix remodelling and restore transparency. To test this hypothesis, a corneal organ culture model was developed to monitor LASIK-like wound healing outcomes. The efficacy of a cell-based therapy, namely OMLP-PCs, on LASIK-like wound healing was evaluated and optimised over four weeks.

The wound healing outcomes of the organ cultured porcine corneas included a significant reduction of percentage α-sma immunopositive cells ($p<0.01$) from ~45% (untreated wounded) to ~25% (OMLP-PC-treated) during weeks 2-3 post wounding. Peak percentage proliferation was 52.2% ±3.7 at 1 week in OMLP-PC treated wounds, earlier compared to 42.2% ±3.3 at 2 weeks in untreated control corneas. OMLP-PCs did not alter stromal percentage apoptosis. Coherence (degree of collagen lamellae alignment) at 4 weeks after wound healing was significantly higher in OMLP-PC treated wounded corneas ($p<0.05$), compared to that in untreated corneas. By 4 weeks corneal transparency in OMLP-PC treated wounded corneas was significantly higher than in untreated corneas ($p<0.01$). To conclude, an OMLP-PC therapeutic application to LASIK-like wounds enhanced stromal cell proliferation and reduced myofibroblast expression, but increased collagen organisation with consequent improved epithelial-stromal flap wound closure and increased corneal transparency.

Acknowledgements

The path to completion of this PhD has been a long and difficult one, and so naturally there are many people to thank for their endless help and support.

First and foremost, I would like to thank my Supervisors Professor. Keith Meek and Dr. Julie Albon. I am very grateful to Keith for his support, guidance and, above all patience (this PhD has been a frustratingly long time in the making!). A special thank you goes to Julie for all her help and understanding in both PhD and personal matters and the long chats (which very often veered off course!). My advisor Dr. Tony Redmond was also incredibly understanding and helpful during my long (and frequently interrupted) path to completion of this thesis. And of course, no PhD in this School would be possible without the fantastic Sue Hobbs- thank you so much!

In pursuit of this PhD I have received help from many people. Firstly, a thank you to Nick White, who we sadly lost in April 2019, for all his help and patient training on various microscopes- I hope you knew how grateful I was. Thank you to Prof. Phil Stephens, as well as Katrina Duggan, Sarah Youde and Emma Board-Davies at Cardiff School of Dentistry provided the cells integral to this study and the invaluable expertise in cell culture. James Galloway, who worked over a summer helping with culture and imaging. A number of statisticians from Cardiff University were consulted in the post-grad statistics clinic over the years- thank you all for your patience! All members of the Structural Biophysics group in the School of Optometry and Vision Sciences are a fantastic set of people who are always ready to lend a hand in anything you need. Professor Andrew Quantock, Dr Justyn Regini, Dr Sally Hayes, Basha, Petar (thank you for your patience with all things computer!!) and Jacek. In particular Dr Phil Lewis and Dr Rob Young with their utmost patience and eagerness to help with TEM (I'm sorry my samples were so squishy and large!). In the Post Grad room many, many, many people have come and gone in my time there; Nada, Tom, Ben, Ellie, Greg, Alina, Elena, Frankie and Stacey (I am SO sorry if I've missed anyone out!), a special thanks to lovely Saleha, who shared the ups and downs of juggling parenthood and research (you felt my pain!). Most importantly Dr Erin Dooley and Dr Sian Morgan, whose work lead the way for me and my PhD. Their generous tutelage through so

many different techniques was incredible! An extra thanks to Sian for her help and encouragement in the last few months in particular- Thank you.

This PhD would certainly not have been possible without the support of my friends. The mums at school (Lydia especially) who have helped with childcare and been so supportive! The awesome Christine and Tash, who were there to support me from the beginning. The rather fabulous ladies of Ardwyn Walk; Jennie, Amy, Sian and Karina who have helped with childcare, venting via messaging and always with a glass of wine (or two?!). Also Lovely Lottie- we both embarked on PhD's, got married, had children, moved houses all at the same time (slightly crazy!) and no one else can really understand just how hard this has been. Thank you for being there for me (albeit 240 miles north)- I wish you lived closer.

The last round of "thank yous" goes to my family. The amount of support from you has been phenomenal. A huge thank you to my Parents- in- Law Rob and Sheila for looking after the children, doing school runs and picking up poorly little ones when I couldn't. For my parents, Wiggy and Alan, who tirelessly and repeatedly made the 4hr journey westwards from Norfolk to help with everything- the children, the house, the shopping, the laundry and you always brought wine and h'uile picante, thank you isn't really enough! You are such supportive parents and fantastic grandparents- I am so lucky. Thank you so much.

And finally, to my little family. My gorgeous husband Tim- this has been such a long "journey" and the last few months have been especially hard. Thank you so much for being my rock and a brilliant father to the sprogs. The biggest thank you though, is reserved for Emilia and Toby, my two (rather beautiful) children who made their appearance during this PhD. You are quite simply the best. And, of course, George. I love you all so much and I am so sorry this has taken me away from you… I'm all yours now!!!

Dedication

To Emilia and Toby.

Love From

Mummy x

In Memory of Nick White.

You will be greatly missed.

Table of Contents

Table of Figures

Table of Tables

Table of Equations

Chapter 1

Introduction

1.1. Corneal Structure

The cornea is the domed, clear, circular "window" at the front of the eye (figure 1.1), allowing the entry of light into the anterior and posterior chambers of the globe. It is exposed anteriorly to the outside environment covered only with a tear film, through which the cornea, being avascular in nature, receives its supply of oxygen. Its metabolic needs are met via its contact posteriorly with the aqueous humour (Oie & Nishida, 2016; Fini, 1999). The outer layers of the eye carry out a number of very important roles in maintaining corneal homeostasis. They form the ocular surface, a complex biological continuum that, as a fibrous tunic, is in its most basic role a protective layer that blocks the invasion of foreign material such as bacteria, fungi and debris (Oie & Nishida, 2016; Delmonte & Kim, 2011). Its smooth surface and tear film gives the eye its most anterior refractive surface.

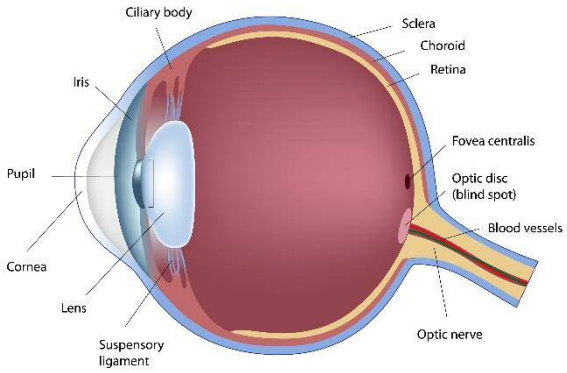

Figure 1.1 Diagram of the eye (Alila Medical Images, Alamy Stock Photo)

The only mammalian tissues that have evolved to be transparent are the cornea and the lens (Christens-Barry et al., 1996). This transparent nature arises from both the organisation of collagen fibrils in the stroma (the central layer of the cornea) and the lack of vasculature (Maurice, 1957; Meek et al., 2003). This provides a pathway for light to travel through to the back of the eye. The cornea also carries out over two-thirds of the eyes refractive function, with the remaining optical power produced by the lens (Krachmer et al, 2011; Forrester et al., 2002), equating to approximately 48 dioptres of power, to create focused

images on the retina. The structure of the cornea provides biomechanical strength in order to maintain its shape, an important factor, as in order to refract light and ultimately maintain normal visual function it must retain not only its transparency, but also its curvature (Müller et al., 2001).

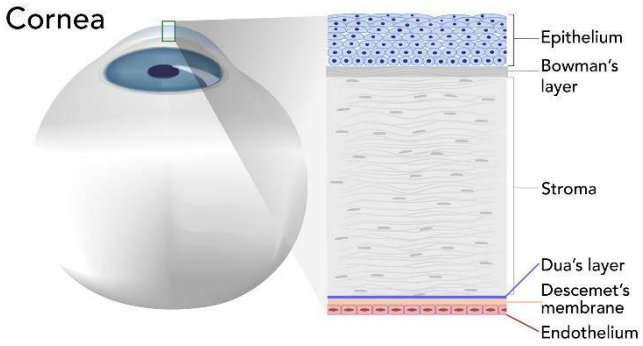

Figure 1.2 Layers of the Cornea (Alila Medical Images, Alamy Stock Photo)

The cornea is divided into five differentiated layers; the epithelium, Bowman's layer, the stroma, Descemet's Membrane and the endothelium. A sixth acellular layer has recently been characterised by Dua et al. in 2013. Found between the stroma and Descemet's membrane, it is referred to as the pre-Descemet's layer (or Dua's Layer) and has a thickness of ~15µm (Dua et al., 2013). There are a number of different substances that make up these layers, namely epithelial and endothelial cells, collagen, water, proteoglycans and keratocytes, the composition of which can be seen in the following table adapted from Hogan et al, 1971 (table 1.1).

Substance	%
Water	78
Collagen	15
Other Proteins	5
Keratocytes	5
Keratan Sulphate	0.7
Chondroitin Sulphate	0.3
Salts	1

Table 1.1 Substances of the cornea, adapted from Hogan et al, 1971

1.1.1. Epithelium

The outermost layer of the cornea, the epithelium, protects the eye as a physical barrier, to a certain extent, against foreign bodies, and although it can certainly be wounded it can heal rapidly helping to minimise scarring as best as possible and therefore maintain transparency and visual function. The epithelium is composed of stratified, non-stratified and squamous cells and is approximately 50-60µm thick; 10% of the total corneal thickness (Forrester et al., 2001). It can be further differentiated into 3 distinct layers of cells; squamous, wing and basal (figure 1.3).

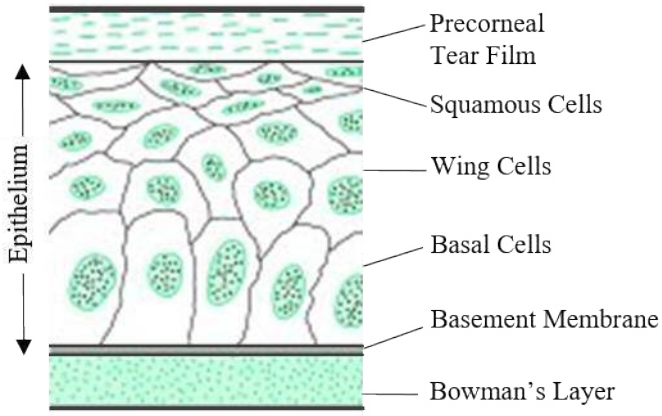

Figure 1.3 Layers of the Epithelium (copied from www.writeopinions.com /corneal-epithelium)

The squamous cells (most anterior, superficial layer) are flat polygonal cells that create a smooth epithelial surface (Saude, 1993). These cells are joined with tight junctions (zonula occludens) and desmosomes that control para-intracellular movement and provide adhesion between the cells. They also have a layer of microvilli that keeps the tear film in place (Forrester et al., 2001).

The wing cells occupy the middle "layer" of the epithelium and are flattened and polygonal in shape. There are 3 layers of these cells attached to each other with desmosomes and gap junctions and joined to the squamous cells (anteriorly) and basal cells (posteriorly) with desmosomes (Remington & McGill, 1998).

The basal cells make up the posterior most layer of the epithelium, which is 1 layer thick. They have a cubical or cylindrical form and are attached to each other via gap junctions and desmosomes and via hemidesmosomes to their basement membrane. This is the layer in which mitosis occurs and some basal cells differentiate to become middle and superficial cells. The stem cells in the corneal limbus are solely responsible for epithelial cell replacement and tissue regeneration, making this layer the most important in corneal epithelial wound healing. These cells also secrete basement membrane that links to the Bowman's layer by hemidesmosomes (zonula adherens), through which anchoring fibrils pass to plaques of extracellular matrix within the stroma (Kaufman & Alm, 2002).

1.1.2. Bowman's Layer

Bowman's layer (or the anterior limiting lamina) is an acellular layer of the cornea consisting of randomly arranged collagen fibrils. It is only ~10μm thick, originating from the mesenchymal processes of the superficial stroma during embryogenesis and is incapable of regeneration (Smolin et al., 2005). Its precise function is unknown, although it has been hypothesised that it may help the cornea maintain its shape, act as a barrier to viral infection and facilitate rapid stromal wound healing following epithelial trauma (Wilson & Hong, 2000; Delmonte & Kim, 2011) It is a layer that is absent in many species.

1.1.3. Stroma

The stroma (or substantia propria) is the thickest of all the corneal layers. At approximately 500μm it makes up 90% of the corneas total thickness (Patel et al., 2001) and is a highly transparent, organised connective tissue that gives the cornea its strength and transparency. It consists mainly of 200-250 lamellae (flattened collagen bundles running parallel to the corneal surface) surrounded by keratocytes, non-fibril forming collagens, proteoglycans, glycoproteins, as well as other soluble proteins and inorganic salts (Smolin et al., 2005; Müller et al., 1995; Forrester et al., 2002). Although this layer has the potential to heal and regenerate it is a complicated process and often results in opacities.

1.1.4. Pre Descemet's Membrane/ Dua's Layer

Pre-Descemet's membrane is a novel layer described by Dua et al., 2013, as a strong, acellular layer between the posterior stroma and Descemet's membrane. It has been postulated that discovery of this layer could make a significant contribution to lamellar corneal surgery, understanding of posterior corneal pathology and biomechanics (Al-Taan, 2018).

1.1.5. Descemet's Membrane

Descemet's membrane (or the posterior limiting lamina) is the 2 layered acellular basement membrane of the corneal endothelium composed of type IV and VIII collagen, laminin, fibronectin and proteoglycans containing heparin sulphate and dermatan sulphate. It is secreted by and adheres to the endothelium, providing some structural integrity and playing a key role in fluid regulation (Hull et al., 1984) It is capable of regeneration, with good antigenic properties, and increases in thickness with age from approximately 3μm thick at birth up to 12μm as an adult (Rodrigues et al., 1982).

1.1.6. Endothelium

The endothelium is the innermost monolayer of the cornea, consisting of flattened cells with oval nuclei and 70-80% of them have a hexagonal "honey-comb like" morphology (Delmonte & Kim, 2011). It is approximately 5μm thick and the posterior most surface of the cornea, adjacent to the aqueous humour (Remington & McGill, 1998). These cells are joined with tight junctions with intercellular communication possible via gap junctions. The function of the endothelium is to maintain the hydration of the cornea, allowing the passage of ions, glucose and amino acids into the stroma, preventing corneal oedema and thus maintaining transparency. The endothelial pump actively transports water and ions across the cell layer from the aqueous humour into the stroma and vice versa via a Na+/K+ -ATPase pump system (Stiemke et al., 1991). Endothelial cell numbers are approximately 2500/mm^2 in middle age. The cells rarely divide and their number decreases with age to 2000/mm^2 in healthy corneas (Rodrigues et al., 1982). Ultrastructural analysis of corneal endothelial cells has found them to have an abundant number of mitochondria, which points to these cells being highly metabolically active (Smolin et al., 2005).

1.1.7. Species Difference

Whilst most mammals have a similar basic ocular anatomy, there are a few interspecies differences due to factors such as size of the animal. In Table 1.2 the differences between pigs and humans have been compared alongside rats to demonstrate the effect of mammal size on dimensions such as corneal thickness. It can be seen that pigs and humans differ mainly by the absence of a Bowman's layer, which, despite the size difference to a human, is present in a rat.

Species	Axial Length (mm)	Corneal Thickness (µm)	Lens Thickness (mm)	Bowman's Layer
Rat	5.98 a	250 a	3.87 a	yes b
Pig	23.9 c	666 f	7.4 c	no c
Human	23.9 d	550 d	4 d	yes b

a Massof et al., 1972 b Hayashi et al., 2002 c Sanchez et al., 2011
d Deering, 2005 e Patel et al., 2001 f Faber et al., 2008

Table 1.2. Corneal structural differences between species

1.2.Corneal Ultrastructure

The mechanical strength of a connective tissue relies upon the interfibrillar interactions of collagen molecules and the interactions of collagen with proteoglycans and water. Central regions of the human corneal stroma consist of approximately 200-250 stacked lamellae running parallel to the corneal surface and each lamella is packed with fibrils in a short-range order (discussed in more detail later in this chapter (Kaufman & Alm, 2002). The axial periodicity of the corneal collagen is 65nm (slightly lower than in other collagenous tissues) and the fibril diameter is 31-34 nm throughout the cornea (Meek et al., 1981; Meek & Leonard, 1993).

Proteoglycans lie between the collagen fibrils maintaining the interfibrillar spacing (important in transparency) and have an intermolecular Bragg spacing of approximately 1.63nm (Meek & Leonard, 1997). Collagen spacing in the periphery of the cornea is greater due to the presence of chondroitin sulphate, a larger proteoglycan. Proteoglycans are

hydrophilic and therefore have a tendency to swell, which, as they maintain interfibrillar spacing, can disrupt the corneal arrangement and result in a reduction in transparency.

1.2.1. Collagen

Collagen molecules have a special amino acid composition whereby one in every three amino acids on an α amino chain is a glycine in the polypeptide chain. These α amino chains form a helical structure, which, when assembled with two other collagen α chains, form a triple helix called tropocollagen. The tropocollagen covalently link to each other in a staggered array creates a rod-shaped macromolecule- a collagen molecule. These molecules are cross-linked to each other and this produces a collagen fibril, a structure with a large amount of biomechanical strength and resilience (figure 1.4) (Woodhead-Galloway, 1980).

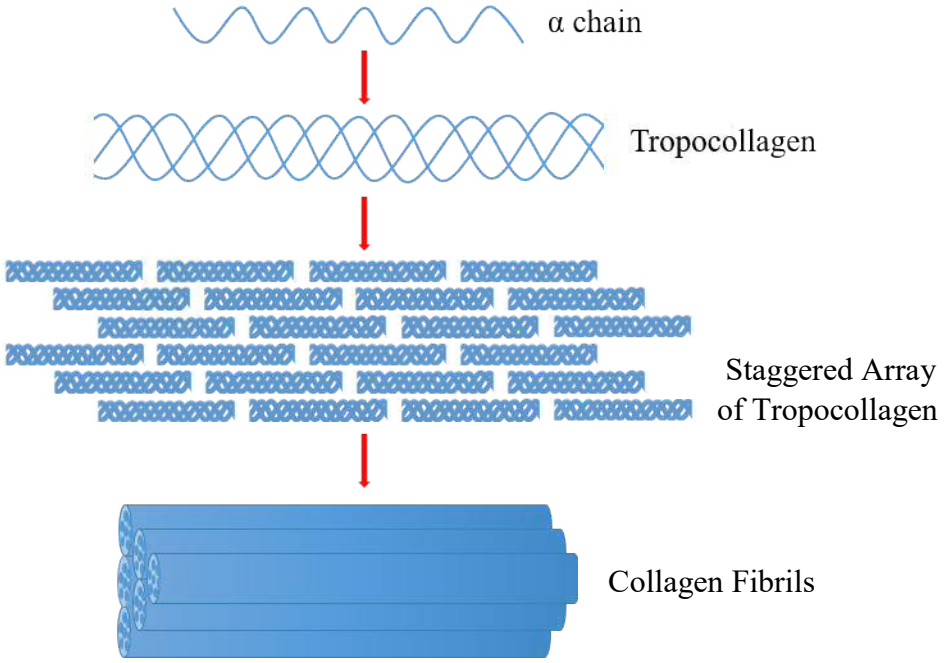

Figure 1.4 Corneal Collagen Hierachy

Collagen types can be classified into 3 sub-families: Class I (Fibril forming collagens, types I, I, III, V and XI) are banded fibrillar collagens with an uninterrupted helix and are

approximately 300nm. These band together to produce fibrils and, in some tissues, fibres. Class II (Fibril-associated collagens with interrupted triple helix domains [FACIT], types IX, XII, XIV and XVI) do not form fibrils by themselves but interact with the surface of fibrillar collagens (Class I) (Shaw & Olsen, 1991; Koch et al., 2001). Class III (Non Fibrillar collagens, types VI, VI and VII) are other forms of non-fibrillar collagen forming basement membrane collagens, microfibrils and anchoring fibrils that form networks (Hirano et al., 1989; Smolin et al., 2005).

The stromal collagen, consisting of type I predominantly and lesser amounts of V, VI, XII, XIII, XIV and XXIV (Ihanamaki & Pelliniemi, 2004), exists in the form of fibrils that have a uniform diameter and spacing throughout the stroma, an essential property for corneal transparency. Collagen type III does exist in the corneal stroma, but only in scarring, which will be discussed later (Smolin et al., 2005). The fibrils are arranged running parallel within lamellae. Lamellae are bands of corneal collagen fibrils approximately 2µm thick and 9-260µm wide that run from limbus to limbus; each one running at a certain angle to each other and parallel to the corneal surface. They bifurcate and interweave intermittently throughout the cornea (figure 1.5) (Meek & Boote, 2009).

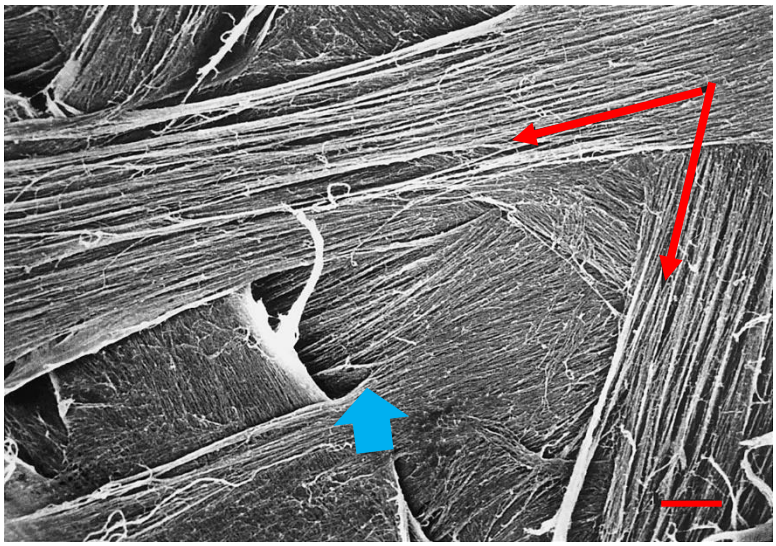

Figure 1.5 Scanning electron micrograph, showing bifurcation and fusion of lamellae in the human corneal stroma. Arrows (red): directions of two separate interwoven lamellae. Arrowhead (blue): point of bifurcation of a lamella. Scale bar: 10 µm. (adapted from Meek and Boote, 2009. Original image from Radner et al., 1998).

Posteriorly these lamellae are arranged in preferentially orthogonal layering (running at right angles to one another) whereas anteriorly the lamellae are organised more obliquely and there is more interweaving between layers (Kaufman & Alm, 2002; Muller et al. 1995). It has been postulated that this increased interweaving may be so that many lamellae can anchor to Bowman's layer for stability (Meek & Boote, 2009).

An extracellular matrix of highly hydrophilic mucopolysaccharides (as part of the glycosaminoglycan side chain on proteoglycans) surrounds the lamellae essentially binding them together. When the endothelial pump breaks down in the cornea due to injury or pathology, these mucopolysaccharides, being highly hydrophilic and at a higher concentration in the stroma than anywhere else in the cornea, are responsible for the ensuing corneal oedema and disruption of the fibril organisation and spacing that ultimately results in loss of transparency (discussed in more detail in section 1.3) (Saude, 1993).

Keratocytes make up 10% of the stroma's volume and are differentiated mesenchymal corneal fibroblasts that produce components important for repair and maintenance of collagen, proteoglycans and keratocytes themselves (Smolin et al., 2005). Generally, keratocytes are flattened cells with long thin processes, however they change morphology throughout the stroma. Anteriorly the cells have a higher density forming an extensive network of branching and interconnecting cell bodies, but have poor lamellar organisation. Towards the centre they have the least cell density and variable organisation, then towards the posterior the keratocytes have a more distinctive morphology, denser population than centrally and are larger and connected by shorter processes. These differences of the keratocytes throughout the stroma have been suggested to correspond to the collagen type and requirements throughout the corneal stroma with regards to transparency (Poole et al., 2003).

1.2.2.Keratocytes

Keratocytes are the corneal fibroblasts and are derived from neural crest cells during embryogenesis (Du et al. 2005). Keratocytes produce type I and V collagen for the stroma during development, as well as other components for the extracellular matrix (Funderburgh et al., 2005; Wilson et al., 2000). These cells can be found throughout the cornea and are transparent, which coupled with their flattened elongated shape helps the cornea maintain its transparency. Keratocytes have a major role in corneal wound healing, which will be discussed in section 1.6.

1.2.3. Proteoglycans

Proteoglycans, the "ground substance" or extrafibrillar material of the cornea, are macromolecules composed of a protein core and a carbohydrate glycosaminoglycan (GAG) polysaccharide chain attached. They are hydrophilic, negatively charged molecules located at specific sites throughout the corneal stroma (Smolin et al., 2005). The protein cores of proteoglycans have 7-10 leucine-rich repeats and belong to the gene family of small leucine-rich repeat proteoglycans. There are 3 major groups of glycosaminoglycan side chains, after which the proteoglycans are named.

There are three different keratan sulphate proteoglycans that are abundant in the posterior stroma which all participate in maintaining corneal transparency alongside collagen types VI and XII; lumican, keratocan and mimecan. Lumican is an 11 leucine rich proteoglycan with a single keratan sulphate side chain, it is known to be important in maintaining corneal transparency by controlling the formation and diameter of collagen fibrils (Kao et al., 2006, Kaufman & Alm, 2002). Keratocan has 10 leucine-rich repeats and three keratin sulphate side chains and is exclusively an ocular proteoglycan. Finally, mimecan has 5 leucine-rich repeats and one keratan sulphate side chain (Kaufman & Alm, 2002).

Decorin, as a chondroitin/dermatan sulphate proteoglycan, has 9 leucine rich repeats and a single glycosaminoglycan side chain. It is more abundant in the anterior cornea than posteriorly and binds to type IV collagen. It is the only chondroitin/dermatan sulphate proteoglycan in the cornea.

The keratan sulphate proteoglycans appear in other connective tissues of the human body, however, they are unique in the cornea as they are highly sulphated. This high sulphation of their glycosaminoglycan side chains increases the water retentive properties of the cornea and thus contributes to the regulation and corneal hydration and consequently its transparency (Funderburgh et al., 1993).

1.3.Corneal Transparency

Transparency of the cornea can be argued to be its most important function, and it achieves this transparency despite having the same composition as the sclera and skin, scattering less than 10% of incident light (Kaufman & Alm, 2002). This transparency becomes all the more impressive when it is considered how densely packed the cornea is with all manner of structures and cells, as discussed above. For an object to be transparent it must adhere to two separate requirements; it must not absorb light and it must not scatter light (Roberts et al., 2001; Meek et al., 2002). These two criteria are certainly met by the cornea as it contains no pigment or other molecules that absorb light in the visible spectrum and the prevention of light scatter is mostly attributable to collagen and proteoglycan organisation in the corneal stroma.

The stromal collagen fibrils require a precise uniform diameter and spacing (controlled by proteoglycans), as originally proposed by Maurice in 1957. However, this hypothesis has since been shown to be incorrect, as modern transmission electron microscopy (TEM) images have revealed that neither fibril diameter nor spacing is strictly constant throughout the cornea (figure 1.6).

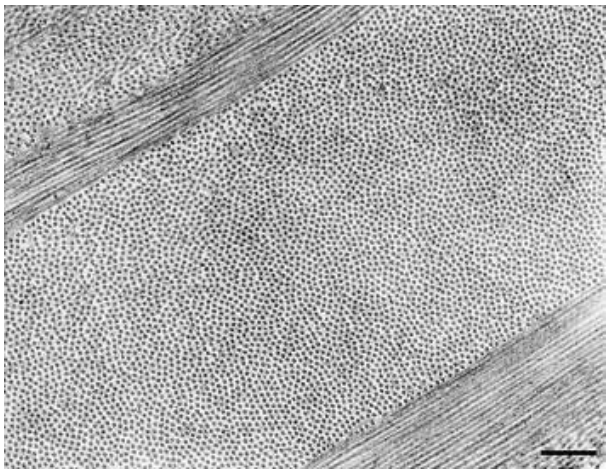

Figure 1. 6 Transmission electron micrograph of the corneal stroma, showing parallel, small diameter collagen fibrils lying within lamellae. Four lamellae are shown, two in longitudinal and two in transverse section. Scale bar: 300 nm. (copied from Meek & Boote 2009, original Image by R. Young)

The control of the scattering of light (to aid transparency), aiming to produce minimal forward scatter relative to light transmission, can also be produced by a uniform refractive index. However, it is known that the components of the stroma have differing refractive indices, Collagen fibres have a refractive index of 1.411 compared with the extrafibrillar matrix's refractive index of 1.365 (Meek & Leonard, 1997), which theoretically should result in light scatter. This is overcome due to the spacing and order of the collagen fibrils. They are arranged in short-range order, examined by Hart and Farrell (1969) who discovered, using a radial distribution function, that a more "liquid crystal" structure of a random yet regular organisation was the answer. It is this short-range order that creates the necessary destructive interference away from the forward direction of light resulting in all the constructive inference energy going only into the light transmitting through to the retina (Meek et al., 2003). This can be demonstrated by imagining each lamella as an individual diffraction grating, and applying the formula $n\lambda=d\sin\theta$, where θ is constructive interference with respect to the incident light and d is the centre to centre distance of the lines on the grating (in this case the collagen fibrils). Where $d>\lambda$ you will see one or more diffraction orders, but where $d<\lambda$, as is the case in the cornea, then you will only see light in the zeroth order, which with respect to the incident is in the forward direction (Roberts et al., 2001; Meek et al., 2002). Essentially, providing the spacing and the arrangement of adjacent

fibrils are such that there is a destructive interference of scattered light, then it is not necessary that the spacing and diameter of the collagen fibrils confirm to a strict "crystalline" structure as described by Maurice (1957) (Hart & Farrell, 1969).

Through all the theories and calculations, the basic proof that corneal transparency largely relies upon basic organisation comes when this organisation is disrupted by either oedema or scarring. In these cases, the collagen fibril spacing is altered and light transmissibility drops, as light is scattered and absorbed, resulting in a milky appearance to the cornea and reduced visual acuity of the patient.

A large number of keratocytes are found throughout the corneal stroma, up to 15% of the total stromal volume (Huang & Meek, 1999; Hahnel et al., 2000), and yet they appear not to scatter light. It has been postulated in the past that keratocytes produce crystalline molecules in their cytoplasm that change their refractive index to match the surrounding extracellular matrix (Jester et al., 1999; Jester, 2008; Møller-Pedersen, 2004). In 2015 Gardner et al. showed that the refractive index of the keratocytes did indeed match that of the surrounding extracellular matrix, but only in their quiescent state. When activated after wounding the refractive index of the cells decreased, no longer matching that of the surrounding tissue and would therefore scatter light, reducing transparency (Gardner et al., 2015).

1.4.Refractive Surgery

Refractive surgery is an increasingly popular and widely available elective, cosmetic treatment for refractive errors such as myopia, hyperopia, astigmatism and even presbyopia (Jester et al., 1999). Originally performed using a blade to make incisions that would flatten the corneal topography (in radial keratotomy) and thus reduce a myopic prescription, refractive surgery has evolved drastically over the last few decades through various permutations (some of which are still used where appropriate) to using excimer lasers (Jester et al., 1999). This is an "excited dimer", popularly an argon-fluoride gas

combination that creates a high power UV light beam and is used to perform precise photoablation to reshape an exposed stromal bed and reduce large and varying types of refractive error to “plano”, with minimal thermal damage to the tissue (Waring & Seiler 1993; Bores, 2001; Singerman & Coscas, 1998). The title of refractive surgery also encompasses implants such as multifocal and phakic IOLs and intacs procedure, however, these will not be discussed in this thesis.

1.4.1. Refractive Conditions

For clear and focussed vision to occur the three components of the eye (the cornea, the lens and the axial length) must interact in the correct proportions and power to bring the incident light beams together in focus on the retina. This state, where no refractive correction is required, is referred to as emmetropia (figure1.7A). When this does not happen and the image is not focused on the retina due to a component being too powerful or not powerful enough, refractive correction is required and the eye is referred to as being ametropic. Ametropia can present in a number of different forms; myopia, hypermetropia, astigmatism and the age related condition of presbyopia.

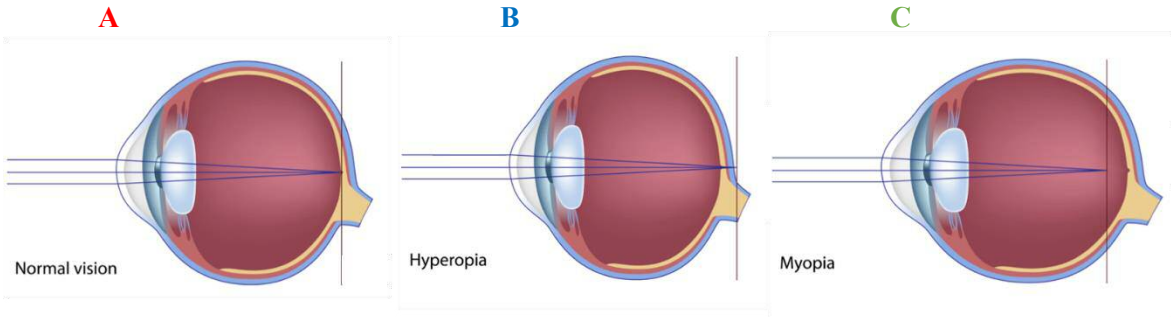

Figure 1.7 Light Diagrams of Refractive Conditions **A** Emmetropia **B** Hyperopia (or hypermetropia) **C** Myopia (Alila Medical Images, Alamy Stock Photo)

i. Myopia

In myopia (or "short/near-sightedness") the incident beams of light entering the cornea in parallel rays, from a distant object, are focussed in front of the retina rather than on it causing a blurred image on the retina (figure 1.7 C). This refractive state is due to an imbalance of the axial length of the eye (too long) and the optical power or curvature of the lens and the cornea (to strong) (Morgan et al., 2012; Upadhyay, 2015). This requires negative spectacle or contact lens correction, to reduce the refractive power of the eye and push the focus of the image back onto the retina, or flattening of the cornea, to reduce its curvature, and therefore its refractive power, using a refractive surgery procedure.

ii. Hyperopia

In hyperopia (or "long/far-sightedness") the refraction of light entering the eye from a distant object is too shallow and the rays are therefore focused behind the retina resulting in a blurry image (figure 1.7 B). This condition is caused by imbalance of the axial length of the eye (too short) and the optical power or curvature of the lens and the cornea (to weak) (Upadhyay, 2015). Whilst mild cases can be naturally compensated, hyperopia requires positively powered spectacle or contact lenses to increase the refractive power of the eye pulling the focused image forward onto the retina. Refractive surgery to correct this form of ametropia involves steepening the curvature of the cornea to increase its refractive power and focus the image on the retina.

iii. Astigmatism

Astigmatism is a more complex form of ametropia caused by a toric cornea or lens- one that is not completely round. This is where there is a larger refractive error (over-powered or under-powered) in one direction (or axis) across the cornea or lens compared to the other, Light entering the eye in this condition is refracted on different axes by differing amounts, resulting in an image being more in focus on one axis than another (Read et al., 2007).

iv. Global Incidence of Refractive Error

The incidence of the different types of refractive error changes depending on ethnicity. There have been many papers reporting incindences of all ages across the world, but in 2018 Hashemi et al., performed a systematic review of databases and studies from 1990-2016 and merged them using a random effect model that reported the results as an estimated pool prevalence (EPP) with a 95% confidence interval (CI). The global incidences of astigmatism, hyperopia and myopia in adults and children can be seen in Table 1.3.

	Astigmatism %EPP (95%CI)	Hyperopia %EPP (95%CI)	Myopia %EPP (95%CI)	Astigmatism %EPP (95%CI)	Hyperopia %EPP (95%CI)	Myopia %EPP (95%CI)
	Children			Adults		
Africa	14.2 (9.9–18.5)	3.0 (1.8–4.3)	6.2 (4.8–7.6)	11.4 (2.1–20.7)	38.6 (22.4–54.8)	16.2 (15.6–16.8)
Americas	27.2 (26–28.4)	14.3 (13.4–15.2)	8.4 (4.9–12.0)	45.6 (44.1–47.1)	37.2 (25.3–49)	22 (16.4–27.7)
South-East Asia	9.8 (6.3–13.2)	2.2 (1.2–3.3)	4.9 (1.6–8.1)	44.8 (36.6–53.1)	28 (23.4–32.7)	32.9 (25.1–40.7)
Europe	12.9 (4.1–21.8)	9.0 (4.3–13.7)	14.3 (10.5–18.2)	39.7 (34.5–44.9)	23.1 (6.1–40.2)	27 (22.4–31.6)
Eastern Mediterranean	20.4 (14.5–26.3)	6.8 (4.9–8.6)	9.2 (8.1–10.4)	41.9 (33.6–50.2)	33 (26.9–39)	24.1 (14.2–34)
Western Pacific	12.1 (8.4–15.8)	3.1 (1.9–4.3)	18.2 (10.9–25.5)	44.2 (30.6–57.7)	28.5 (20.1–37)	25 (20–30.1)
All	14.9 (12.7–17.1)	4.6 (3.9–5.2)	11.7 (10.5–13.0)	40.4 (34.3–46.6)	30.9 (26.2–35.6)	26.5 (23.4–29.6)

EPP: Estimated pool prevalence. CI: Confidence interval.

Table 1.3 Estimated pool prevalence (EPP) of myopia, hyperopia, and astigmatism in children and adults by WHO regions. Table adapted from Hashemi et al., 2018.

v. Presbyopia

Presbyopia is an age onset refractive error (usually in middle age at around 40-50 years old) that occurs due to increasing stiffness of the crystalline lens. In its young and flexible

state its shape can be changed by the contraction or relaxation of the ciliary muscle surrounding the lens to change the focus of the eye from a distance to a near object, known as accommodation. Once the lens stiffens there is a progressive loss of accommodative amplitude and the near vision is no longer clear (Mantry & Shah, 2004). In this instance positively powered lenses are needed purely for near work to provide the patient with clear near vision. This is therefore harder to correct with Laser refractive surgery, as the correction is not required at all times in the distance (although it can obviously occur alongside a longstanding refractive error that does require distance correction). It can be corrected by performing intraocular surgery, such as refractive lens exchange, going to the more obvious root of the problem, or extraocular surgery using a number of laser techniques (Mantry & Shah, 2004). There are a number of differing approaches using Laser in situ keratomileusis (LASIK- see section 1.4.3) to create a multifocal corneal surface from the most commonly performed technique, central PresbyLASIK (Yin et al., 2016), to the more straight forward monovision LASIK technique (Vargas-Fragoso & Alió, 2017) where one eye (the dominant eye) is corrected for distance vision and one eye for near vision.

1.4.2. PRK

Photorefractive keratectomy (PRK) is a procedure whereby the corneal surface is re-sculpted via excimer laser ablation. Firstly, the epithelium is removed using one of three methods; mechanically (using a blade or a spatula), chemically (usually using alcohol) or by using an excimer laser to de-epithelialise the cornea via photoablation (Bansal & Veenashree, 2001). The centre of the exposed cornea is then ablated using the excimer laser to either flatten or steepen the curvature depending on the original refractive error (figure 1.8). The wound will re-epithelialise in a matter of days after the procedure (during which time a protective membrane is placed over the wound, usually a bandage contact lens), however, as discussed previously, stromal healing can take months and the final refractive result cannot be ascertained until this has happened. Each pulse of the excimer laser disrupts the molecular bonds in the cornea and can remove 0.25μm of tissue centrally, controlled by a computer (Coscas & Singerman, 1999), the laser beam quality and the frequency of its pulses are derived by an algorithm (Fagerholm, 2000).

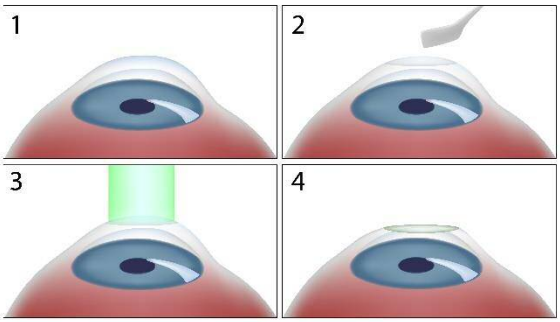

Figure 1.8. PRK Procedure- 1. Untreated cornea 2. Epithelium is removed 3. Laser ablates and reshapes corneas 4. Exposed PRK wound (Alila Medical Images, Alamy Stock Photo)

Although PRK has a long visual recovery and can be quite painful for a few days after the procedure and it can result in complications such as damage to the central cornea, corneal haze or decentred ablation causing irregular astigmatism, it does not involve the creation of a corneal flap and is therefore considered safer than LASIK.

1.4.3. LASIK

The first to combine the excimer laser and microkeratome technology were Buratto and Pallikaris in the late 1980's, first attempting the procedure on rabbits, then blind human eyes in 1989 and finally sighted patient eyes in 1991 (Pallikaris et al., 1990; Pallikaris et al., 1991). Laser in situ keratomileusis (LASIK) involves the photoablation of the mid-stroma of the cornea to correct refractive error, after creating a flap out of approximately the upper 150μm of the cornea (comprising of the epithelium, Bowman's membrane and the anterior stroma) using either a microkeratome or a femtosecond laser (a laser delivering laser pulses of infrared wavelength-1053nm- to disrupt the tissue at a specified level within the stroma) (Kezirian & Stonecipher, 2004; Montes-Mico et al., 2007). Once the flap has been created by either method it is lifted and the mid stroma undergoes reshaping by photoablation to correct the refractive error, much the same as with PRK. The flap is then repositioned and left to heal (Bansal & Veenashree, 2001) (figure 1.9).

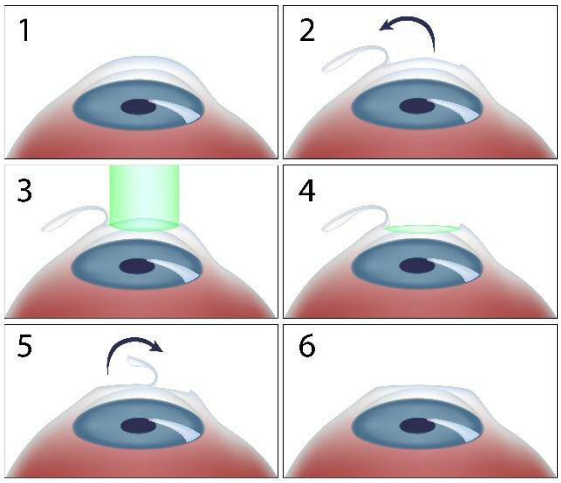

Figure 1.9 - LASIK procedure 1. Untreated cornea 2. Flap creation using Microkeratome and lifted 3. Laser ablates and reshapes cornea 5. Flap is repositioned 6. Post-operative eye (Alila Medical Images, Alamy Stock Photo)

LASIK can be considered superior to PRK in terms of visual outcomes and patient comfort. In general, the patient experiences very little if any discomfort and the visual recovery is quick and more predictable than with PRK. However, the creation of a flap out of the outermost layers of the cornea creates some very serious risks of complications (see section 1.4.5).

1.4.4. LASEK

Laser assisted sub-epithelial keratectomy (LASEK) is similar to PRK. However, instead of removing the epithelium and disposing of it, this procedure involves the peeling back of the epithelium and repositioning after the stroma has been photoablated. This is an improvement on PRK as it results in less central postoperative corneal haze (as the epithelium and Bowman's layer are not disrupted as much) and less postoperative pain for the patient, yet it maintains the advantages of PRK over LASIK by not creating a flap. LASEK is mostly used for patients who have a thinner cornea and so would be left with an insufficient amount of residual stroma post operatively with LASIK. It has more discomfort

than LASIK and slightly increased healing time (Ambrosio & Wilson, 2003; Taneri et al., 2004).

1.4.5. LASIK Post-operative Complications

Refractive surgery procedures in general result in a number of associated post-operative complications. However, LASIK has the most worrying of complications due to the manner in which it is performed. Complications range from visual symptoms such as glare, haloes and reduced night time vision to the more serious recurrent epithelial erosion and corneal ectasias that cause, not only visual disturbances, but also discomfort and require medical intervention (Pallikaris et al., 2001; Perez-Santonja et al., 1998). The corneal nerves are also severed and their number decreases by 90% after LASIK. This number gradually increases, however after one year there will still be less than half the original number (Lee et al., 1982). This potentially reduction in sensitivity could be responsible for reduced rate in blinking and the dry eye problems that ensue; another common complication following surgery (Toda et al., 2001; Chuck et al., 2000; Rosen, 2000)

As there is a flap created, which is then smoothed back down, there is great potential for complications with this flap. Diffuse lamellar keratitis (DLK, “sands of the sahara”) is a sterile inflammation that can occur under the space in the flap/stroma interface. This can cause a decrease in vision and in severe cases require the flap to be lifted and “washed” out. This complication has an incidence rate of 6% 18 months post-operatively in microkeratome created flaps and 10.6% in those created with a femtosecond Laser, making it the most common post-operative complication (Moshifar et al., 2011). This has been known to happen up to 12 years after LASIK (Kamiyaki et al., 2010). Other particles such as cellular debris and even metallic components of the microkeratome blade can be found in the flap interface (Kaufman et al., 1998; Dawson et al., 2005). Another disruption of vision involving the flap/stroma interface is the occurrence of epithelial ingrowth whereby the epithelium can grow under the flap edge and can induce astigmatism and encroach on vision if left untreated. This happens in under 1% of patients with LASIK for both microkeratome and femtosecond LASER created flaps (Moshifar et al., 2011). The treatment for this is, again, to lift the flap and wash out the cells. These both require a

surgical intervention that causes the patient more discomfort and requires another course of antibiotics and anti-inflammatory therapeutics.

The most potentially damaging of the LASIK flap complications, however, is flap dislocation. This occurs due to an aspect of corneal wound healing, whereby the stromal wound healing is triggered adjacent to the epithelial wound (see section 1.6). This was found to happen in 2.5% of microkeratome LASIK patients and 1.1% of those created with a femtosecond Laser one-day post operatively by Moshifar et al. in 2011. As the flap created means that only a circular incision is made through the epithelium around the mid-periphery of the cornea this is where the epithelial and stromal healing takes place, and the wound healing of the incision through the stroma in the middle of the cornea parallel to the epithelium remains potentially incomplete, leaving a hypocellular scar (Schmack et al., 2005).

This means that the flap retains only an estimated 2-28% of its original strength (Schmack et al., 2005; Randleman et al., 2008). The peripheral wound healing is often not enough to secure the flap making it vulnerable under mechanical stress and some flaps can easily, with trauma such as eye rubbing or car accidents, become wrinkled, folded (figure 1.10) or, in extreme cases entirely dislocated (Melki et al., 2000; Iskander et al., 2001; Heickell et al., 2004; Landau et al., 2006). Whilst in most cases this can be resolved it causes great discomfort and distress to the patient.

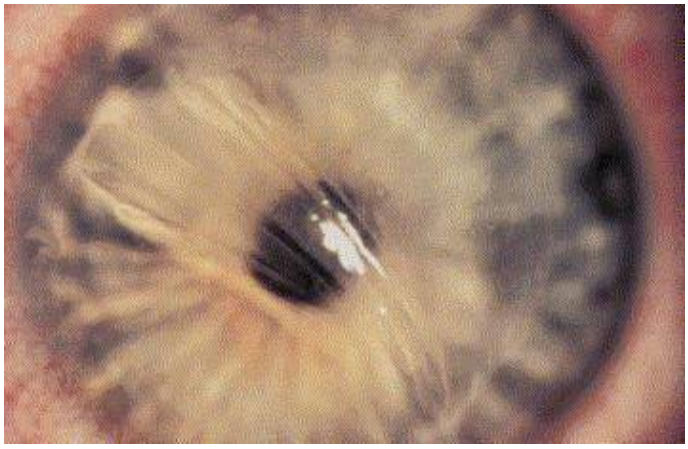

Figure 1.10. Large LASIK Flap Wrinkle (copied from Melki & Azar, 2001)

1.5.Wound Healing

Wound healing is the necessary response of a mammalian body to close and clean a wound, preventing invasion of foreign bodies that may be harmful and returning the body to homeostasis as soon as possible. There are four different stages of wound healing; haemostasis, inflammatory stage, granulation and re-epithelialisation stage, wound contraction and tissue re-modelling (Falabella & Kirsner, 2005). At the end of this process a scar will have formed at the wound site comprising of fibrous tissue produced by activated fibroblasts that are activated during wound healing. This scar, once healing has finished and the wound is closed, remains as a tissue with a different phenotype and mechanical properties to that of the original tissue, giving not only a different appearance but also a permanently weaker tensile strength to that of the original tissue.

The coagulation stage occurs immediately after injury and prevents blood loss via vasoconstriction. Platelets are then activated by exposure to collagen from the surrounding tissue (such as collagen type I) and this creates a fibrin clot at the site of injury that provides an initial wound matrix. The platelets are also responsible for the initial release of cytokines and growth factors (Falabella & Kirsner, 2005).

The inflammatory stage follows the initial response to injury and can last for as long as 14 days after wounding in normal wound healing (Falabella & Kirsner, 2005). This helps to minimise foreign body invasion via the migration of neutrophils and macrophages to the injury site. This is followed by the granulation and re-epithelialisation stage whereby once the wound has been temporarily closed by the two initial stages the fibroblasts start to lay down and other ECM (extra cellular matrix) components creating scar tissue, further healing the wound.

The final stage of wound healing is in the contraction of the wound and remodelling of the tissue. The wound is contracted, bringing the edges of the wounds together, by the final stages of the formation of scar tissue and this seals the injury site. This scar tissue is then remodelled, very slowly, as a result of the action of matrix metalloproteinases (MMP's)

and various collagenases that will bring the scar tissue closer to the phenotype of the original tissue (Clark, 1996).

1.6.Corneal Wound Healing

No matter where the injury or what type of injury has occurred, wound healing follows the same basic sequence across any one organism. The cornea is no different, however, due to its avascular nature, some stages of the sequence do not apply. Figure 1.11 shows a flow diagram of the corneal wound healing cascade.

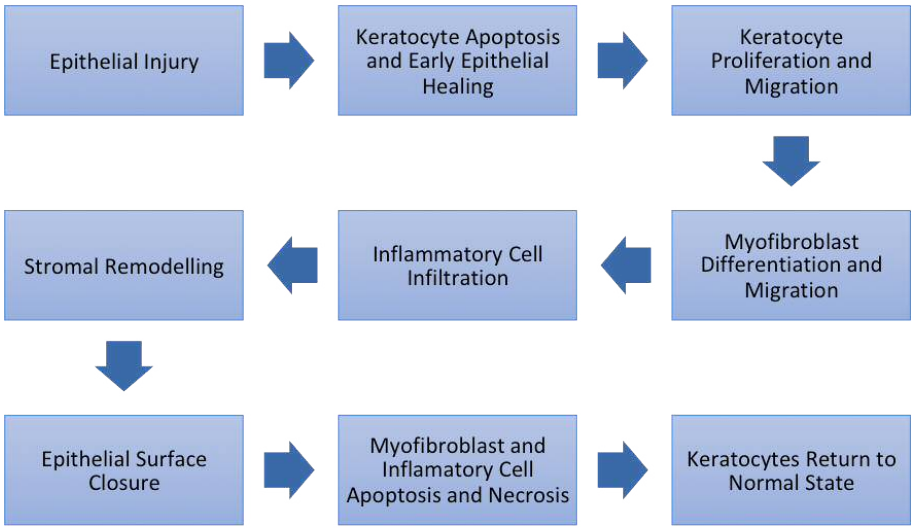

Figure 1.11. Corneal Wound Healing Cascade-
adapted from Eraslan & Toker, 2009

Corneal wound healing can be approached by looking at each of the three major layers of the cornea separately (the epithelium, stroma and endothelium), as each one has its own characteristic sequence of events. Wound healing of both the stroma and the epithelium will be discussed here, as there is significant interaction between the epithelium and stroma during corneal wound healing and both are injured during the creation of LASIK-like wounds with a microkeratome. The production of metalloproteinases, collagenases and other enzymes that restore the damaged stromal tissue is stimulated by cytokines and

interleukins produced by the epithelium (see section 1.6.1) (Mohan, et al., 1999; Masur et al., 1996; Wilson et al., 1996). This is known as an epithelial-stromal interaction. In turn the myofibroblasts secrete cytokines (the receptors for which are up-regulated in the epithelium during injury) that aid regulation of healing of the epithelium directly above in aspects such as proliferation, migration and differentiation; this is referred to as a stromal-epithelial interaction (Wilson et al., 1999).

Wound healing can of course also extend to the endothelium, raising a number of complications as damage to the endothelium will interfere with the endothelial pump and therefore have an impact on corneal clarity. However, this will not be covered in the following paragraphs.

1.6.1. Epithelial Wound Healing

The epithelial response to injury is, as would be expected, the first in the sequence of corneal wound healing, whether it be for a superficial wound (such as and abrasion) or a penetrating wound (such as LASIK). There are three main, but continuous stages to this process; the latent stage, epithelial cell migration and re-epithelialisation (Zieske, 2001; Fini, 1999; Dua et al., 1994).

Following injury in the latent phase (within 4-6 hours) (Lu et al., 2001), any necrotic or damaged cells are either sloughed off via the tear film or engulfed by polymorphonuclear cells in the tear film (Lee et al., 1982). The introduction of intracellular material into the extracellular space triggers apoptosis and results in the release of interleukins and growth factors such as transforming growth factor (TGF) α and β, Platelet derived growth factor (PDGF) and interleukins (IL)-1, -6 and 10 (Ljubimov & Saghizadeh, 2015; Lu et al., 2001; Yu et al., 2010; Netto et al., 2007). The normal mitosis of the basal cell layer (for normal corneal maintenance) at the wound edge ceases and the basal layer cells loosen their hemidesmosome attachments to the basement membrane (Kaufman & Alm, 2002). In this latent phase the wound edge retracts and actin filaments are generated in its vicinity. The

phenotype of the epithelial cells on the edge of the wound starts to change as the cells flatten and enlarge, causing a thinning of epithelium immediately adjacent to the wound (Lu et al., 2001; Kaufman & Alm, 2002). Extensions from the changing epithelial cells called filopaedia and lamellapodia project forward onto the wound site where fibronectin is now present, most likely derived from the tear film, acting as a provisional matrix (very much like the fibrin clot in general wound healing in vascular tissue) (Gipson et al., 1993).

Epithelial cell migration, begins as a sheet of epithelial cells. The cell-cell junctions (the desmosomes) remain intact, creating an "ameboid"-like crawling motion (Kaufman & Alm, 2002). Cell migration is usually completed 36 hours after wounding (Dua et al., 1994), although this will be largely dependent on the initial size of the wound.

Re-epithelialisation happens alongside cell migration. Hemidesomosomes are re-formed once the wound closure is complete (Steele, 1999). New epithelial cells at this juncture are derived from those proliferating at the limbal edge of the epithelium which migrate in a centripetal pattern towards the wound area. The wound is eventually covered by 1-2 layers of cells and a new basement membrane is developed. The release of cytokines and growth factors also stops (Kaufman & Alm, 2002).

Complete epithelial wound healing takes approximately 48-72hrs in normal healing. Until it is complete the patient can experience visual fluctuations.

1.6.2. Stromal Wound Healing

Due to its varied structure and composition when compared to the epithelium, stromal wound healing differs significantly to epithelial wound healing. The healing process in the stroma, however, is "kick started" by the epithelial wound healing process. When cytokines, namely TGFβ 1 and 2, are produced by the apoptotic cells in the wounded epithelium (Masur et al., 1996; Wilson et al., 2012; Ljubimov & Saghizadeh, 2015; Mohan et al., 1997), they bind to receptor sites on the keratocytes almost immediately, which in

turn triggers keratocyte apoptosis (Wilson et al., 1999), leaving an acellular zone. This apoptosis can last a week or more (Gao et al., 1997; Mohan et al., 2001). The remaining quiescent keratocytes surrounding the void that remains after apoptosis then undergo rapid proliferation and their numbers increase and begin activation into keratocyte-derived myofibroblast phenotypes. These then migrate to the injury site where they produce collagen, proteoglycans and other ECM components to restore Bowman's layer and the damaged stromal tissue (Wilson et al., 2012; Fini, 1999; Jain & Azar, 1994) (see section 1.6.3).

The production of metalloproteinases, collagenases and other enzymes that restore the damaged stromal tissue, as described above, is stimulated by cytokines and interleukins produced by the epithelium. This is known as an epithelial-stromal interaction. In turn the myofibroblasts secrete cytokines (the receptors for which are up-regulated in the epithelium during injury) that aid regulation of healing of the epithelium directly above in aspects such as proliferation, migration and differentiation. This is referred to as a stromal-epithelial interaction (Wilson et al., 1999). There are many interactions between the stroma and the epithelium during the overall corneal wound healing processes that are mediated by cytokines.

The final phase of healing in the stroma involves remodelling of the damaged tissue in an attempt to bring it back as close as possible to its native state. The success of this process however, is dependent on the type of wound originally inflicted on the cornea. Shallow abrasions on the cornea (such as those inflicted during PRK and LASEK that run horizontal to the surface) heal over approximately a year in humans (Smolin et al., 2005). The number of myofibroblasts decrease through apoptosis (Kaur et al., 2009; Wilson, 2012; Gao et al., 1997) and the basement membrane is restored leaving minimal scarring. A penetrating, gaping wound however (one that runs perpendicular to the corneal surface, such as surgical incisions and penetrating trauma), stimulate the synthesis of abnormal ECM repair components and collagens not habitually found in the stroma, namely collagen type III and abnormally large "repair type" proteoglycans by the myofibroblasts (Borcheding et al., 1975; Wilson, 2012). This therefore results in abnormal collagen inter-fibril spacing

leading to a lack of the level of transparency found in the native tissue (Fini, 1999). This could take years to remodel and may not ever reach the optical clarity of the original un-injured cornea (Zieske, 2001).

1.6.3. Myofibroblasts and Alpha Smooth Muscle Actin (α-sma)

Myofibroblasts are fibroblastic cells found in stromal wound healing that arise from quiescent keratocytes and corneal fibroblasts derived from keratocytes, activated by TGF-β1 and TGF-β2 released by apoptotic epithelial cells after epithelial injury (Masur et al., 1996; Wilson, 2012; Ljubimov & Saghizadeh, 2015). The activated myofibroblastic cell phenotype changes into an elongated morphology from a stellate one and remodel their actin cytoskeleton to acquire stress fibres (intracellular microfilament bundles) and express alpha smooth muscle actin (α-sma, associated with the contractile forces that are necessary for wound closure) (Ljubimov & Saghizadeh, 2015; Jester & Ho Cheng, 2003) in essence adopting a smooth muscle cell phenotype (Wilson, 2012).

The expression of α-sma in the myofibroblast has become a reliable and widely used immunohistochemical marker for myofibroblasts in vitro and in vivo (Chaurasia et al., 2009) (figure 1.12)

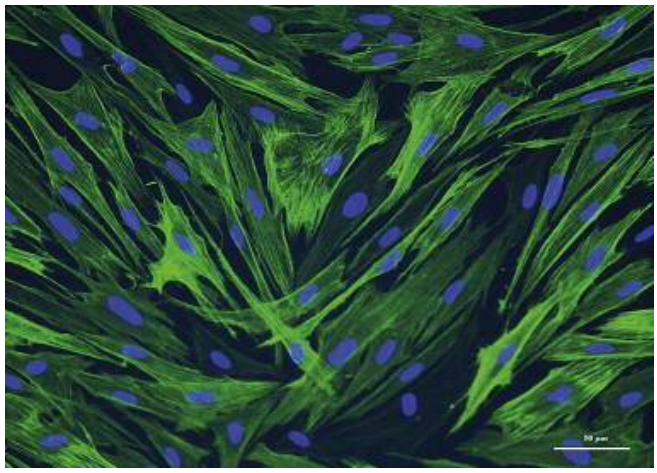

Figure 1.12. α-Smooth muscle actin (green) staining in myofibroblasts cultured in RSF with 1% FBS and 2 ng/ml TGF β1. Blue is DAPI stained nuclei. Magnification 200× (copied from Kaur et al., 2009)

Myofibroblasts produce a number of ECM components including collagen I and III and large proteogylcans as well as fibronectin receptor α5β1 and αvβ3 integrins that are involved in the assembly of fibronectin fibrils (Jester et al., 1999; Zieske, 2001; Wilson, 2012) The myofibroblastic exertion of contractile forces and high motility (migrating to the wound site) are aided by the presence of this fibronectin as well as chondroitin sulphate that open up the stromal fibrils and promote invasion of fibroblasts to the wound site (Andresen et al., 2000; Taliana et al., 2000; Jester et al., 1995). The large amounts of ECM laid down by the myofibroblasts play an important role in wound healing by aiding with wound closure and the regeneration and remodelling of the stromal tissue. However, the activation of myofibroblasts can also have a negative impact on the outcome of the wound healing process by contributing to a more opaque stroma (Ishizaki et al., 1994; Wilson, 2012) This is due to a number of myofibroblastic characteristics; the contractile forces altering the stromal collagen fibril organisation, the laying down of excess repair ECM and the diminished concentration of intracellular corneal crystallins compared to the quiescent (due to the dramatic increase in their size) (Jester et al., 2005; Jester et al., 2012; Ljubimov & Saghizadeh, 2015; Ishizaki et al., 1994; Wilson, 2012; Fini, 1999).

Whilst the activation of myofibroblasts is an integral part of the wound healing process, elucidated by the production of TGF-β1 and TGF-β2 (Carrington et al., 2006), they are not generally detectable in the normal unwounded cornea and so their presence during wound healing is a balancing act between TGF-β1, TGF-β2 and interleukin-1 (IL-1) (Wilson, 2012; Kaur et al., 2009). Sufficiently high enough levels of TGF-β activates the transformation of keratocytes into myofibroblasts, and maintain their presence by inhibiting IL-1 stimulated myofibroblast apoptosis (Kaur et al., 2009, Wilson, 2012). As the levels of TGFβ fall, the numbers of myofibroblasts decrease as IL-1 triggered apoptosis occurs.

1.7.Scarless Wound Healing in the Oral Mucosa

1.7.1. Oral Mucosa

The oral mucosa describes the mucous membrane epithelial lining of the mouth, gums and internal surface of the cheek. It is a multi-layered structure, consisting of the oral epithelium (which is either keratinized or non-keratinized depending on the location within the oral cavity), lamina propria and sub mucosa. The oral mucosa is multifunctional; it helps to regulate temperature and hydration and, like the cornea, acts as a barrier to external environmental damage and infection (Stephens & Davies, 2015). Due to high frequency of mechanical trauma from mastication and the need to close wounds rapidly (to prevent infection) and limit scarring (so as not to restrict the flexibility of the oral mucosa) it has unique preferential healing (Lee & Eun, 1999; Shannon et al., 2004; Szpaderska et al., 2003; Enoch et al., 2007). This healing characteristic of the oral mucosa has previously been postulated as being a result of environmental factors such as saliva (Bodner et al., 1992; Hutson et al., 1979) however studies have confirmed that the scarless wound healing properties are inherent to the oral mucosa (Szpaderska et al., 2003).

1.7.2. Oral Fibroblasts

The oral mucosal healing characteristics have been likened to that of foetal scarless wound healing and, focussing on the fibroblasts with respects to wound healing, it has been postulated that oral fibroblasts represent a subpopulation of foetal fibroblasts that have undergone clonal expansion (Sloan, 1991; Irwin et al., 1994; Stephens et al., 1996).

The characteristic preferential wound healing of the oral mucosa includes the rapid re-epithelialisation, an increased ability to remodel ECM (especially in the re-organisation of 3D collagen lattices when compared to skin grafts (Shannon et al., 2005) and a short inflammatory phase (Stephens et al., 1996; Stephens et al., 2001; Enoch et al., 2009; Enoch et al., 2010). The reduced scarring potential of the mucosa may be due to the inhibition of hyaluronan (HA) synthesis by oral fibroblasts that modulate TGFβ1 dependent responses

(discussed in section 1.6.3), in essence preventing fibroblast differentiation into the myofibroblast which would maintain the non-scarring phenotype associated with oral mucosa (Meran et al., 2007; Enoch et al., 2008). This lower myofibroblastic differentiation would mirror the lack of myofibroblasts seen in early gestational wounds that exhibit scarless wound healing (Estes et al., 1994).

Oral fibroblasts also express greater quantities of the cytokines hepatocyte growth factor (HGF or scatter factor) and keratinocyte growth factor (KGF) which both have a role in the regulation of wound healing in the cornea (Shannon et al., 2004; Enoch et al., 2008; Ljubimov & Saghizadeh, 2015). Elevated HGF is also associated with the foetal phenotype in wound healing (Enoch et al., 2008).

1.7.3. Oral Mucosal Lamina Propria Progenitor Cells (OMLP-PCs)

Recently a population of pluripotent stem/progenitor cells were discovered in the lamina propria of the oral mucosa that are thought to contribute to the foetal like scarless wound healing of the oral mucosa (Davies et al., 2009; Widera et al., 2009). These oral mucosal lamina propria progenitor cells (OMLP-PCs) are isolated from buccal mucosal biopsies by differential adhesion to fibronectin (Board-Davies et al., 2015; Davies et al., 2009) are neural crest derived and are highly multipotent with the ability to differentiate down both mesenchymal and neuronal lineages (Stephens & Davies, 2015; Locke et al., 2015).

Furthermore, studies have demonstrated not only the immunological properties of OMLP-PCs, showing their ability to potently suppress the proliferation of peripheral blood leucocytes (PBLs) in a dose and contact-independent manner (Davies et al., 2012), but also the potent antibacterial properties (Board-Davies, 2015). OMLP-PCs were shown to halt the growth of both Gram-negative, by the secretion of haptoglobin (Hp), and Gram-positive bacteria, via the secretion of osteoprotegerin (OPG) (Board-Davies et al., 2015).

OMLP-PCs are of particular interest in the field of future therapeutics as these cells are reliably reproducible, can differentiate down multiple distinct lineages and are easily accessible from a biopsy site that, by the very nature of the characteristics the cells are being collected for, result in minimal or no scarring for the donor (Stephen & Davies, 2015). The potent immunosuppressive and anti-bacterial properties of the OMLP-PCs provide the potential for clinical therapeutic applications. For example, the treatment of immune related disorders, allogeneic tissue engineering and the treatment of infectious diseases such as bacterial pneumonia (Board-Davies et al., 2015; Davies et al., 2012; Stephen & Davies, 2015).

1.8.Aims and Objectives

The hypothesis of this study is that OMLP-PCs will augment corneal healing of a LASIK-like wounded flap such that stromal remodelling and transparency is improved.

To test this hypothesis, the overall aim of this study was to determine the effect of OMLP-PCs as a cell based therapy on corneal wounds in an organ culture model.

To achieve this, the following objectives were performed;

1. Development of a porcine organ culture model that could be used to evaluate the physical properties (transparency and biomechanical strength) of the wound healing cornea.

2. Optimisation of the cell therapy application to LASIK-like wounded organ cultured porcine corneas.

3. Determination of the efficacy of OMLP-PCs on the cellular processes involved in corneal wound healing.

4. Determination of the efficacy of OMLP-PCs on stromal matrix organisation and wound resolution.

Chapter 2

General Materials and Methods

2.1 Source of Tissue

2.1.1. Porcine Eyes

Enucleated whole porcine eyes were procured from a local abattoir within 6 hours of sacrifice, and transported to the laboratory on ice. The eyes were examined (any with epithelial/corneal defects were discarded) and any excess tissue (including muscle, fat and optic nerve) was removed using dissection scissors, in a separate room adjacent to the culture room, to avoid contamination. Next the eyes were rinsed in PBS (phosphate buffered solution) and transferred to a beaker of sterile PBS (see Appendix for solution preparation details) on ice, then rinsed in new PBS, before being transferred to a sterile beaker containing 2.5% betadine, in which they were immersed for 5 minutes. This beaker was re-covered with autoclaved foil, sprayed with 70% IMS (industrial methylated spirit) externally and transferred to a previously cleaned and prepared class II biological safety cabinet. From this stage on, all solutions (see Appendix for methods and preparation details), instruments and containers were prepared using aseptic technique, autoclaved/filtered or purchased as sterile.

Porcine eyes were transferred into fresh PBS and rinsed twice, before being placed into moist chambers (i.e. 60ml sterile pots with a few drops of PBS). Eyes were left at 4°C overnight. Attempts were made to measure the central thickness of the porcine cornea after overnight storage, however this was not possible as it exceeded the limit of the ultrasonic pachymeter (>1000μm).

2.2 Corneal Wounding

A LASIK-like wound flap was created in the stromal portion of each porcine corneas of intact globes using a microkeratome (figure 2.1) (Hansatome Bausch & Lomb, Germany).

Figure 2.1. Hansatome microkeratome (Bausch & Lomb,Germany)www.brusselseyecenter.be accessed 2012

The wounding of the corneas took place in the culture cabinet to maintain sterile conditions. The head components of the microkeratome hand piece were autoclaved at 120°C for 40 minutes. The hand piece (as a motor connected to an electrical supply) as well as the connecting wires and suction tubing were cleaned as thoroughly as possible using an antimicrobial reagent, Microsol, followed by 70% IMS. The operating unit and foot pedals remained outside of the culture cabinet.

The suction ring was placed carefully over the central cornea, using the pupil as a guide and placing the hinge superiorly. The suction was then turned on via a foot pedal and the pressure in the globe was increased to approximately 26mmHg to allow safe operation of the blade and a more accurate incision depth. The wound flap incision was then made by activating the oscillating blade (mounted on a motor) to cut forward into the cornea in a guided arc and then reversed. Once the blade was clear of the cornea, the suction ring was disengaged and the microkeratome head removed from the globe. This resulted in a corneal flap, approximately 200μm thick (the first fifth of the corneal thickness), that remained attached to the peripheral cornea via a “hinge” (figure 2.2). The flap was then examined for quality to ensure it was properly placed and intact.

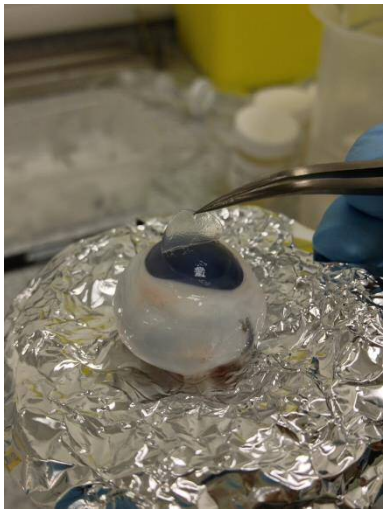

Figure 2.2. Microkeratome corneal wound flap.

2.3 Organ Culture

An organ culture method, used successfully in previous research into corneal wound healing (Foreman et al. 1996; Carrington et al. 2006; Kamma-Lorger et al. 2009; Dooley et al. 2012; Morgan, et al. 2014) in bovine and ovine eyes, was used to create an *ex vivo* model of wound healing with an air interface, representative of that *in vivo.* This organ culture protocol was based on the protocol outlined by Carrington et al., 2006.

A highly important aspect of organ culture is to maintain as sterile an environment as possible to avoid contamination and infection by bacteria and fungi. The class II biological safety cabinet (BSC) and the incubator were thoroughly cleaned 24 hours in advance with 1% Virkon solution followed immediately by Microsol, and then 70% IMS on the day of culture. All items introduced into the cabinet were sprayed liberally with 70% IMS. Nitrile gloves and a culture lab coat were worn at all times and gloved hands and arms were sprayed with 70% IMS before beginning, and repeated as necessary during the process.

2.3.1. Preparation of Solutions

A number of solutions were prepared in advance and autoclaved before use (see Appendix I for full preparation methods). These included sterile phosphate buffer saline (PBS) pH 7.4, 500ml DMEM organ culture media, agar/gelatin support matrix (Invitrogen, UK), 300ml of 7.4% NaHCO3, pre-prepared stock antibiotic solution. Where appropriate, autoclaving was performed at 120°C for 40 minutes. 1L PBS was prepared by adding PBS pH 7.4 tablets (Sigma, UK) to double distilled water (ddH_2O). A 1% agar (Sigma, UK)/1% gelatin (Sigma, UK) solution/gel was prepared by dissolving 2g agar and 2g gelatin in 200ml of ddH_2O, then autoclaved in a 300ml dewar bottle.

A 7.4% sodium bicarbonate ($NaHCO_3$) solution was prepared in a flask by stirring 22.2g of $NaHCO_3$ in 300mls of ddH_2O. Once dissolved this was then stored at room temperature in a 300ml dewar. Stock antibiotic solution, required for both the agar/gelatin support matrix and the DMEM media solution, was prepared by dissolving 500mg streptomycin sulphate (Sigma, UK), 500mg of kanamycin, 300mg penicillin and 730mg L-glutamine in 50ml ddH_2O. The solution was then filtered, through a 0.2µm filter, in 10ml aliquots into bijoux. Aliquots were stored in the freezer until needed.

The agar/gelatin support solution matrix and the DMEM media for the culture were prepared in the culture cabinet in advance. The 200ml 1% agar/1% gelatin stock solution was heated in a microwave at 5 second intervals on low power until liquefied, and then, along with the following items, sprayed with 70% IMS, before introduction into the class II BSC; fungizone™ (Invitrogen, UK), 10ml stripettes, 2ml syringes, 60ml sterile pots and 0.2µm filters. The final support matrix was prepared by filtering 20ml of DMEM media, 10ml of 7.4% $NaHCO_3$ and 2ml of both the 250 µg/ml amphotericin B (Gibco™ Amphotericin B 15290026, Invitrogen, UK) and stock antibiotic solution into the 1% agar/1% gelatin solution (using the 0.2µm filters). This was then decanted into sterile 60ml pots and stored in the fridge until needed.

Organ culture DMEM (21969035, Invitrogen, UK) media was prepared by filtering 5ml of stock antibiotic solution and 5ml of amphotericin B into the 500ml media bottle. This was stored in the fridge until the day of use.

2.3.2. Materials

All required instruments and solutions, detailed in Table 2.1, were sprayed liberally with 70% IMS and introduced into the BS cabinet.

	Pre-packed Sterile	Autoclaved		Prepared Sterile
Instruments	· Individually wrapped pasteur pippettes · Petri Dishes · Microtome pump tubing · 10ml Stripettes	· 3x 250ml Beakers (Foil Covered) · 1x 1L Beaker (Foil Covered) · Razor Blades · Universal Lids · Foil	· 2x Dissection Packs (2x Forceps, 1x Scissors) · Microkeratome Blades · Microkeratome Head Parts · Eyeball Stand · Tip Boxes	-
Solutions	-	· 1L PBS		· DMEM culture Media · Agar Gelatin Support Matrix · 100% IMS

Table 2.1 Materials required for organ culture

When the workspace inside the BS cabinet was arranged and the microkeratome made ready to use, the 60ml pots containing the decontaminated porcine eyes (see section 2.1.1) were also introduced into the BS cabinet.

2.4 Organ culture of porcine corneas

After the LASIK-like flap wound was created in each cornea using a microkeratome (Hansatome, Bausch & Lomb, Germany) as previously described in section 2.2, the wounded corneo-scleral discs were dissected from the globes by cutting circumferentially 3-4mm below the corneal limbus using razor blades and dissection scissors. Taking care not to disturb the wound, the iris and lens were peeled away using forceps and disposed into the waste beaker with the posterior globe. In preparation for the agar support, and to ensure corneas did not dry out whilst the process was repeated with 3 subsequent eyes, each cornea was placed inverted into the plastic lid of an autoclaved universal tube lid, rinsed and filled with Media.

To avoid contamination as much as possible, the eyes were wounded in batches of 4. Additionally, the microkeratome blade was changed every 2 eyes and the instrument head cleaned with 70% IMS and rinsed with PBS between each wounding. The instrument set (including the disposable razor blade) was changed between each dissection with the unused instrument set stored in a beaker of 70% IMS in between uses (each instrument was rinsed in PBS before use). The 70% IMS and PBS were changed out every 8 eyeballs.

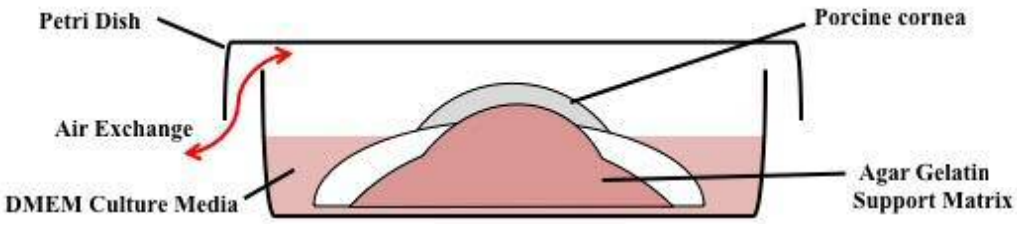

Figure 2.3. Diagram of organ culture model showing the air interface.

Agar/gelatin corneal support matrix was pipetted into the corneal cavity until filled to the scleral rim (approximately 2ml) and allowed to set for a few minutes. Sterile petri dishes were labelled with the appropriate initials, date and experimental details. Once the agar/gelatin support matrix had set, each cornea was placed into its appropriately labelled sterile petri dish, with the epithelial surface uppermost, ensuring all the flaps on the LASIK-

like wounded corneas were in place and unwrinkled. The flap was carefully lifted using a disposable pipette tip and 10µl DMEM culture media was pipetted onto the stromal bed of the LASIK-like wound, close to the hinge to aid even distribution as the flap was carefully replaced using a pipette tip, with great care so as not to damage either the corneal epithelium or the stroma. Using a stripette, 5ml of the DMEM culture media was added to each petri dish (starting with a few drops to the corneal surface) (figure 2.3). The petri-dishes were then transferred to the incubator at 37^{o}C, 95% O_2/5% CO_2.

In order to keep the corneas hydrated and nourished over the culture time period of 1-4 weeks, media was removed and replaced in the petri dishes, and a few drops of fresh organ culture DMEM media solution were applied to the corneal surface once every 1-2 days.

For characterisation of the porcine organ culture model, 4 corneas were cultured at each of 0, 1, 2, 3 and 4 week time points. For the 0 week time point the eyes were wounded, treated and processed (for transparency and/or histology) within 30 minutes of wounding. Due to the practicalities of organ culture and the capacity of the incubator the corneas were cultured in batches containing 2-3 corneas (to avoid batch bias) for each time point and group in a rolling culture to achieve the numbers required.

2.5 Culture and application of Oral Mucosa Lamina Propria Progenitor Cells (OMLP-PCs) to LASIK-like wounds

2.5.1. Source of cells

Oral Mucosa Lamina Propria Progenitor cells (see chapter 1) were provided by the wound biology group at Cardiff School of Dentistry. Normal, disease-free buccal mucosa biopsies were obtained from consented patients undergoing routine dental procedures. Local ethical committee approval had been previously obtained for the study and donors were informed in accordance with the Helsinki convention (Davies et al., 2010). OMLP-PCs were isolated

(as described by Davies et al., 2010), counted and their viability determined using trypan blue exclusion (1:1 dilution of cell suspension in 0.4% Trypan blue). The cell lines of 3 different patients were transported to the School of Optometry and Vision Sciences on dry ice, having been previously frozen in 9:1 Fetal Calf Serum (FCS):dimethyl sulfoxide (DMSO) freezing media. On delivery they were placed immediately into a liquid nitrogen cell storage dewar. Three different cell populations acquired from different participants were provided.

2.5.2. Cell Culture

i. Media and solutions

Prior to commencing the cell culture, culture media solution was prepared (see Appendix I for more detailed methods of solution preparation). Complete culture media was made up in a class II culture cabinet by adding 5ml of 200mM L-glutamine (Life Technologies, UK) and 5 ml 100X Antibiotic/Antimycotic mix (Life Technologies, UK) to 500ml of DMEM (Life Technologies, UK). This solution was stored for up to a month at 4°C. For cell feeding, 10% heat-inactivated fetal calf serum (FCS; Life Technologies, UK) was added to media to provide 10% DMEM. This complete media was stored for up to 1 week at 4°C.

ii. Thawing Oral Mucosal Fibroblasts and OMLP-PC's

The cells were thawed rapidly by agitation in a 37°C water bath. In a culture cabinet the cell suspension was transferred into 5ml of complete culture media (see above) and spun down in a centrifuge at 1500 RPM and 4°C for 5 minutes to remove the freezing medium. The supernatant was discarded into a 50ml waste tube and the cell pellet was re-suspended in 5ml fresh media by scratching the bottom of the flask against the tip box. Complete media was added to the 15ml centrifuge tube to make it up to 5ml and the cells were spun down once more at 1500 RPM 4°C for 5 minutes and the supernatant discarded into the waste tube. The cell pellet was re-suspended in 1ml of complete media, and an aliquot removed for counting (see below). Once counted the cells were seeded at $2x10^3$ cells cm^{-2} into a T75 flask.

iii. Cell Counting

To count viable cells, 10µl of 0.4% trypan blue (Sigma, UK) was pipetted into a well plate and, using a fresh tip, 10µl of the cell suspension was added to the trypan blue to create a 1:1 suspension. This solution was then pipetted up and down gently to ensure mixing and 10µl was then pipetted into a haemocytometer.

To count viable cells, 10µl of 0.4% trypan blue (Sigma, UK) was pipetted into a well plate and, using a fresh tip, 10µl of the cell suspension was added to the trypan blue to create a 1:1 suspension. This solution was then pipetted up and down gently to ensure mixing and 10µl was then pipetted into a haemocytometer. The haemocytometer was then placed on the stage of a Leica inverted microscope (Leica IX70, Germany) and the numbers of viable cells (those that had not taken up the trypan blue) were counted. This has a grid of 5x5 squares of 1/25 sq mm^2 and 4 x 4 squares of 1/400mm^2. An average cell number was calculated and represented the cell count for 10µl. To calculate the number of cells in 1ml this number was multiplied by 100.

iv. Passaging of the OMLP-PCs

OMLP-PCs were seeded at a density of $2x10^3$ cells cm-2 per cm2 i.e. 1.5 x 10^5 cells in a T75 flask. To the T75 flask, 12ml of complete media was pipetted in and the appropriate amount of the cell suspension required to reach the seeding density was added. Once the lid was replaced the T75 flask was gently swirled to ensure an even distribution and the flask was placed into an incubator at 37˚C and 5% CO_2. The cells were monitored on the inverted microscope (Leica IX70, Germany) and the media replaced every 3-4 days.

Once cells had reached 90% confluent, the cell culture media was removed from the flask and the cells were washed liberally with 10ml sterile PBS (Invitrogen, UK). The PBS was swirled gently around the flask to ensure washing of the complete surface area, as complete removal of the serum is essential before addition of trypsin. PBS was removed and 2ml of 0.05%Trypsin/0.53mM EDTA (Life Technologies, UK) was added and swirled over the

cells to ensure complete coverage before being replaced into the 37˚C/5% CO_2 for 5 minutes (no longer due to the toxic effect on the cells). The side of the flask was tapped gently to encourage detachment of the cells, and the cells were viewed under the Leica Light Microscope to confirm they had rounded up and were free floating. A 2x volume of complete media (FCS inactivates the trypsin) was added to the flask (4ml for the T75) and the cell suspension trypsin/media mix was pipetted out into a centrifuge tube and spun at 1500RPM for 5 minutes.

The supernatant was then removed and the cell pellet re-suspended by scratching the bottom of the tube against the tip rack. This re-suspended pellet was made up to a volume of 1ml by the addition of complete media and the cells counted as previously described. Cells were re-seeded at a cell density of $1.5x10^5$ cells/cm^2.

The remaining cells were frozen down by suspending the cells in 90% complete media/10% DMSO solution (prepared in advance in a class II culture cabinet and stored at 4°C). The suspension was then pipetted into a 1ml cryo-vial, which was appropriately labeled and placed into a Mr. Frosty^{TM} freezing container (Thermoscientific, UK) and stored for 24hrs at -80°C. The vial was then transferred to a liquid nitrogen cell storage dewar until needed.

iv. Application of Cells to Wounded Cornea

10µl of OMLP-PC cell suspension at appropriate cell concentration was applied to the wound bed. For determination of optimal cell concentration $1.5x10^4$, $1.5x10^5$ and $1.5x10^6$ cells ml^{-1} were applied to wounded corneas (n=3). Next, once the optimal cell concentration was determined, this cell concentration was applied to n=4 corneas for each of the three different donor cell lines at each time point.

2.6 Tissue Preparation for wax and cryoembedding

To ensure that each section obtained would have an entire flap (consisting of flap edge, center and hinge) across the cornea, the hinge of the LASIK-like wound on the porcine corneas was visualised and the cornea cut, using a scalpel blade, straight across the middle, endothelium up, to bisect the flap hinge (see figure 2.4). One half was fixed in 4% PFA for wax embedding, the second half was snap frozen as described below.

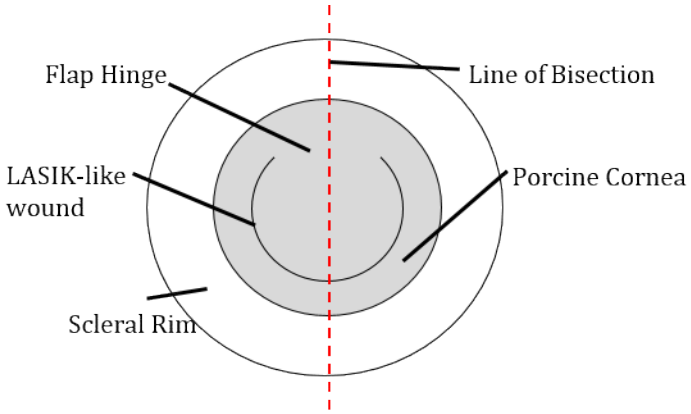

Figure 2.4 Diagram showing bisection (red line) of LASIK-like wounded organ cultured porcine cornea.

2.6.1 Snap Freezing

Foil moulds were created by forming the foil around the base of a 5ml sample pot, which were then labelled with date, name and sample type. These moulds were then filled with cryoembedding media (RA Lamb, UK). Isopentane (Fisher, UK) was placed in a beaker and cooled by placing the beaker into a Styrofoam box of liquid nitrogen. Each bisected corneal sample was then briefly immersed in isopentane to freeze, before being placed, cutting edge (i.e. bisect edge) down, into the mould (figure 2.5). Then the mould was held in the isopentane using forceps until the embedding media had frozen completely and the sample was then transferred to a -20°C freezer until day of cryosectioning. If long term, samples were stored in a -80°C freezer.

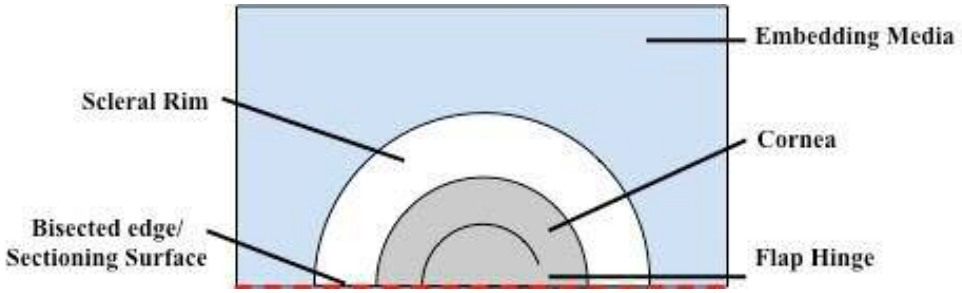

Figure 2.5 Diagram of embedding orientation

2.6.2 Wax Embedding

The bisected corneal samples were fixed by carefully, so as not to dislodge the flap, placing the sample in 4% PFA within a 5ml bijou, and stored at 4°C for at least 24 hours before processing.

The corneal samples were labelled using pencil on paper strips. Each sample was then immersed in 50% IMS (Fisher, UK) (vol/vol with dH20) for 30 minutes, this was then poured off and replaced with 70% IMS for 1 hour after which the 70% was replaced with 90% IMS for at least 1 hour (it could also be left overnight at this juncture). The 90% IMS was then replaced with 100% IMS for 1 hour, followed by a final 30 minutes in fresh 100% IMS. The samples were transferred to glass vials and moved to a fume cupboard where the 100% IMS was discarded and replaced with a 50% vol/vol mixture of IMS and chloroform (Fisher, UK) for 30 minutes followed by 100% chloroform for 30 minutes. The chloroform was replaced with a final 100% chloroform immersion for a further 30 minutes after all but a little chloroform was poured off and the vials placed on top of the wax oven to warm for 10 minutes.

The samples were blotted on filter paper and placed in fresh vials filled with molten wax and transferred to an oven (Thermofisher, UK) for 1 hour at 63°C. The sample was then transferred to a fresh glass vial full of molten wax and placed in the oven for another 30 minutes. During this time a wax block mould was partially filled with molten wax to cover

the base and placed on a refrigerated base (RA Lamb, UK) at -12°C to part solidify. The tissue samples were then placed onto the solidified wax with the bisected surface down, an embedding ring was placed on top of the wax mould, trapping the paper specimen label, and filled with molten wax to the top. This was then allowed to completely solidify and then placed in a 4°C fridge until sectioning.

2.7 Sectioning

2.7.1. Wax Sectioning

Using a razor blade (Fisher Scientific, UK), the wax block was trimmed around the corneal sample. The wax block was then clamped into the microtome chuck (after ensuring the blade guards were in place and the wheel locked) in an orientation such that the hinge of the flap in the section was inferior most. Using a Feather® s35 microtome blade (PMF medical, UK) the wax block was trimmed until sample to be cut was observed, then 7µm thick sections were cut on a microtome MICROM HM 325 (Thermo Scientific, UK). Ribbons of wax sections were transferred to cardboard folders.

Three porcine cornea wax sections were cut from a ribbon using a razor blade and floated out in a cold-water bath. The sections were then picked up using a glass slide and transferred to a hot water bath set at 42-45°C to flatten and free of bubbles. The sections were floated onto a HistoBond® slide (RA Lamb, UK), and placed onto a heated platform for 30 minutes, then placed in a 56°C oven (GenLab, UK) overnight.

2.7.2. Cryosectioning

The cryostat chamber and sample holder was set to -20°C. The snap frozen sample was trimmed with a razor blade and mounted on a metal chuck using a small amount of freezing medium, then placed in the cryostat to set.

An MX35 blade (Thermo Scientific) was placed into the blade holder and the platform was securely fastened into the sample holder, which was moved forward as close as possible to the blade. The block was trimmed, by turning the handle, until the sample was visible. 10µm sections were cut and carefully rolled out using a fine paintbrush, then picked up onto a Superfrost Plus Slide (Thermo Scientific, UK); placing 3 sections per slide. The slides were labelled and sections were air dried for 30 minutes, then transferred to a -20°C freezer until needed.

2.8 Histological Analysis

2.8.1. Morphology: H&E Staining

i. Wax sections

Harris hematoxylin and 1% aqueous eosin were decanted into two separate staining dishes. The prepared porcine cornea wax sections were immersed in xylene twice, for 5 minutes each time. Following this the sections were taken to water, through decreasing concentrations of IMS; 100% for 5 minutes, 100% for 3 minutes, 90% for 2 minutes, 70% for 20 seconds and 50% for 20 seconds. The slides were then immersed in gently running tap water for 3 minutes before being immersed in Harris' hematoxylin for 4 minutes. After this the slides were washed in running tap water for 2 minutes, followed by an immersion in the 1% aqueous eosin for 5 minutes. The slides were briefly rinsed in tap water once more before being taken back up through decreasing IMS concentrations, briefly dipped in each before a final two immersions in xylene for 2 minutes each. The slides were mounted in DPX (RA Lamb 03703596) and left to dry overnight.

ii. Cryosections

The prepared cryosections were brought to room temperature and subjected to three 5 minute PBS washes. They were then placed directly into the Harris hematoxylin for 5 minutes followed by a rinse in gently running tap water for 3 minutes. The sections were then placed into the eosin for 3 minutes, then washed briefly in running tap water. Sections

were then dipped in increasing concentrations of IMS before being mounted in DPX and allowed to dry overnight.

2.8.2. Keratocyte Activation and transformation: α-sma Immunofluorescence

Cryosections were brought to room temperature and a water immiscible outline was drawn around each section using a PAP pen. PBS was applied gently to each section for three 10 minute washes. 60µl of primary antibody solution, mouse monoclonal anti-α-smooth muscle actin (A2547 Clone 1A4, Sigma, UK) diluted 1 in 100 in PBS was applied to each section. For a negative control solution, monoclonal mouse anti-green fluorescent protein (GFP) antibody (Sigma, UK) was prepared at the same dilution, and applied to control sections (figure 2.6).

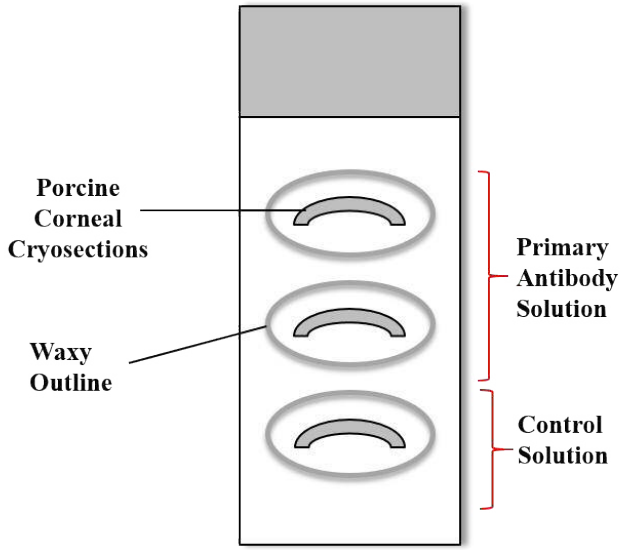

Figure 2.6 Cryosection slide for α-sma immunofluorescence

These cryosections were incubated in primary antibody solutions for 2 hours in a sealed humidity chamber, after which time the excess antibody solution was gently poured off and the slides were subjected to 3 PBS washes for 10 minutes each. During the PBS washes, the secondary antibody solution was prepared.

Secondary antibody, donkey anti-mouse IgG (H+L) Alexa Fluor®488 (Invitrogen, UK) at a 1 in 1000 dilution in PBS, containing 2µl (for every ml of secondary antibody solution) of 1mg/ml Hoechst 33342 stock solution was added to all sections, which were then sealed in a humidity chamber for 2 hours.

After this, three 5 minute PBS washes were applied to the slides and the samples were mounted in Hydromount (BDH, UK), covered in foil to maintain the signal, and stored at 4°C until the day of imaging.

The sections were imaged using a Leica DM6000 flouorescent Micropscope (Leica, Germany). A 100µm square was drawn onto the image in Image J software and the total number of cells (those exhibiting a blue Hoechst signal stain of the nucleus) were counted within the square. The cells that were labeled with a green fluorescent signal from the α-sma immunolabelling, were also counted and percentage myofibroblasts was determined using the following equation (equation 2.1).

$$\frac{\textbf{Total Cells with Green Signal (α-Sma)}}{\textbf{Total Cells with Blue Signal (Hoechst Stained Nuclei)}} \textbf{ X 100}$$

Equation 2.1 Equation to determine percentage of myofibroblasts.

This was performed on 3 adjacent 100 µm squares at each region of interest (flap edge, mid-flap and hinge) above and below the wound (18 squares per section) for each time point.

2.8.3. Cell Proliferation; PCNA immunofluorescence

Cryosections were brought to room temperature and a water immiscible outline was drawn around each section using a PAP pen. PBS was applied gently to each section for three 10 washes minutes. 60µl of primary antibody solution, rabbit polyclonal anti-PCNA (Proliferating Cell Nuclear Antigen) antibody (ab18197, Abcam, UK) diluted 1 in 100 in PBS was applied to each section. These cryosections were incubated in primary antibody solutions for 2 hours in a sealed humidity chamber, after which time the excess antibody solution was gently poured off and the slides were subjected to 3 PBS washes for 10 minutes each. During the PBS washes the secondary antibody solution was prepared.

Secondary antibody, Donkey Anti-Rabbit IgG H&L Alexa Fluor® 555 (Abcam, UK) at a 1 in 1000 dilution in PBS, containing 2µl (for each 1ml of secondary antibody solution) of 1mg/ml Hoechst 33342 stock solution was added to all sections, which were then sealed in a humidity chamber for 2 hours.

After this, three 5 minute PBS washes were applied to the slides and the samples were mounted in Hydromount (BDH, UK), covered in foil to maintain the signal, and stored at 4°C until day of imaging.

The sections were imaged using a Leica DM6000 fluorescent Micropscope (Leica, Germany). A 100µm square was drawn onto the image in Image J software and the total number of cells (those exhibiting a blue Hoechst signal stain of the nucleus) were counted within the square. The cells producing a green fluorescent signal from the α-sma were also counted and the percentage cell proliferation was determined using the following equation (equation 2.2).

$$\frac{\text{Total number of cells with Red Signal (PCNA)}}{\text{Total number of cells with Blue Signal (Hoechst Stained Nuclei)}} \text{ X } 100$$

Equation 2.2 Equation to determine percentage cell proliferation.

This was performed on 3 adjacent 100 μm squares at each region of interest (flap edge, mid-flap and hinge) above and below the wound (18 squares per section) for each time point.

2.8.4. Cell Apoptosis; TUNEL and Caspase-3 immunofluoresence

TUNEL

A terminal deoxynucleotidyl transferase-dUTP nick end labeling (TUNEL) assay (Click-iT™ Plus TUNEL Assay, C10617, Invitrogen, UK) was attempted to determine apoptosis. Working solutions of 1X Click-iT™ Plus TUNEL Supermix, Click-iT™ TUNEL Reaction Buffer Additive and 1X Proteinase K Solution were prepared in advance and stored appropriately (see appendix). Cryosections were brought to room temperature and PBS applied to each section for three 10 minute washes. The sections were then fixed in 4% paraformaldehyde for 15 minutes at 37°C followed by 2 applications of PBS for 5 minutes each.

Sections were incubated in 60μl of Proteinase K solution for varying amounts of time (see optimisation) followed by a 5 minute wash in PBS, a further 5 minutes in 4% paraformaldehyde at 37°C and a final rinse in deionized water.

Sufficient quantity of TdT Reaction buffer was added to each slide to allow the solution to spread and cover the samples completely. The slides were incubated for 10 minutes at 37°C whilst the TdT reaction mixture was prepared (see appendix). After removal of the TdT

reaction buffer, 50µl of the prepared TdT reaction mixture was added to each section and incubated for 60 minutes at 37°C. Upon removal the slides were rinsed with deionized water and washed with 3% BSA and 0.1% Triton™ X100 in PBS for 5minutes before a final rinse in PBS.

A Click-iT™ Plus TUNEL Reaction Cocktail was prepared (see appendix) and 50µl applied to each section before an incubation of 30 minutes at 37°C, followed by a 5 minute rinse in 3% BSA in PBS and a final rinse in PBS.

A 50µl of 1mg/ml solution of Hoechst 33342 was added to each section for 15minutes at room temperature before removal and three 5 minute washes in PBS. The slides where then mounted in Hydromount (BDH, UK), covered in foil to maintain the signal, and stored at 4°C until the day of imaging.

TUNEL Optimisation

The initial attempt at TUNEL assay on the samples resulted in indiscriminate immunolabelling of all cells in the corneal samples, therefore optimisation was attempted as outlined in figure 2.7.

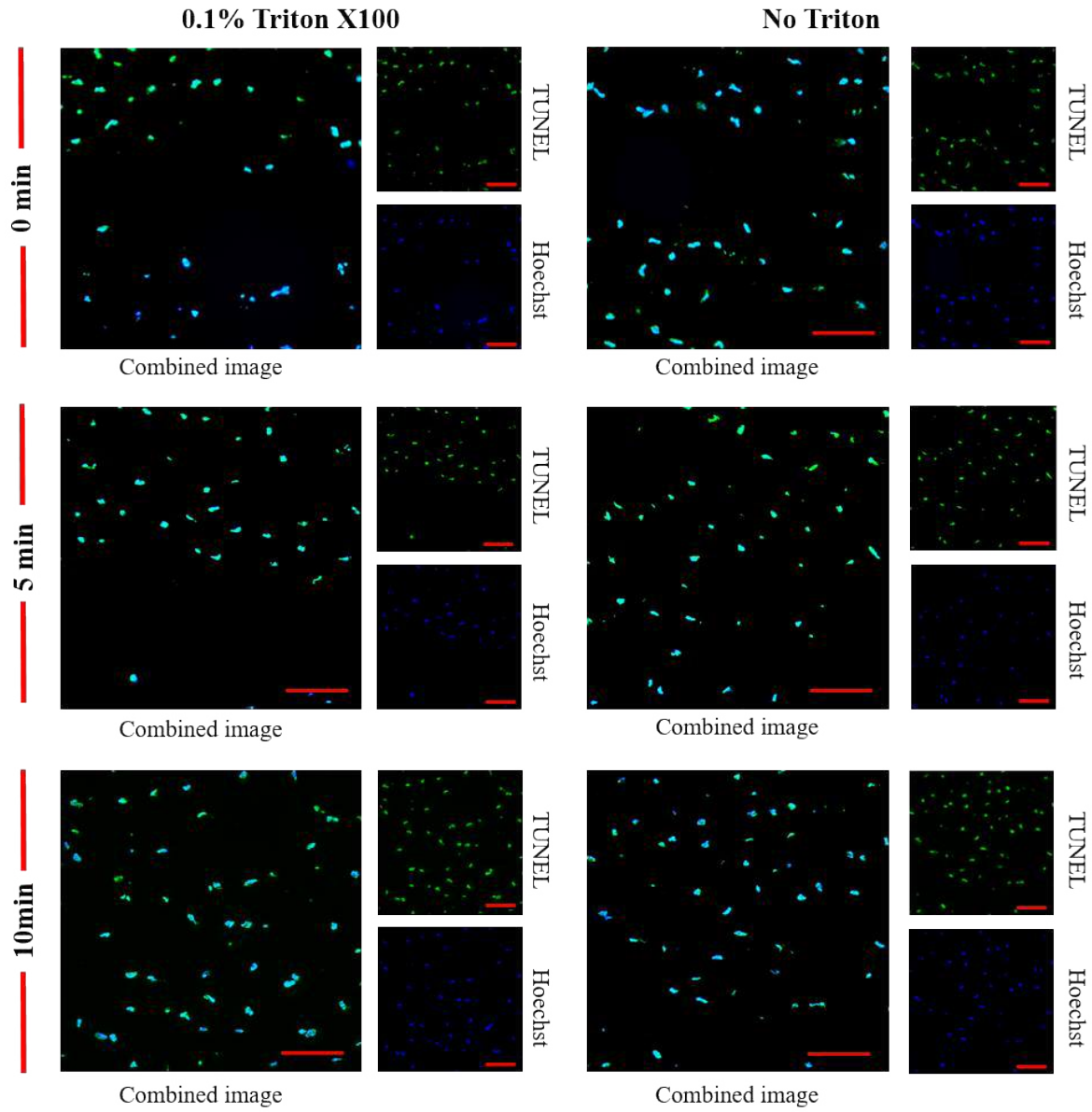

Figure 2.7 TUNEL Assay Optimisation images demonstrating the period of time incubated with proteinase K and the application of 0.1% Triton X100 of LASIK-like untreated wounded corneas after 1 week in organ culture. The results show Hoeschst labelling of cell nuclei (Blue) an indiscriminate immunolabelling of TUNEL positive cells (Green). This demonstrates a failure of the TUNEL protocol. Scale bars represent 100µm

The TUNEL assay on these sections failed, despite optimisation attempts, and so apoptosis was detected by immunolabelling for caspase-3.

Caspase-3

Cryosections were brought to room temperature and a water immiscible outline was drawn around each section using a PAP pen. PBS was applied gently to each section for three 10 washes minutes. The sections were incubated in 0.1% Triton-X100 for 10 minutes, followed by three 5 minute PBS washes. 60µl of primary antibody solution, rabbit polyclonal anti-active Caspase-3 (ab49822, Abcam, UK) diluted 1 in 500 in PBS was applied to each section. For a positive control an apoptosis positive slide of 4-day post-weaning rat mammary gland was used (ApopTag® Positive control slide, S7115, Sigma, UK).

These cryosections were incubated in primary antibody solutions for 2 hours in a sealed humidity chamber, after which time the excess antibody solution was gently poured off and the slides were subjected to 3 PBS washes for 10 minutes each. During the PBS washes, the secondary antibody solution was prepared.

Secondary antibody, donkey anti-rabbit IgG H&L Alexa Fluor® 555 (Abcam, UK) at a 1 in 1000 dilution in PBS, containing 2µl (for every ml of secondary antibody solution) of 1mg/ml Hoechst 33342 stock solution was added to all sections, which were then sealed in a humidity chamber for 2 hours.

After this, three 5 minute PBS washes were applied to the slides and the samples were mounted in Hydromount (BDH, UK), covered in foil to maintain the signal, and stored at 4°C until the day of imaging.

The sections were imaged using a Leica DM6000 flouorescent Micropscope (Leica, Germany). A 100µm square was drawn onto the image in Image J software and the total number of cells (those exhibiting a blue Hoechst signal stain of the nucleus) were counted

within the square. The cells that were labeled with a red fluorescent signal from the Caspase-3 immunolabelling, were also counted and percentage of apoptotic cells was determined using the following equation (equation 2.3).

$$\frac{\textbf{Total Cells with Red Signal (Caspase-3)}}{\textbf{Total Cells with Blue Signal (Hoechst Stained Nuclei)}} \textbf{ X 100}$$

Equation 2.3 Equation to determine percentage of apoptotic cells.

This was performed on 3 adjacent 100 μm squares at each region of interest (flap edge, mid-flap and hinge) above and below the wound (18 squares per section) for each time point.

2.9 Transmission Electron Microscopy

Transmission electron microscopy (TEM) was used to observe the corneal ultrastructure up to x100 000 magnification. Corneas were removed from organ culture and fixed in a 2.5% glutaraldehyde solution overnight. They were then rinsed twice in 0.1M cacodylate buffer pH7.4 at room temperature for 10 minutes each, before storing at 4°C until needed (see appendix for solution preparation).

The samples were dissected under a light microscope with a razor into tissue blocks, isolating the wound edges of the trephine and LASIK-like wounded corneas, keeping the flap intact and on the stromal bed. These tissue blocks were placed into glass vials appropriately labelled and then placed into 1% osmium tetroxide in 0.1M cacodylate buffer for 1 hour, after which they were rinsed in distilled water (dH_2O) three times for five minutes each. After the last rinse, 0.5% aqueous uranyl acetate was decanted into the glass vials and the tissue blocks were stored in this for one hour.

The samples were then dehydrated through increasing concentrations of ethanol solution (70%, 90% and 100% twice) for 15 minutes each. After the last ethanol change, the samples were immersed in propylene oxide for 15 minutes twice. Finally, the vials were drained and samples immersed in 1:1 mixture of propylene oxide and araldite resin for 1 hour.

The tissue blocks were infiltrated with araldite resin in glass vials placed in a rotator within a fume cupboard. This resin was changed thrice, approximately every 2 hours before being left to infiltrate. A further three changes of resin were repeated again, every 2hours. The samples were placed into moulds, filled with fresh araldite resin and placed in a 60°C oven for 24hrs, thus creating resin blocks for sectioning. Each sample was labelled appropriately and great care was taken to orientate the samples correctly so that when they were sectioned and placed on the electron microscope the desired location was imaged.

A Leica UC6 ultramicrotome (Leica, Germany) was used to cut ultrathin sections (~90nm thick) using a glass knife made using a Leica EMKMR2 knifemaker (Leica, Germany) (figure 2.8). Once the sections were lifted and placed on grids, they were examined and imaged using a Jeol 1010 transmission electron microscope (Jeol, USA).

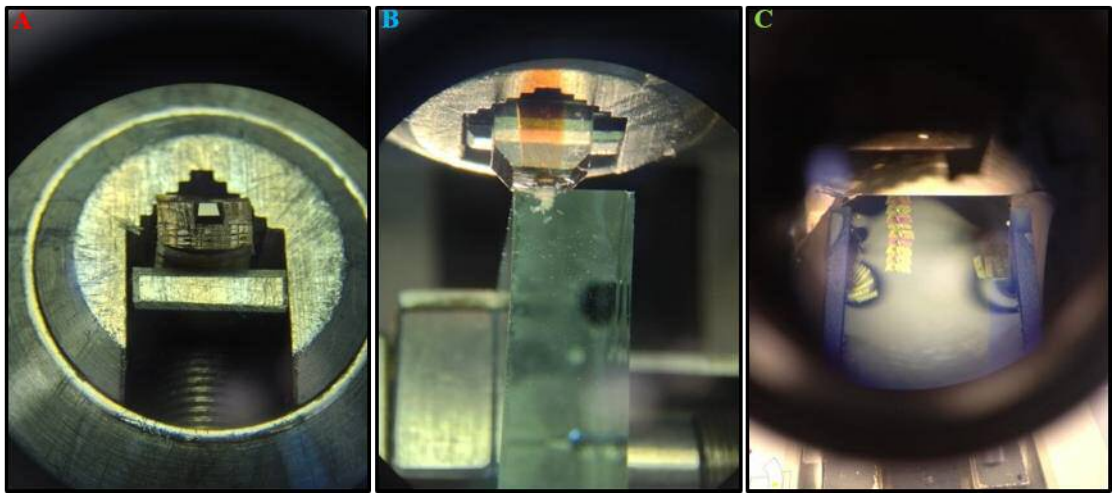

Figure 2.8. TEM Sectioning - A- Polished resin block sample prior to sectioning. B- Sectioning with glass knife. C- Ribbon of ultrathin sections

2.10 Extensometry

The corneas were loaded into the Barons Artificial chamber (figure 2.9). This chamber allowed a pressure to be introduced into the system via injection of PBS into a valve, to mimic intraocular pressure, as well as a support to orientate the cornea in a vertical position.

Figure 2.9. Barons Artificial Anterior Chamber. (www.bpic.com accessed 2013)

The PBS was injected into the chamber with care, until the cornea adopted the normal domed shape and the valve was clipped shut. The chamber was then attached to a vertical support, fixed to the bottom chuck of the extensometer (figure 2.10), ensuring that the hinge of the LASIK-like flap was in the superior position. Attached to the vertical chuck, a clamp, lined in sandpaper to provide grip and friction, held a stiff strip of card, the end of which had an area of 5x5mm that was glued (with a thin layer of superglue) to the centre of the corneal flap (figure 2.11).

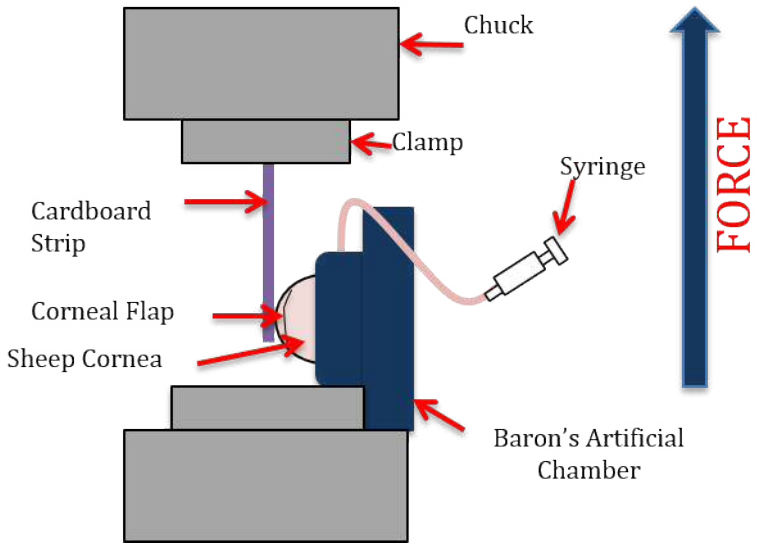

Figure 2.10. Diagram of extensometer set up to measure vertical shear.

The extensometer slowly pulled the cardboard strip upwards at a set rate and force, creating a direct shear effect. The programme was set to the following parameters (table 2.2);

Nexygen Parameters	
Preload	0.20N
Speed	1.50mm/min
Gauge Length	N/A
Area	5mm x 5mm
Break	Load Drops to 10%

Table 2.2. Nexygen 4.1 programme parameters for pull to break testing

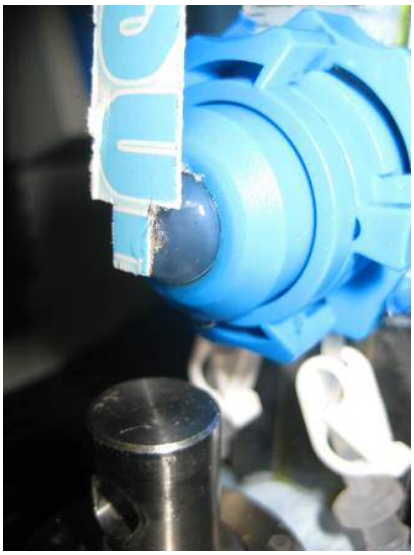

Figure 2.11. Image of cornea loaded into Barons Artificial Chamber before pull to break cycle is started.

The stress and strain forces on the corneal flap were recorded by the extensometer, controlled by the Nexygen 4.1 user interface software (Lloyd Instruments, Bognor Regis, UK). A graph of force versus time was automatically produced by the software. The dehiscence/break point of the LASIK-like wound can be determined by a sharp drop in force (seen on the realtime data plotted on the graph by Nexygen software), but was also monitored by eye. Time to flap detachment was recorded and compared to the data collected by the software.

2.11 Transparency Measurements

2.11.1. Spectrophotometry

Spectrophotometry quantitatively measures the ability of a material to transmit light as a function of wavelength. The spectrophotometer, in this study, generated a 1mm beam of light at a given wavelength that passed through a sample and the amount of light transmitted through the sample was measured via a detector.

An SP8-100 UV/VIS spectrophotometer (PYE Unicam ltd) was switched on at least one hour before use, to warm up. Ensuring no sample or cuvette was in its path, the transmission was measured at 100% (by altering the zero dial). A cuvette was filled with silicon oil (Dow Corning, UK) and placed in the beam path (figure 2.12). Starting at 400nm the transmission % was recorded at 10nm intervals up to 700nm. This provided a "blank" measurement used to normalise the data.

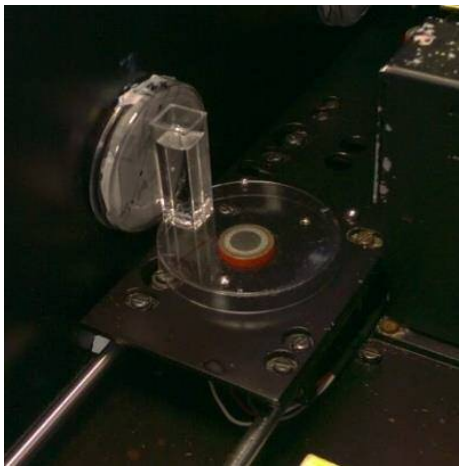

Figure 2.12 Silicone oil filled cuvette placed in beam line

A porcine corneal sample was placed in the custom-made sample holder (figure 2.13 A). Syringing through valves, containing 5 mm stoppers (SGE Analytical Science, Australia), silicon oil was added to both the anterior and posterior chamber of the sample holder to

reduce the scattering of light. The prepared sample holder with the porcine cornea sample was then placed into the spectrophotometer (figure 2.13 B) and the % transmission was recorded at 10nm intervals from 400 to 700nm. These measurements were repeated 3 times for each corneal sample and the blank measurement of silicon oil was performed between each sample to ensure stability in the reading.

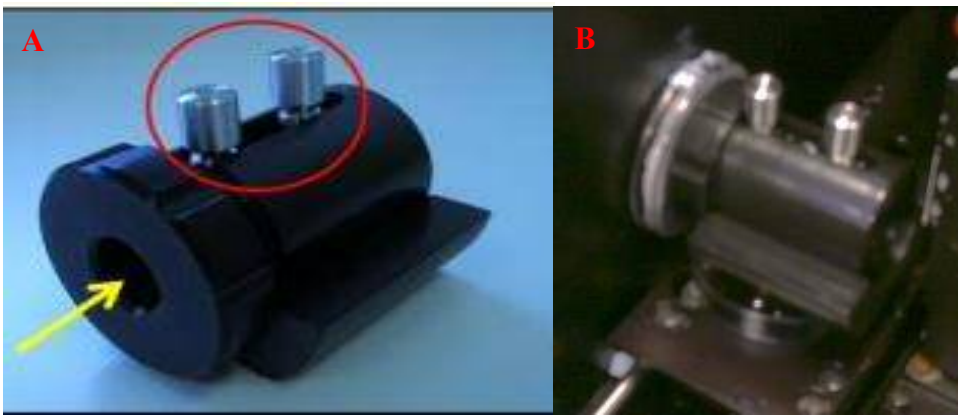

Figure 2.13 A Custom-made corneal sample holder. Yellow arrow indicates passage of light beam. B Sample holder placed in beam line.

The data, once collected, was normalised against the blank reading of the silicon oil and statistical analysis was performed.

2.11.2. Visual Transparency Assessment

The use of spectrophotometry, although useful in the provision of detailed data on the transmission of different wavelengths through the wounded organ cultured cornea, destroys the sample as it becomes irreversibly coated in silicon oil and damaged by the sample holder. In order for transparency and cellular/collagen to be analysed in the same sample, an alternative measure of transparency was required.

Once removed from organ culture, but before fixation or cryoembedding, each cornea was photographed, epithelium down, at a fixed distance and illumination, over a page of graph paper. The same sample was then moved to a dissecting microscope (Leica, UK) and imaged.

These images were arranged in random tiled order and presented to 10 different individuals, who were shown the grading scale as a guide, and then assigned a level of clarity to each image (figure 2.14). This method was successfully employed in previous research by Kamma-Lorger et al. (2009) and Dooley et al. (2012).

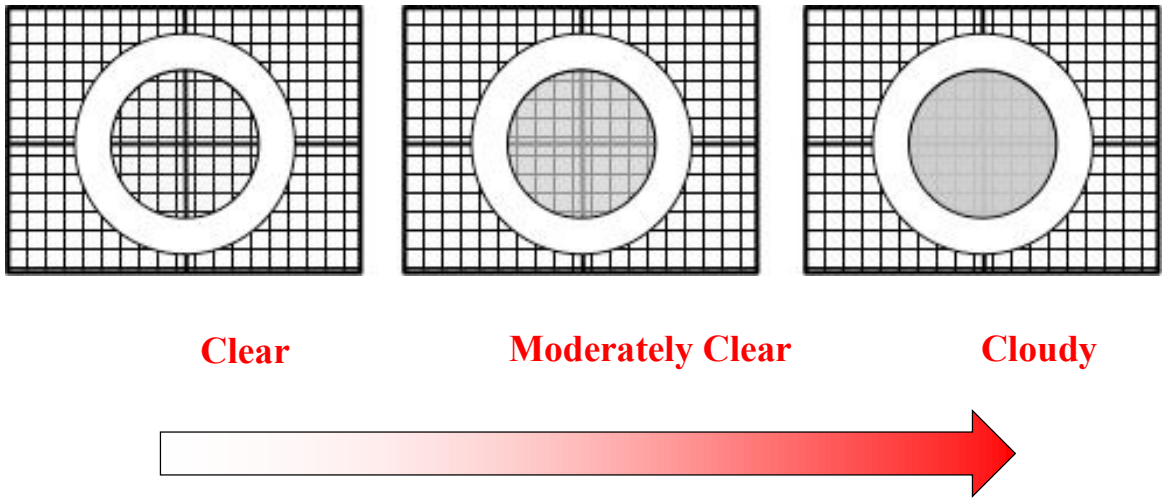

Figure 2.14 Demonstration of visual grading of cornea transparency

Data were collected for n=3 corneas at each time point for each treatment and each level of clarity was assigned a numerical value (3= Clear, 2= Moderately Clear 1= Cloudy) to allow graphical representation of the transparency and statistical analysis.

2.12 SHG Imaging

2.12.1. Non Linear Microscopy

The imaging of the 3D architecture of tissues such as the cornea has been possible using non-invasive methods since the advent of non-linear microscopy techniques. This non-linear optical microscopy technique was employed to examine the fibre organisation of the corneal sections, using second harmonic generation (SHG) (λex/em=800nm/ 400nm).

10µm cryosections were brought to room temperature and subjected to three 5 minute PBS washes. Then sections were mounted in VECTASHIELD® with propidium iodide (PI) (Vector Labs, UK), as PI excites at about 535nm and emits at about 615 nm when bound to DNA, producing a red fluorescence, this provided a nuclear stain. The sections were then allowed to air dry (in the dark) for 1 hour and sealed with clear nail varnish before being wrapped in foil and stored at 4°C.

The laser scanning microscope (LSM) 880 NLO on Axio Examiner fixed stage upright microscope (Carl Zeiss Ltd., Cambridge, UK) was turned on, being careful to adhere to instructions and ensure that the coolant temperature was 25°C. The Zen software was initialized and the microscope configured as below (figure 2.15A). Once set up as such, the ocular tab in Zen was chosen to enable safe viewing of the slide so that the appropriate area of interest could be located. Once located and brought into focus, the “acquisition” tab was selected and “live scan” selected, ensuring that the Channel panel was set up as follows (figure 2.15B).

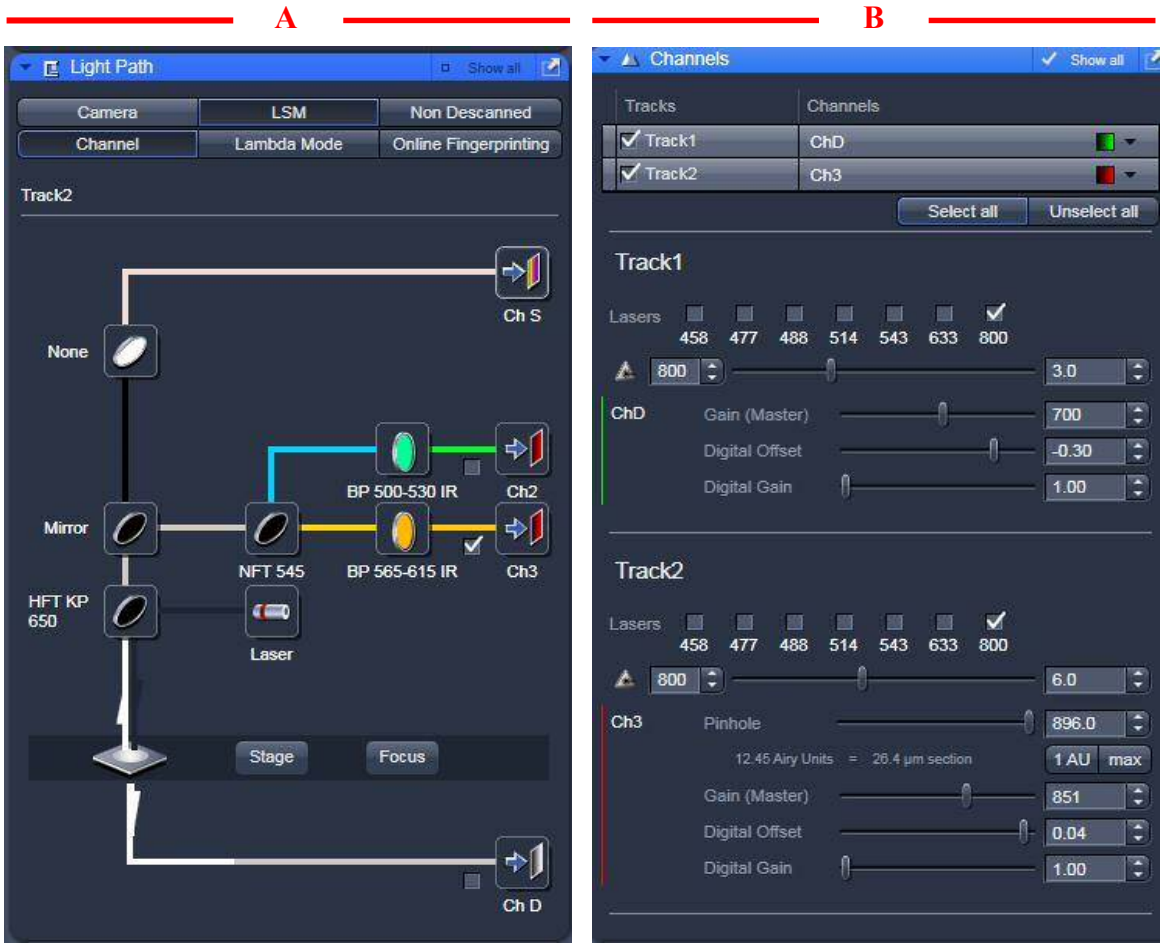

Figure 2.15 **A** Saved configuration 'SHG PI' to be used when viewing samples mounted with VECTASHIELD® with PI **B** Drop down menus showing setting for channels used viewing samples mounted

The desired pseudocolouring for forward scattered SHG and PI fluorescence were also selected for the image (Green- SHG, Red- PI) (see figure 2.16). A focus step of 1µm for corneal sections was also selected. The wounds in the corneal sections were tracked by finding an initial reference point, such as the flap edge, setting that point to zero and tracking along the wound until the hinge was identified. Once these two points were determined the distance moved in the X and Y directions, calculated from the x,y co-ordinates of each position, were used to estimate the location of the mid-flap region (figure 2.17). Images were collected with Plan-Apochromat 20x/0.8NA objective lens (Zeiss). Configuration of the scans is covered in Chapter 6.

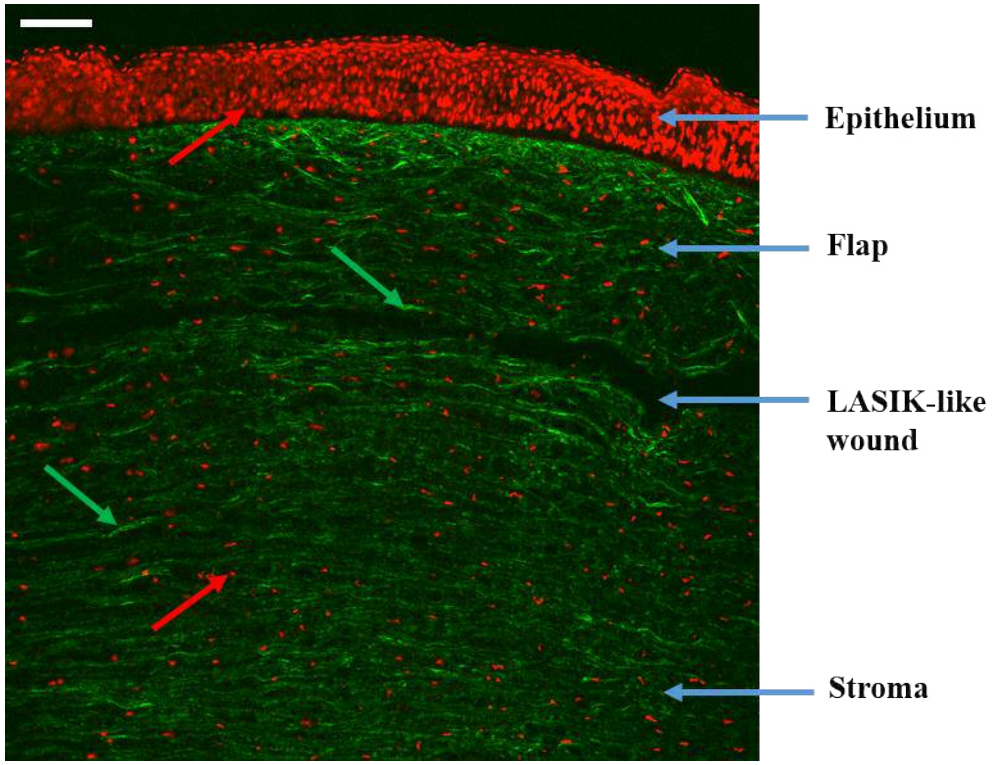

Figure 2.16 SHG (Green Arrows) and PI fluorescence (Red Arrows) image of LASIK-like Wounded porcine cornea cryosection mounted in VECTASHIELD® with PI (Vector Labs, UK)

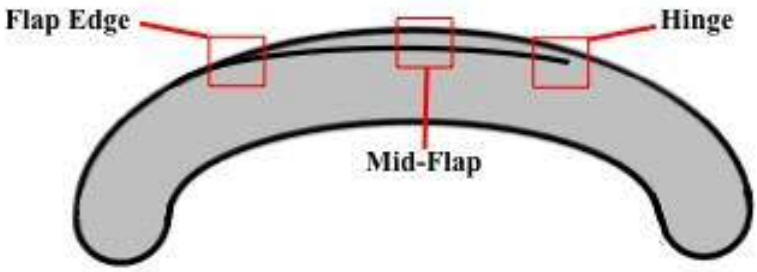

Figure 2.17 Diagram of LASIK-like wounded porcine cornea. Red boxes demonstrate ROI's; Flap Edge, mid-flap and hinge.

These images were saved as .lsm files and the fibrillar collagen bundle coherence and distribution of orientation at each region of interest were determined using Image J Orientation J Analysis software (version 1.52a, National Institutes of Health, USA) as previously described by Rezakhanih et al. (2011). Detailed methods of application of Orientation J image analysis will be provided in Chapter 6.

2.13. Statistical Analysis

In the analysis of data compiled in the experiments it was necessary to compare the results of a particular test such as percentage α-sma immunopositivity for each group of samples against each other and each time point. For this a 2-way ANOVA (analysis of variance) was used to compare the mean differences between groups split on two independent variables, to understand if there was an interaction (significant difference) between the independent variables on the dependant variable.

Multiple comparisons were run on a single data set and so a post-hoc test to adjust for this and reduce error rates, such as Bonferroni, Scheffes's or Tukey HSD (Honest Significant Difference), was needed. With these results multiple pairwise comparisons were required and so a Tukey HSD test was used as a post-hoc test. The 2-way ANOVA tells of significance but can't tell you where the significance lies, so the Tukey HSD was used to run comparisons between all possible pairs of groups to find out which specific groups are significantly different to one another.

The lack of statistical power to these analyses from the low sample numbers throughout these experiments was something to bear in mind during the evaluation of the results.

Chapter 3

Characterisation of LASIK-like wound healing during organ culture

3.1 Introduction

Refractive corneal surgery has become an increasingly popular method of vision correction over the years. However, due to the incomplete healing of LASIK-treated corneas they maintain only 2-28% of the tensile strength of the native cornea (Schmack et al., 2005; Randleman et al., 2008). This limited wound healing is of significant clinical importance and can ultimately result in dehiscence of the flap created during the LASIK procedure (figure 3.1). Although this dehiscence can be treated with mostly positive results, it can be extremely painful and traumatic for the patient and can result in a significant reduction in functional vision.

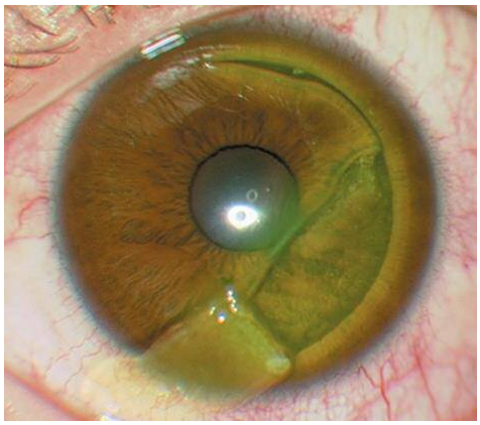

Figure 3.1. Corneal Flap Dehiscence Following Screwdriver Trauma 10 Years After Lasik (Rodriguez & Ascaso, 2013) Reproduced with permission from Rodriguez & Ascaso, 2013, Copyright Massachusetts Medical Society.

Researchers have tried to resolve this issue by improving flap adhesion using "biologic tissue glues" and attempting to modify the stromal healing process. The properties of quiescent keratocytes at the wound edge alter in the early stages of wound healing; the cells become activated fibroblasts and migrate towards the wound bed. These fibroblasts then transform into myofibroblasts on reaching the wound bed and begin expressing α-smooth muscle actin (sma), as well as desmin and an increased amount of vimentin (Chauraisia et al., 2009). The α-sma expression directly correlates with the contractile forces exerted by the myofibroblasts, thus closing the wound gap (Jester et al., 1995). Concurrently, fibroblast expression of corneal crystallins are downregulated and the transparency of the

cornea is reduced through the contractile forces and deposition of opaque ECM (Jester et al., 1999; Fini, 1999; Jester et al., 2005). The expression of α-sma then ceases on completion of the wound healing process and the disappearance of myofibroblasts (Fini, 1999). The activation of keratocytes into the myofibroblast phenotype, and the presence of α-sma, can therefore be associated with the corneal haze that accompanies corneal wound healing.

Dooley et al. (2012) used an organ culture model of LASIK-like wounded ovine corneas to investigate the effect of cell applications, and evaluated the activation of keratocytes to fibroblasts and myofibroblasts using alpha smooth muscle actin (α-sma) in treated and control corneas to investigate the role of these cells in producing scarless wound healing and a subsequently clear cornea. The potentially improved wound healing was tested by assessing the strength of the flap adhesion at various time points during the culture. An extensometer was used to subject the flap to a known vertical force and the time to dehiscence (or break) was recorded (figure 3.2A). However, a vertical force is not representative of the naturally occurring shear force that is the cause of most cases of post-LASIK flap dehiscence (e.g. eye rubbing and other abrasive forces) and was performed in the absence of any other natural forces acting on the cornea, such as intraocular pressure.

Littlechild et al. (2012) constructed a rig to apply a shear force to corneal tissue. Various combinations of fibrinogen “glue” and riboflavin/UVA crosslinking were used to adhere corneal strips from rabbit or shark corneas together. Their adhesion was measured by pulling apart the corneal strips via scleral tags using a motorised horizontal test stand and measuring time to break and the force required (see figure 3.2B).

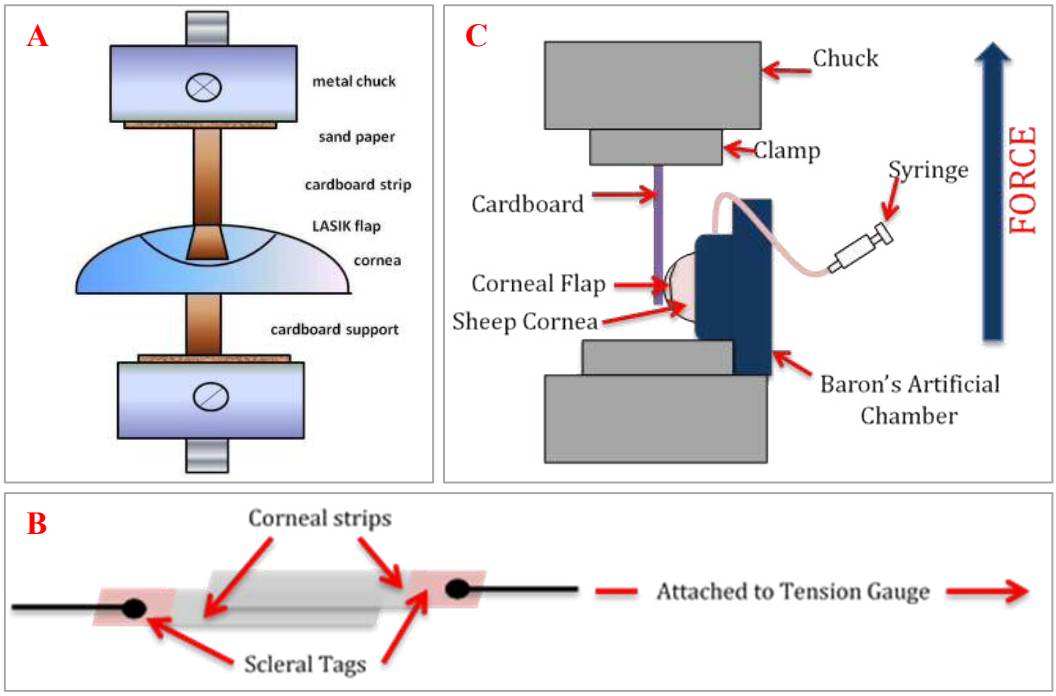

Figure 3.2. A Dooley's 2012 Extensometer design- Reproduced with authors permission (Dooley et al., 2012) B Littlechild's method of measuring flap adhesion (Littlechild et al. 2012) C Final vertical shear extensometry design.

This method was found to markedly increase the biomechanical adhesion strength of the wound after 30 minutes. Finally, Randelman and Dawson (2008) evaluated the biomechanical strength of a LASIK-like wounded cornea by applying a force along their axis and measuring the elasticity based on Young's Modulus. As Randelman and Dawson stated themselves, this method does not reflect an *in vivo* trauma. The force they used to measure Young's Modulus exerted over the X or Y axis, was one that would be very unlikely to cause flap dehiscence and that, in reality, a compressive or shear force with a degree of torque would be the more natural event to result in this specific trauma. A vertical shear extensometry rig was constructed to measure the shear force that also incorporated a Baron's Artificial Chamber to introduce the more natural intraocular pressure and shape of an eye (figure 3.2C).

3.2 Aim

Porcine organ culture was carried out to ascertain whether the fibrinogen glue had any effect on the corneal wound healing of LASIK-like wounded corneas as a function of time in organ culture.

The objectives of this chapter were to:

- Evaluate porcine cornea wound healing of LASIK-like flaps in an organ culture model
- Use fibrinogen as an example of a therapeutic agent to determine the efficacy of the model in evaluating change in healing outcome measures as a function of treatment.

3.3 Experimental design

The following investigations used the application of fibrinogen solution as outlined by Littlechild et al. (2012) as a model to develop a porcine corneal wound organ culture model that could later be used to test the efficacy of potential therapeutics. Outcome measures for evaluation of change were: morphological and structural assessment (Haematoxylin and Eosin staining and electron microscopy), α-sma immunopositivity (i.e. myofibroblastic transformation), cell number (cell proliferation/movement), transparency (spectrophotometric analysis) and mechanical properties (shear force) of the treated and untreated cornea.

To characterise the wound healing of LASIK-like wounded corneas during organ culture, and to assess the effects of fibrinogen treatment, porcine corneas were procured and wounded and treated before being placed into organ culture (see section 2.1-3). Corneas were wounded with the microkeratome to create a LASIK-like wound. Wounded, but not cultured, corneas provided 0 time point samples.

Half of the corneas were left as controls, the other half were treated by adding 10µl of a 180mg/ml fibrinogen solution (see Appendix) to the stromal bed under the epithelial-stromal flap of the LASIK-like wound. Corneas were examined using spectrophotometry immediately after treatment to assess the effect of the addition of fibrinogen on corneal light transmission, unwounded controls.

After 4 weeks in culture, corneas were examined using spectrophotometry (see section 2.11.1), extensometry (see section 2.10), electron microscopy (see section 2.9), α-sma immunofluorescence (see section 2.8.2) and H&E (see section 2.8.1). The number of corneas used is outlined in Table 3.1.

	Treatment	Time point	Processes	
LASIK-like Wounded Porcine Corneas n=34	Fibrinogen Treated n=17	0 week n=7	Electron Microscopy	n=2
			Immunofluorescence & H&E	n=2
			Spectrophotometry & visual grading of transparency	n=3
		4 week n=10	Electron Microscopy	n=2
			Immunofluorescence & H&E	n=2
			Spectrophotometry & visual grading of transparency	n=3
			Extensometry	n=3
	Untreated Controls n=17	0 week n=7	Electron Microscopy	n=2
			Immunofluorescence & H&E	n=2
			Spectrophotometry & visual grading of transparency	n=3
		4 week n=10	Electron Microscopy	n=2
			Immunofluorescence & H&E	n=2
			Spectrophotometry & visual grading of transparency	n=3
			Extensometry	n=3
Unwounded Porcine Corneas n=6	-	0 week n=3	Spectrophotometry & visual grading of transparency	n=3
		4 week n=3	Spectrophotometry & visual grading of transparency	n=3

Table 3.1 Table demonstrating porcine cornea number.

An additional organ culture was carried out with LASIK-like wounded porcine corneas for 1, 2, 3 and 4 week time points to further refine the immunofluorescence protocol. The number of corneas used is outlined in Table 3.2.

	Treatment	Time point	Process	
LASIK-Like Wounded Porcine Corneas n=15	Untreated Controls n=15	0, 1, 2, 3 & 4 week n=3 for each time point	αsma Immunofluoresence Protocol Refinement	n=15

Table 3.2 Table demonstrating the number of porcine corneas used in αsma immunofluorescence protocol refinement.

Results

3.4 Morphology:

3.4.1. H&E staining

Haematoxylin and eosin stained images of fibrinogen-treated and untreated wounded corneas, captured using a Leica AF6000 microscope (Leica, UK) and analysed using the LF software (Leica, UK), can be seen in figure 3.3. Higher cellularity was observed above and below the wound in the untreated LASIK-like wound (figure 3.3A,B), compared to the fibrinogen treated LASIK-like wound (figure 3.3C,D). The stroma-flap interface of the wound can be clearly seen. In figure 3.3D the wound appeared to have been stained more heavily with blue, unlike image B where the wound has not been stained a significantly different colour to the rest of the sample.

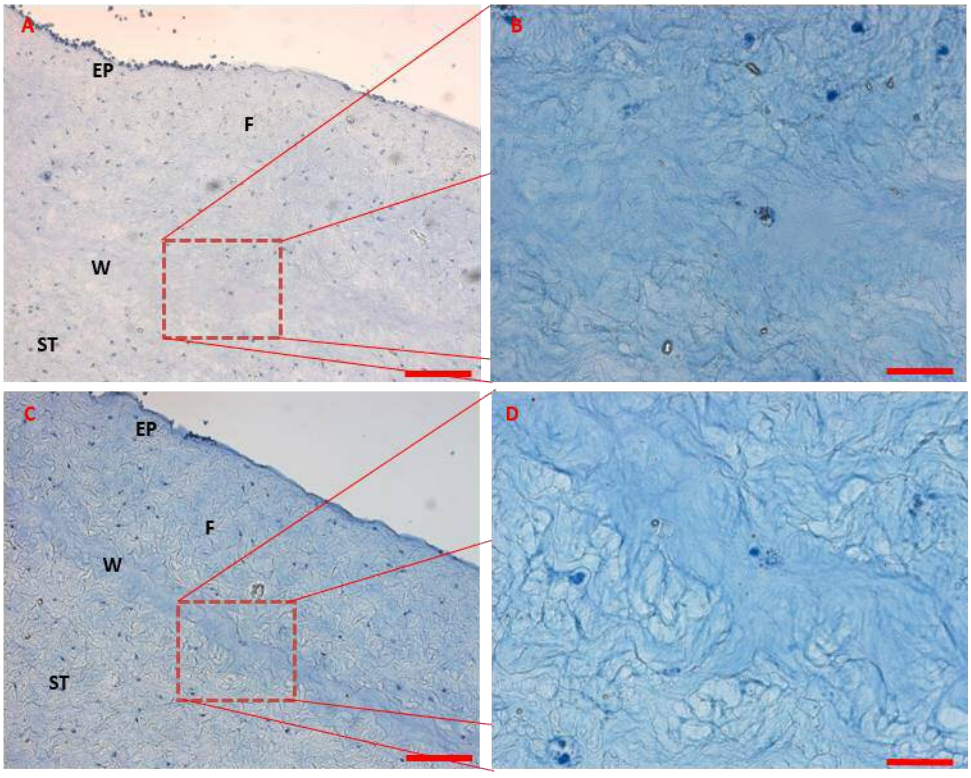

Figure 3.3. Haematoxlin and eosin stained organ cultured porcine corneal wound. A untreated LASIK-like wounded cornea after 4 weeks in organ culture. Region of interest (ROI) outlined in red is magnified in B to show the wound interface (W) between the flap (F) and the stromal wound bed (ST) Epithelium (EP). C fibrinogen treated LASIK-like wounded cornea after 4 weeks in organ culture, with D magnified ROI. Scale bars represent 100µm for A and C, and 25µm for B and D.

Cell counts were performed in 100µm^2 squares at 3 adjacent sites above and below the wound in figure A and C and recorded in Table 3.3.

	Position of Counts	Cell Count			Total	Average	Total Average
Untreated LASIK-like Wounded Cornea	Above the Wound	6	6	7	**19**	**6.3**	**5.7**
	Below the Wound	5	3	7	**15**	**5**	
Fibrinogen treated LASIK-like Wounded Cornea	Above the Wound	5	4	4	**13**	**4.3**	**3.8**
	Below the Wound	4	4	2	**10**	**3.3**	

Table 3.3 H&E Cell counts for Fibrinogen treated and untreated LASIK-like wounded corneas.

Figure 3.4 demonstrates a lower overall cellularity ($p<0.05$) in the untreated LASIK-like wounded cornea after a culture period of 4 weeks when compared to the fibrinogen treated LASIK-like wounded cornea, cultured for the same period.

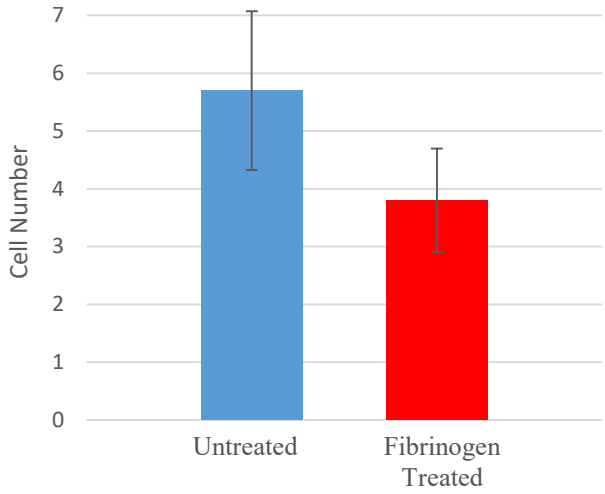

Figure 3.4 Comparison of Average Cell Counts for Fibrinogen Treated and Untreated LASIK-like wounded porcine corneas after 4 weeks in organ culture. Fibrinogen treated corneas had significantly lower cell count than untreated ($p<0.05$ t-test)

3.4.2. Corneal Ultrastructure

Specific areas of the LASIK-like wounds were unable to be identified in the electron micrographs, however, other features were determined. The images obtained were not directly comparable due to the differing magnifications, however some general observations were possible. Figure 3.5A, the 4 week organ cultured untreated wounded cornea, demonstrated collagen disarray and areas without collagen fibrils in the matrix. In figure 3.5C, although swollen by the culture incubation, this part of the untreated cornea has aligned, undamaged collagen fibrils. As well as a degree of warping, alignment was also visible in figure 3.5E. The fibrinogen treated corneas also demonstrated aligned, albeit, swollen collagen fibrils (figure 3.5F). However, disarrayed and damaged collagen can be seen in the micrographs shown in figures 3.5B and D. In these micrographs, there were patches of intense amorphous background staining suggesting the presence of non-collagenous material, possibly fibrinogen.

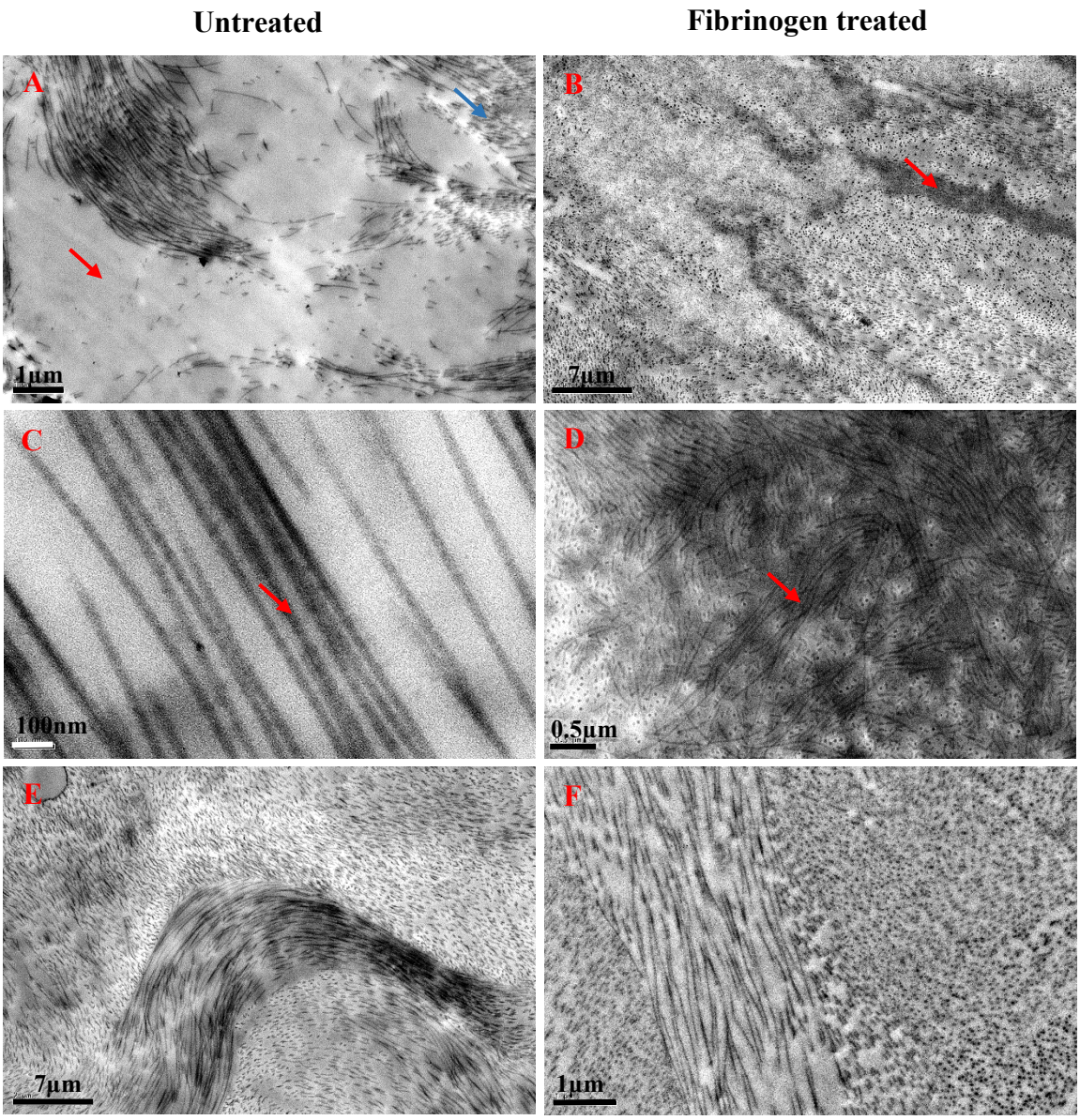

Figure 3.5. Electron micrographs of 4wk organ cultured porcine corneas. A-Untreated wounded cornea- showing spaces in matrix (red arrow) and collagen disarray (blue arrow). B-Fibrinogen treated cornea- showing collagen disarray and presence of non-collagenous substance (red arrow). C-Untreated cornea- demonstrating swollen extracellular matrix but with aligned collagen (red arrow). D-Fibrinogen treated cornea- shows damaged cornea with collagen in disarray (red arrow). E-Untreated cornea- demonstrates warping of collagen in stroma. F-Fibrinogen treated cornea- area of organised collagen structure.

3.5 Corneal Stromal Cellularity

3.5.1. Keratocyte Activation: α-sma immunofluorescence

The activation and transformation of keratocytes into myofibroblasts can be detected by the presence of alpha smooth muscle actin (α-sma). The number of myofibroblast was ascertained using ex/em λ =494nm/520nm, which has a maximum emission of 520nm (bright green). Therefore, a myofibroblast had the combination of the Hoescht nuclei labelling in blue and α-sma in green, resulting in a blue-green cell. Figure 3.5 shows α-sma immunolabelling in wax sections for the treated and untreated 4 week organ cultured LASIK-like wounded corneas.

A small number of myofibroblasts were observed above the wound in the untreated cornea after 4 weeks in organ culture (figure 3.6A). The number of myofibroblasts in the untreated LASIK-like wounded cornea (figure 3.6A) was higher than that in the Fibrinogen treated LASIK-like wounded cornea (figure 3.6B) as recorded in Table 3.4.

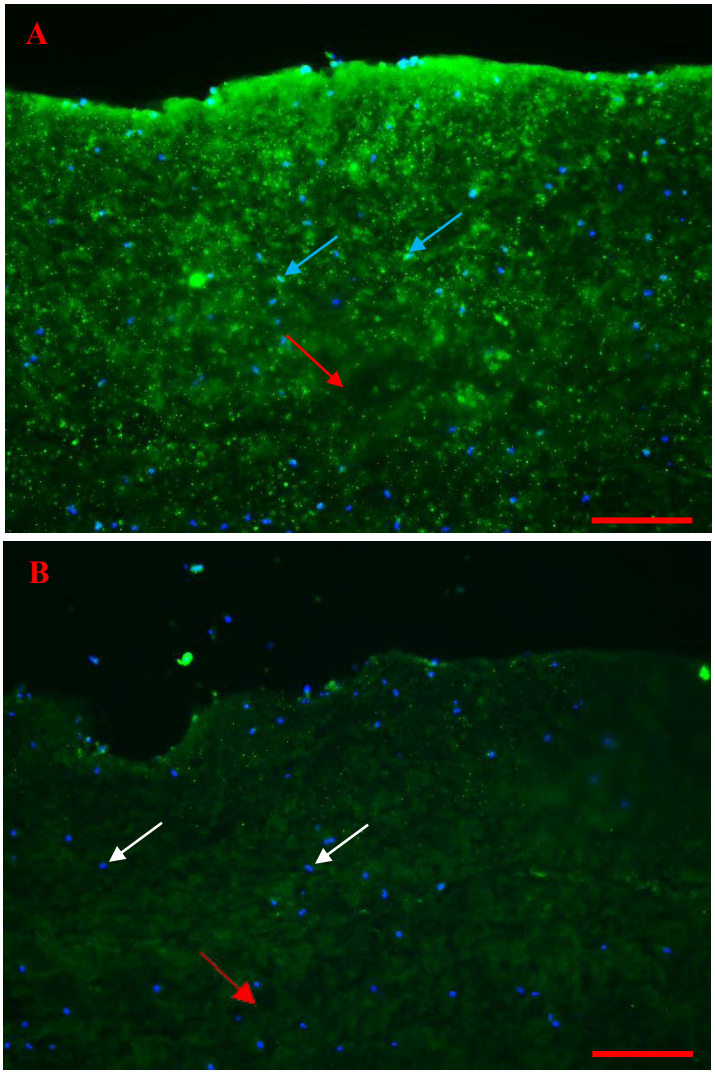

Figure 3.6 Immunolocalisation of α-sma in wax sections. A-LASIK-like wounded cornea after 4 weeks in organ culture. B- Fibrinogen treated LASIK-like wounded cornea after 4 weeks in organ culture. Blue arrows indicate α-sma immunopositive cells. Red arrows indicate the wound. White arrows indicate hoescht labelled cell nuclei. Scale bars represent 100µm

The percentage activation of keratocytes denoted by the α-sma positive cells was significantly higher ($p>0.01$) in the untreated LASIK-like wounded cornea than the fibrinogen treated LASIK-like wounded cornea (table 3.4) that had no activation of α-sma, with only the blue Hoescht labelled nuclei being visible (figure 3.6B). Again, the flap-stroma interface of the wound was seen (indicated by the red arrow), but not as clearly as in figure 3.5A of the untreated LASIK-like wounded cornea. There was a large amount of background fluorescence in this sample, but the flap-stroma interface of the LASIK-like wound was clearly demarcated (indicated by the red arrow).

	Area of Counts	Total Cell Count			α-sma Positive Cells			Percentage Activation/%			Mean Percentage /%
Untreated LASIK-like Wounded Cornea	Above the Wound	6	6	5	1	2	1	17	33	20	21
	Below the Wound	4	5	3	1	1	0	25	20	0	
Fibrinogen treated LASIK-like Wounded Cornea	Above the Wound	3	3	2	0	0	0	0	0	0	0
	Below the Wound	3	4	2	0	0	0	0	0	0	

Table 3.4 Myofibroblast (α-sma-positive cell) counts for Fibrinogen treated and untreated LASIK-like wounded corneas.

3.5.2. Immunofluorescence Protocol Refinement

For optimisation of α-sma immunolabelling for future investigations, the quality of the immunolabelling when using wax sections was compared to that of samples prepared using cryosections (see section 2.7) to determine the most appropriate tissue preparation method using LASIK-like wounded porcine corneas organ cultured for 4 weeks (figure 3.7).

It was determined that cryosectioned corneal tissue produced a better immunolabelling of cells (figure 3.7 B,D,F), with less background signal, with retention of the corneal epithelium, when compared to images produced from wax sections (figure 3.7A, C, E) immunolabelled using the same protocol.

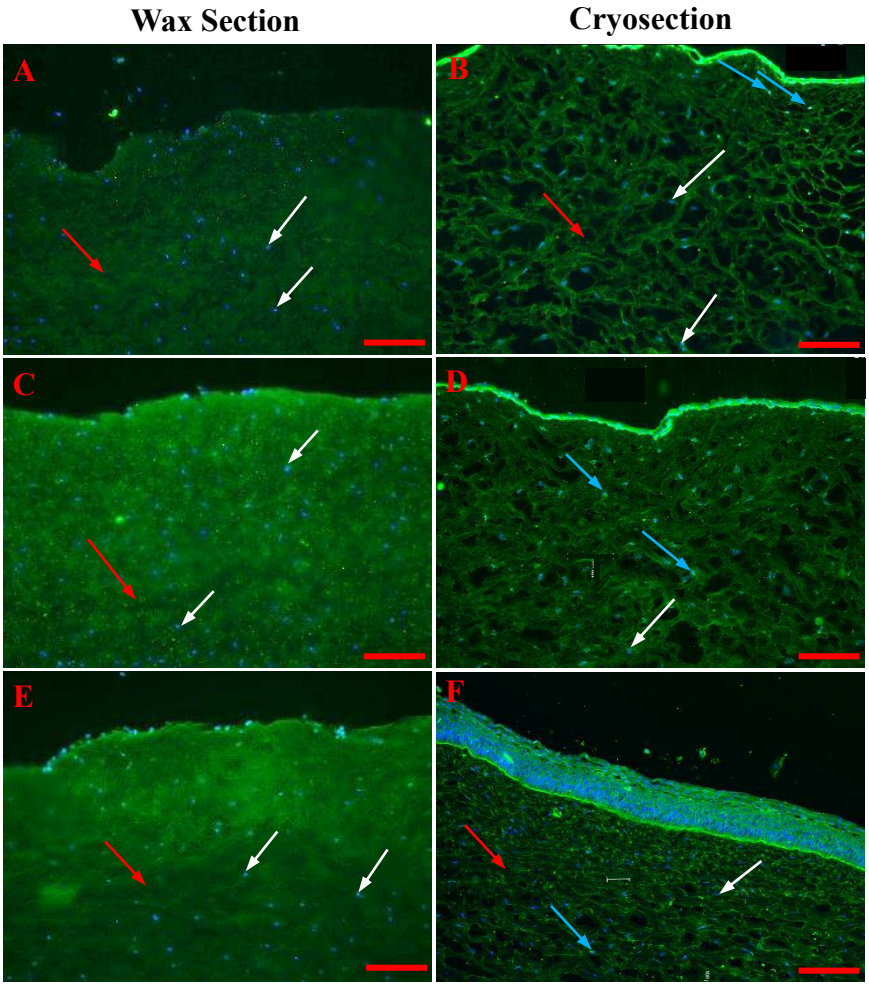

Figure 3.7 Comparison of Wax sections (A, C & E) and Cryo-sections (B, D & F) in immunofluorescence. Images show immunolabelled with 1 in 100 primary antibody concentration and goat anti-mouse IgG (H+L) Alexa Fluor 488 secondary antibody, cryosectioned porcine cornea after 2 weeks in organ culture. Blue arrows indicate α-sma immunopositive cells. Red arrows indicate the wound. White arrows indicate hoechst labelled cell nuclei. Scale bars represent 100µm

The necessity of using a block during the immunolabelling process (see section 2.8) was determined when comparing the use of 5% goat serum (Sigma, UK) to block the signal on cryosectioned LASIK-like wounded 2 week organ cultured porcine corneas with no blocking (figure 3.8). It was determined that no block was required in future immunolabelling as the signal from 5% blocking was too weak (figure 3.8B and D) and no block resulted in good signal and easy detection of immunopositive α-sma cells with a low level of background signal in corneal cryosections (figure 3.8A & C).

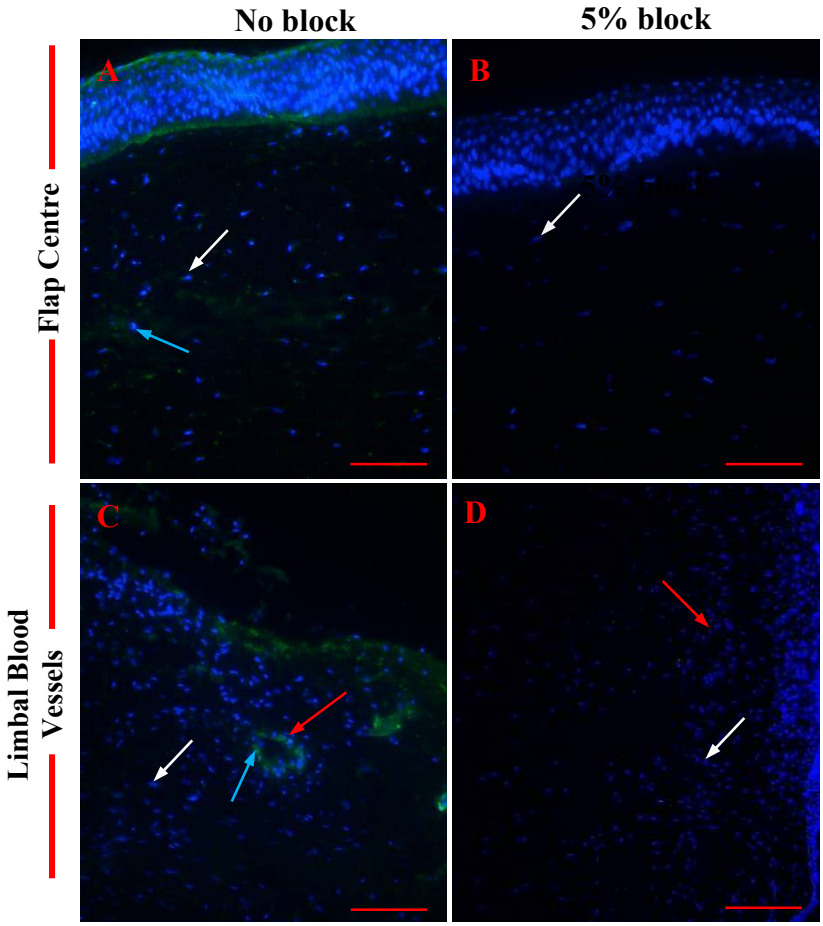

Figure 3.8. Determination of necessity of blocking with goat serum during immunolabelling. Images A, B, C & D show immunolabelled with 1 in 100 primary antibody concentration and goat anti-mouse IgG (H+L) Alexa Fluor 488 secondary antibody, cryosectioned porcine cornea after 2 weeks in organ culture. White arrows indicate α-sma immunopositive cells, Red arrows indicate Limbal Blood Vessels and Blue arrows indicate hoescht labelled cell nuclei. Scale bars represent 100µm

The type of secondary antibody was determined on cryosectioned 2week organ cultured LASIK-like wounded porcine corneas, using a 1 in 100 concentration of primary antibody with no block. The immunolabelled images were examined for signal strength and presence of background (figure 3.9). 3 different secondary antibodies were considered; “Goat” goat anti-mouse IgG Alexa Fluor 488 (figure 3.9C & F) and 2 separate batches of Donkey anti-mouse IgG Alexa Fluor 488, “Donkey 1” (figure 3.9A & D) and “Donkey 2” (figure 3.9B & E).

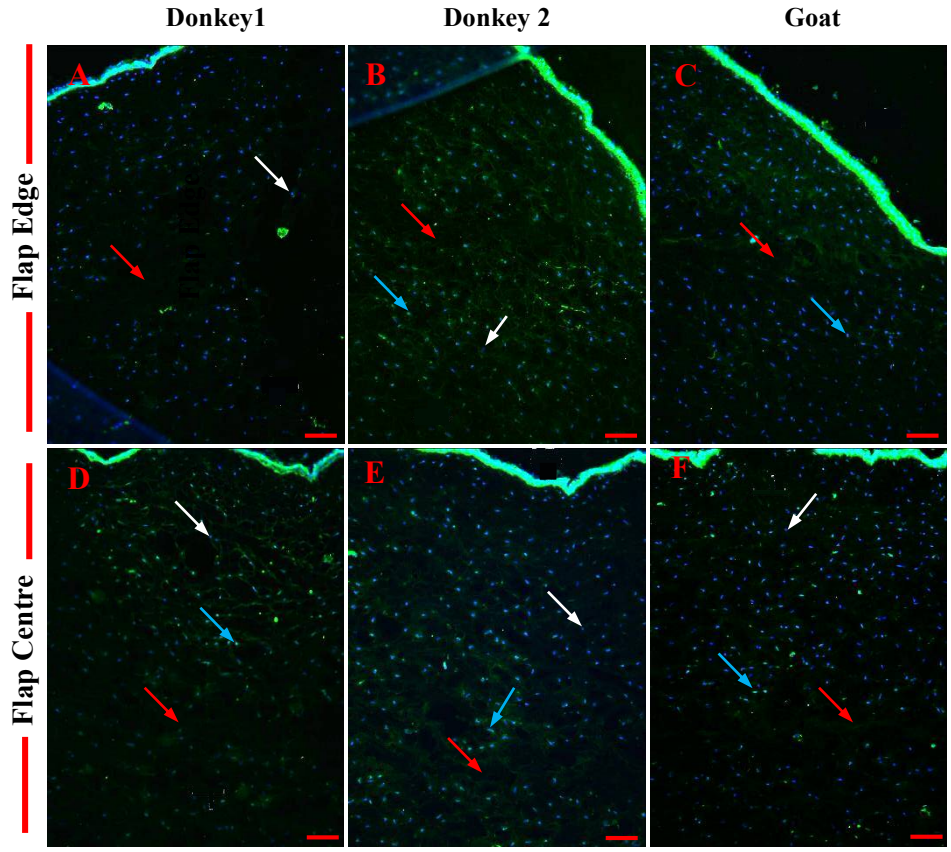

Figure 3.9 Determination of Secondary antibody type. Images show immunolabelling with 1 in 100 primary antibody concentration and cryosectioned porcine cornea after 2 weeks in organ culture. White arrows indicate α-sma immunopositive cells. Red arrows indicate the wound. Blue arrows indicate Hoescht labelled cell nuclei. Scale bars represent 100µm.

The donkey anti-mouse IgG Alexa Fluor 488 secondary antibody produced a good signal allowing for easy identification of α-sma immunopositive cells with low background signal (figure 3.9B and E) and would therefore be used going forward.

Finally, the concentration required of the primary antibody, mouse monoclonal anti-α-smooth muscle actin (sigma UK), during immunolabelling was refined using cryosectioned 2 week organ cultured LASIK-like wounded porcine corneas with no block and the chosen secondary antibody. The images were compared for signal strength and background fluorescence (figure 3.10).

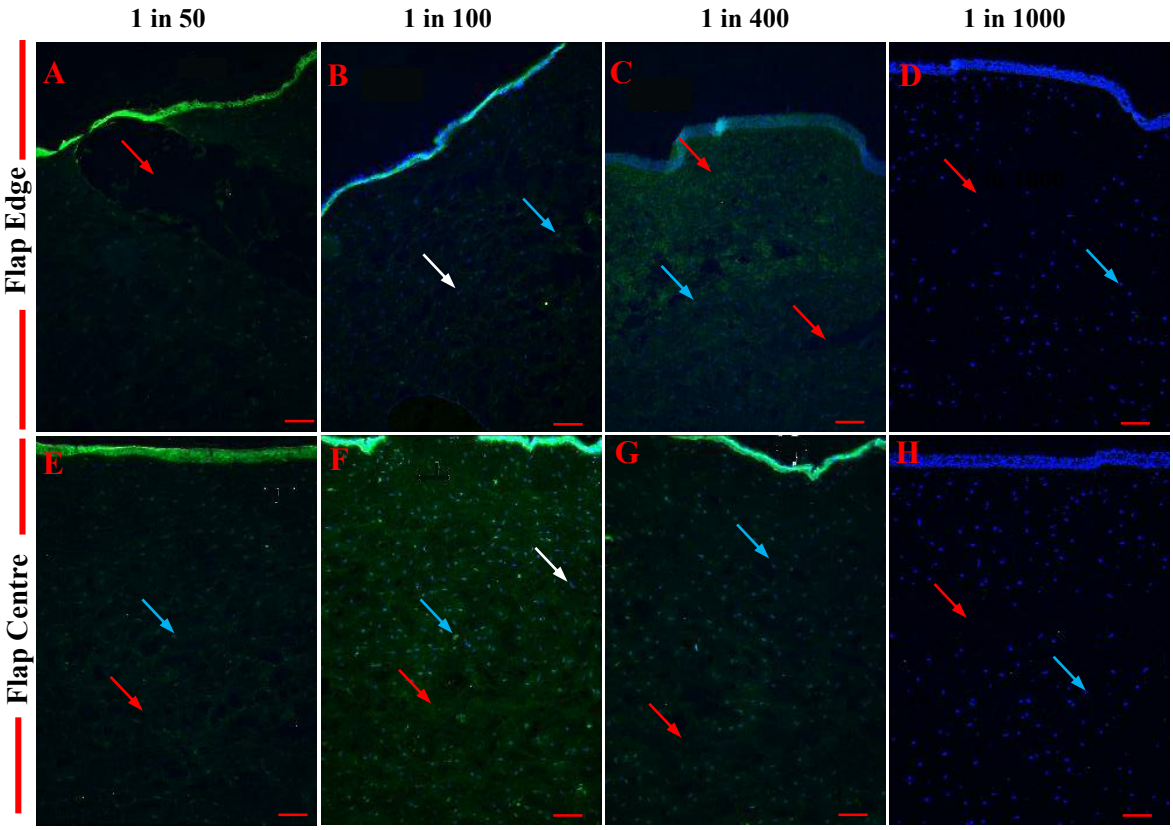

Figure 3.10 Determination of Primary Antibody Concentration. Images show alpha sma immunofluorescence following incubation of organ cultured corneal cryosections in primary antibody dilutions at 1in50 (A,E), 1in100 (B,F), 1in 400 (C,G) and 1in1000 (D,H) . Blue arrows indicate α-sma immunopositive cells. Red arrows indicate the wound. White arrows indicate Hoechst labelled cell nuclei. Scale bars represent 100µm

The 1 in 100 concentration of the primary antibody was determined to produce the clearest cell signal to identify the α-sma immunopositive cells with the lowest background signal (figure 3.10B & F).

Following these protocol refinements snap frozen porcine corneal cryosections would be immunolabelled with 1 in 100 dilution of the primary antibody mouse monoclonal anti-α-smooth muscle actin, and donkey anti-mouse IgG (H+L) Alexa fluor 488 with hoescht, and no blocking step.

The following images in figure 3.11 show the first panel of this refined protocol imaging the 3 separate regions of interest (ROI's) the flap edge, flap centre and flap hinge

(demonstrated in chapter 2 section 2.12) at the uncultured 0 time point and following 1, 2, 3 and 4 week time points. The appearance of two layers pf epithelium seen at flap edge at 0 week time point (figure 3.11) is due to the disruption of the morphology of the flap when placed into the moulds with no wound healing. The flap edge can misalign causing the observed appearance.

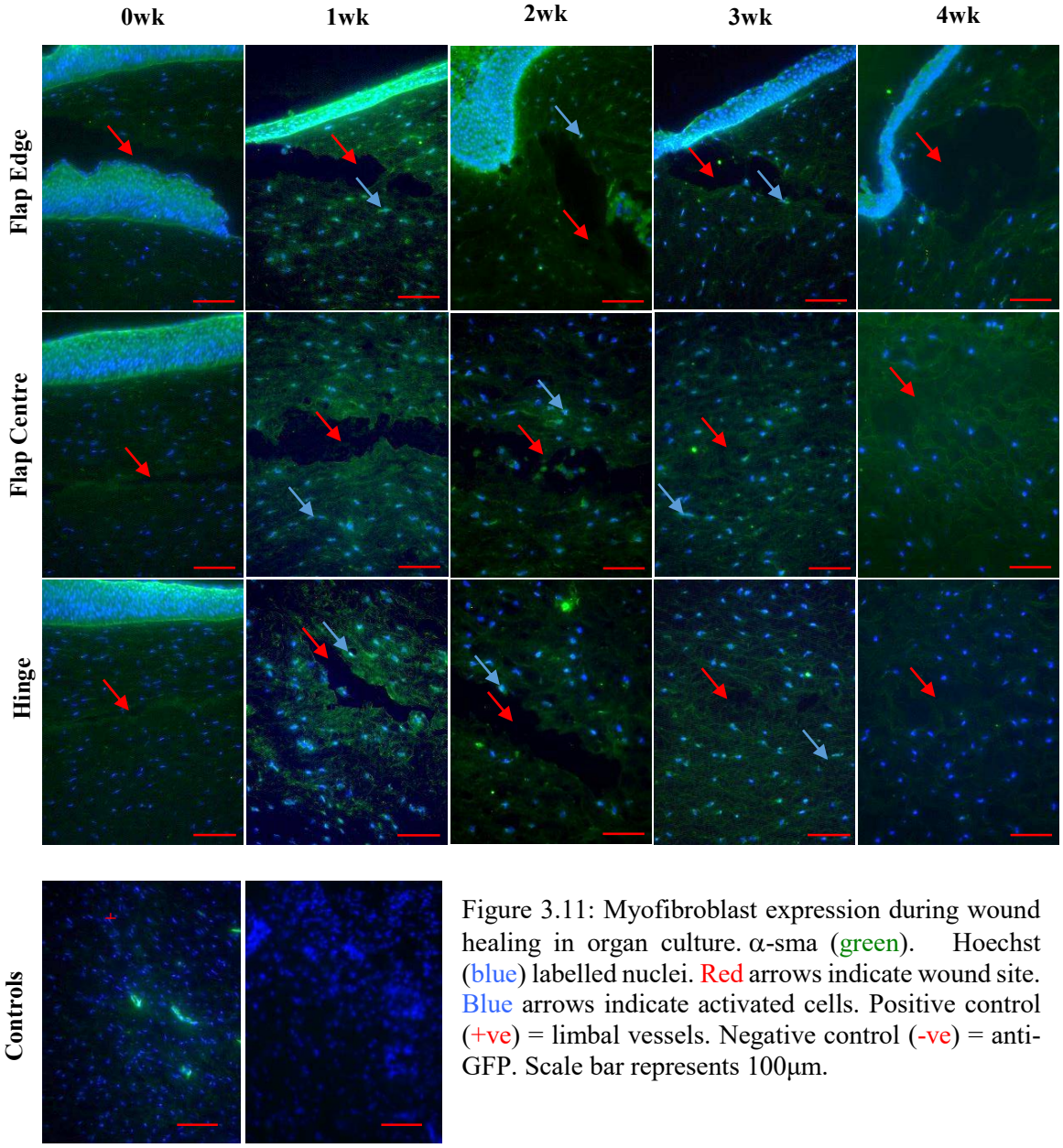

Figure 3.11: Myofibroblast expression during wound healing in organ culture. α-sma (green). Hoechst (blue) labelled nuclei. Red arrows indicate wound site. Blue arrows indicate activated cells. Positive control (+ve) = limbal vessels. Negative control (-ve) = anti-GFP. Scale bar represents 100µm.

3.6 Corneal Transparency

Spectrophotometry was used to assess the transparency of the wounded corneas at 0 time point after wounding and after 4 weeks in organ culture for both the LASIK-like wounded and the trephine wounded corneas. Figure 3.12 shows the spectrophotometry results for all wounded organ-cultured corneas.

The unwounded controls showed a significant ($p<0.01$) reduction in transparency after 4 weeks in culture (figure 3.12A), dropping by about 45% at 550nm. The creation of the LASIK-like flap also causes a significant ($p<0.01$) reduction in transparency (figure 3.12C) when compared to the unwounded cornea at 0 time point. This reduction in transparency was maintained during the culture incubation such that after 4 weeks there was no significant change (figure 3.12B) and the transmission was similar to that of the unwounded ($p>0.01$) cornea at this time point (figure 3.12D).

Figures 3.12E and 3.12F show that fibrinogen treatment has very little effect on the LASIK-like corneal transmission either after wounding (figure 3.12E) or after 4 weeks in culture (figure 3.12F) with no significant difference found between the transmission curves ($p>0.05$).

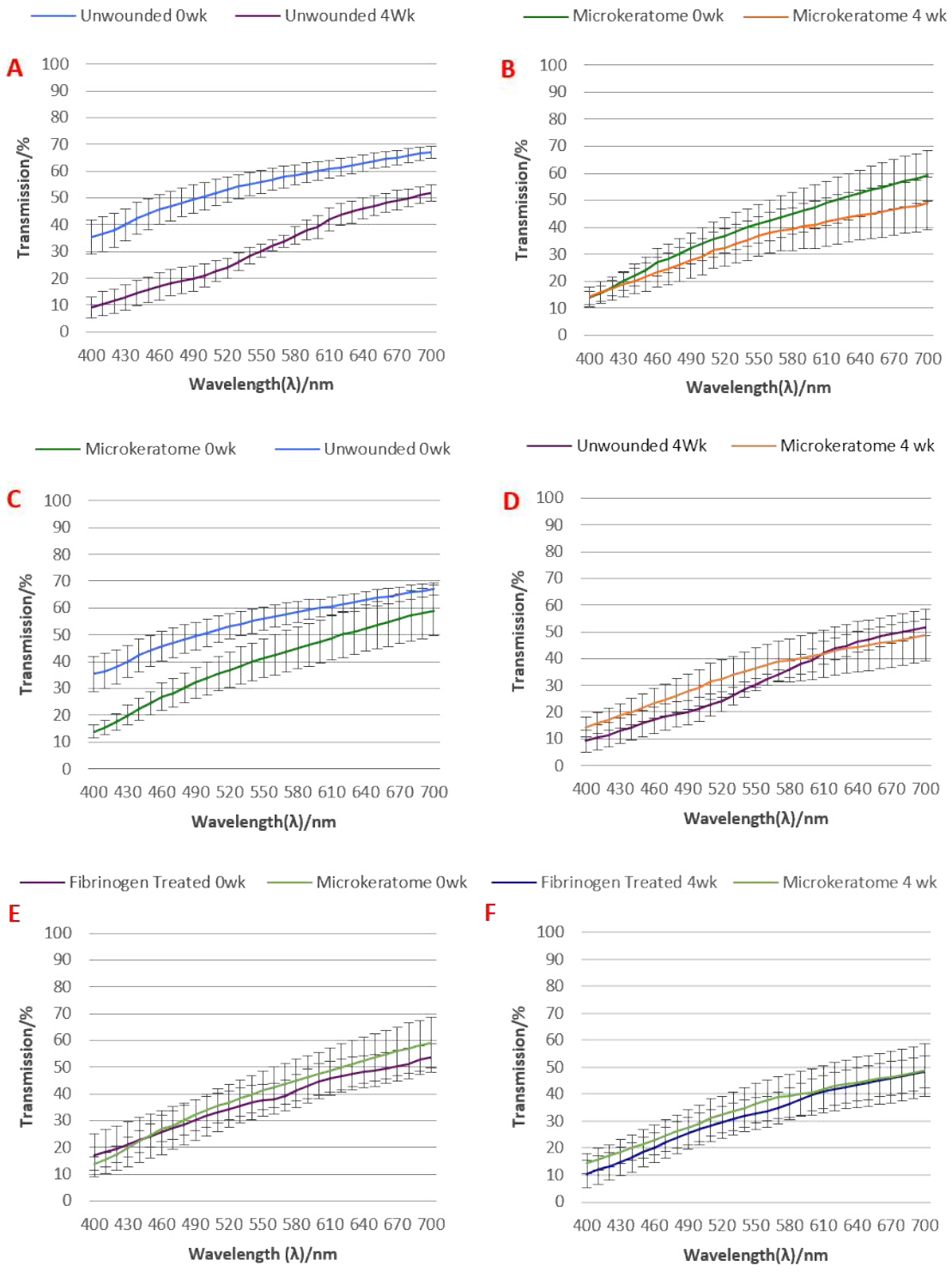

Figure 3.12 Normalised data showing the percentage transmission of light through a wounded, treated and untreated corneas plotted as a function of the wavelength of light. A: Unwounded corneas at 0 and 4 weeks in culture. B: LASIK-like wounded corneas 0 and 4 weeks in culture. C: Comparison of LASIK-like wounded and unwounded corneas at 0 weeks. D: Comparison between LASIK-like wounded and unwounded corneas at 4 weeks in culture. E: Effect of fibrinogen treatment at 0 weeks. F: Effect of fibrinogen treatment at 4 weeks.

Some corneas were examined at 0 and 4 weeks using a visual transparency assessment as described in section 2.11.2 (figure 3.13) and the assigned numerical value was used to facilitate graphical representation (figure 3.14A)

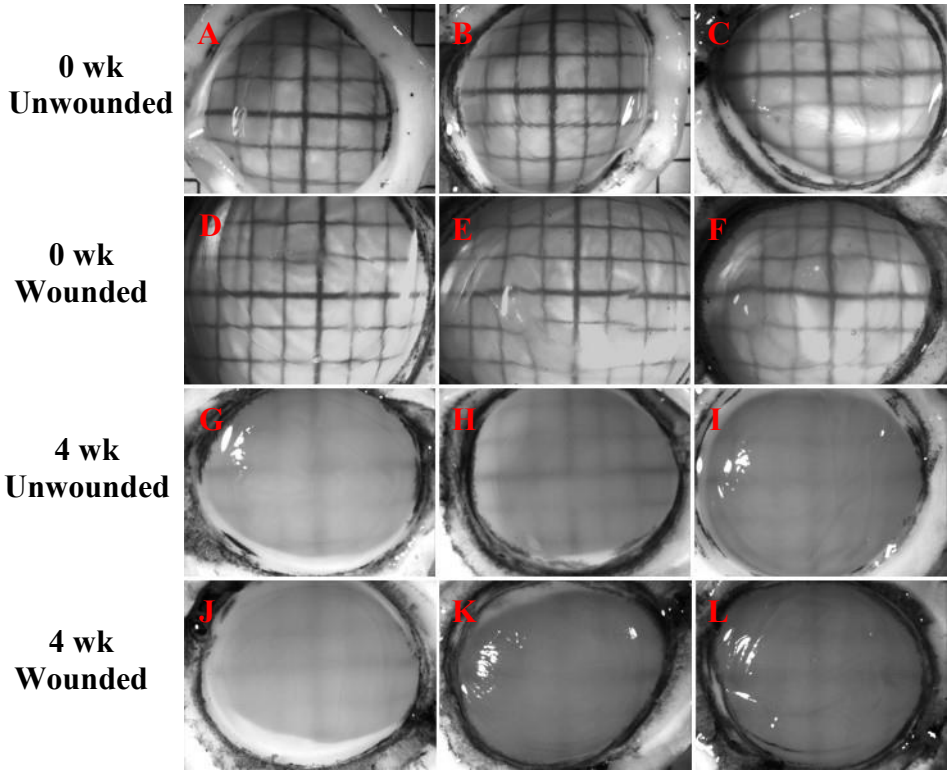

Figure 3.13 Visual Grading Images. Images of LASIK-like wounded (n=6) (D-F,J-L) and unwounded (n=6) (A-C,G-I) porcine corneas at 0 time point (A-F) and after 4 weeks in organ culture (G-L), used to determine the transparency of corneas (as described in chapter 2 section 2.9).

The LASIK-like wounded corneas appear less transparent than the unwounded corneas at 0 time point (figure 3.13A-F) before being placed in organ culture, although there is no significant difference ($p<0.01$), but appear to be similarly cloudy after 4 weeks in organ culture (figure 3.13G-L). This is demonstrated graphically in figure 3.14A.

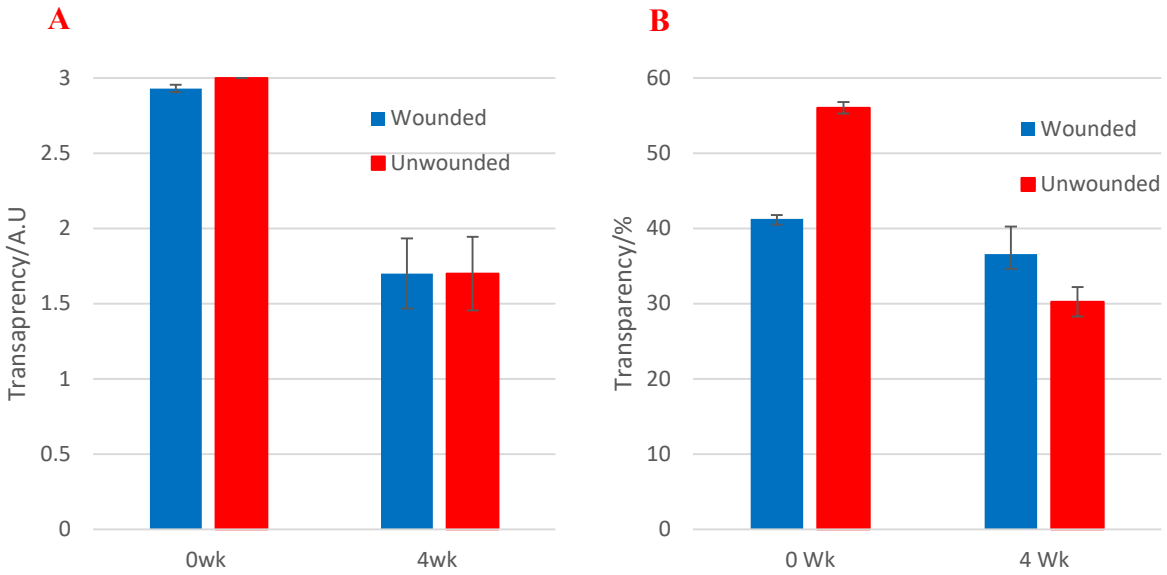

Figure 3.14 Visual Grading Vs. Spectrophotometry. Averaged data comparing the results of visually graded transparency (A) and spectrophotometry determined transparency at 550nm (B) for both wounded and unwounded porcine corneas at 0 time point and organ cultured for 4 weeks.

The decision was made to continue with the visual grading as the process of spectrophotometry destroyed the cornea, and so no further analysis of a particular sample would be able to take place. Using the visual grading technique would enable the same cornea to be subjected to snap freezing, cryosectioning and analysis of α-sma immunolabelling. This would enable a correlation between transparency and myofibroblast expression to be determined in the same cornea.

3.7 Mechanical Properties

After 4 weeks in culture the wounded control and treated corneas were placed into an extensometer and tested, as outlined in section 2.10. The results produced by the Nexygen 4.1 software are shown in figure 3.15A-F

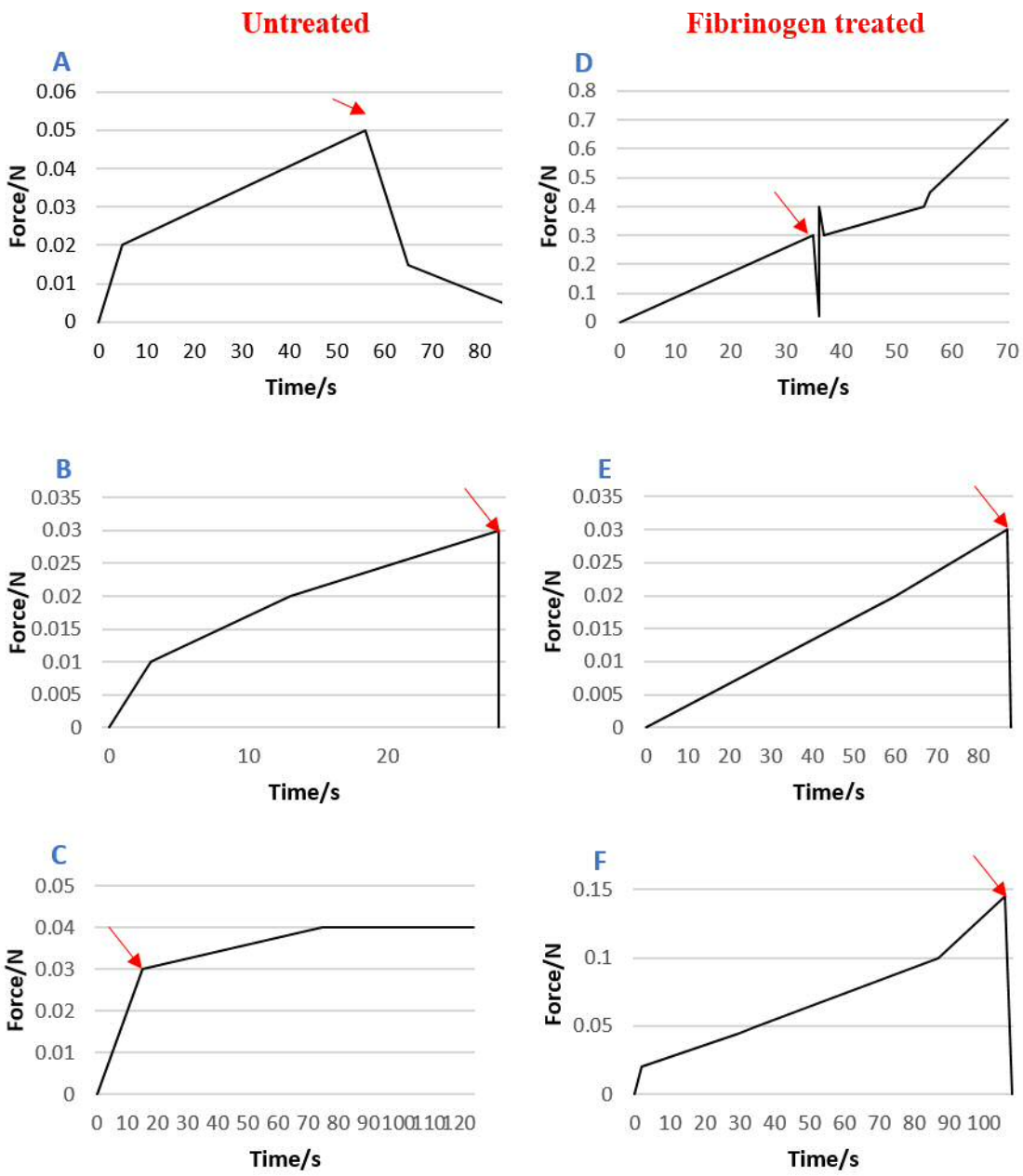

Figure 3.15 Extensometry: Force and time required to detach flap from wound bed in LASIK-like wounded untreated (A-C) and Fibrinogen treated (D-F) porcine corneas. Red arrows indicate the time of observed break.

The figures demonstrated the time taken in seconds for the flap edge of the wound in the corneas to become detached from the surrounding cornea against the force required for dehiscence to occur. Notably, each graph had a different line profile and an observed time of detachment was necessary to interpret the graphs. The following table (table 3.5) demonstrates both the observed and recorded data.

Specimen Nº	Treatment	Force (N) at Break	Observed Time of Break	Observed Factors Effecting Outcome
A	Control	0.050N	56s	None
B	Control	0.030N	28s	None
C	Control	0.030N	15s	Flap possibly pre-detached by high IOP
D	Fibrinogen	0.300N	35s	Graph shows pull to complete detachment
E	Fibrinogen	0.030N	87s	Flap possibly pre-detached by high IOP
F	Fibrinogen	0.145N	106s	None

Table 3.5 Force required to detach corneal flaps in treated and untreated corneas: observed break time and any factors observed effecting the outcome

The control corneas (LASIK-like wounded, without treatment) required, on average, a lower force and shorter time (figure 3.16) to detach the flap from the wound bed than the fibrinogen treated corneas, although the differences were not significant with the sample numbers used in this study.

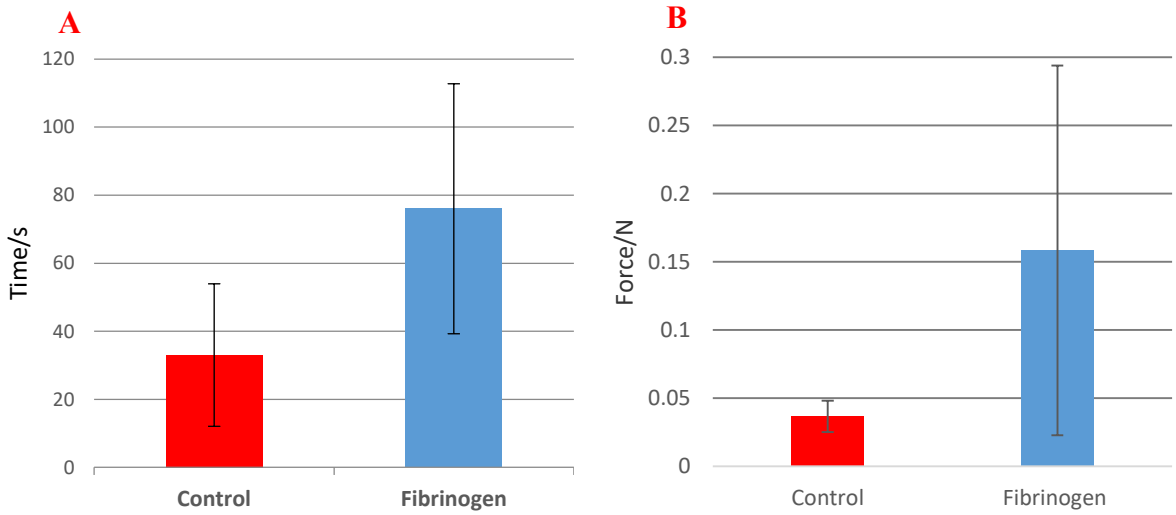

Figure 3.16 A Average Time Required to break for Control (untreated LASIK-like wounded corneas) vs. Fibrinogen (treated LASIK-like wounded corneas) B Average force required to break for control (untreated LASIK-like wounded corneas) vs. fibrinogen treated LASIK-like wounded corneas.

3.8 Discussion

The aim of the preliminary experiments described in this Chapter was to assess the optical, histological and biomechanical effects of LASIK-like flap creation in the porcine cornea, and to establish effective protocols using fibrinogen as a model treatment for stabilising the flaps.

The electron micrographs produced from the TEM processing of the samples showed areas of organised and disorganised stroma in all samples after wounding and following a period of organ culture. This is as would be expected. The regions of disarray and lamella warping are almost certainly due to damage to the cornea from the wounding itself, as collagen synthesis during wound healing is minimal at the flap/bed interface. Some disruption will also be caused by tissue swelling in the culture medium. Interestingly, the presence of additional background staining in the fibrinogen-treated samples probably reflects the penetration of fibrinogen into the ECM. Although the possibility of the fibrinogen solution filling the interface would appear to solve the dehiscence problem by acting as a "biologic glue" increasing the adhesion strength of the flap, this presents its own potential problems. Fibrinogen is an extra substance of a different refractive index, 1.347 compared to the corneas 1.376) that has been introduced into the corneal structure. *In vivo* this would most certainly interfere with the visual acuity of the cornea by changing the overall refractive index (Meek & Leonard, 1997) and therefore altering the refraction of the cornea, resulting in a different focus for the eye. The presence of fibrinogen within the ECM would also be expected to cause an interruption in the collagen fibril organisation that is partially responsible for maintaining the transparency of the cornea (Meek et al., 2003; Meek, 2002). Therefore, a topical treatment that would not just simply glue the flap down, but enhance the wound healing of the stroma, as well as maintaining the transparency needs to be found.

As the wound was by its nature easily detached, in order to preserve the morphology of the wound during processing, the size of each sample needed to be unusually large for TEM. This larger size resulted in poorer quality embedding, and the resultant inability to locate any wound landmarks. The morphology of the wound and the identification of the activated

cells during wound healing can be investigated by utilising H&E staining and immunolabelling instead.

The images of the H&E staining of the fibrinogen treated and untreated LASIK-like wounded corneas showed an increased cellularity in the untreated corneas and the presence of the fibrinogen filling the wound in the treated corneas. The wax sections of the samples provided good morphology of the corneal wound for H&E staining and can therefore be used to evaluate the wound healing process throughout the organ culture period.

Keratocyte activation occurs in the wound healing process of the cornea and can be identified using immuno-labelling to detect the presence of α-sma (an indicator of keratocyte activation). A higher cell number and presence of α-sma activated cells were observed in the immunolabelled samples of the untreated LASIK-like wounded organ cultured corneas as opposed to the fibrinogen treated samples (table 3.2). This may indicate a difference between the natural wound healing process of the untreated cornea and the possibly altered healing process of the fibrinogen treated cornea.

Use of this method to perform cell counts at all time points to follow cell number and percentage activation, as well as utilising Caspase-3 active immunolabelling to assess cell apoptosis and confirm the fate of the cells, would allow a more in depth analysis of corneal wound healing over the culture period. Both images obtained from the samples subjected to immunofluorescence showed a large amount of background staining which is not optimal for analysis and signal identification. The use of wax sections to evaluate keratocyte transformation into myofibroblasts using immunolabelling did not result in a good quality of image. A refinement of the protocol found that cryosectioned samples provided more distinct labelling with improved immunoreactivity resulting in stronger signals of the α-sma immunopositive cells and a reduced background signal.

The transparency of unwounded corneas reduced significantly after 4 weeks in organ culture (figure 3.12A). Whilst the Foreman air-interface method (Foreman et al., 1996) of

organ culture was an improvement over earlier methods where the tissue was immersed, it is impossible to entirely eliminate tissue swelling, which is responsible for the loss of transparency observed. The transparency of the unwounded corneas at 0 time point was higher than the microkeratome wounded corneas at 0 time point (figure 3.12C). This would most likely be due to the creation of the flap interface (with accompanying wrinkling) within the body of the stroma. When the wounded cornea was incubated for 4 weeks there was no further loss of transparency (figure 3.12B). This could be because the flap interface wrinkling had smoothed out, but the cornea had swollen during the 4 week incubation, resulting in a lower drop in transparency than would have been expected. Due to this swelling, the transparency had dropped to the same level as the unwounded cornea (figure 3.12D). There was no difference in the transparency between the fibrinogen treated and un-treated LASIK-like wounded corneas for either time point (figures 3.12E & F).

Spectrophotometry of the corneal samples provides numerical data relating to their transparency as a function of wavelength before and after organ culture, however it destroys the sample. Comparative analysis against visual transparency measurements using graph paper, as used in previous studies by Dooley et al. (2012) and Kamma-Lorger et al. (2010), provided a good comparative assessment method by which data could be collected for samples which would then be processed for histological analysis to maintain a narrative.

The data profiles of the graphs from the biomechanical testing in this study using the extensometer were not significant. Additionally, data profiles were inconsistent and showed that the time of detachment, and therefore the force required to do so, could not be reliably ascertained from the graph alone and required visual confirmation. The inconsistency of the profiles also suggested that other factors relating to the biomechanical testing of the corneas, such as the intraocular pressure (IOP) of the corneal sample, would need much tighter regulation. The testing also completely destroyed the corneal sample and rendered any further processing impossible. For these reasons, it was decided that a custom-built shear rig or rheometer would be a more appropriate method, so this line of investigation was discontinued for this current study.

Chapter 4

Optimisation of Application of OMLP-PCs to a Corneal Wound Bed

4.1. Introduction

Oral Mucosa Lamina Propria Progenitor cells (OMLP-PCs) are multipotent neural crest-derived progenitor cells found in the oral mucosa lamina propria that have been shown to demonstrate potent immunosuppressive qualities (Davies, et al., 2012). Their presence in the buccal mucosa is thought to promote preferential wound healing and accounts for the low rate of recurrent infections in the oral cavity despite the exposure to repeated mechanical trauma and the presence of diverse microflora and potentially harmful bacteria (Board-Davies et al., 2015).

In corneal wound healing, due to the optical necessity of maintaining the transparent nature of the tissue, the aim is to improve wound healing by increasing the biomechanical strength of the wound area in the healed cornea and reducing the formation of scar tissue and corneal haze. Research in recent years has explored the possibility of using topical applications of cells from varying sources as a potential stem cell-based therapy to realise this aim. Proposed cell-based therapies have included stem cells isolated from adult human corneal stroma with the potential for treatment of corneal opacity (Dua et al., 2009). This direction of research was continued by Morgan et al. (2014), using human corneal stromal stem cells to heal LASIK-like wounds i.e. penetrating wounds in ovine corneas, whilst Dooley et al (2012) investigated the use of oral mucosal fibroblasts as a potential therapeutic agent for corneal wound healing in similarly wounded ovine corneas.

Both of these studies used an organ culture model to test efficacy of these cell therapies on wound biomechanical strength, stromal cell number, keratocyte to myofibroblast transformation and percentage transparency over a 3-week period. Both experiments had positive outcomes (i.e. an increased transparency in treated corneas, an increase in biomechanical strength and a reduced myofibroblast expression). However, the source of cells for these cell-based therapies would require the *ex vivo* culturing of cells harvested from the patient (an autologous donation), over a period of weeks before the treatment could be applied to the wound without risk of rejection or infection. This may not be appropriate in all situations such as a traumatic injury where the therapy may be required

in a short time frame. Therefore, a non-autologous source of cells, in plentiful supply, that could aid the wound healing process of the cornea needs to be identified.

Such a potential source of non-autologous cells could be the previously mentioned oral mucosa lamina propria progenitor cells due to their possible preferential wound healing properties and potent immunosuppressive qualities (Davies et. al., 2012; Board Davies et al., 2015). A supply of OMLP-PCs as a cell-based therapy could potentially be ready to apply in an emergent situation.

Both ovine and bovine eyes have been used by previous researchers (Kamma-Lorger et al., 2010, Dooley et. al., 2012; Morgan et al., 2014) in their investigations into corneal wound healing using organ culture models. Bovine corneas used by Kamma-Lorger et al. (2010) in a manually induced flap wound were determined too large and inappropriate for creating semi-automatic LASIK-like flaps using a microkeratome. The ovine corneas used by Morgan et al. (2014) and Dooley et al. (2012) were an excellent substitute for human eyes, however during the early stages of protocol optimisation (Chapter 2), a high proportion of ovine eyes, in batches procured from local abattoirs, were found to have significant corneal scars and traumatic injuries (approximately 30%) which rendered them unviable for this research project. Pigs have been shown to be one of the best animals to be used in both *in vivo* and *ex vivo* organ culture models due to the similarity to the anatomy and physiology of humans (Jian Fei Wang et al., 2000) and have already been used in investigations into the promotion of scarless wound healing using oral mucosal fibroblasts in skin (Mak et al., 2009). The porcine cornea itself, although lacking a Bowmans layer, is similar in structure to the human cornea with both stromas containing a large amount of Type I collagen (Delmonte & Kim, 2011; Sanchez et al., 2011). The porcine central corneal thickness has been measured as approximately 666 µm *in vivo* and 1013 µm *ex vivo* (Faber et al., 2008), whilst a human cornea is approximately 500-550 µm *in vivo* (Delmonte & Kim, 2011). During the protocol optimisation of organ culture, it was found that the batches of porcine eyes procured had significantly lower percentage of scarred and injured corneas when compared to ovine eyes (Chapter 2). Therefore, the choice was made to use porcine eyes in this research.

Corneal injury usually results in altered collagenous structure within the extra-cellular matrix (ECM) (Jester et al., 1999; Piatigorsky, 2000) which can have a detrimental effect on the transparency of the cornea and subsequently the vision of the patient (Girgis et. al., 2007). During corneal healing of a penetrating wound, the damage to the epithelium initiates a wound healing cascade that results in keratocyte apoptosis and the activation of corneal keratocytes (Wilson et al., 2001). These activated cells have significantly reduced levels of crystallin proteins, ALDH1A1 and ALDH3A1 (Jester et. al., 2012) and a lowered refractive index compared to that of the quiescent keratocyte that no longer matches that of the surrounding tissue and therefore scatters light, reducing transparency (Gardner et al., 2015). They also produce ECM materials that have been shown to reduce corneal transparency and increase light scattering or 'corneal haze' (Jester et al., 1999; Pei et al., 2006, Jester et al., 2012). The success of the application of the OMLP-PC to a corneal wound could be measured by a reduction in activation of keratocytes, indicated by reduced expression of α-sma (Jester et al., 1999), and in turn, the subsequent maintenance or even improvement of corneal transparency.

4.2. Aim

The aim of this chapter was to optimise conditions, including finding the optimal cell concentration, for application of OMLP-PCs to a corneal wound bed (using a LASIK-like penetrating injury) in porcine corneas in an organ culture model for future experiments.

Towards this aim, the efficacy of three different concentrations of OMLP-PCs on cellularity, transparency and myofibroblast activation in the wounded porcine corneas was assessed at five different time points during LASIK-like corneal wound healing in the organ culture period.

4.3. Experimental Design

The concentration of the cell-based therapies applied to the stromal wound bed has varied in previous research and the reasoning for the selection of these concentrations has seemed arbitrary and unsupported by any evidence as to how they were chosen. Therefore, a determination of the optimal concentration of OMLP-PC solution to be applied to the wound bed was deemed necessary. The experimental design of this investigation also enabled the comparison of efficacy of OMLP-PCs to that of other previous cell-based therapies on corneal wound healing.

Fresh porcine eyes were procured from a local abattoir, disinfected, dissected and wounded as outlined in section 2.1.1. Three different cell lines of frozen human OMLP-PCs were obtained by Cardiff School of Dentistry and passaged as outlined in section 2.5.2. The cells were made up into concentrations of $1.5x10^4$, $1.5x10^5$ or $1.5x10^6$ OMLP-PCs ml^{-1} and a control solution of culture medium without cells, was also prepared. These three cell concentrations were selected based on previous successful cell-based applications to wounded corneas in a similar organ culture model. For instance, Dooley et al. (2012) applied $1.5x10^5$ cells ml^{-1} of oral mucosa fibroblasts and Morgan et al. (2014) applied $6.5x10^4$ cells/ml of corneal stromal stem cells in ovine organ culture models.

A 10 µl volume containing $1.5x10^4$, $1.5x10^5$ or $1.5x10^6$ OMLP-PCs ml^{-1} was applied to the wound bed of corneas in triplicate, and cultured in organ culture for 0, 1, 2, 3 and 4 weeks (see Table 4.1). At each time point, triplicate wounded corneas, treated with a 10 µl volume of media without cells were cultured as control corneas. At each appropriate time point, treated and control corneas were removed from culture and assessed for transparency, cellularity and α-sma expression. Transparency was assessed in triplicate corneas as outlined in section 2.11.2. These same corneas were then snap frozen and cryosectioned as described in sections 2.6.1, and 2.7.2. Myofibroblast transformation was assessed in these cryosections as a measure of percentage α-sma positivity. In brief, sections were incubated in primary antibody, mouse monoclonal anti-α-smooth muscle actin (A2547 Sigma, UK, 1 in 100 dilution) for 2 hours, rinsed and then incubated in donkey anti-mouse IgG (H+L)

Alexa Fluor®488 (Invitrogen, UK, at a 1 in 1000 dilution), with 2µl of 1mg ml^{-1} Hoechst 33342 solution (see section 2.8.2) added to each millilitre of secondary antibody solution.

Images of each section were acquired using a Leica DM6000 fluorescent microscope (Leica, Germany), α-sma positive cells and Hoechst labelled cell nuclei were counted above and below the wound edges at 3 sites (flap edge, centre and hinge region) across the wound. Percentage myofibroblast transformation was calculated as a measure of α-sma positivity i.e. the number of α-sma cells divided by the number of Hoechst labelled cells in a given area, multiplied by 100.

The number of corneas used is outlined in Table 4.1.

	Treatment	Time point	Processes
LASIK-like Wounded Porcine Corneas n=60	$1.5x10^4$ OMLP-PC ml^{-1} Concentration n=15	0, 1, 2, 3 & 4 week n=3 for each time point	·Visual Grading for Transaprency ·Immunofluoresence to Determine Keratocyte Activation and Cellularity
	$1.5x10^5$ OMLP-PC ml^{-1} Concentration n=15	0, 1, 2, 3 & 4 week n=3 for each time point	
	$1.5x10^6$ OMLP-PC ml^{-1} Concentration n=15	0, 1, 2, 3 & 4 week n=3 for each time point	
	Control Solution n=15	0, 1, 2, 3 & 4 week n=3 for each time point	

Table 4.1 Table demonstrating porcine cornea number.

Statistical analyses

Statistical analysis, using 2-way ANOVA and Tukey HSD, was carried out to compare the results of transparency, cellularity and percentage α-sma positivity of differing concentrations of OMLP-PCs at each time point and wound site for treated and control corneas.

Although the 2-way ANOVA was used as a statistical analysis for transparency, the results for transparency were in the form of ordinal data and so a Kruskhal Wallis was run, and the resulting statistics were the same.

Results

4.4. Effect of OMLP-PC therapy on keratocyte activation

Percentage activation of keratocytes, identified by α-sma-immunopositive cells (labelled with green fluorescence, figure 4.1), was ascertained at 3 adjacent sites in 3 different regions of interest (ROIs; flap edge, flap centre, flap hinge) in the epithelial-stromal flap (above the wound site) and the stromal wound bed (below the wound site). This was repeated for $1.5x10^4$, $1.5x10^5$ and $1.5x10^6$ OMLP-PC ml^{-1} applications and the wounded untreated control corneas at each organ culture time point.

Percentage α-sma immunopositivity was significantly increased ($p<0.001$) in all ROIs in both treated and control corneas (figure 4.2) at weeks 1, 2 and 3, compared to week 0 corneas. This was followed by a significant decrease at 4 weeks in the percentage of α-sma immunopositivity ($p<0.001$) in all treated corneas for each cell concentration. An apparent decrease in untreated control corneas was not statistically significant ($p>0.05$). Notably, the percentage α-sma immunopositivity was significantly lower at 1,2,3 and 4 week time points in cell treated corneas (figure 4.2), compared to control corneas at the same time points ($p<0.001$). There was no significant difference in α-sma immunopositivity in corneas treated with $1.5x10^4$, $1.5x10^5$ or $1.5x10^6$ OMLP-PCs ml^{-1} at any time points during the organ culture period.

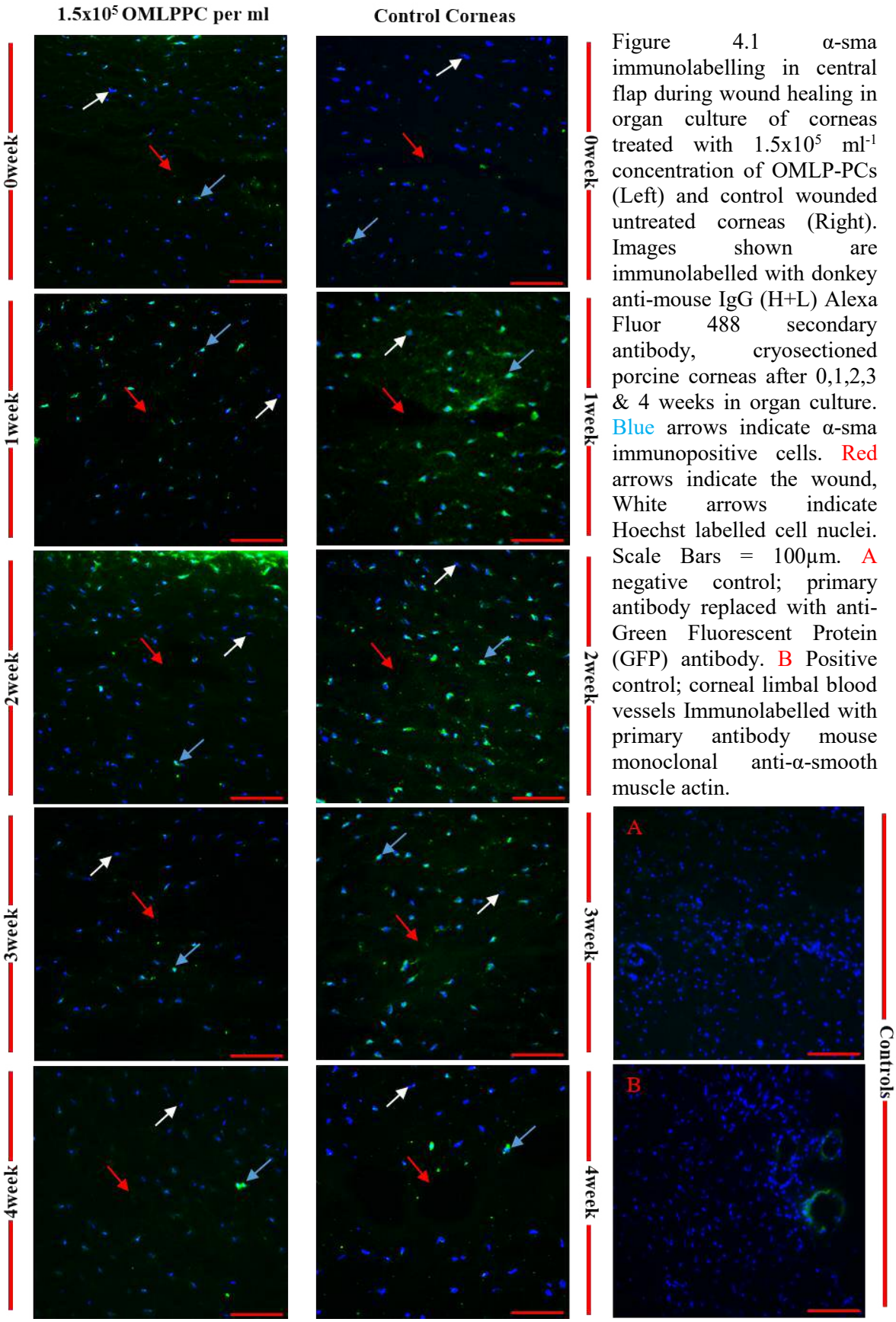

Figure 4.1 α-sma immunolabelling in central flap during wound healing in organ culture of corneas treated with $1.5x10^5$ ml^{-1} concentration of OMLP-PCs (Left) and control wounded untreated corneas (Right). Images shown are immunolabelled with donkey anti-mouse IgG (H+L) Alexa Fluor 488 secondary antibody, cryosectioned porcine corneas after 0,1,2,3 & 4 weeks in organ culture. Blue arrows indicate α-sma immunopositive cells. Red arrows indicate the wound, White arrows indicate Hoechst labelled cell nuclei. Scale Bars = 100µm. A negative control; primary antibody replaced with anti-Green Fluorescent Protein (GFP) antibody. B Positive control; corneal limbal blood vessels Immunolabelled with primary antibody mouse monoclonal anti-α-smooth muscle actin.

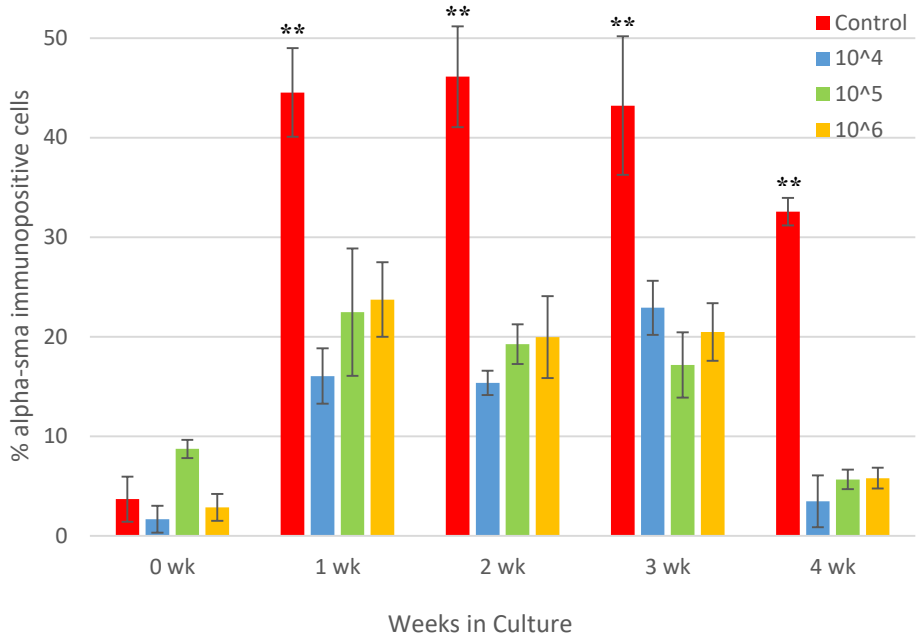

Figure 4.2 Total percentage α-sma immunopositive cells at wound site (above and below wound) in all three ROIs during 4 weeks organ culture. OMLP-PC treated corneas, for all cell concentrations, had a significantly lower percentage of α-sma immunopositive cells (**p<001) compared to untreated control corneas at 1, 2, 3 and 4 week time points.

The percentage activation of keratocytes in the epithelial flap wound (above the wound) across all ROIs (figure 4.3) followed the same trend as was seen in figure 4.2 across the entire corneal sample. Increased keratocyte activation at 1, 2, and 3 weeks for cell treated and control corneas was observed, when compared to 0 time point ($p<0.05$). At 4 weeks there was a significant reduction in keratocyte activation for cell-treated samples ($p<0.05$), and once more a noticeable decrease for untreated control corneas not statistically significant ($p>0.05$) (figure 4.3). In the epithelial-stromal flap wound the percentage of keratocyte activation for corneas treated with OMLP-PCs was significantly higher that untreated control corneas at weeks 1, 2, 3 and 4 (figure 4.3).

Keratocyte activation of the stromal wound bed across all ROIs, whilst showing a visible increase after 0 time point for weeks 1, 2 and 3, had no statistically significant difference between all OMLP-PC treated corneas at all time points (figure 4.3). There was a significantly lower percentage of keratocytes in the OMLP-PC treated corneas when compared to untreated control corneas ($p<0.001$) during the organ culture period for weeks 1, 2, 3 and 4 (figure 4.3).

The 3 different concentrations of the cell solution all showed that the keratocyte activation above the wound was statistically higher when compared to below the wound at weeks 1, 2 and 3 ($p<0.05$), whereas the keratocyte activation above and below the wound in the control corneas showed no significant difference throughout the organ culture period (figure 4.3).

Whilst the percentage of α-sma immunofluorescent cells was significantly different depending on whether it was observed above or below the wound in the cell-treated corneas, the regional site of the cell count i.e. flap edge, flap centre or flap hinge, revealed no statistically significant effect on the α-sma expression at any time points for both cell treated or control samples ($p>0.05$).

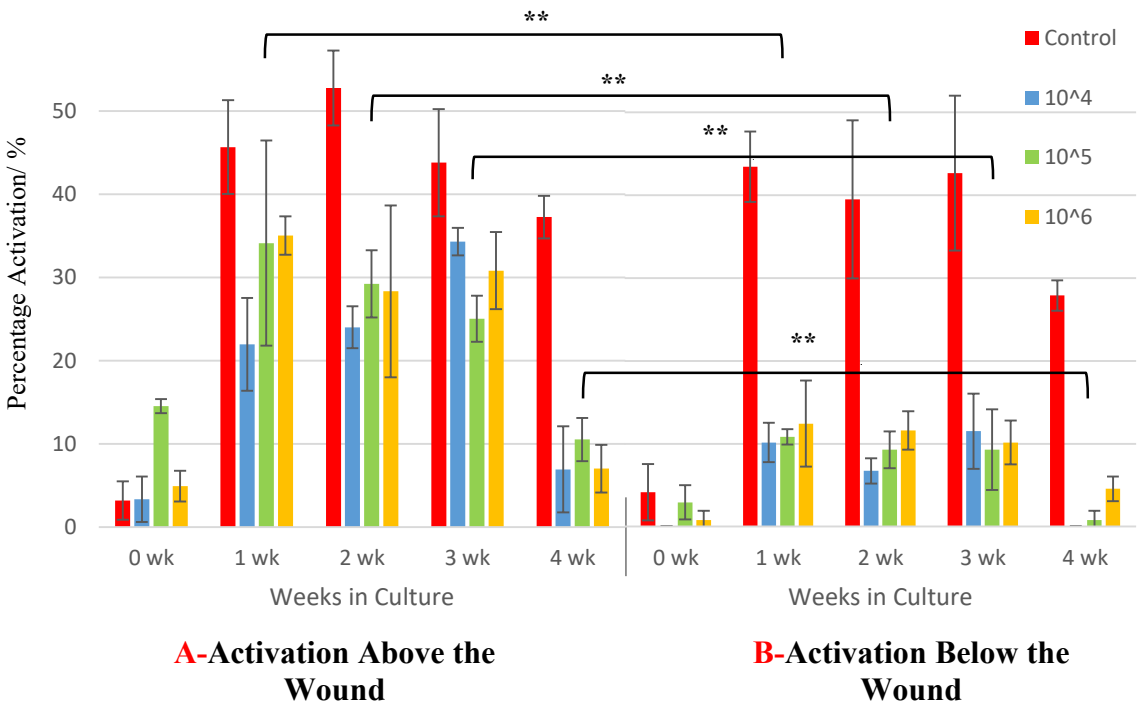

Figure 4.3 Percentage Activation of Keratocytes (Percentage α-sma immunopositive cells) above and below the wound Site A Percentage α-sma immunopositivity in epithelial flap (above) and B stromal (below) wound bed (averaged data across all 3 ROI sites for controls and cell treated corneas) as a function of culture time. All concentrations showed a significantly higher activation above the wound than below for weeks 1, 2, 3 and 4 ($p<0.01$, marked on the graph for only $1.5x10^5$ cells ml^{-1}).

4.5. Keratocyte cellularity

Keratocyte cellularity during organ culture refers to the number of cells counted as a measure of Hoechst-labelled nuclei (labelled blue in figure 4.1). Figure 4.4 shows that the cellularity at the wound site was significantly higher in corneas treated with $1.5x10^5$ cells ml^{-1} at 2 and 4 weeks, than in the respective controls ($p<0.05$). Interestingly, corneas treated with $1.5x10^4$ and $1.5x10^6$ cells ml^{-1} had significantly higher cellularity at 3weeks, when compared to the control corneas ($p<0.05$, figure 4.4).

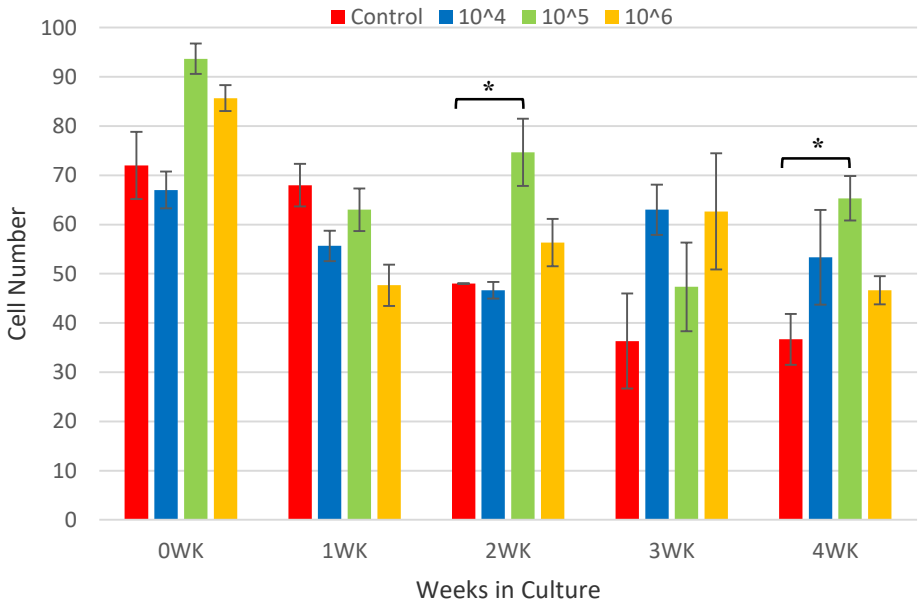

Figure 4.4 Total Cell Count in corneal wound area calculated as the total number of Hoechst labelled cell nuclei in all 3 ROIs above and below the wound (average of n=3 for each time point) over a 4 week organ culture period.

When treated with different cell concentrations, appart from the differences in cellularity seen in figure 4.4 between the control corneas and the corneas with cell solutions applied to the LASIK-like wound bed, there were no significant differences between the cellularity above (figure 4.5A) and below (figure 4.5B) the wound for cell treated or control and no significant difference between each ROI (figures 4.5 C, D & E).

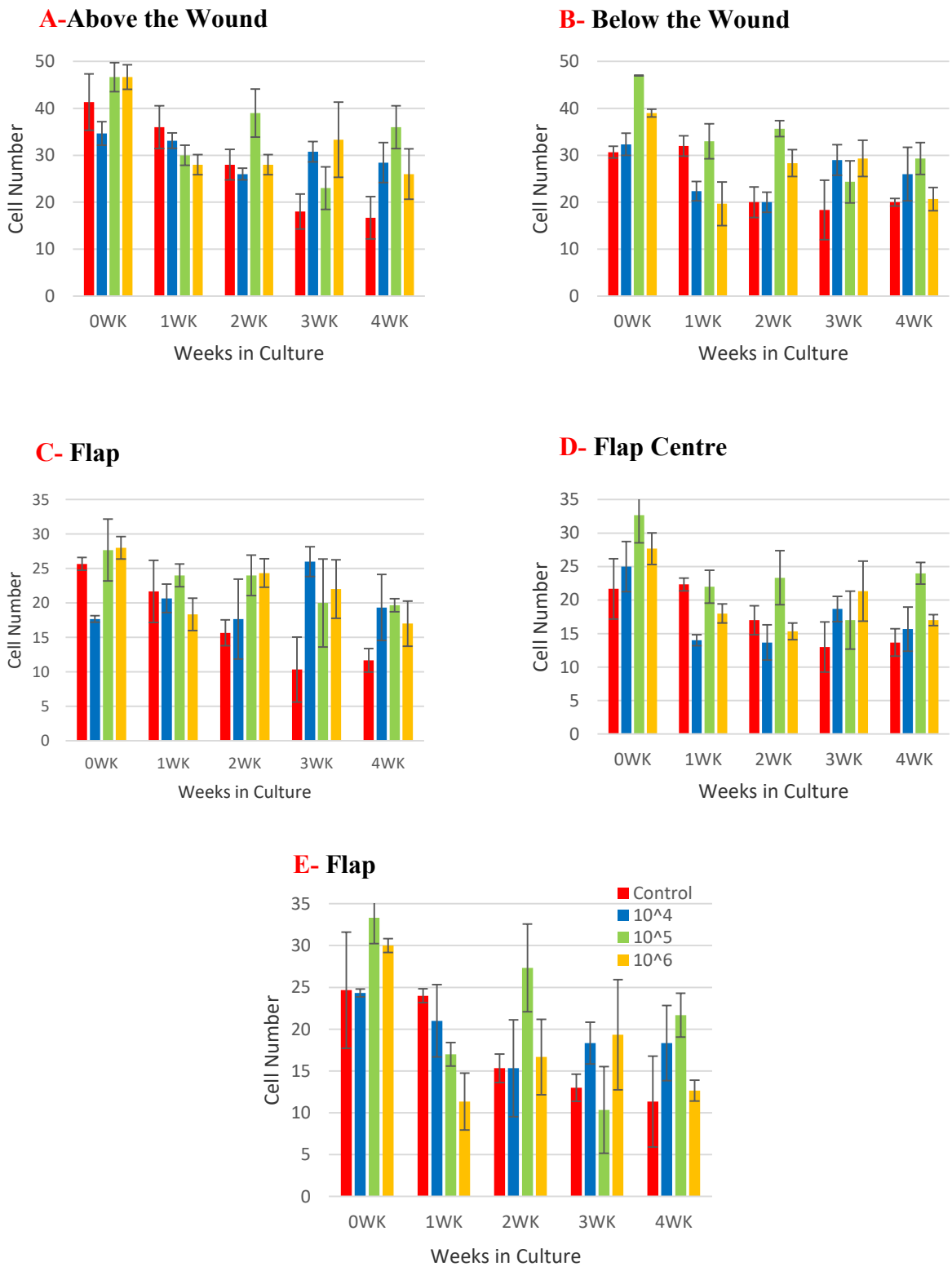

Figure 4.5 A Cell Count above wound. B Cell Number Below Flap below wound (A & B show Number of Hoechst labelled cells at all 3 ROI's for above the LASIK-like wound for an n=3 over a 4 week organ culture period). C Cell Count at Flap Edge. D Cell Count at Flap Centre E Cell Count at flap Hinge (C, D & E show number of Hoechst labelled cells above and below the LASIK-like wound at each ROI for an n=3 over a 4 week organ culture period

4.6. Transparency Measurements

Figure 4.6 demonstrates representative images of corneas used for transparency grading; acquired immediately following removal from organ culture. The corneas (n=3 for each cell concentration and control at each time point) were imaged using a Leica MZ10F dissecting microscope (Leica, UK) while overlying scaled graph paper (as described in section 2.11.2).

Images were masked and placed in random order. Ten people, masked to organ culture time and treatment, were asked to determine whether the corneas appeared “clear”, moderately cloudy” or “cloudy”. Arbitrary numerical values, 1 to 3, were then applied to these ‘grades’ to allow for statistical analysis (figure 4.7).

The data for the transparency is shown in Figure 4.7, the higher the value on the y axis the higher the transparency. The transparency for all samples decreased similarly after the initial time point and the remained constant with no significant difference between the control corneas and those treated with OMLP-PCs at all concentrations.

The transparency of the corneas was found to be significantly higher ($p < 0.001$) in all 0 time point corneas compared to those subjected to organ culture (figure 4.7).

During the organ culture period, no significant difference in corneal transparency was observed between corneas treated with OMLP-PCs and control corneas at weeks 0, 1, 2 and 3. However, at week 4, the porcine corneas treated with a $1.5x10^5$ OMLP-PCs ml^{-1} had a significantly higher visually graded transparency than, not only the control corneas, but also the other OMLP-PC treated corneas ($p<0.001$, see figure 4.7)).

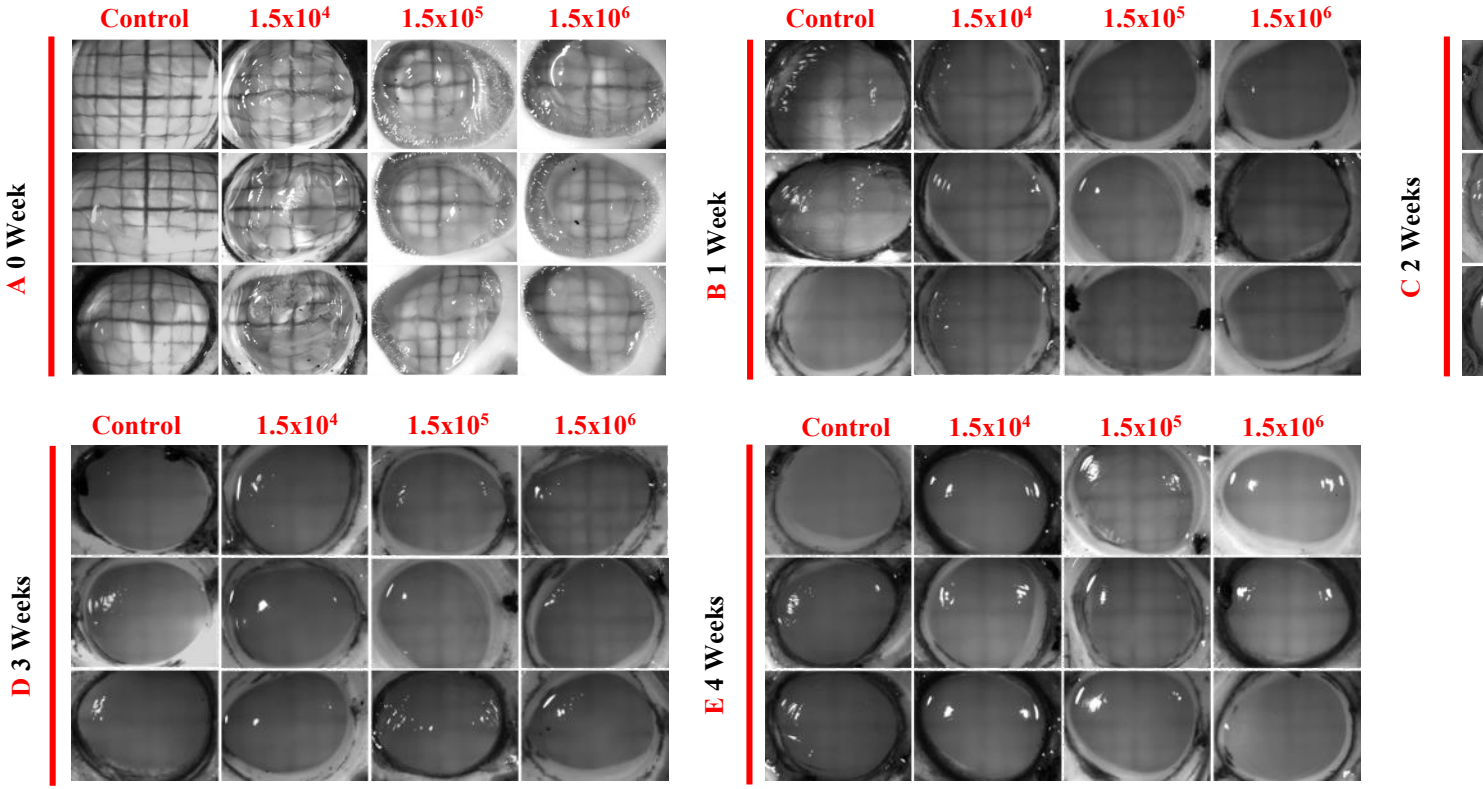

Figure 4.6 Images of LASIK-like wounded corneas; control and treated (cell concentrations of $1.5x10^4$ 1.5x10 used to grade corneal transparency at 0 time point (A), 1 (B), 2 (C), 3 (D) and 4 (E) weeks in organ culture.

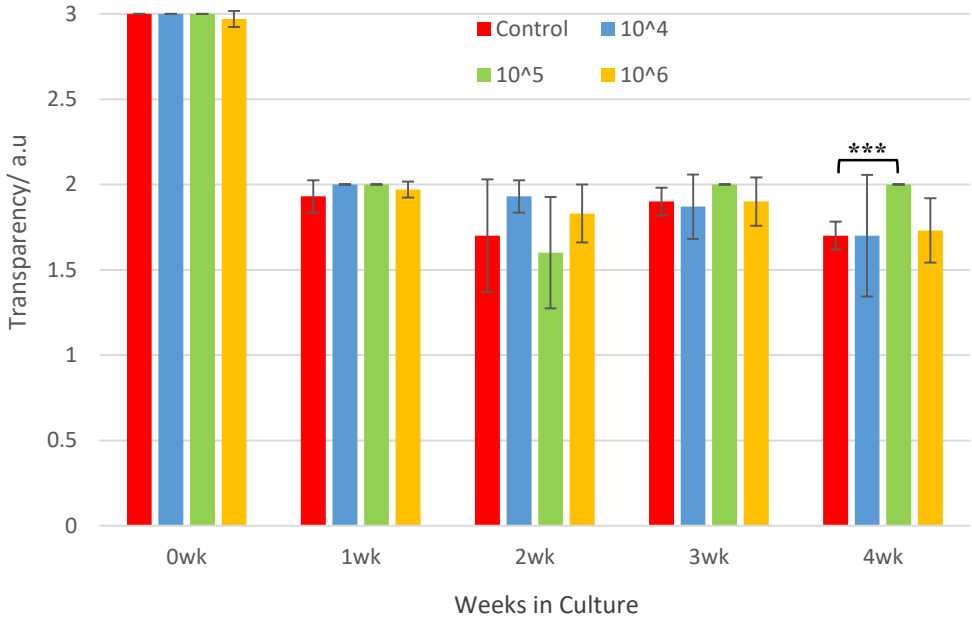

Figure 4.7 Corneal Transparency. Visually graded transparency of LASIK-like wounded corneas with an application of either a control solution or a cell solution of OMLP-PCs at 3 different concentrations at 5 time points over an organ culture period. Treated corneas at $1.5x10^5$ OMLP PC ml^{-1} concentration were significantly more transparent at 4week time point than untreated controls (***$p<0.001$)

4.7. Discussion

In this experiment, the organ culture model based on Foreman et al. (1996), and refined over subsequent investigations into corneal wound healing by Carrington et al. (2001), Kamma-Lorger et al. (2009), Mi et al. (2011), Dooley et al. (2012) and Morgan et al. (2013) was used to assess the wound healing of LASIK-like wounds in porcine corneas over a 4 week culture period. Three concentrations of the OMLP-PCs from a single donor source, were applied to the wound bed under the LASIK-like flap, which was then relayed back, prior to being placed in organ culture. These were varied by a factor of ten ($1.5x10^4$, $1.5x10^5$ and $1.5\ x10^6$ cells ml^{-1}, to include cell numbers used in previous cell therapy investigations) and cultured alongside un treated control corneas.

The main question under investigation in this chapter was the determination of the optimum concentration of OMLP-PC solution for application to the stromal wound bed of LASIK-like wounds in porcine corneas. In order to determine the optimum cell concentration to be applied to the wound bed in future experiments, three different OMLP-PC concentrations were examined with regards to α-sma expression (an indication of keratocyte activation and transformation in myofibroblast phenotype (Jester et al., 1999), cellularity, and transparency, over an organ culture period of 4 weeks.

However, another important question in these initial experiments was the viability of the protocols in general and whether the results of the application of OMLP-PCs to the LASIK-like wound, regardless of concentration, would yield comparable results to those therapeutic cell solutions used in previous research (Dooley et al., 2012; Morgan et al., 2013) and therefore allow us to proceed with this line of investigation.

During normal corneal wound healing, myofibroblastic transformation of keratocytes plays a major role in ECM deposition, collagen fibril organisation and wound contraction (Petroll et al., 1993; Jester et al., 1999). These myofibroblasts can be detected by the intracellular appearance of α-sma (Jester et al., 1987 & 1995). Therefore, in this study percentage activation of keratocytes in the wounded corneas was determined following cell counts of Hoescht labelled cell nuclei and α-sma immunopositive cells in organ cultured porcine corneas over the organ culture period. This was compared to previous research by Dooley (2012) and Morgan (2014). Dooley applied a solution of oral mucosal fibroblasts to LASIK-like wounded ovine corneas which were then placed in organ culture alongside controls for 3 weeks. The results showed that the percentage activation for the keratocytes was significantly reduced by approximately 20-30% for the corneas treated with oral mucosa cells, when compared to the control corneas after weeks 1, 2 and 3 in organ culture (Dooley, 2012). Similarly, Morgan et al. (2014) found that the percentage keratocyte activation for wounded corneas treated with a solution of corneal stromal stem cells (CSSCs) was significantly reduced compared to the control corneas at 1, 2 and 3 weeks in organ culture, by approximately 20%. The results observed in this experiment were favourably comparable to the outcomes of these previous studies; the averaged percentage

activation of all the different cell concentrations and the average results of the control corneas showed an overall reduction of approximately 20-30% in activation of keratocytes over the same 3 weeks in organ culture as Dooley and Morgan (table 4.2), indicating a successful experimental design.

	% Activation		
	1 week	2 week	3 week
Dooley (2012)			
Oral Mucosal	26.63%	17.10%	21.62%
Control	49.84%	49.11%	41.65%
Morgan (2014)			
CSSC	19%	30%	29%
Control	24%	48%	44%
Current Study			
OMLP-PC	20.8%	18.2%	20.2%
Control	44.5%	46.1%	43.2%

Table 4.2 Comparison of % Keratocyte Activation to Previous Research.

The percentage activation of keratocytes across the entire cornea for the differing cell concentrations applied (figure 4.5) was not statistically significantly different from one another throughout all time points during the organ culture period. Whilst the cell-treated corneas exhibited a significant difference between the keratocyte activation in relation to the LASIK-like wound (higher activation above the wound when compared to below), the difference between the varying concentrations was not significant.

Following penetrating corneal injury and subsequent scarring, the decrease in transparency has been shown to be associated with disorganised collagen fibril structure compared to the native tissue in the unwounded cornea (Cintron et al., 1981; Rawe et al., 1994). As previously mentioned, these changes are largely brought about by the activation of keratocytes into myofibroblasts, characterised by the expression of α-sma and have

significantly reduced corneal crystallin expression (Pei et al., 2006; Jester et al., 1999), which in turn, also has a negative impact on corneal transparency. The transparency of the corneas over the organ culture period was significantly reduced from the initial measurements at 0 week for both the control and the cell solution-treated corneas, to the 1 week time point, and this level of transparency was then maintained throughout the remainder of the organ culture. This would be partly due to corneal swelling caused by time in organ culture which increases the thickness of corneal tissue, which, in turn has a negative impact on the propagation of light through the cornea (Hart and Farrell, 1969; Freund et al., 1991; Farrell & McCally, 2000; Meek et al., 2003; Doutch et al., 2008).

Therapies reducing the appearance of myofibroblasts by suppressing the release of TGFβ (Shii et al., 2009) and neutralising antibodies to TGFβ (Møller-Pedersen et al., 1998) have been shown to reduce the appearance of corneal haze, thus improving the transparency, in the healed cornea. Cell based therapies used by Dooley (2012) and Morgan (2013) showed that the transparency for those corneas subjected to an application of a therapeutic cell solution was significantly increased by approximately 10% in both cases when compared to the control corneas. The outcomes of this experiment, whilst not improving the transparency of the cornea during wound healing, did not significantly reduce it. At week 4, the end of the organ culture period, the transparency of those corneas treated with a $1.5x10^5$ cells per ml concentration OMLP-PC solution significantly increased when compared to the control corneas, and those treated with the other 2 cell concentrations. This indicated that a concentration of OMLP-PC at $1.5x10^5$ cells per ml had a statistically significant positive effect on corneal transparency towards the end of organ culture period.

The cellularity of the corneas treated with $1.5x10^5$ OMLP-PC ml^{-1} was significantly higher at 0 week, 2 weeks and 4 weeks when compared to the other treated and control corneas. The increased number of Hoechst labelled cells counted at the 2 week time point in the$1.5x10^5$ OMLP-PC ml^{-1}-treated LASIK-like wounded corneas could be indicative of increased proliferation during the cell replenishment that follows apoptosis during initial wound healing (Wilson, 2002). Oral mucosal fibroblasts have been shown to proliferate faster than dermal fibroblasts (Lee & Eun, 1999) and so could account for the significantly

increased cellularity of those corneas treated with a $1.5x10^5$ OMLP-PC ml^{-1} solution compared to the controls. The other concentrations did not show a similarly significant difference in cellularity, indicating that perhaps the lower and higher concentrations of OMLP-PCs had a negative effect on the efficacy of the OMLP-PCs due to under-population and over-population, respectively.

During the course of this study to determine the optimal concentration of OMLP-PCs for application to the wound bed, the results showed significant differences between the cell-treated and the control corneas in line with previous research by others, especially with respect to the keratocyte activation. When compared to each other, however, the 3 concentrations of OMLP-PCs were not statistically different to one another throughout the organ culture time points when investigating keratocyte activation. However, there was a positive result of the increasing transparency of those corneas treated with $1.5x10^5$ cells per ml of OMLP-PC solution at the end of the organ culture period when compared to other concentrations and the controls. Also the significantly higher cellularity of the corneas treated with $1.5x10^5$ cells ml^{-1} of OMLP-PC solution at the 2 week time point could indicate an increased rate of proliferation of the OMLP-PCs at this concentration. There were statistically significant results in this chapter, however the low number of samples used in this determination may have elicited unreliable results and so the concentration $1.5x10^5$ cells ml^{-1} of OMLP-PC would be logical to use as it was similar to concentrations used in previous research and the middle concentration. Therefore, the decision was made to proceed in all subsequent experiments with the application of a cell concentration of $1.5x10^5$ OMLP-PCs ml^{-1} prepared as outlined in section 2.5.2.

Chapter 5

Application of OMLP-PCs to Penetrating Corneal Wounds: Effect on Stromal Healing and Transparency

5.1 Introduction

The inflammatory and proliferative stages in the complex biological process of corneal wound healing (as described previously in section 1.5) often leads to significant changes in the organisation of the stromal collagen which, in turn, negatively effects the corneal transparency and biomechanical properties that rely on the highly ordered nature and precise spacing of the native tissue (Meek, 2009). Transparency in the wounded cornea can be negatively affected by the natural need to rapidly close the wound in order to provide protection to the underlying structures and avoid potential infection. The laying down of disorganised stromal collagen that reduces the efficacy of light transmission, increasing light scatter results in an opaque cornea. Also contributing to corneal haze are the fibroblastic changes following activation with cytokines and inflammatory growth factors (Jester et al., 1999; Piatigorsky, 2000) These include a reduction in crystallin protein concentration that alters the refractive properties of myofibroblasts and fibroblasts (Jester et al., 2012) causing light scatter.

Whilst, following the initial wound healing response, the cornea can continue to remodel over many months, a return to the exact original organised nature of the native tissue never occurs and significant scarring can be the result (Lee et al., 1982; Cintron et al., 1990). If this scarring is unfortunately located on the visual axis this can be permanently detrimental to the patient's vision potentially requiring surgical treatment such as keratoplasty (corneal transplant). Research into novel cell-based therapies to improve the biomechanical strength and ameliorate the formation of corneal haze and scarring is, therefore, clinically important.

Recent research has looked into the application of fibronectin based glues and the use of corneal cross linking (Littlechild et al., 2012, Mi et al., 2011), as well as application of corneal stromal stem cells, activated corneal fibroblasts and various signal inhibitors and growth factors (Kamma-Lorger 2007; Müller et al., 2005; Morgan, 2015) with varying results. More recently, attention has been brought to the oral mucosa as a potential future source for non-autologous cell based therapies, with Dooley, 2012, successfully applying oral mucosal fibroblasts cells to the wound bed of LASIK-like wounded corneas.

There is a history of autologous oral tissue transplantation to repair ocular conditions, including OOKP (osteo-odonto-keratoprosthesis) (Liu et al., 2005) and tissue engineered oral mucosal epithelial cell sheets (Nishida et al., 2004) with good reason. The oral mucosa undergoes mechanical trauma on a regular basis due to mastication and so requires a rapid cell turnover and benefits from privileged wound repair. Whilst early studies involving de-salivated animal models suggested that saliva was the origin of the oral mucosa's enhanced wound resolution (Bodner et al., 1992; Hutson et al., 1979), more recently it has been determined that, rather than being due to environmental factors such as saliva and temperature, this is related to the intrinsic characteristics of the oral mucosa (Szpaderska et al., 2003). Oral mucosa fibroblasts have been shown to exhibit both adult and foetal-like properties (Sloan, 1991), resulting in the preferential wound healing observed in the oral mucosa, with rapid re-epithelialisation, remodelling with minimal scarring and very rare formation of keloid or hypertrophic scarring that is comparable to foetal wound repair (Stephens et al 1996; Mak et al., 2009). The intra-oral mucosal fibroblasts differ from the superficial extra-oral epithelium due to their ability to synthesise collagen and ECM components without expressing excessive amounts of alpha-smooth muscle actin (α-sma), associated with a myofibroblast phenotype. Therefore, it is thought that these cells produce factors that are possible inhibitors of fibroblast cells returning to homeostasis (Wilson et al., 2000). Due to these properties, cells and tissues from the oral mucosa have been widely utilised successfully in attempts to enhance wound healing properties of other organs (Ohki et al., 2006) including the cornea (Nishida et al., 2004; Nakamura et al., 2004).

A population of multipotent neural crest-derived progenitor cells within the lamina propria of the oral mucosa (figure 5.1), oral mucosa lamina propria progenitor cells (OMLP-PCs), have demonstrated not only potent immunological properties but also innate broad spectrum antibacterial properties. OMLP-PCs, therefore, are an ideal source for non-autologous cell-based therapies (Davies et al., 2012; Board-Davies et al., 2015).

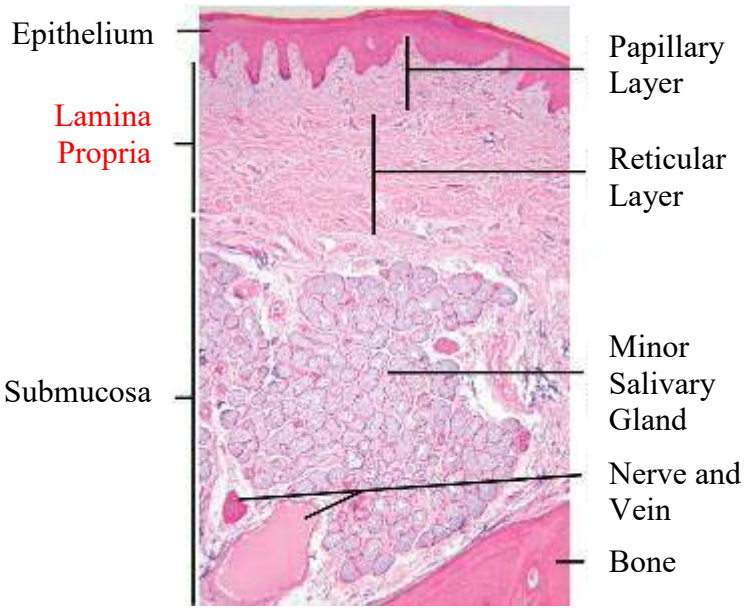

Figure 5.1 Histology section through the Oral Mucosa. The location of the Oral Mucosa Lamina Propria Progenitor cells (OMLP-PCs) within the Lamina Propria (Adapted from Fleisch et al., 1978).

It is well established that alpha smooth muscle actin (α-sma) is expressed in activated myofibroblasts during the contraction phase of a wound (Jester et al., 1987 & 1995). Their presence, as previously discussed, not only reduces the production of crystalline proteins in the cells, increasing light scatter, but also increases the deposition of opaque ECM and contractile forces, therefore diminishing transparency in the cornea. Whilst OMLP-PCs have been found to have the ability to differentiate into tissue lineages removed from their origin (Davies et al., 2012), and can differentiate into myofibroblasts, they have also been shown to express significantly lower levels of α-sma (Shannon et al., 2006). Interestingly, Tsai et al. (1995) and Lee and Eun (1999) found oral fibroblasts to have the smaller contractile potential compared to dermal fibroblasts during wound healing. These differences in phenotype between the native myofibroblast and the potentially differentiated OMLP-PCs as a therapy to apply to corneal wounds, could have a positive effect on the wound resolution resulting in improved transparency and a tissue closer to that of the native unwounded cornea.

5.2. Aim

Following determination that OMLP-PCs, at an optimal concentration, can affect corneal transparency and α-sma expression following application to a penetrating corneal wound (Chapter 4), in this chapter the optimised OMLP PC concentration from different donor sources will be applied to corneal wounds.

The aim of this chapter was to determine whether or not the wound healing of LASIK-like wounded porcine corneas could be improved by the application of OMLP-PCs to the wound bed over a course of 4 weeks. This would be assessed by measuring the cell proliferation and cellularity, monitoring and quantifying the transparency of the wound healing cornea, determining the level of apoptosis and calculating the percentage α-sma expression.

5.3. Experimental Design

Fresh porcine eyes were procured, dissected and wounded as outlined in sections 2.1 and 2.2. OMLP-PCs were obtained from Cardiff School of Dentistry from 3 different human donors and passaged as outlined in section 2.5.1.

10 µl aliquots, containing $1.5x10^5$ OMLP-PCs/ml in culture media or control media (i.e. the same media without cells) were applied to the wound bed of quadruplicate corneas, and subjected to organ culture as previously described (see section 4.7). Quadruplicate corneas were removed from corneal organ culture at each time-point, namely 0 (not cultured), 1, 2, 3 or 4 weeks. Additionally, to determine corneal changes as a function of organ culture, 4 unwounded, untreated corneas were also cultured for each time point. On removal from culture, transparency was assessed immediately in quadruplicate corneas as outlined in section 2.11.2. These same corneas were then snap frozen and cryosectioned as described in sections 2.6.1, and 2.7.2 for subsequent labelling.

Myofibroblast transformation was assessed in these cryosections as a measure of percentage α-sma positivity. In brief, sections were incubated in primary antibody, mouse monoclonal anti-α-smooth muscle actin (A2547 Sigma, UK, 1 in 100 dilution) for 2 hours, rinsed and then incubated in donkey anti-mouse IgG (H+L) Alexa Fluor®488 (Invitrogen, UK, at a 1 in 1000 dilution) with 2µl 1mg/ml Hoescht 33342 added to each millilitre secondary antibody solution (see section 2.8.2).

Cell proliferation was assessed as a measure of percentage proliferation, and followed the same immunolabelling procedure described for α-sma immunolocalisation, except that the primary antibody used was a rabbit anti-PCNA antibody (ab18197 Abcam, UK), at a 1 in 100 dilution and the secondary antibody was a donkey anti-rabbit IgG (H&L) Alexa Fluor®555 (ab150062 Abcam, UK at 1in 1000 dilution).

To determine cell apoptosis at the wound site immunolocalisation of anti-active caspase-3 antibody (ab49822, Abcam, UK) was performed on cryosections as detailed in section 2.8.3.

Images of each corneal section were acquired using a Leica DM6000 fluorescent microscope (Leica, Germany), from three wound sites (flap edge, centre and hinge region), and labelled cells were counted above and below the wound edges and expressed as a percentage of total cells (i.e. number of Hoechst labelled cell nuclei). For the unwounded corneas, as the regions of interest could not be dictated by an inflicted wound, surrogate areas at similar corneal depths and regions were imaged and analysed.

The number of porcine corneas used for each cell line and control group for LASIK-like wounded corneas and for unwounded corneas at each time point is outlined in Table 5.1

	Treatment	Time point	Processes
LASIK-like Wounded Porcine Corneas n=80	OMLP-PC Cell Line 1 n=20	0, 1, 2, 3 & 4 week n=4 for each time point	·Visual Grading for Transaprency ·Immunofluoresence to Determine Keratocyte Activation and Stromal Cell Proliferation and Apoptosis
	OMLP-PC Cell Line 2 n=20	0, 1, 2, 3 & 4 week n=4 for each time point	
	OMLP-PC Cell Line 3 n=20	0, 1, 2, 3 & 4 week n=4 for each time point	
	Control Solution n=20	0, 1, 2, 3 & 4 week n=4 for each time point	
Unwounded Porcine Corneas n=20	-	0, 1, 2, 3 & 4 week n=4 for each time point	

Table 5.1 Table demonstrating porcine cornea number.

Statistical Analysis

Statistical analysis, following determination of a normal data distribution a 2-way ANOVAs and Tukey HSD were performed to determine the effect of OMLP-PC application on corneal transparency, total stromal cellularity, percentage α-sma positivity, percentage stromal cell proliferation and apoptosis as a function of culture duration. Additionally, inter-donor cell line application of 3 differing OMLP-PCs cell lines was also analysed.

Results

5.4. Keratocyte activation and myofibroblast activation: α-sma immunopositivity

The green fluorescently labelled α-sma immunopositive cells were identified amongst non-activated keratocytes (Hoechst-blue labelled nuclei) in treated and control wounded corneas at all time points in organ culture (figure 5.2). Overall, there was a significant increase ($p<0.01$) in percentage α-sma immunopositive cells from the 0 time point to the 1 week time point in all wounded corneas, those treated with three different cell lines of OMLP-PCs and untreated controls (figure 5.3). This increase was maintained across the organ culture weeks 1, 2 and 3; then at week 4, percentage α-sma immunopositivity significantly decreased in both treated and untreated wounded corneas ($p<0.01$, figure 5.3). The unwounded control corneas maintained a low percentage α-sma immunopositivity throughout organ culture week ($p<0.05$, figure 5.3).

The wounded OMLP-PC treated corneas (all three cell lines) had a significantly lower percentage keratocyte activation at weeks 1, 2, 3 and 4 when compared to the untreated wounded control corneas ($p<0.001$, figure 5.3), and significantly higher percentage α-sma expression than the unwounded control corneas at all time points ($p<0.001$, figure 5.3). There was no significant difference in the percentage α-sma immunopositivity between cell lines at all points during the organ culture ($p>0.05$).

No significant difference was found with regards to α-sma expression, whether above or below the wound, in both the OMLP-PC treated controls and the untreated wounded control samples ($p>0.05$) during the organ culture in the differing regions of interest of the wound site (flap edge, flap centre, flap hinge).

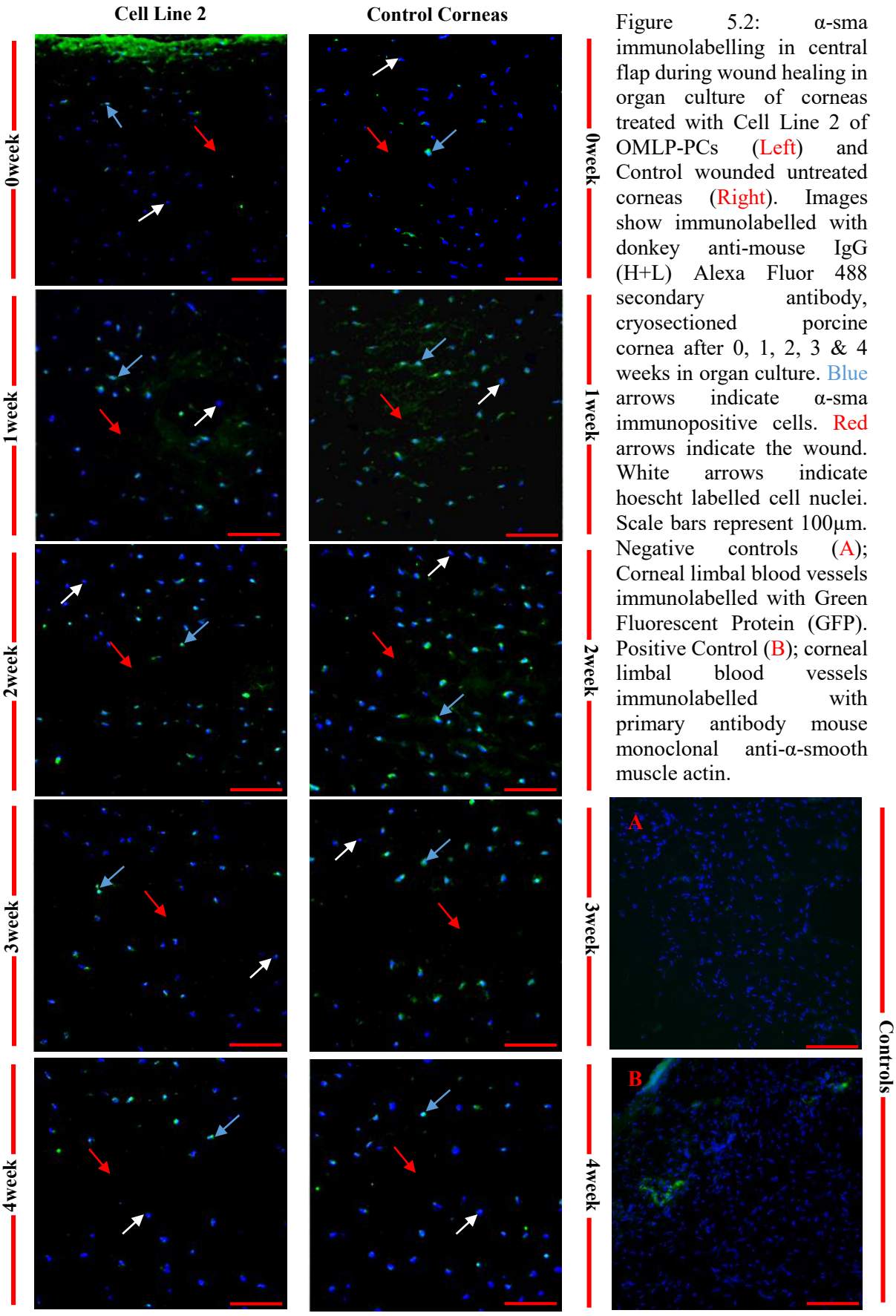

Figure 5.2: α-sma immunolabelling in central flap during wound healing in organ culture of corneas treated with Cell Line 2 of OMLP-PCs (Left) and Control wounded untreated corneas (Right). Images show immunolabelled with donkey anti-mouse IgG (H+L) Alexa Fluor 488 secondary antibody, cryosectioned porcine cornea after 0, 1, 2, 3 & 4 weeks in organ culture. Blue arrows indicate α-sma immunopositive cells. Red arrows indicate the wound. White arrows indicate hoescht labelled cell nuclei. Scale bars represent 100µm. Negative controls (A); Corneal limbal blood vessels immunolabelled with Green Fluorescent Protein (GFP). Positive Control (B); corneal limbal blood vessels immunolabelled with primary antibody mouse monoclonal anti-α-smooth muscle actin.

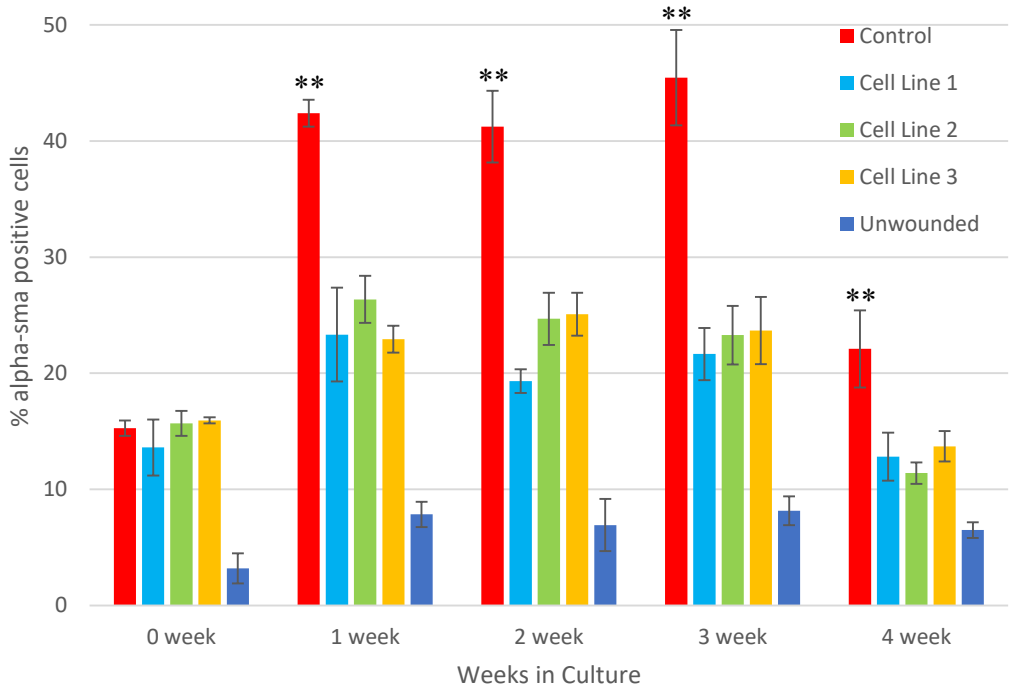

Figure 5.3 Total percentage α-sma immunopositive cells across wound site (above and below wound in all 3 ROIs.) during 4 weeks organ culture. OMLP-PC treated corneas, for all cell concentrations, had a significantly lower percentage of α-sma immunopositive cells (**p<001) compared to untreated control corneas at 1, 2, 3 and 4week time points and a significantly higher percentage keratocyte activation compared to unwounded control cornea at all time points. Error bars represent SD.

However, across all time points during the organ culture in all OMLP-PC treated wounded corneas (with all three cell lines), the percentage α-sma immunopositivity was significantly higher when measured above the wound in the epithelial stromal flap compared to in the stromal wound bed below the wound, ($p<0.001$, figure 5.4). This significant higher α-sma immunopositivity above the wound compared to below ($p<0.001$) was also observed in the control wounded corneas at all 5 time points during the organ culture period (figure 5.4).

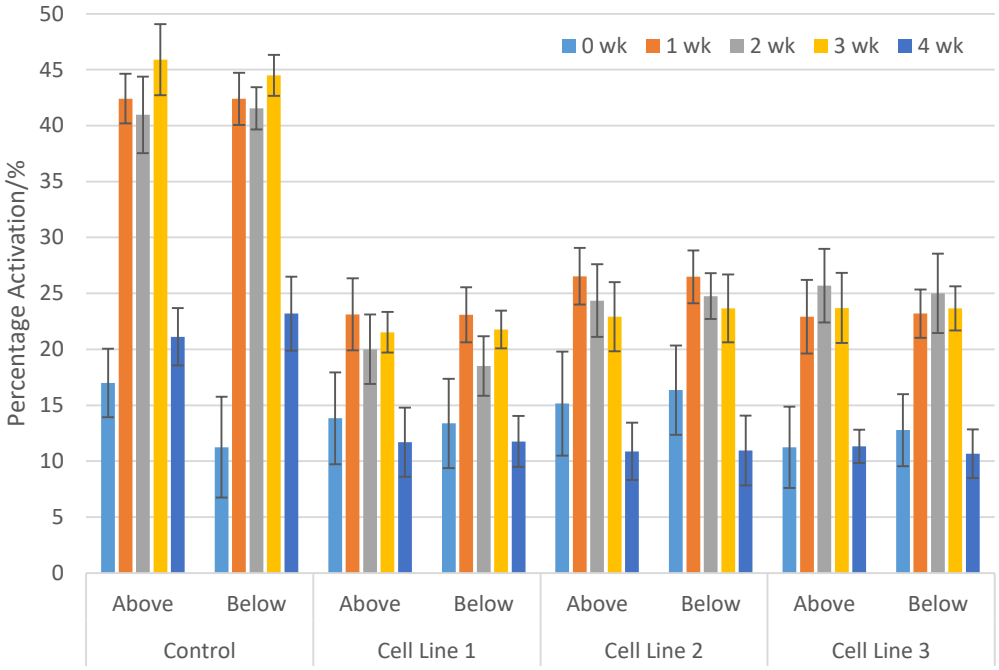

Figure 5.4 Percentage α-sma immunopositive cells above and below the wound site. All cell lines showed a significantly higher α-sma concentration in the epithelial-stromal flap (above the wound) than the stromal wound bed (below the wound) for weeks 1,2,3 and 4 ($p>0.01$, marked on the graph for cell line 2 only for clarity). Wounded untreated control corneas also demonstrated higher percentage activation above the wound compared to below for weeks 1, 2, 3 and 4 ($p>0.05$).

5.5. Keratocyte cellularity

A steady reduction of the number of blue Hoechst-labelled nuclei (figure 5.2) during the organ culture period was seen in all treated corneas and controls (figure 5.5). There was no significant difference between the cellularity of the OMLP-PC treated corneas and the untreated wounded controls for 0 time point and weeks 1, 2 and 4, however the treated corneas had a significantly higher cell number at week 3 when compared to the wounded controls ($p<0.01$, figure 5.5).

The cellularity, although showing no difference at 0 and 4 weeks in organ culture, was significantly lower in wounded corneas, treated and untreated corneas, at weeks 1, 2 and 3 ($p<0.001$, figure 5.5), compared to unwounded corneas.

When assessed separately, the same overall trends were noted above and below the wound site and at all three ROI's (flap edge, flap centre and flap hinge) for all treated and untreated wounded corneas and unwounded cornea. However, there was no significant difference above and below the wound or at any of the ROIs ($p>0.05$).

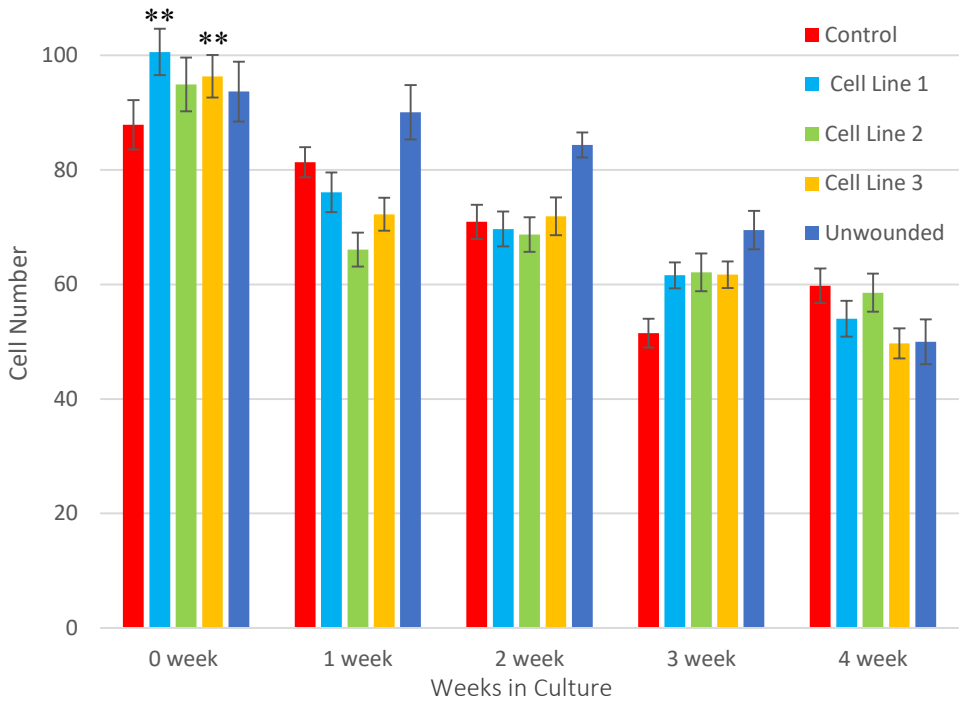

Figure 5.5 Total Cell Count in corneal wound area calculated as the total number of Hoechst labelled cell nuclei in all 3 ROI's above and below the wound (average of n=4) over a 4 week organ culture period. Cell number for cell line 1 and 3 treated wounded corneas was significantly higher at 0 time point compared to control treated corneas (**$p<0.01$). Error bars represent SD.

5.6. The Effect of OMLP-PC Therapy on Stromal Cell Proliferation

Percentage stromal cell proliferation, calculated as a proliferating cell nuclear antigen imunopositive cells (PCNA, labelled red, figure 5.6) percentage of total cell number in same region, for both treated and control wounded porcine corneas significantly increased from 0 time point to 1 week ($p<0.001$, figure 5.7). For those corneas treated with cell line 1 OMLP-PCs the peak percentage of proliferating cells was 52.20% ±3.73 at 1 week and was significantly higher than 35.89% ±5.89 the untreated wounded controls ($p<0.05$). At subsequent time points the percentage cell proliferation decreased at a steady rate (figure 5.7).

The untreated wounded controls, reached a peak proliferation 42.17% ±3.38 at 2 weeks, albeit at a lower percentage proliferation than the cell-treated wounded corneas, in particular cell line 1 ($p<0.05$, figure 5.7). After this 2 week time point the cell proliferation in the untreated wounded corneas decreased steadily up until week 4.

At weeks 1, 2, 3 and 4, wounded corneas, treated with OMLP-PCs and untreated, had a higher percentage proliferation than the unwounded control corneas ($p<0.001$). The unwounded controls maintained a low rate of proliferation throughout the organ culture period from 0 to 4 weeks (figure5.7).

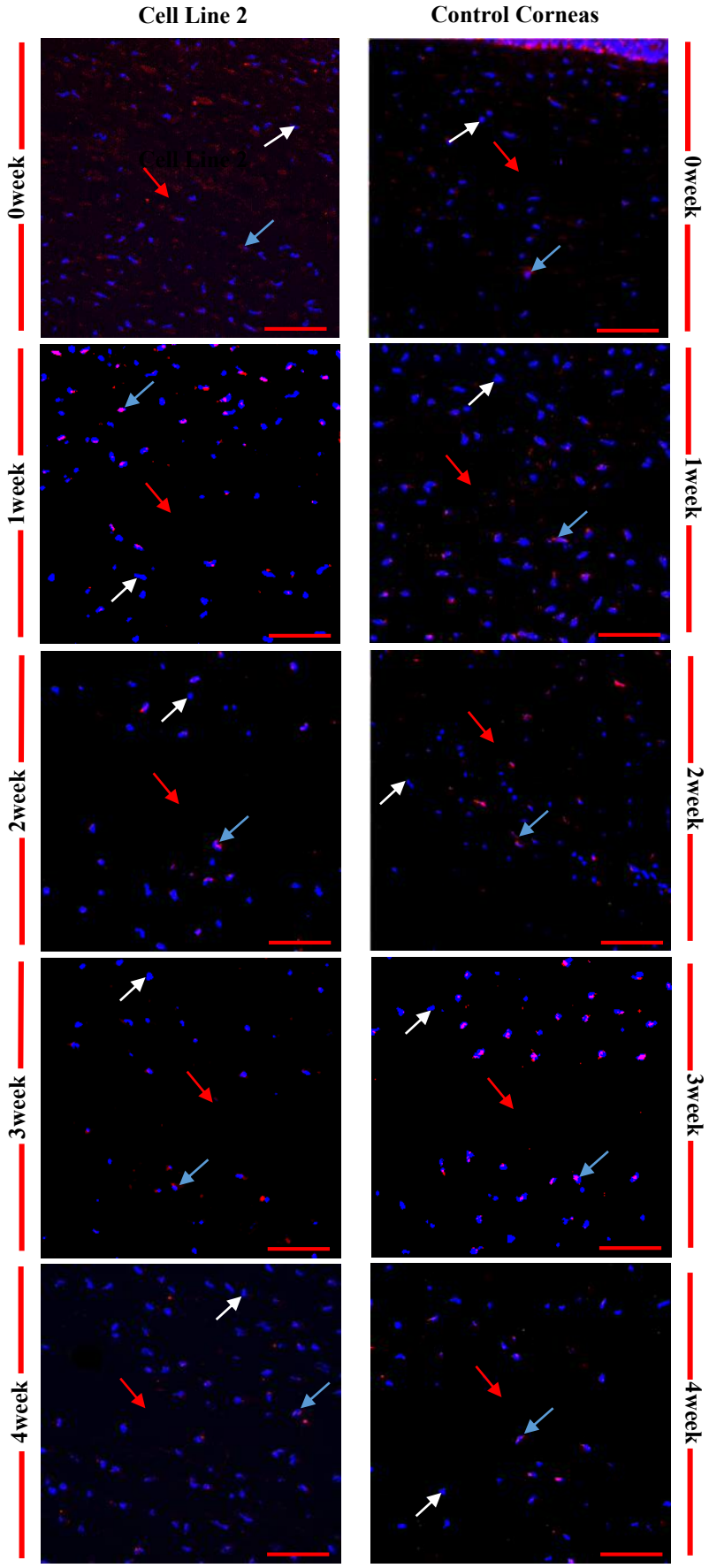

Figure 5.6: Representative images of PCNA immunolabelling in the central wound area during wound healing in organ culture of corneas treated with OMLP-PC Cell Line 2 (Left) and Control untreated wounded corneas (Right). Images show immunopositive cells (red fluorescence) indicated by Blue arrows, whilst Red arrows point to the wound site White arrows indicate Hoechst labelled cell nuclei. Scale bars represent 100µm.

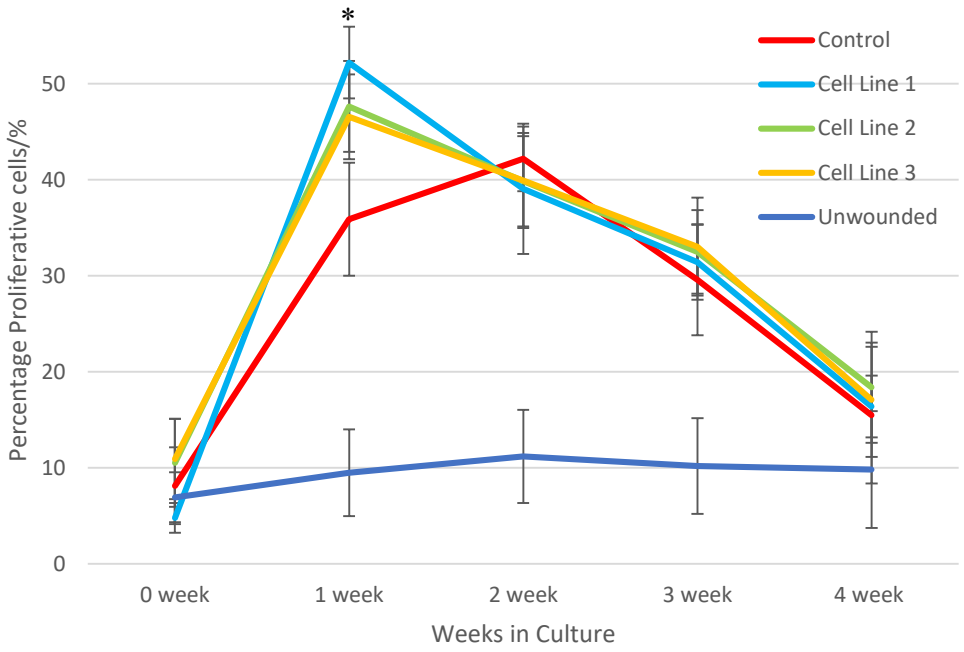

Figure 5.7 Mean percentage cell proliferation throughout wound area (i.e. above and below wound in all 3 ROIs.) as a function of organ culture time. OMLP-PC treated corneas, for cell line 1, had a significantly higher proliferation percentage than untreated wounded controls at 1 week (*$p<0.05$). All untreated and OMLP-PC treated corneas had a significantly higher proliferation at weeks 1, 2, 3 and 4 weeks compared to the unwounded controls ($p<0.001$). Error bars represent SD.

There was no significant difference in percentage cell proliferation between ROIs (flap edge, flap centre and flap hinge) for all wounded and unwounded corneas at all time points during the organ culture.

However, there was no statistically significant difference between the percentage of proliferating cells for the OMLP-PC treated and control treated LASIK-like wounded corneas and the unwounded corneas when comparing above and below the wound ($p>0.05$), although there was a consistent trend of higher proliferation above the wound in the epithelial-stromal flap (figure 5.8 A, B, C and D).

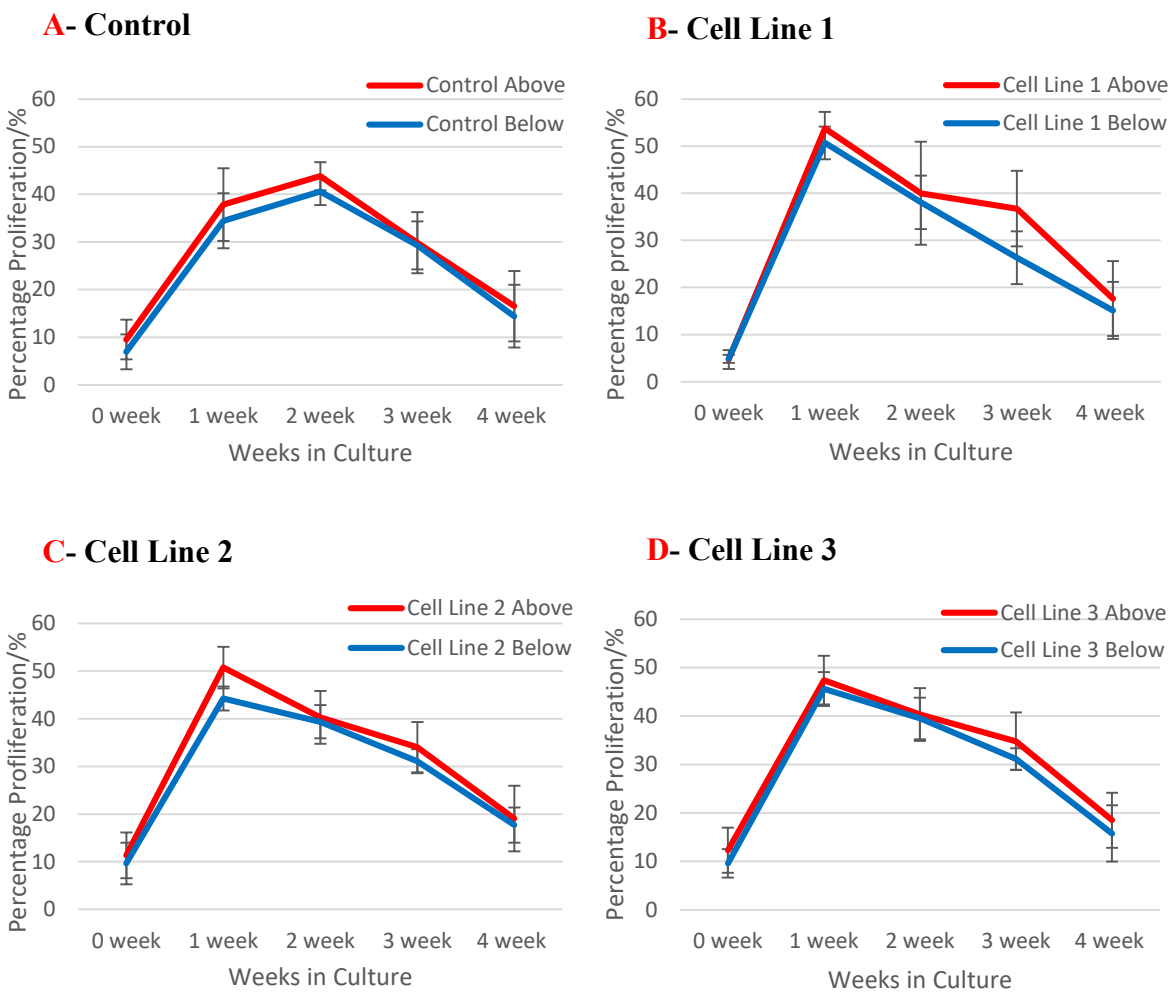

Figure 5.8 Percentage Proliferation Above and Below Wound Site (at all 3 ROIs.) during 4 weeks organ culture. Despite proliferation being consistently higher above the wound than below in all wounded porcine corneas (control and treated) there was no significant difference (p=>0.05). Error bars represent SD.

5.7. Keratocyte apoptosis during organ culture:

Percentage stromal cell apoptosis, calculated as caspase 3 imunopositive cell (labelled red, figure 5.9) percentage of total cell number in same region, for both treated and control wounded porcine corneas significantly increased from 0 time point to 1 week ($p<0.001$, figure 5.10).

From week 1 to week 3 the percentage of apoptosing stromal cells showed a very slight decrease for both treated and untreated wounded corneas (figure 5.10), however, this was not significant ($p>0.05$).

At week 4 the percentage Caspase-3 immunolabelled cells decreased significantly ($p<0.01$, figure 5.10). There was no significant difference between the OMLP-PC treated LASIK-like wounded corneas and wounded corneas left untreated throughout the organ culture period ($p>0.05$).

The unwounded corneas showed caspase-3 immunopositive cells at 0 time point and a very low percentage in subsequent weeks (figure 5.10).

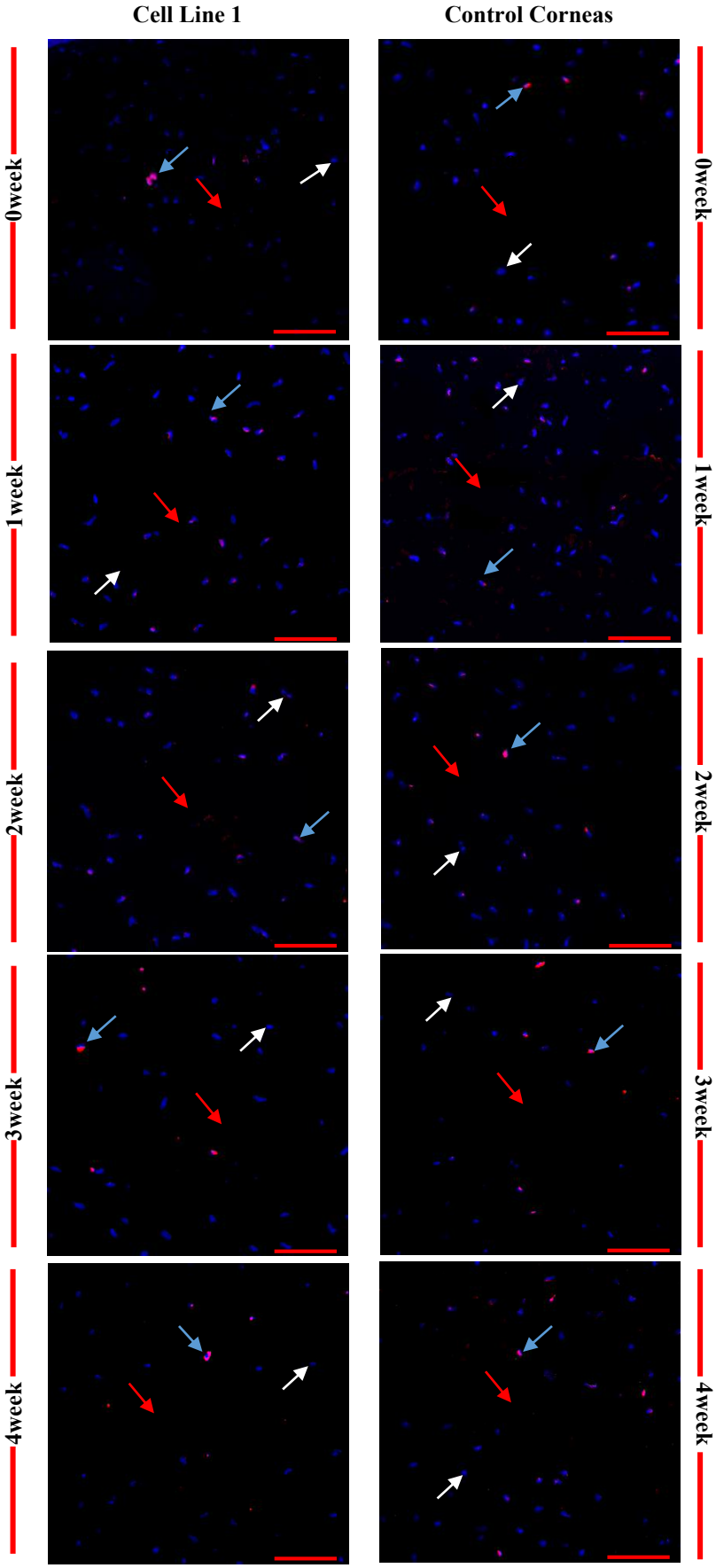

Figure 5.9: Representative images of Caspase 3 immunolabelling in the central wound area during wound healing in organ culture of corneas treated with OMLP-PC Cell Line 2 (Left) and Control untreated wounded corneas (Right). Images show immunopositive cells (red fluorescence) indicated by Blue arrows, whilst Red arrows point to the wound site White arrows indicate Hoechst labelled cell nuclei. Scale bars represent 100µm.

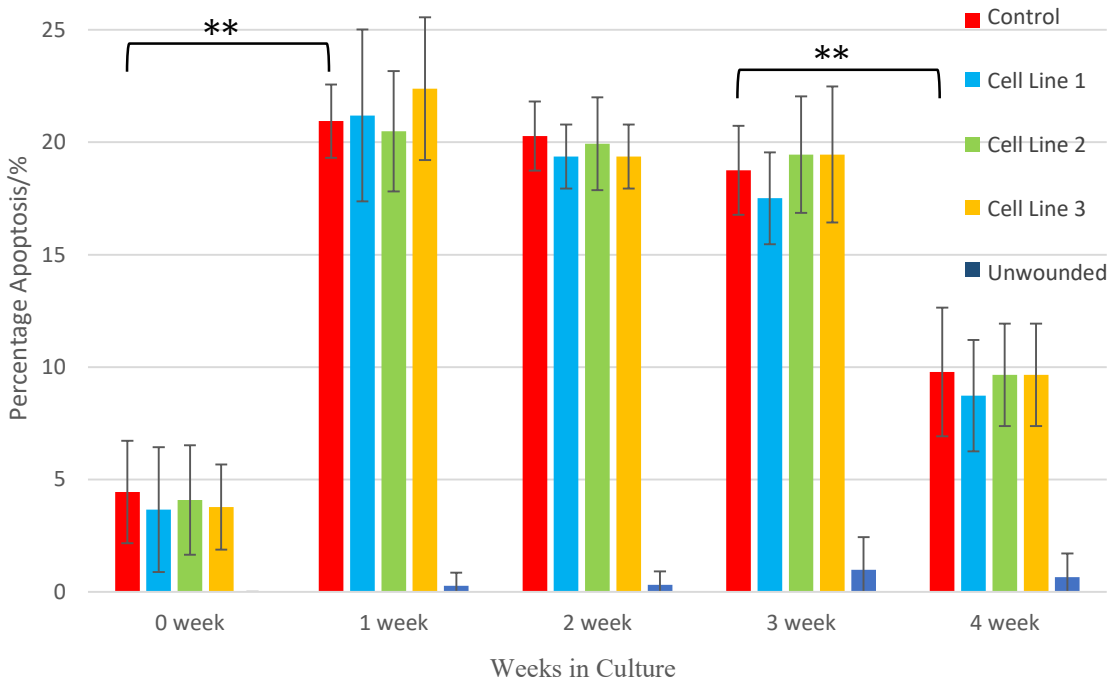

Figure 5.10 Mean percentage cell apoptosis throughout wound area (i.e. above and below wound in all 3 ROIs.) as a function of organ culture time. There was no significant difference between the wounded treated and untreated corneas throughout the organ culture ($p>0.05$). All wounded corneas had a significant increase (**$p<0.001$) in apoptosis from 0 time point to 1 week. The percentage of apoptosis was maintained from weeks 2-3, followed by a significant decrease at week 4 (**$p<0.001$) (significance shown on controls only for clarity). The unwounded corneas showed very little apoptosis during the organ culture period. Error bars represent SD

5.8. Transparency Measurements

The transparency of the corneas during the organ culture period, shown in figure 5.11, was visually graded as previously outlined in sections 2.11.2 and 4.6.

The cell-treated and untreated wounded corneas, and the unwounded corneas all underwent a significant decrease in transparency between 0 time point and week 1 ($p<0.001$, figure 5.12). In weeks 1 to 3 there was a slight, albeit not statistically significant, decrease in transparency although there was no difference between any of the samples ($p>0.05$).

At week 4 there was no significant increase in transparency, however those wounded corneas treated with a solution of OMLP-PCs had a significantly higher transparency when compared to the untreated wounded controls ($p<0.01$). Representative corneal images demonstrate this in figure 5.11. Most notably, the wounded corneas treated with OMLP-PCs showed no statistically significant difference in transparency when compared to the unwounded control corneas ($p<0.01$, figure 5.12).

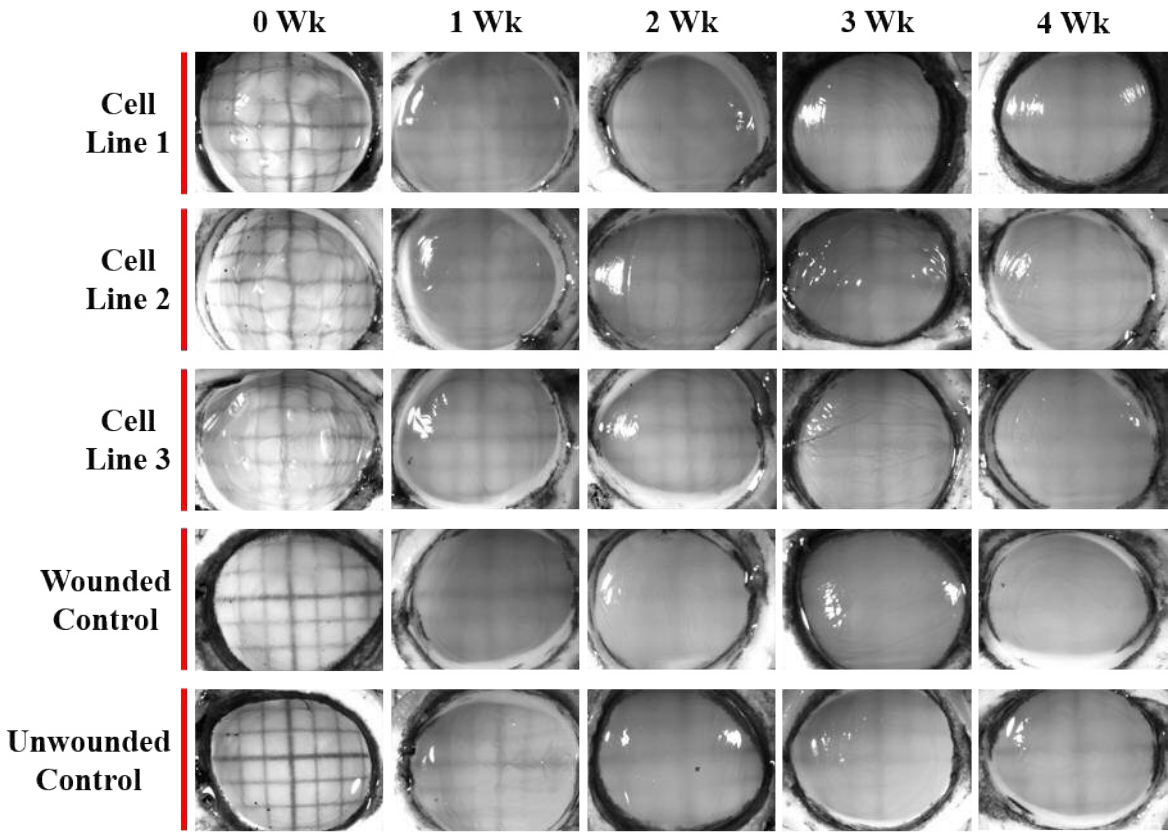

Figure 5.11 Visual Transparency Grading Images. Used to assess corneal transparency for LASIK-like wounded corneas with applications of $1.5x10^5$ cells per ml concentration of OMLP PC solution from 3 cell lines, untreated LASIK-like wounded corneas and unwounded corneas at 0 time point and after 1,2,3 and 4weeks in organ culture.

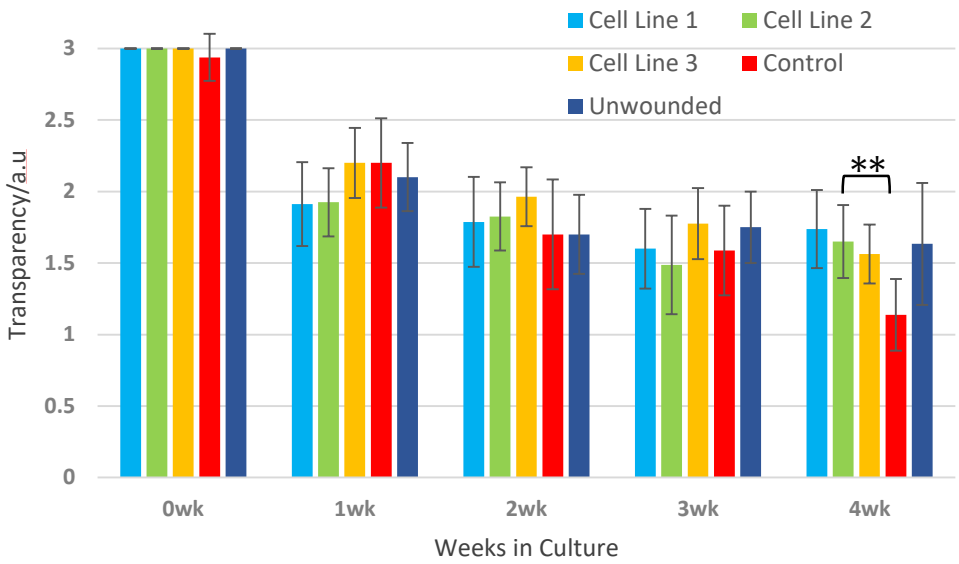

Figure 5.12 Corneal Transparency. Visually graded transparency of unwounded porcine corneas and LASIK-like wounded corneas with an application of either a control solution or a $1.5x10^5$ cells per ml cell solution of OMLP-PCs from 3 different patients at 5 time points over an organ culture period. Cell Lines 1, 2 and 3 were significantly more transparent at week 4 than untreated wounded controls (**$p<0.01$, shown only on Cell Line 2. Error Bars represent SD

5.9. Discussion

On wounding of the cornea the complex cascade of cellular responses begins with epithelial loss mediating the apoptosis of keratocytes immediately below the epithelial wound by release of cytokines such as IL-1 and TGFα (Wilson et al., 1996; Masur et al., 1996; Mohan et al., 1997). The site of this apoptosis is dependent on the original injury; an abrasion or epithelial scrape will elicit keratocyte apoptosis immediately below the initial wound in the superficial stroma, whereas a penetrating lamellar cut (such as those inflicted by microkeratomes in LASIK) produce keratocyte apoptosis in the stroma anterior and posterior to the lamellar interface of the wound as well as below the original injury site of the epithelium (Wilson et al., 2001). This apoptosis is the first observable sign of wound healing to take place after epithelial wounding and can occur for several days at a minimum, after initial injury (Gao et al., 1997).

Following this, in the first 24 hours, the keratocytes remaining after apoptosis begin proliferation and keratocyte numbers increase rapidly (Zieske et al., 2001). However, with the increasing number of keratocytes, apoptosis of the new cells occurs cause a rolling simultaneous occurrence of apoptosis and proliferation over a number of days (Mohan et al., 2001). The activation of these keratocytes and transformation into myofibroblasts takes place and they begin to acquire temporary expression markers of smooth muscle differentiation, α-sma, in the microfilaments of myofibroblasts. This α-sma expression is regarded as a reliable indicator of the presence of myofibroblastic cells (Darby et al., 1990; Gabbiani, 2003). Whilst the appearance of α-sma is necessary and contributes to the contractile forces of myofibroblasts (Gabbiani, 2003) this has a negative impact on transparency of the cornea through a markedly diluted concentration of intracellular corneal crystallins due to a dramatic increase in the cell size of activated keratocytes (Jester et al., 2005; Jester et al., 2012).

The repair of the stroma ensues as collagen and other ECM components, such as glycoproteins and proteoglycans, are synthesised by the activated fibroblasts. A lack in organisation compared to the native cornea results and therefore contributes to the reduced transparency of the wound healing cornea. Remodeling of this newly laid down ECM, controlled by matrix metalloproteinases (MMPs) such as collagenase and gelatinases, potentially continues for years and can result in tissue that does not closely resemble the organisation or strength of the native corneal tissue (Lee et al., 1982; Cintron et al., 1990; Steele et al., 1999).

In this study, the activation of keratocytes into myofibroblasts was ascertained by determining the percentage of cells expressing α-sma at different time points during the organ culture period following creation of a penetrating wound, similar to that created in a LASIK-like flap, in porcine corneas, using a microkeratome.

In order to determine the effect of OMLP-PCs on wound healing, they were inserted into the wound bed under the epithelial-stromal flap. The cell response, in terms of cell apoptosis and proliferation, cell number and presence of myofibroblasts, within the wound area, was then compared to untreated wounded corneas and unwounded porcine corneas cultured for up to four weeks. Whilst the unwounded corneas showed a significantly low activation of keratocytes across the organ culture, this has not been seen in *in vivo* studies of the unwounded cornea. In 2003 Mohan et al. observed no α-sma in the unwounded cornea of an *in vivo* rabbit model. The low level of activation shown in the organ cultured unwounded porcine corneas could be a result of epithelial damage during the organ culture, leading to an initiation of the wound healing cascade.

As was also shown in chapter 4 (sections 4.4 and 4.7), the OMLP-PC treated corneas once more, had a significantly lower percentage of cells with α-sma expression, and therefore number of myofibroblasts, than the untreated wounded corneas from week 1 in organ culture. This was consistent to that observed in previous studies of cell-based therapies applied to corneal wounds in an organ culture model; oral mucosal fibroblasts and corneal stromal stem cells (CSSCs) (Dooley et al., 2012; Morgan et al., 2014).

The lowering of the percentage of myofibroblastic transformation in the organ cultured wounded porcine corneas should have positive ramifications for corneal transparency during wound healing as it has less of a negative effect on the expression of corneal crystallins and reduced production of disorganised ECM products. The significant lowering of keratocyte activation when compared to the untreated wounded corneas also indicates that the OMLP-PC treatment is having an effect on the wound healing of the cornea, potentially introducing some of the characteristics of oral mucosa wound healing into that of the wounded cornea.

The privileged repair of the oral mucosa has been well documented as having rapid re-epithelialisation and remodeling (Stephens et al., 1996) and the intra-oral mucosal

fibroblasts have been shown to exhibit foetal-like phenotypes that are consistent with the scarless wound healing associated with the foetal-like behaviours of the oral mucosal (Sloan, 1991). Oral mucosal fibroblasts have demonstrated they have the ability to accelerate collagen gel contraction whilst lowering the expression of α-sma (Shannon et al., 2006), a faster proliferation than dermal fibroblasts (Glim et al., 2014; Lee & Eun, 1999) and a significantly increased ability to reorganise ECM (Stephens et al., 1995). The foetal like wound healing of the oral mucosa led researchers to hypothesise that a progenitor cell population was yet to be discovered in the lamina propria that was contributing to the preferential wound healing. This hypothesis was proved correct in 2010 by Davies et al., when OMLP-PCs were discovered and shown to be multipotent with the ability to differentiate down different lineages, potently immunosuppressive and possessing anti-microbial properties (Davies et al., 2010 & 2012; Board-Davies et al., 2015).

The apoptosis of keratocytes in corneal wound healing, triggered by cytokine release from the epithelium, occurs almost immediately after wounding (Wilson et al, 2001), which can be seen in this study. Apoptosis was seen in the wounded corneas at 0 time point (detected by caspase-3 immunolabelling), compared to no apoptosis in the unwounded corneas. A significant increase in apoptosis occurred at 1 week and continued until a significant reduction at 4 weeks. There was a low amount of apoptosis in the unwounded corneas from 1 week onwards, potentially triggered by low level damage to the epithelium as a consequence of organ culture. Interestingly there was no difference in apoptosis between the wounded and unwounded corneas at any time point during the organ culture, indicating that the application of OMLP-PCs had no effect on the apoptotic stages of wound healing in the LASIK-like wounded cornea.

In this study attempts were made to follow the fate of the OMLP-PCs within the porcine cornea throughout the organ culture by labelling with a human antigen Anti-Histone H2B antibody - N-terminal (Abcam, UK,). However, the antibody indiscriminately labelled all cells (results not shown), and it was later found that porcine and human proteins have a high homology (Franek & Sorm, 1970). Despite numerous protocol optimisations, it is

likely that cross reaction between porcine and human antigen is high and, therefore the OMLP-PCs could not be tracked.

The proliferation within the organ cultured porcine corneal stroma, in the wound area, showed an earlier and higher peak at 1 week post wounding, when treated with OMLP-PCs. This peak appeared at a lower level, and at 2 weeks in the untreated wounded corneas, indicating the cell proliferation progressed at a faster rate in treated corneal wounds. The comparatively faster cell proliferation in the OMLP-PC treated corneas suggests that potentially the OMLP-PCs produce growth factors that trigger stromal cell proliferation within the porcine cornea as they have been shown to proliferate faster than other fibroblasts (Lee & Eun, 1999; Glim et al., 2014). The peak in proliferation for the untreated wounded porcine corneas may be indicative of the keratocyte replenishment that takes place following apoptosis in the corneal stromal wound healing process (Wilson, 2002).

The cellularity of the corneas throughout the wound healing process followed an overall trend of reduction over the organ culture period. The number of stromal cells in the corneas treated with OMLP-PCs decreased from 0 time point to 1 week significantly ($p<0.001$), whereas the consequent weeks, although showing a decreasing trend, did not show a consistently significant reduction in cell number. At 0 time point there was a significantly higher number of cells in the wounded corneas treated with OMLP-PCs compared to the untreated corneas, but once again no consistently significant reduction in numbers between the untreated corneas and when compared to the cell treated corneas. However, the trend for the unwounded corneas is interesting as it shows a smooth non-linear decrease in cell number, from 0 to 4 weeks in organ culture. During organ culture the porcine corneas have a tendency to swell (Van Horn et al., 1975; Summerlin et al., 1973) resulting in an increasing thickness over the organ cultured period. This would lower the number of cells per area in the assessment of cellularity and result in a steady decrease over the organ culture period.

This increased thickness of the cornea can also have a negative impact on the transparency of all corneas over the 4 week organ culture period (Hart & Farrell, 1969; Cox et al., 1970, Meek et al., 2003; Doutch et al., 2008). During the wound healing of the untreated wounded corneas a number of factors, as previously discussed can have a negative impact on the transparency. The activation of myofibroblasts is a major determinant as, due to the increase in size of the keratocytes, the intracellular corneal crystalline concentration is effectively diluted, thus reducing the transparency (Jester et al., 2005 & 2012), as well as the laying down of new disorganised ECM components by the newly activated keraocytes causing opacification. In the wounded corneas treated with OMLP-PCs, there was a similar reduction in transparency over the organ culture period, as in the unwounded corneas. However, at the 4 week time point the transparency of the OMLP-PC treated corneas and the unwounded corneas were not only similar, but significantly more transparent than the untreated corneas. As the increase in thickness due to the corneal oedema caused by the organ culture was a common factor between the untreated and treated wounded corneas and the unwounded corneas, the low percentage of myofibroblasts present in the wound area must have a positive effect on the transparency of the cornea, as previously discussed.

The success of previous researchers using cell based therapies to improve the wound healing capabilities of the organ cultured corneas (Dooley et al 2012; Morgan et al., 2014) have led the way to utilising the OMLP-PCs as possible source of cell based therapy that could provide immunosuppressive, anti-microbial, and self-renewing properties from an easily accessible biopsy site. Due to the very nature of cells, these could be collected easily, induce rapid healing with minimal scar formation, similar to the foetal like characteristics of oral mucosal wound healing (Sloan, 1990; Davies et al., 2010 & 2012; Board Davies et al., 2015).

These cells appear to have been successful in improving the wound healing properties of the wounded porcine cornea; their application increased the rate of cell proliferation, lowered the number of keratocytes transformed into myofibroblasts, and significantly improving corneal transparency to the level of an unwounded cornea by 4 weeks in organ culture.

Chapter 6

Collagen microarchitecture during wound healing and OMLP-PC application

6.1. Introduction

The stroma makes up the bulk of the human cornea, accounting for 90% of its thickness (500µm) (Rodrigues et al., 1982) and has a unique homogeneity of cell types, consisting of keratocytes, proteoglycans and collagen (Hogan et al., 1971; Fini, 1999). The organisation of the collagenous stroma is highly specialised; collagen fibrils of narrow and uniform diameter and spacing are aligned in parallel within stromal lamellae and surrounded by proteoglycans (Maurice, 1957). Lamellae, numbering approximately 300 in the central corneal to 500 in the periphery (Radner et al., 1998), are orthogonally stacked with respect to each other (Fini, 1999) and run from limbus to limbus.

The transparency of the cornea, which is crucial for functional vision, is reliant, not only on its avascular nature, but also on the uniquely organised ultrastructure, as described in brief above. Disruption of this specific arrangement results in the loss of corneal transparency (Meek et al., 2003). There are a number of potential causes for the loss of transparency with respect to wound healing, the stromal collagen arrangement is disrupted during the wound healing process due to swelling, laying down of repair ECM components and eventual remodelling (Zieske, 2001; Fini, 1999).

The initial damage to the epithelium releases cytokines such as TGFβ and IL-1 (see section 1.6) that mediate apoptosis in the adjacent keratocytes via the fas-fas ligand system (Toricelli & Wilson, 2014), resulting in an acellular zone (Zieske, 2001). Proliferation of remaining nearby keratocytes ensues and fibroblast activation and transformation into myofibroblasts begins; with a fibroblastic phenotype (Jester et al., 1999; Funderburgh et al., 2003). As previously discussed in Chapters 4 and 5, appearance of myofibroblasts negatively impacts on transparency due to the decreased concentration of corneal crystallins compared to keratocytes (Jester et al., 2005 & 2012), but also due to their excessive deposition of repair ECM products (Masur et al., 1996; Moller-pedersen et al., 1997; Jester et al., 1999; Mohan et al., 2003) and contractile forces (Ishizaki et al., 1994).

The concurrent apoptosis, proliferation and activation of keratocytes and transformation into myofibroblasts continues for days or weeks and stromal remodelling begins. Over many months, the ECM is remodelled with continuous collagen (and other component) synthesis, degradation and re-synthesis (Fini, 1999). The parallel lamellar layers are gradually reformed across the wound site as deposited collagen lamellae in the repair tissue interleaves with the cut collagen (Davison & Galbavy, 1986). The collagen fibrils return to a more uniform size and become more organised (Cintron et al., 1978). This stromal remodelling is dependent on the wound type of the initial injury; wounds that run parallel to the corneal surface such as PRK, heal with minimal scarring and may take up to a year or more to heal. Incisional wounds, where the cut occurs perpendicular to the surface (e.g. gaping wounds) require the deposition of collagens and abnormally large proteoglycans which may take many years of healing to return to its native opacity, if at all (Zieske et al, 2001; Funderburgh et al., 1998). The deposition of these proteoglycans has a significant effect on corneal transparency as, due to their hydrophilic nature, they play a major role (along with the corneal endothelial pump, as previously discussed in chapter 1) in regulating the collagen fibril spacing (Hassell et al., 1983). The presence of these larger proteoglycans can therefore not only increase the fibril spacing due to their size, but also increase corneal hydration, thereby disrupting the specific corneal collagen organisation required for normal visual function (Funderburgh et al., 1998; Saika, 1998; Ishizaki et al., 1994).

The collagen ultrastructure of the cornea is traditionally imaged using transmission electron microscopy (TEM). However, second harmonic generation (SHG) microscopy can be used to investigate fibrillar collagen (Han et al., 2005). In this non-linear microscopy technique, two photons with the same frequency can interact with a structure that has non-centrosymmetric molecular organisation, with consequent scatter in a non-random phase (Zipfel et al., 2003). Two near infrared incident photons are converted into one photon with twice the energy of the incident laser beam; twice the frequency and half the wavelength (figure 6.1) (Mohler et al., 2003; Strupler et al., 2007). SHG conserves the energy and the coherence of laser light, as it does not involve an excited state (Campagnola & Loew, 2003) The near infrared wavelengths used allow excellent depth penetration without the need for

confocal optics (Cox et al., 2003; Campagnola & Loew, 2003). Without the need for dyes such as fluorophores, SHG is non-invasive and can image samples without degrading or destroying them, specifically targeting fibrillar collagen I and has had a significant impact on biomedical research (Mohler et al., 2003; Brown et al., 2003).

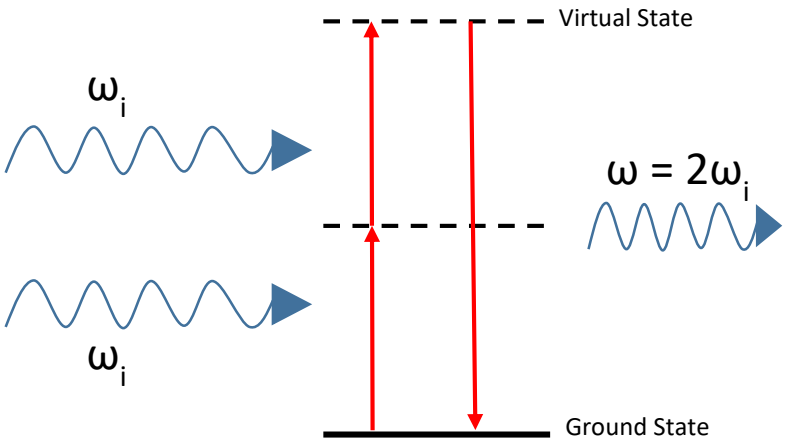

Figure 6.1 Diagram showing Second Harmonic Generation (or frequency doubling). Two incident photons with the same frequency (ω_i) interact with non-centrosymmetric molecules and a photon with twice the frequency and half the wavelength ($2\omega_i$) is produced and energy is conserved.

The activation and transformation of keratocytes into myofibroblasts in the process of corneal wound healing results in many processes that decrease the corneal transparency including altered collagen organisation within the cornea. Additionally, a decrease in corneal crystallins, production of contractile forces and the excessive deposition of repair ECM occurs. The presence of myofibroblasts was shown to be significantly reduced by the application of OMLP-PCs to the wound bed of LASIK-like wounded porcine corneas over a 4 week organ culture, when compared to the wounded untreated control corneas (Chapter 5). The structure of collagen is non-centrosymmetric, being made up of repeating units of parallel cross-linked triple helical molecules (tropocollagen) (Thomas et al., 2007). As has been reported on numerous occasions, collagen is a very effective "upconverter" of light by SHG and so is ideal for this non-linear imaging method (Georgiou et al., 2000; Cox et al., 2002). Therefore, in this study SHG imaging was used to assess the collagen fibril organisation within the stromal cornea as a function of wound healing to assess whether

the application of OMLP-PCs to the LASIK-like wounded cornea improved the remodelling of corneal ECM back to, or as near as possible to, the native unwounded state.

6.2. Aim

The aim of this chapter was to determine the effect of OMLP-PCs on the stromal collagen organisation in corneal wound healing.

The results were used to assess the efficacy of OMLP-PCs in remodelling stromal collagen to improve healing and consequent corneal transparency after LASIK-like wounding.

6.3. Experimental Design

Corneal cryosections obtained from the organ cultured LASIK-like wounded porcine corneas from section 5.3 were used in this experiment (Sections 2.1- 2.7.2.).

The morphology of the stromal wound area was assessed using Haematoxylin and Eosin staining (H&E). In brief, triplicate corneal cryosections from unwounded, treated ($1.5x10^5$ OMLP-PCs ml^{-1}, Cell line 2) LASIK-like wounded and untreated wounded corneas were immersed in Harris haematoxylin followed by 1% aqueous Eosin and then mounted in DPX (03703596, RA Lamb, UK). Images of these sections were acquired using a Leica DMRA2 Microscope (Leica, Germany) and Zen image capture software (Zeiss, Germany). The images were assessed for differences in the corneal stroma morphology during wound healing, between the treated and untreated corneas, over an organ culture period of 4 weeks.

Triplicate 10µl cryosections from OMLP-PC treated (at $1.5x10^5$ cells ml^{-1}) LASIK-like wounded corneas and similarly wounded (media without cells) and unwounded control corneas were mounted in Vectorshield® with propidium iodide (PI) (Vector Labs, UK) (section 2.12.1) and imaged using a Laser scanning microscope (LSM) 880 NLO on Axio Examiner fixed stage upright microscope (Carl Zeiss Ltd., Cambridge, UK). A tuneable ultrafast (< 140fs) titanium-sapphire laser (Cameleon, Coherent, Inc., UK) operating at 800 nm. Second harmonic emission was collected in the forward propagating direction through a 400 +/-3nm near infrared (NIR) blocking band pass filter. Serial optical sections at 1024x1024 resolution were collected at 3µm *z*-focus intervals. The resulting image datasets were analysed using the OrientationJ plugin to ImageJ version 1.52a (National Institutes of Health, USA). All images were equally adjusted for brightness and contrast and despeckled.

A maximum intensity profile image was created from the z stack and an orientation colour overlay applied (figure 6.2), the settings in figure 6.3 were applied. The coherence of orientation (a measure of the degree of the number of fibres aligned in a preferred orientation) and the distribution of the orientation across the sample were analysed at adjacent triplicate points for each sample above and below the wound in the flap centre.

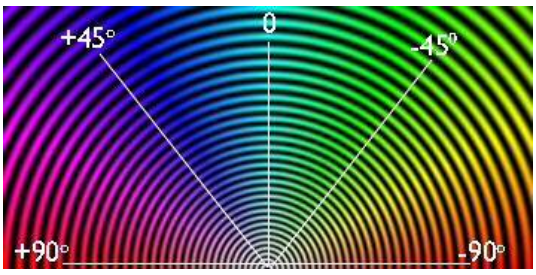

Figure 6.2 Circular colour survey map coding, Original image courtesy of Urszula Zajaczkowska.

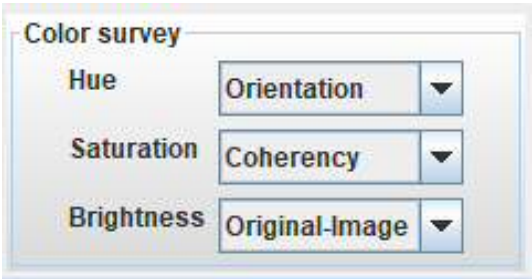

Figure 6.3 OrientationJ plugin (ImageJ version 1.52a National Institutes of Health, USA) settings for OrientationJ Analysis tool.

For the unwounded corneas, as the regions of interest could not be dictated by an inflicted wound, surrogate areas at similar corneal depths and regions were imaged and analysed.

The number of unwounded and LASIK-like wounded porcine corneas (treated with cell line 2 OMLP-PC solution and those treated with a control solution) used is outlined in Table 6.1.

	Treatment	Time point	Processes
LASIK-like Wounded Porcine Corneas n=30	OMLP-PC Cell Line 2 n=15	0, 1, 2, 3 & 4 week n=3 for each time point	·Non-Linear Microscopy for Orientation Analysis ·H&E Staining to Assess Morphology
	Control Solution n=15	0, 1, 2, 3 & 4 week n=3 for each time point	
Unwounded Porcine Corneas n=15	-	0, 1, 2, 3 & 4 week n=3 for each time point	

Table 6.1 Table demonstrating porcine cornea number.

Statistical Analysis

Following determination of a normal data distribution a 2-way ANOVAs and Tukey HSD were performed to determine the effect of OMLP-PC application on corneal collagen orientation coherency and distribution as a function of culture duration.

Results

6.4. H&E

Morphological traits of the wound healing stroma (Haematoxylin labelled blue cell nuclei with pink eosinophilic background) were assessed at 3 different regions of interest (ROIs); namely flap edge, flap centre and flap hinge within the stroma. Wounded corneas treated with a $1.5x10^5$ cells ml^{-1} OMLP-PCs (cell line 2), untreated and unwounded corneas were compared at each organ culture point.

At 0 time point the stroma of all corneas appeared dense with a regular distribution of cells. The corneas that were wounded had an easily observable gaping epithelial wound at the point of entry of the microkeratome blade (the flap edge), and a defined lateral incision running parallel to the epithelium (flap centre) culminating in the end of the incision within the stroma (flap hinge) (figure 6.4).

Through weeks 1, 2 and 3 after wounding an epithelial plug had formed at the incision wound site (the flap edge) in the treated and untreated wounded corneas. The stromal lamellae in all corneas became less compact, with a less organised appearance and the spacing of the nuclei and matrix had increased. The wounded corneas, treated with the OMLP-PCs, showed better wound closure in the central cornea compared to those untreated wounded corneas, which appeared closed at 4 weeks (Fig 6.6). Untreated wounded corneas had larger central areas where the epithelial-stromal flap had not fully adhered to the stromal wound bed (figures 6.5 & 6.6).

By week 4, whilst the epithelial wound at the flap edge showed a varying degree of wound closure (complete healed epithelium, epithelial ingrowth and markedly thinned epithelium), the central stroma, particularly at the flap-wound bed interface, demonstrated a degree of stromal organisation that more closely resembled the unwounded organ cultured cornea than the untreated wounded cornea (figure 6.6).

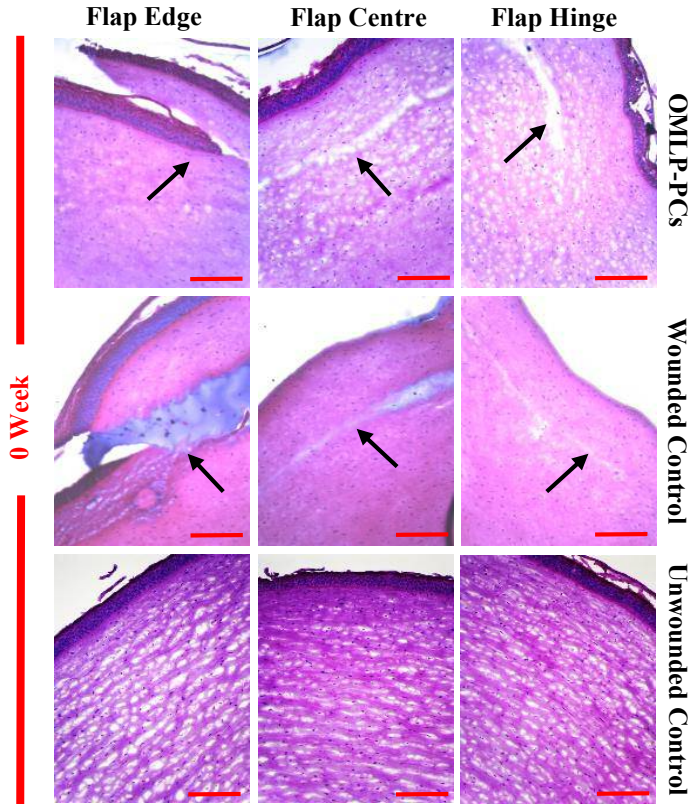

Figure 6.4 H&E stained cryosections of LASIK-like wounded porcine treated with a $1.5x10^5$ cells ml^{-1} solution of OMLP-PCs, LASIK-like wounded control corneas with no treatment and unwounded porcine corneas at 0 time point. Arrows indicate the wound site. Scale bars represent 100µm.

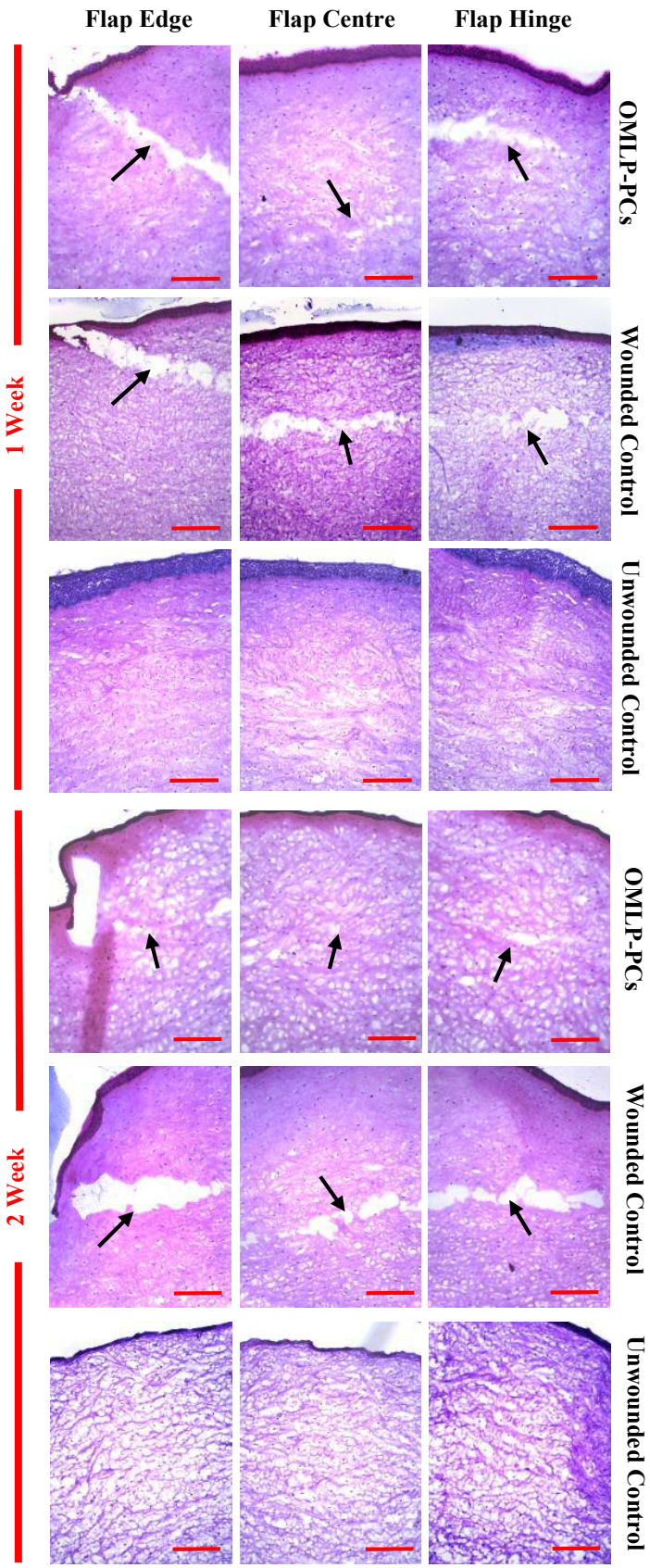

Figure 6.5 H&E stained cryosections of LASIK-like wounded porcine treated with a $1.5x10^5$ cells ml^{-1} solution of OMLP-PCs, LASIK-like wounded control corneas with no treatment and unwounded porcine corneas after 1 and 2 weeks in organ culture. Arrows indicate the wound site. Scale bars represent 100µm.

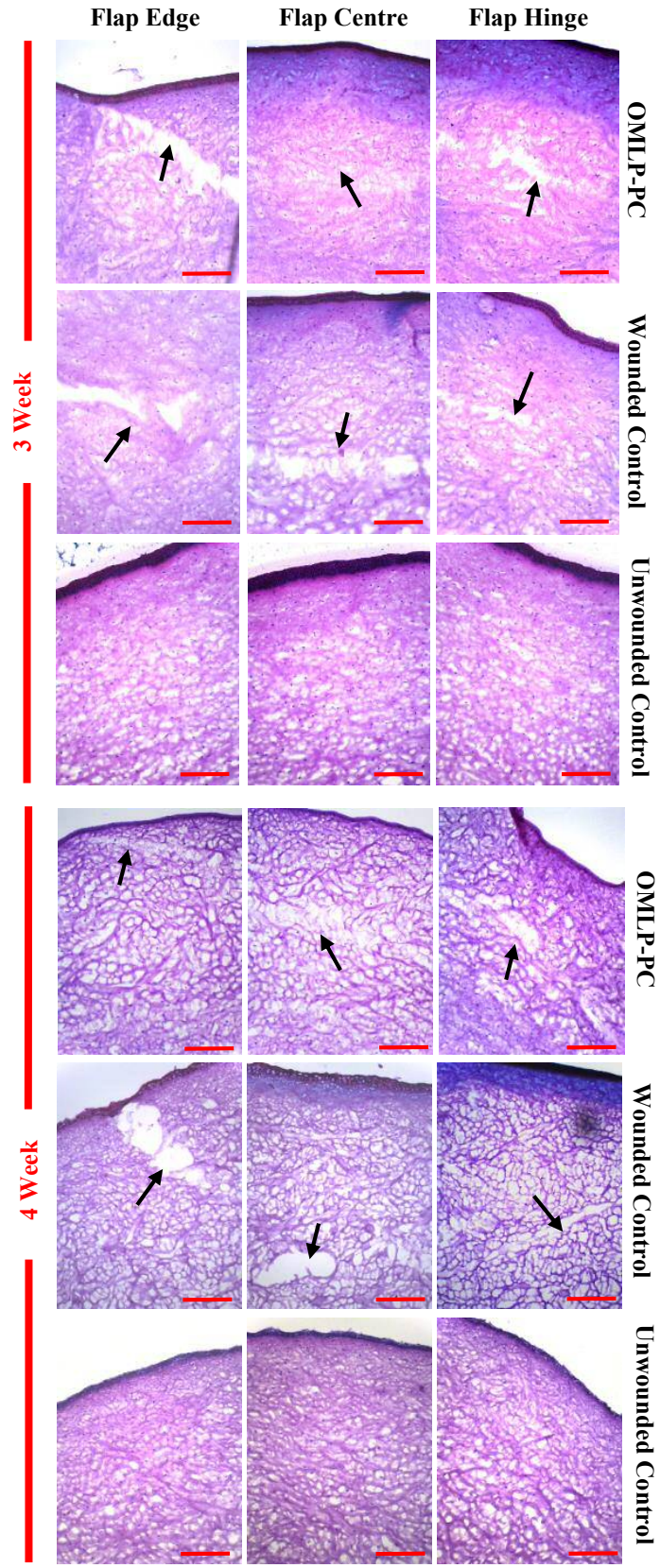

Figure 6.6 H&E stained cryosections of LASIK-like wounded porcine treated with a $1.5x10^{5}$cells ml^{-1} solution of OMLP-PCs, LASIK-like wounded control corneas with no treatment and unwounded porcine corneas after weeks 3 and 4 in organ culture. Arrows indicate the wound site. Scale bars represent 100µm.

6.5. Non-Linear Imaging

Figure 6.7 demonstrates SHG signals generated in a full thickness corneal section of an untreated LASIK-like wounded porcine cornea at 0 time point, with propidium iodide labelling the cell nuclei (red fluorescence). The collagen organisation within stromal lamellae are clearly seen, with LASIK-like wound running parallel to the epithelium clearly defined.

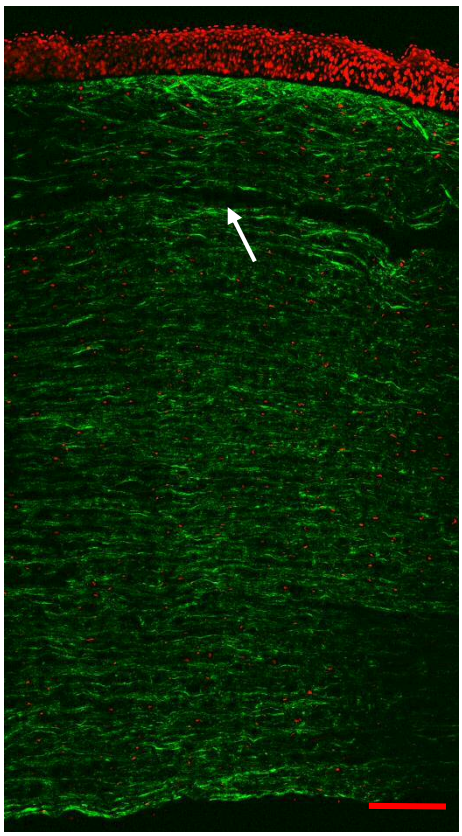

Figure 6.7 Non-linear Second Harmonic Generation (SHG) image of corneal collagen (green) with propidium iodide (PI) fluorescence of labelled cell nuclei (red) within the central cornea (from epithelium to endothelium) of a 0 time point LASIK-like wounded porcine cornea. Arrow indicates wound site. Scale bar represents 200µm

6.6. Orientation Analysis

Triplicate corneas for each time point (0, 1, 2, 3 and 4 weeks) for OMLP-PC treated, untreated wounded and unwounded corneas were subjected to SHG imaging at the flap centre. Images were then assessed using OrientationJ analysis (ImageJ version 1.52a (National Institutes of Health, USA) where a colour survey map overlay image was generated and data collected with regards to preferred fibre orientation, coherence of orientation and distribution.

At 0 week (figure 6.8), the stromal collagen lamellae appeared to be mostly horizontally aligned, parallel to the epithelium in wounded and unwounded corneas and collagen lamellae appeared condensed and tightly pack within the stroma. Analysis of coherence showed a significantly higher coherence in unwounded corneas compared to treated and untreated corneas ($p<0.001$), but no significant difference between treated and untreated wounded corneas ($p>0.05$) (figure 6.11). The stromal incision inflicted by the microkeratome was clearly seen in both of the images of LASIK-like wounded corneas.

At 1 week in organ culture, the alignment of the collagen lamellae in all samples appeared to decrease (figure 6.8), however analysis of the coherence indicated an increase in the coherence in unwounded corneas, compared to 0 time point. The spacing of the collagen lamellae appeared to have increased from 0 time point for both the wounded samples and, to a lesser degree, in the unwounded samples. The stromal wound was still evident in both the cell treated and untreated wounded corneas, with a clear gap at the interface, however, there appeared to be evidence of small areas of intermittent wound closure. Coherence of the cell-treated and control corneas decreased from 0 time point to 1 week, but there was no distinct observable differences between them (figure 6.11). The gaping at the stromal flap interface in the OMLP-PC treated cornea appears greater at 1 week than for the control untreated corneas at the same time point. However, although not significantly different, the coherence of the OMLP-PC treated corneas does appear to be slightly greater than the untreated controls at this time point.

At weeks 2 and 3 in organ culture the stromal wound appeared to have closed more in the OMLP-PC treated corneas compared to the untreated wounded corneas (figure 6.9). There was a large amount of disorganised collagenous stroma seen in all samples, but, once again, to a lesser extent in the unwounded cornea. Analysis of coherence showed significantly higher coherence in the unwounded corneas compared to the wounded at 2 weeks ($p<0.001$), however there was no significant difference between wounded and unwounded at 3 weeks ($p>0.05$). Once more there was no significant difference between the treated and untreated wounded corneas at either 2 or 3 weeks ($p>0.05$) (figure 6.11).

By week 4 the stromal wound was mostly closed in the OMLP-PC treated LASIK-like wounded corneas, whilst the similarly wounded untreated control corneas showed more open gaping wounds at the flap interface (figure 6.10). The LASIK-like wounded corneas treated with OMLP-PCs showed a small, but significant increase in collagen coherence when compared to the similarly wounded untreated corneas ($p<0.05$). Notably, there was no significant difference between the coherency of the unwounded and OMLP-PC treated wounded corneas at this point ($p>0.05$) (figure 6.11).

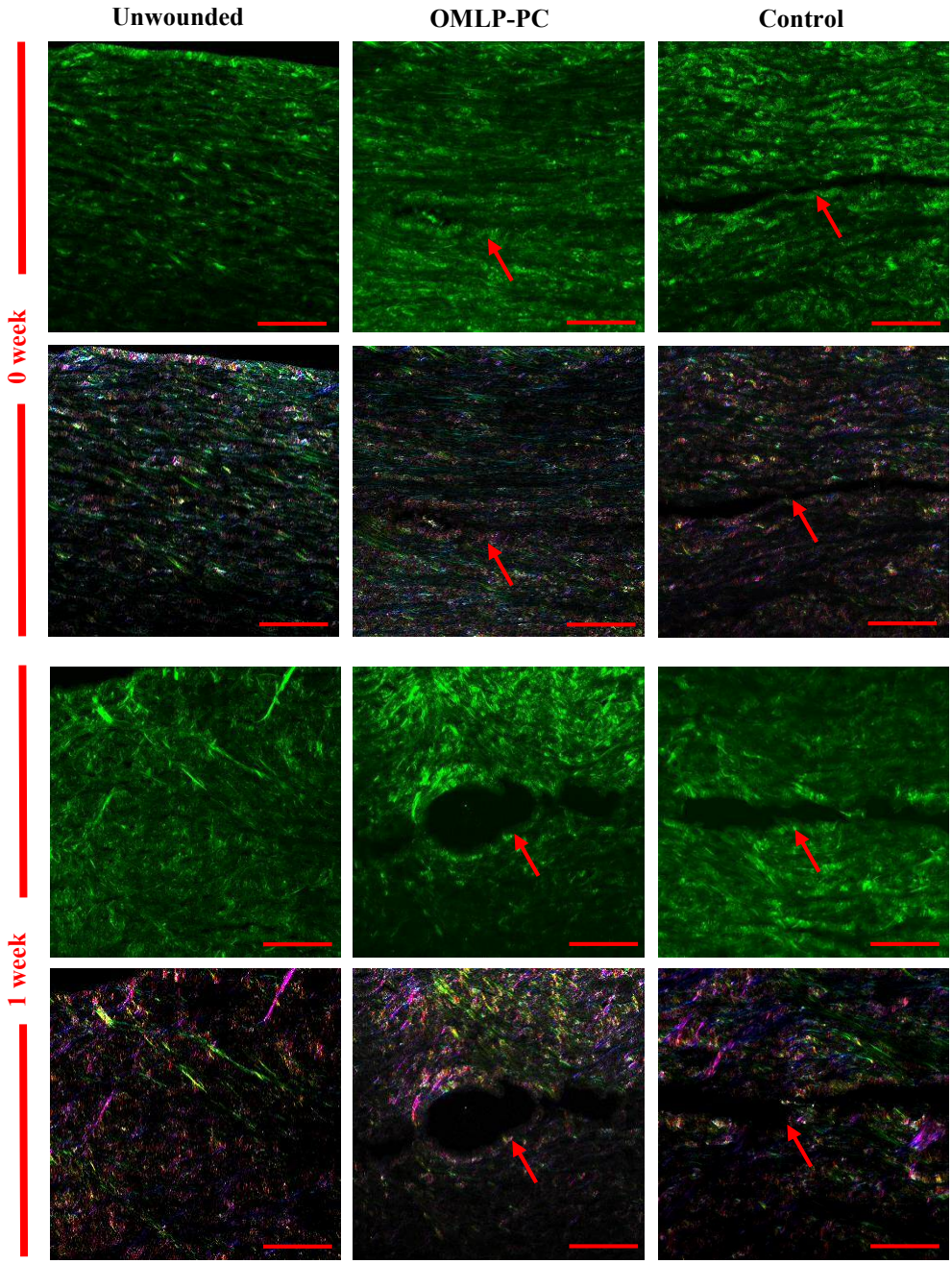

Figure 6.8 SHG imaging of the collagenous stroma (green) in treated and untreated LASIK-like wounded and unwounded corneas at 0 week and after 1 week in organ culture. Aligned and organised collagen stromal lamellae at 0 time point becomes more disorganised 1 week after wounding. Collagen lamellae orientation coherence is represented by the colour map overlay generated by OrientationJ plugin for Image J version 1.52a (National Institutes of Health, USA). Arrows indicate wound site. Scale bars represents 100µm.

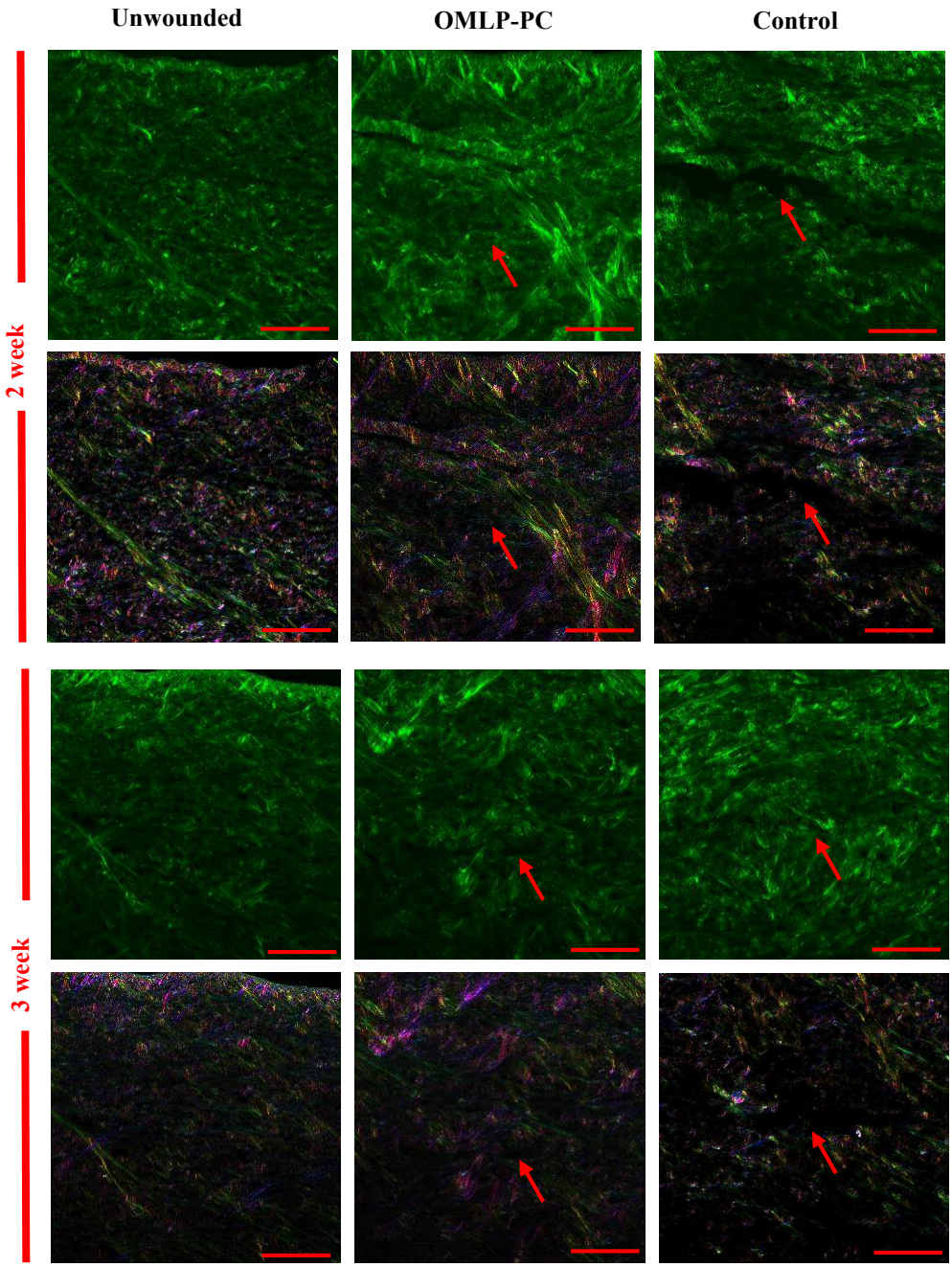

Figure 6.9 SHG imaging of the collagenous stroma (green) of treated and untreated LASIK-like wounded and unwounded corneas at 2 and 3 weeks in organ culture. Collagen lamellae appear increasingly disorganised in all corneas. Colour map overlay orientation generated by OrientationJ plugin for Image J version 1.52a (National Institutes of Health, USA). Arrows indicate wound site. Scale bar represents 100µm.

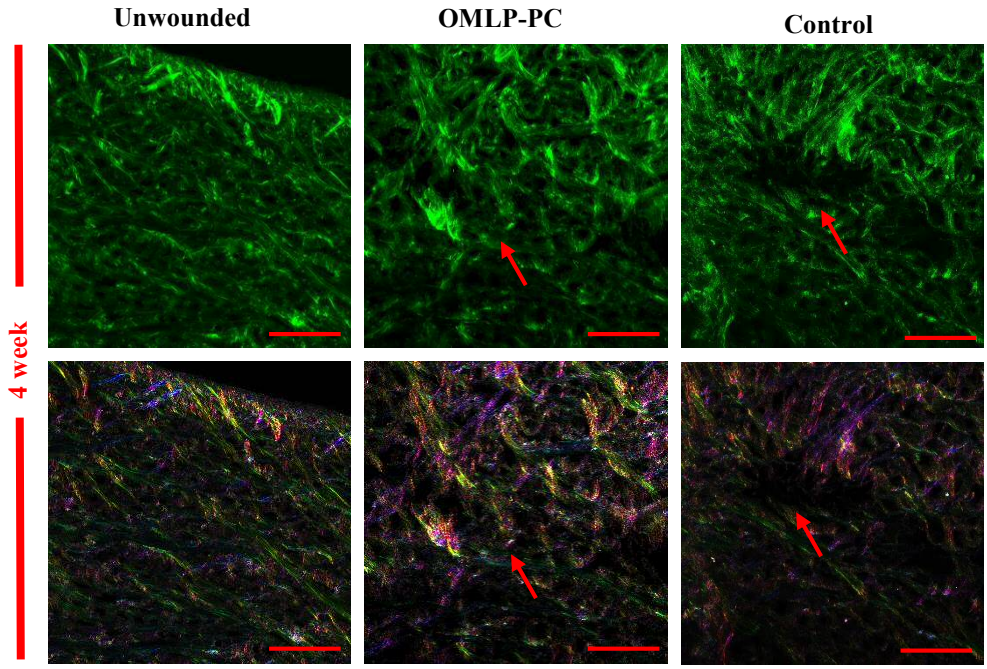

Figure 6.10 SHG imaging of the collagenous stroma (green) of treated and untreated LASIK-like wounded and unwounded corneas after 4 weeks in organ culture. Collagen lamellae appear more disorganised in the wounded corneas compared to the unwounded corneas. Colour map overlay orientation generated by OrientationJ plugin for Image J version 1.52a (National Institutes of Health, USA). Arrows indicate wound site. Scale bar represents 100µm.

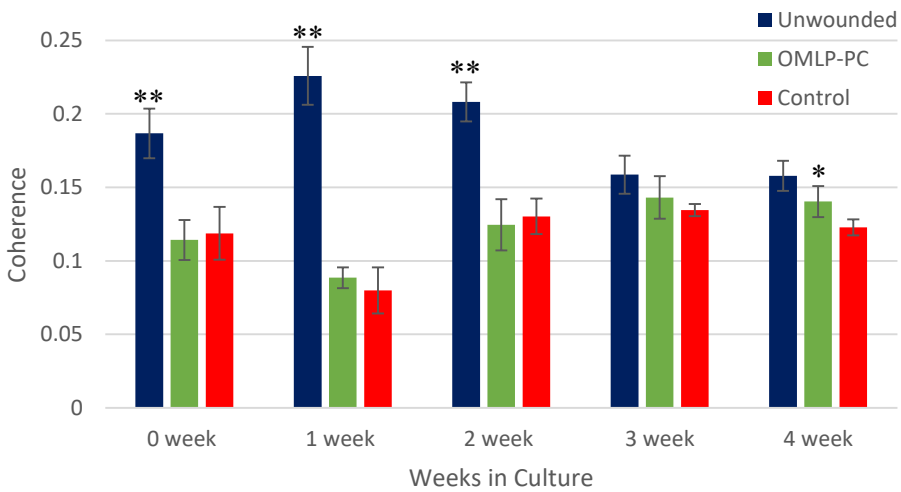

Figure 6.11 Coherence of collagen lamellae orientation in the flap centre of LASIK-like wounded corneas treated with$1.5x10^5$ cells ml^{-1} solution of OMLP-PC Cell line 2 and untreated and unwounded corneas at 5 time points during organ culture. Unwounded corneas showed a significantly higher coherence (**$p<0.001$) than wounded corneas at 0, 1, and 2 weeks. Cell treated corneas and unwounded corneas showed no significant difference in collagen coherency ($p> 0.05$) until week 4 where OMLP-PC treated corneas showed a significantly higher coherency than untreated wounded corneas (*$p<0.05$) and no significant difference when compared to unwounded corneas.

Distribution of collagen orientation was analysed using OrientationJ plugin (ImageJ, version 1.52a National Institutes of Health, USA). The wounded corneas showed a lack of any distinct peaks in distribution of stromal collagen lamellae orientation throughout the organ culture period (figure 6.12).

At 0-time point wounded corneas showed peaks in distribution at approximately 0º (horizontally), (figure 6.12A). At weeks 1, 2 and 3, definition of any peaks were less prominent in the LASIK-like wounded corneas and the treated and untreated samples appeared indistinguishable from one another (figure 6.12 B, C & D).

At the end of the organ culture period the LASIK-like wounded corneas showed a more defined peak distribution of approximately horizontal collagen lamellae orientation compared to the untreated control corneas that showed a lesser distribution peak off the horizontal axis (figure 6.12 E).

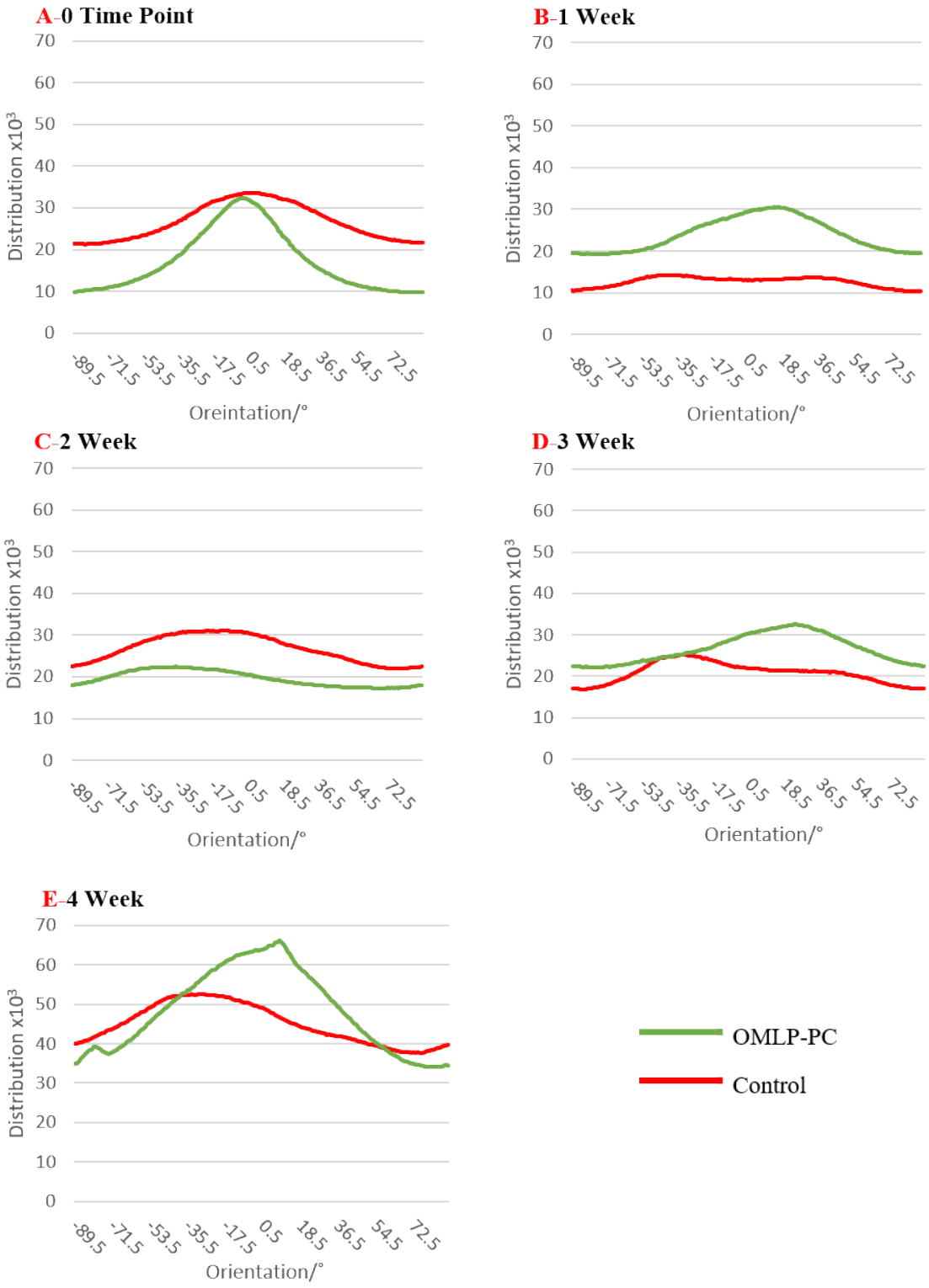

Figure 6.12 Weekly Time Points of Distribution of Collagen Lamellae Orientations over an organ culture period of LASIK-like wounded corneas treated with a control solution (Control) and similarly wounded corneas treated with OMLP-PCs (OMLP-PC). Distinction of peaks in collagen lamellae orientation distribution decreases from time point 0 over weeks 1, 2 and 3 before increasing at week 4 for both treated and untreated LASIK-like wounded corneas.

6.7. Discussion

The stromal collagen lamellae organisation of the cornea can potentially undergo dramatic changes during corneal wound healing, largely due to the deposition of repair extracellular matrix ECM and abnormally large proteoglycans produced by activated myofibroblasts during the granulation and remodelling stages of wound healing (Kamma Lorger et al., 2009; Zieske, 2001; Fini, 1999; Funderburgh et al., 1998). Whilst this study of collagen organisation during wound healing after LASIK-like incision in an organ culture model can be used to assess the efficacy of OMLP-PCs in improving the wound healing outcomes in the porcine model, the effects on orientation of the stromal lamellae can only derive a general comparison as the lamellar orientation of humans and pigs is different.

A diffraction study by Meek et al., in 1987 determined that the orthogonal preferential orientation of stromal collagen appears unique to humans and in recognition of the fact that research in this area would be heavily reliant on specimens obtained from abattoirs, a need for a comparative study was suggested. This was later confirmed by Hayes et al., (2007) who ran a comparative study of fibrillar collagen arrangement in the corneas of primates and other mammals using X-ray scattering patterns, and included porcine corneas. The corneal collagen arrangement of pigs was found to be circumferential compared to orthogonal in humans.

In this study the crucial organisation of collagen fibres was assessed in the central section of the stroma (flap centre) of LASIK-like wounded porcine corneas treated with $1.5x10^5$ cells ml^{-1}, similarly wounded control porcine corneas treated with a control solution and unwounded porcine corneas over a 4 week organ culture period. An overview of the structural changes within the wound healing organ cultured porcine corneas was performed by looking at stromal wound morphology using H&E staining. A more in-depth investigation into the microstructural changes in the collagenous stroma over the same time period was carried out using SHG imaging, taking advantage of the non-centrosymmetric nature of corneal collagen. The stromal collagen organisation was quantitatively analysed

from these images using OrientationJ plugin (ImageJ, version 1.52a (National Institutes of Health, USA), whereby the coherency of orientation was determined and the distribution of orientation over the entire image was determined.

All corneas treated, wounded or unwounded, exhibited signs of stromal swelling during organ culture. Consequently, the collagen appeared more disorganised and the cell density reduced over the 4 week period. The corneas treated with the OMLP-PCs demonstrated a faster, more comprehensive closure of the stromal wound inflicted, compared to the gaping between the epithelial-stromal flap and the wound bed still evident in the control untreated wounded corneas, seen at equivalent time points. The cell-treated corneas also demonstrated a close resemblance to the unwounded control corneas in the central flap region by week 4. The central wound area of the OMLP-PC treated wounded corneas at 4 weeks was relatively acellular with warped and stretched appearance to the ECM. However, the ECM collagen had been laid down sufficiently at the wound site to effectively close the wound, compared to the remaining space and gaping viewed in untreated control corneas at the same time point.

The results of the orientation analysis of coherence and distribution of corneal collagen lamellae orientation showed that both the treated and untreated wounded porcine corneas exhibited a significantly reduced coherence of collagen lamellae orientation compared to the unwounded porcine corneas in the first 3 time points during organ culture ($p<0.001$). Although at different amplitudes, the dominant orientation for wounded corneas at 0 time point appeared to be horizontal. The coherency of the collagen lamellae orientation of the wounded corneas was significantly lower than the unwounded controls immediately after wounding at 0 time point. This is possibly a result of the incision severing lamellae that run from limbus to limbus (Radner et al., 1998) and so releasing the mechanical tension that would be present in the collagen fibres running through the lamellae resulting in an instant reduction in orientation coherency at the time of wounding.

At week one the coherency of the collagen lamellae orientation had significantly dropped in both the wounded treated and untreated corneal samples, this would reflect the activation of keratocytes and their transformation into myofibroblasts, which begin to lay down disorganised repair extracellular matrix (Masur et al., 1996; Møller-Pedersen et al., 1997; Jester et al., 1999; Mohan et al., 2003). Likewise, the distinction of any preferential orientation distribution decreased in the wounded samples. The remodelling that takes place during wound healing occurs concurrently with apoptosis and proliferation in a rolling wound healing cascade (Mohan et al., 2001; Fini et al., 1999) and ECM can continue to remodel for weeks. Over weeks 2 and 3 of organ culture wound healing in this study, the coherence of orientation in the wounded, untreated and treated corneas gradually increases from the low point at 1 week, whilst peaks in orientation distribution show gradually increasing definition in the wounded corneas. The OMLP-PC treated LASIK-like wounded porcine corneas demonstrated no significant difference to the control untreated wounded corneas during this organ culture up until and including the 3 week time point ($p>0.05$). Interestingly, over the same period the coherence of orientation in the unwounded corneas, whilst remaining significantly higher than that of the wounded corneas ($p<0.001$), gradually decreases and at 3 weeks shows no significant difference in orientation coherency compared to both wounded corneas ($p>0.05$).

Certainly, this study is limited by the fact that the analysis was only undertaken in a 2D plane, not allowing full appreciation and analysis of the 3D structural organisation of the stromal collagen. Future works should be aimed at analysis of collagen nanostructure using WAXS (wide angle x-ray scattering) in serial sections through the cornea, looking at 3D analysis of fibril orientation to gain further insight into the changes that occur in the 3 dimensional plane in organ culture and during wound healing to better characterise stromal matrix changes.

By 4 weeks the coherence of collagen lamellae orientation in the OMLP-PC treated wounded corneas had increased and was significantly higher than that of the control wounded cornea ($p<0.05$) and showed no significant difference to the unwounded control

cornea ($p>0.05$). The distribution of orientation of all wounded corneas showed increased definition compared to previous weeks at this time point, and the OMLP-PC treated LASIK-like wounded corneas showed a more prominent peak at an approximately near horizontal orientation.

The initial closure of epithelial wounds in the cornea close via an epithelial plug rapidly after the initial infliction, closing the wound completely to potential infection and debris up to 48-72hrs. The initial stages of the wound healing of the underlying corneal stroma (apoptosis and proliferation) take place relatively quickly within the first week or so (Zieske et al., 2001; Mohan et al., 2001; Wilson et al., 2001), however, complex stromal remodelling can continue for years before possibly reaching the native phenotype (Cintron et al., Fini, 1999; Lee et al., 1982). The OMLP-PC treated LASIK-like wounded corneas in this study seemed to reach an appearance (seen in H&E stained cryosections) after 4 weeks in organ culture that more closely resembled that of the unwounded porcine corneas at the same point and definitely demonstrated a more competent stromal wound closure than that observed in the control wounded corneas. Similarly, by the 4 week time point in organ culture the SHG analysis of LASIK-like wounded OMLP-PC corneas showed more definite distribution of orientation peak and had a significantly higher orientation coherence than the control wounded corneas and was not significantly different to the unwounded corneas.

Cells originating in the oral mucosa have repeatedly demonstrated their propensity for preferential wound healing; accelerating collagen gel contraction, whilst lowering α-sma activation (Shannon et al., 2006), a faster rate of proliferation, compared to dermal fibroblasts (Glim et al., 2014; Lee & Eun, 1999) and, most notably, a significantly increased ability to reorganise ECM (Stephens et al., 1995). They have been shown to express foetal stem-like wound healing characteristics (Sloan, 1991) in rapid remodelling of tissue (Stephens et al. 1996; Mak et al., 2009). Previous chapters have demonstrated that the application of OMLP-PCs to the wounded cornea, in comparison to the untreated cornea, reduce the expression of α-sma, (a marker for the transformation of corneal fibroblasts into

myofibroblasts) and improve transparency (Chapter 5). Whilst the results of this study by no means demonstrate a return to the native state of wounded stromal ECM in the 4 weeks of organ culture, it does demonstrate the potential of OMLP-PCs to augment corneal wound healing.

Chapter 7

Discussion and Future Work

7.1. Discussion

The biological priority of the complex cascade of corneal wound healing is to close the epithelial wound site to maintain the smooth refractive surface of the eye and protect the cornea from potential infection and invasion of foreign particulates that could compromise health and function. The epithelial defect caused by injury closes rapidly and efficiently, as outlined in chapter 1, and initiates wound healing in the stroma via cytokine release (section 1.6). This stromal healing, whilst also efficient and complex, can have detrimental effects on the long term quality of vision of the patient. The cytokine release from the wounded epithelium triggers keratocyte apoptosis and activates neighbouring quiescent keratocytes that then undergo myofibroblastic transformation. (Masur et al., 1996; Mohan et al., 1997; Wilson et al., 2012). These myofibroblasts are responsible for the potential wound healing related complications that lead to reduction in visual function, via the dilution of corneal crystallin concentration, the laying down of excess repair extracellular matrix (including disorganised collagen fibrils and abnormally large proteoglycans that can over hydrate the cornea resulting in a loss in transparency) and exerting the contractile forces that enable wound closure (Wilson et al., 2012; Ljubimov & Saghizadeh, 2015; Masur et al., 1996; Mohan et al., 1997).

This fibrotic response in the eye has been reviewed extensively by Shu & Lovicu (2017) and Fini (1999); it can lead, not only to a poor outcome of accidental injury and trauma, but also to poor surgical outcomes, namely corneal procedures, but this can also effect other parts of the eye; potentially blocking aqueous outflow facility after laser surgery for the treatment of glaucoma and causing secondary cataracts and subcapsular pathologies of the lens to name but a few.

This study focuses in particular on the unique wound-type inflicted on the cornea by the popular corrective refractive procedure, laser assisted in-situ keratomileusis (LASIK). The procedure creates a circular penetrating epithelial wound in the mid peripheral cornea that then extends parallel to the epithelium through the anterior third of the corneal stroma; a

wound that results in the incomplete healing and closure of the stromal wound. This has been observed on numerous occasions post-operatively *in vivo,* for example, a case described by Crawford et al. (2003) where artifactitious separation of the flap and the underlying stroma was noted in a cornea 13 months after LASIK treatment and another case 20 months after uncomplicated LASIK where a similar separation was noted by Anderson et al., 2002.

Peripheral flap melt and epithelial ingrowth are just some of the flap related complications associated with LASIK created by a microkeratome, including flap dislocation (Ivarson et al., 2003). This is of particular interest when discussing the potential reduction in biomechanical strength of the stromal wound after LASIK surgery. Whilst dislocation is rare, it has been reported up to 38 months post-operatively after impacts from airbags, dog paws, basketballs, snowballs, and fingers (Lemley et al., 2000; Melki et al., 2000; Patel et al., 2001; Iskander et al., 2001). Increasingly, femtosecond laser is becoming the preferential method of flap creation, due to its precision and superior post-operative outcomes, including greater biomechanical stability (although still inferior to that of the native unwounded cornea) and fewer post-operative complications (Kezirian & Stonecipher, 2004; Stonecipher et al., 2006; Alio et al., 2005). Therefore, although there may be a case to be made that investigating the wound healing of LASIK-like flaps created by a microkeratome is no longer relevant, the microkeratome is still used in practice.

Additionally, the microkeratome-created LASIK flap has been posited as an interesting repeatable wound model of corneal wound healing. Keratocyte apoptosis occurs along the flap interface (Wilson et al., 2000) thus potentially stimulating a healing response. It could be used to provide further insight into the wound healing response in LASIK as a model to study the basic regulation of corneal epithelial and stromal wound repair (Ivarson et al., 2003; Zieske, 2001). The improvement of corneal wound healing after trauma or surgery is a research goal and has had many permutations over the years. A selection of the wide range of corneal therapies and treatments, not discussed in this thesis can be seen in Table 7.1.

	Procedure/Therapy	Reference
Implant	Osteo-Odonto-Keratoprosthesis (OOKP)	Liu et al., 2005; Zerbe et al., 2005; Tan et al., 2012
	Boston Keratoprosthesis	
	Penetrating Keratoplasty	
	Lamellar/Deep Anterior Lamellae/endolthelial Keratoplasty	
Graft	Limbal Epithelial Cell Transplantation	Pellegrini et al., 1997; Nishida et al., 2004
	Corneal reconstruction with autologous oral mucosal Epithelium	
Cell Therapy	Dental Pulp Stem Cells	Syed-Picard et al., 2015; Basu et al., 2014; Hertsenberg & Funderburgh, 2016
	Human Limbal Biopsy Derived Stromal Cells	
	Embryonic stem cell derived keratocytes	
Bio-engineering	Human Stromal Equivalent constructed from cell Lines	Griffith et al., 1999; Buznyk et al., 2015
	Bioengineered corneas	

Table 7.1 Corneal Therapies

The overall aim of this study was to determine the effect of OMLP-PCs as a cell based therapy on corneal wounds in an organ culture model.

To achieve this aim, first an organ culture model of corneal wound healing was developed to attempt to evaluate and improve the physical outcomes of corneal wound healing of a LASIK-like flap. A porcine organ culture model that could be utilised to assess the wound healing of a LASIK-like corneal wounds was established (Chapter 3), and the application of a cell based therapy was optimised. Oral mucosal lamina propria progenitor cells (OMLP-PCs) were applied to the wound bed of the LASIK-like microkeratome inflicted wounds using an optimised $1.5x10^5$ cells ml^{-1} concentration (Chapter 4) and placed in organ culture. These were cultured alongside similarly wounded and unwounded controls, in order to determine the comparative effect of OMLP-PCs on corneal wound healing, for 0, 1, 2, 3 and 4 weeks. Once removed from culture the corneas were assessed to determine the

efficacy of the OMLP-PCs on the cellular processes involved in wound healing (Chapter 5) and the extent of wound resolution by examining the stromal matrix organisation (Chapter 6).

The use of porcine organ culture over other animals used in previous research (such as ovine used by Dooley, 2012, and bovine by Kamma-Lorger, 2007) was chosen due to the inappropriate size of bovine eyes. Previous studies involving LASIK-like wounds in bovine corneas had to use custom-made devices to create the incisions (Kamma-Lorger et al., 2009) and so wounding was not created by a microkeratome. There was also a high incidence of corneal injury in incoming ovine eyes (Chapter 4).

The pig has been shown to be an excellent animal for comparative studies with humans due to their similar anatomy and physiology (Wang et al., 2000). The success of this porcine model can be ascertained in terms of the wound healing response in the LASIK-like wounded (untreated) corneas. The keratocyte apoptosis and proliferation that occur concurrently in corneal wound healing following the initiation of cytokine-mediated stromal wound healing (Masur et al 1996; Wilson et al., 2012; Gao et al., 1997; Ljubimov & Saghizedah, 2015; Mohan et al., 1997) were evident in this organ culture. Apoptotic cells in the stroma were seen at 0 time point and increased significantly at 1 week to over 20%. Concurrently the percentage of proliferating cells in wounded (treated) corneas followed a similar trend reaching a peak of 45% at 1 week (see table 7.2). This has been seen in other previous research, namely a similar *in vivo* study using rabbits by Mohan et al. (2003), although they found this happened in a much shorter time frame, as rabbits are known to have aggressive wound healing responses and are temporally distinct from other species in this respect (Cintron & Kubin, 1977; Thomasey et al., 2012 & 2014). The myofibroblastic transformation seen in the wounded control corneas (determined by the presence of α-sma) mirrored that seen in previous successful corneal organ culture studies (Dooley, 2012; Morgan, 2015) and represented the keratocyte activation and eventual transformation into myofibroblasts.

It was found in work outlined in chapter 3, that in order to obtain a consistent biomechanical evaluation of the flap adhesion using extensometry, a customized device would have had to be made from scratch. Therefore, it was decided not to pursue this line of investigation for this thesis. The analysis of transparency using spectrophotometry was also abandoned due to the irreparable damage caused to the corneas. Hence, in order to maintain the same corneas throughout the investigation all subsequent chapters used a Visual grading system to assess corneal transparency. The concentration of the solution of OMLP-PCs to be applied to the wound bed was determined after a 4 week organ culture using 3 separate OMLP-PC solution concentrations on LASIK- like wounded corneas, compared to control wounded (untreated) corneas. Once removed from culture the α-sma immunopositivity and transparency of the cells was assessed and the concentration resulting in a significantly more transparent cornea, when compared to the wounded controls ($p<0.01$), was selected; $1.5x10^5$ OMLP-PC ml^{-1}.

Having established a porcine organ culture model, the next step was to determine if OMLP-PCs could augment the healing process following a LASIK-like wound. The effect of the application of OMLP-PCs on the LASIK-like wounded porcine corneas in this study reduced the percentage expression of α-sma by ~20%, when compared to the similarly wounded untreated control corneas (table 7.2). This was favourably comparable to the outcomes of previous studies by Dooley (2012) and Morgan (2014) whose results showed that the percentage activation for the keratocytes was significantly reduced by approximately 20-30% for the corneas treated with oral mucosa cells (Dooley, 2012), and by approximately 20% for wounded corneas, treated corneal stromal stem cells (CSSCs) (Morgan, 2014) compared to the control corneas at weeks 1, 2 and 3 in organ culture.

Interestingly the site of the expression of α-sma in LASIK-like wounded corneas appears to differ between studies. In the results of this thesis α-sma positive cells were found along the flap bed at all time points, however Kamma-Lorger (2007) found α-sma positive cells only adjacent to the epithelial incisional wound in bovine eyes at all time points, in line with studies by Ivarsen et al. (2004) and Wilson et al. (2002). Dooley (2012) and Morgan

(2014), found α-sma positive cells at the flap bed, which is supported by the literature which states that LASIK-like wounds are known to induce apoptosis at the flap interface and so would likely induce wound healing (Zieske, 2001; Wilson et al., 2000). Likewise, Mohan et al. (2003) found α-sma positive cells along the wound bed in an *in vivo* study on rabbit eyes, but only at a later point in wound healing (4 weeks). It has been suggested that the onset of myofibroblastic transformation depends on the injury inflicted, the conditions of the injury and the species used (Kamma-Lorger et al., 2009). It may also be true that the site of myofibroblastic transformation in LASIK-like wounds could possibly be species dependent.

The visually graded transparency of the OMLP-PC treated LASIK like wounded corneas was found to be significantly greater ($p<0.01$) by week 4 of the organ culture compared to untreated corneas (table 7.3). Although this is a similar overall outcome to previous work by Dooley (2012) and Morgan (2014), their results showed improved transparency at all time points across the wound healing in organ culture. This may be attributed to their attempts to return the corneas to homeostasis by de-swelling in dextran after removal from organ culture, a step not included in these studies due to the known adverse effects on cells (van der Want et al., 1983). This will be discussed later in this chapter.

Collagen lamellae coherence (a measure of the number aligned in a similar direction) in OMLP-PC treated wounded corneas was found to be significantly higher than that of untreated corneas but not significantly different to unwounded corneas (table 7.3). Additionally, in H&E histological sections the stromal wound of OMLP-PC treated corneas bore a closer resemblance to unwounded corneas at week 4; the wound gap appeared to have closed compared to the gap still seen in untreated corneas (table 7.3). The gaping of LASIK treated central corneal wounds has been noted years after surgery in various *in vivo* studies (Anderson et al., 2002; Crawford et al., 2003). The initial disorganisation of the corneal collagen in the first weeks after wounding likely occurs due to the laying down of disorganised ECM, including large proteoglycans that alter the spacing of stromal collagen, as well as stromal swelling during organ culture (see more details of this later in this

discussion). The disorganised collagen is then slowly reorganised during wound healing. The corneas treated with OMLP-PCs appear to have been remodelled closer to the native stromal state. Consistent with this, previous studies by Morgan (2014). Dooley et al. (2012) and Meek & Leonard (1997) when examining the collagen fibril spacing and diameter using SAXS (small angle X-ray scattering) analysis on LASIK-like wounded ovine eyes and wounded rabbit eyes *in vivo* (respectively), found that wounded corneas demonstrated increased Bragg spacing (i.e. interfibrillar spacing) compared to unwounded corneas. Whilst both wounded corneas in Dooley et al. (2012) study demonstrated increased Bragg spacing, those treated with oral mucosa fibroblasts showed spacing near to homeostasis. These findings are consistent with the improved corneal organisation found in this thesis after treatment of LASIK-like wounds with OMLP-PCs.

The cells used in this study were neural crest derived, multipotent progenitor cells recently found in the lamina propria of the oral mucosa; OMLP-PCs (Davies et al., 2010). Cells from the oral mucosa have been studied at length over the years due its foetal-like privileged wound repair (Stephens et al., 1996; Sloan, 1991). Their desirability as a potential cell-based therapy is heightened by their potent immunosuppressive and antimicrobial properties and ease of access. The foetal-like wound healing characteristics of oral mucosal cells have been demonstrated during this study in the LASIK-like wounded corneas treated with an application of OMLP-PCs.

After the application of OMLP-PCs under the epithelial-stromal flap of LASIK-like wounded corneas the keratocyte activation and consequential transformation into the myofibroblast phenotype was significantly reduced during organ culture, when compared to the wounded control corneas. This mirrors the decreased expression of α-sma in oral mucosal tissue, described by Shannon et al., (2006). The proliferation of the stromal cells in the wounded corneas, detected by immunolabelling of proliferating cell nuclear antigen (PCNA), was seen to peak at an earlier time point of 1 week in the OMLP-PC treated corneas compared to the wounded untreated corneas peak of proliferation a week later at a lower percentage. This demonstrated an increased earlier proliferation of cells in the

OMLP-PC treated corneas, which aligns with the faster proliferation seen in oral mucosal tissue when compared to dermal fibroblasts (Glim et al., 2014; Lee & Eun, 1999).

The analysis of the coherence of collagen lamellae in (i.e. degree of alignment) LASIK-like wounded and unwounded corneas throughout the 4 week organ culture demonstrated that by 4 weeks in culture the coherence of orientation in the OMLP-PC treated corneas had increased from initial wounding, and was significantly higher than untreated wounded corneas. There was also no significant difference in coherence compared to the unwounded corneas. The distribution of preferred orientation angles of the same samples, indicated that the collagen lamellae orientation, aligned in the horizontal axis at 0 time point in all samples, showed a reduction in alignment over the organ culture period. At week 4, the OMLP-PC treated corneas showed a more defined alignment of collagen lamellae when compared to the untreated wounded corneas indicating an advanced stage of stromal wound remodelling when compared to the untreated wounded corneas. Assessment of the morphology of the corneas, using H&E staining, reinforced this return towards native structure is a result of potentially improved stromal remodelling. The OMLP-PC treated LASIK-like wounded corneas demonstrated a close resemblance to the unwounded corneal stroma, with a closed epithelial-stromal interface at 4 weeks compared to the visible gaping still present at the wound site in the untreated wounded corneas. This is much like the significant increase in ability of oral mucosa cells such as fibroblasts to reorganise ECM shown in the oral mucosa (Stephens et al., 1995).

These foetal-like wound healing traits, observed in recent studies on the oral mucosa, appear to have been expressed in the wound healing of the LASIK-like wounded corneas treated with an application of OMLP-PCs. The reduced amount of myofibroblastic transformation reduces their negative impact on corneal crystallin concentration, whilst also reducing the laying down of excess disorganised repair ECM and the exertion of contractile forces which can further disrupt the corneal collagen organisation during wound healing. Combined with the improved remodelling of the stroma, these findings correlated with an increased transparency of the LASIK-like wounded corneas treated with OMLP-

PCs, which, by week 4 in organ culture, had a significantly higher transparency than untreated wounded corneas when compared to untreated wounded corneas, and no significant difference when compared to unwounded corneas at the same time point.

The results of these studies have been summarised in Table 7.2 and 7.3.

Apoptosis	Caspase-3 (red) and cell nuclei (blue) immunolabelled to determine percentage apoptosis of stromal cells.	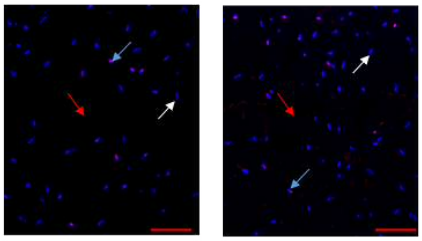 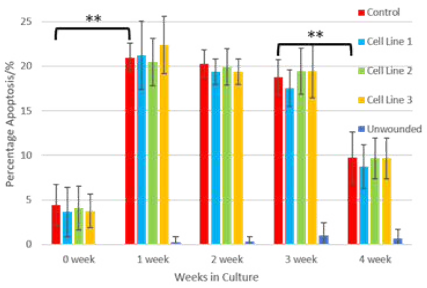	Apoptosis increased after wounding and decreased at 4 weeks. There was no significant difference between treated and untreated wounded corneas ($p>0.05$).
Cellularity	Cell nuclei immunolabelled to determine cell number.	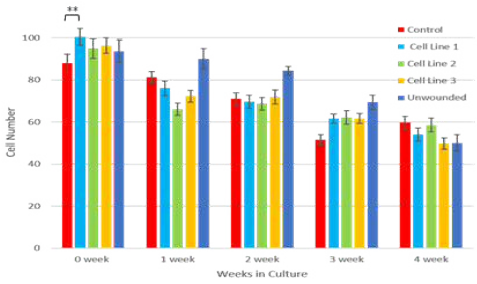	Cell number in OMLP-PC treated corneas was significantly higher (**$p<0.05$) than controls at 0 time point. A decreasing trend in cellularity was seen for all corneas from 0-4 weeks.
Proliferation	Proliferating cell nuclear antigen (PCNA) (red) and cell nuclei (blue) immunolabelled to ascertain stromal cell percentage proliferation.	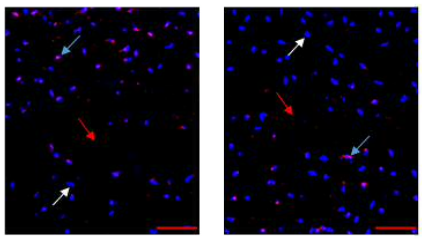 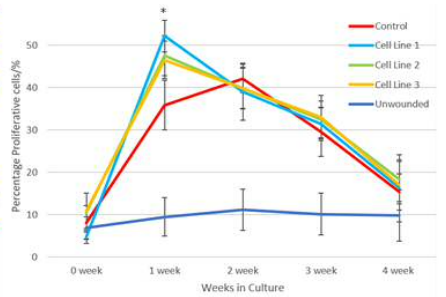	Peak percentage proliferation was 52.2% ±3.7 at 1 week in OMLP-PC treated wounds, earlier compared to 42.1% ±3.3 at 2 weeks in untreated control corneas
Myofibroblastic Transformation	α-sma (green) and cell nuclei (blue) immunolabelled to ascertain percentage keratocyte activation.	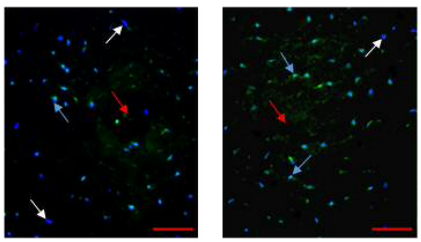 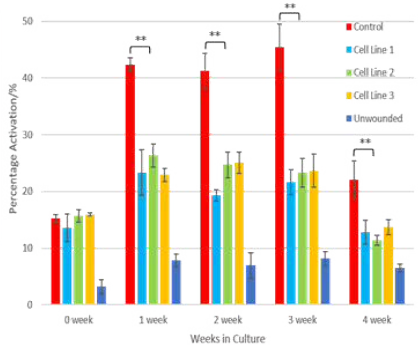	There was a significant reduction of percentage α-sma immunopositive cells (**$p<0.01$) from ~45% (untreated wounded) to ~25% (OMLP-PC-treated) during weeks 1-3 post LASIK-like wounding

Table 7.2 Summary of Cellular Processes Pertinent to Wound Healing

Transparency	Visually graded corneal transparency.	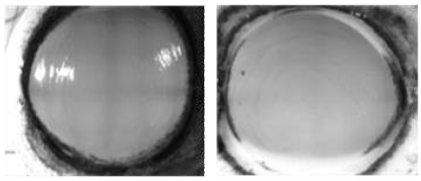 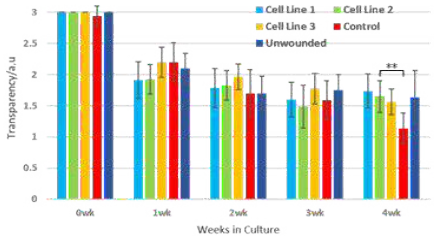 By 4 weeks corneal transparency in OMLP-PC treated wounded corneas was significantly higher than in untreated corneas (**p<0.01)
Morphology	Stromal morphology assessment using H&E staining.	Scale bars =100μm 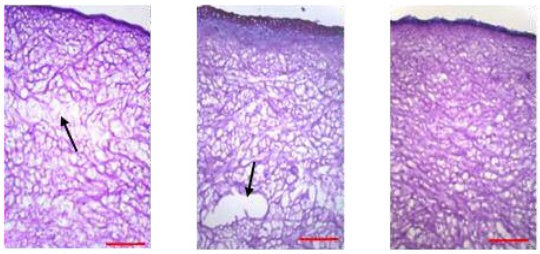 = wound By 4 weeks OMLP-PC treated wounded corneas demonstrated a close resemblance to unwounded control corneas (central flap region) compared to gaping at the wound site still evident in untreated wounded corneas.
SHG	Corneal lamellae coherence of orientation analysis of SHG images.	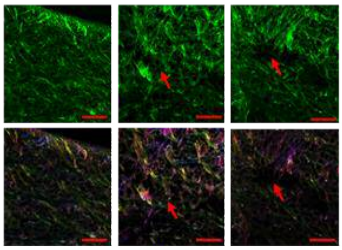 Scale bars =100μm = wound 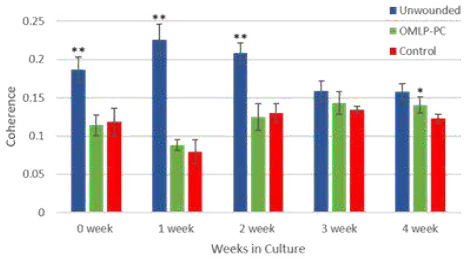 Coherence (degree of collagen lamellae alignment) at 4 weeks after wound healing was significantly higher in OMLP-PC treated wounded corneas (*p<0.05), compared to that in untreated corneas.

Table 7.3 Summary of Pertinent Physical and Morphological Outcomes

There were several limitations in this study which need to be addressed. The swelling of the porcine corneas in organ culture was noted throughout the experiments. Corneal hydration homeostasis is a result of a balancing act between the natural tendency of the cornea to take up fluids, due to the highly hydrophilic nature of proteoglycans glycosaminoglycan (GAG) side chains, and the dehydrating mechanism of the stroma in

the form of the endothelial pump (Hodson, 1997). During wound healing in organ culture the cornea swells, possibly due to a disruption in the endothelial barrier function (Kamma-Lorger et al., 2007). The wound healing process itself is thought to increase the uptake of water as the energy requirements of the tissue itself increase (Kamma-Lorger et al., 2009) The production of abnormally large proteoglycans by myofibroblasts during ECM deposition (Funderburgh et al., 1998; Saika et al., 1998; Ishizaki et al., 1994) and higher cell number as a result of proliferation can contribute to corneal swelling (Mohan et al., 2003; Wilson & Kim, 1998).

Previous studies by Dooley et al., (2012) and Morgan et al., (2014) attempted to return the cornea to homeostasis after organ culture incubating corneas in 8% dextran at 37˚C, for 3hrs and overnight respectively. This was successful in terms of reduction of swelling and potentially improved the results of corneal transparency. However, this was not carried out in this study as the 3hr or overnight immersion in dextran may have had negative impacts on the cellular processes and the LASIK-like flap morphology, thereby not generated results true to the time point. However, the consequent swelling of the cornea would have falsely altered the stromal cell number (as the number of cells in the same 100μm^2 area of the stroma would have decreased as stromal swelling increased during the organ culture period) and so the actual stromal cell number may in fact be higher than that recorded. The collagen orientation may also have been affected by corneal swelling as the increase in interfibrillar spacing may have contributed to stromal disorganisation, which would have negatively impacted on the transparency of the corneas. The results were compared to the unwounded corneas, which were subjected to identical organ culture conditions and so would serve as a baseline comparison. The issue of excess corneal hydration will be addressed in future work section.

Several lines of investigation for this study were discontinued relatively early on. The use of transmission electron microscopy (TEM) was not possible as the LASIK-like wound to be imaged was, by its nature, easily detached. Therefore, in order to preserve the morphology of the wound during processing, the size of each sample needed to be

unusually large for TEM. This larger size resulted in poorer quality embedding due to the inability of solutions to penetrate into the tissue, and the resultant inability to locate any wound landmarks.

In extensometry tests of the samples, the results were not consistent to deliver reliable results. Unfortunately, epithelial-stromal flap adherence to the stromal bed could not be determined. Data profiles were inconsistent and showed that the time of detachment and force required could not be reliably ascertained from the graph alone; visual confirmation was required. The inconsistency of these profiles suggested that other factors such as the intraocular pressure (IOP) of the corneal sample would need much tighter regulation. The testing also completely destroyed the corneal sample and rendered any further processing impossible. It was decided that a custom-built shear rig or rheometer would be a more appropriate method, so this line of investigation was discontinued for this current study.

It was anticipated that spectrophotometry of the corneal samples would provide numerical data relating to their transparency as a function of wavelength before and after organ culture. However, it destroyed the sample rendering any further processing impossible. Previous studies (Kamma-lorger et al., 2009) had used visual transparency grading and it was decided to employ this method instead as analysis of cell processes could be undertaken on the same corneas. This method however, did have its limitations. The visual grading (as described in section 2.11.2) provides a gross result in terms of perceived transparency. This could be improved by the use of diffuse sheet lighting when imaging to eliminate corneal reflections. Additionally, a more robust unbiased method of analysis of transparency by software such as ImageJ (National Institutes of Health, USA) would be an improvement.

Conclusions

To conclude, an OMLP-PC therapeutic application to LASIK-like wounds enhanced stromal cell proliferation and reduced myofibroblast expression, but increased collagen organisation with consequent improved epithelial-stromal flap wound closure and increased corneal transparency

7.2. Future Work

1. Follow the OMLP-PC's during wound healing in organ culture using fluorescent labelling/tagging to determine whether they remain in the wound integrate into the matrix, and then differentiate into fibroblasts or augment the wound healing process by the excretion of various factors into the ECM needs to be determined. If the latter, the known combination of optimal mediators could be determined, so that a cell–free therapy could be applied to the wound.

2. TUNEL analysis to confirm the caspase-3 active immunolabelling detection of apoptosis during wound healing.

3. Testing of the biomechanical strength of the wounded corneas at set time points during organ culture to determine the biomechanical strength of the wound healing cornea. A custom made rig would be necessary to ensure uniform force and detachment in a shearing action was possible.

4. Establish a protocol to control corneal swelling during organ culture either by additions made to the media during incubation or by a process on removal from organ culture.

5. Examine in more detail the first week of wound healing with time points set at 4hrs, 8hrs, 12hrs, 24hrs, 48hrs and 72 hrs (etc.) to observe the changes in wound healing that occur during the first few hours.

6. Apply the OMLP-PCs to different wound models e.g. PRK or trephine to determine their efficacy within different wound types, as this could be a therapy for other ocular wound types.

7. Placing human cells in porcine organs appears to elucidate positive results, however species matching future *in vitro* and, possibly *in vivo,* studies could potentially improve results.

8. 3D analysis of fibril orientation to gain further insight into the changes that occur in the 3 dimensional plane in organ culture and during wound healing to better characterise stromal matrix changes

9. Examination of collagen ultrastructural parameters using SAXS to determine collagen fibril diameters and interfibrillar spacing and using WAXS to determine collagen intermolecular spacing and orientation.

10. Create 3D models of human wound healing which could be used to test drug/therapies before application in culture.

.

References

Alió, J. L., Claramonte, P. J., Cáliz, A. and Ramzy, M. I. (2005) Corneal modeling of keratoconus by conductive keratoplasty. *J Cataract Refract Surg*. 31: 190–197.

Al-Taan, S.L.M., 2018. *Characterisations of Pre-Descemet's (Dua's) layer for its clinical application in keratoplasty* (Doctoral dissertation, University of Nottingham).

Ambrósio, R. Jr and Wilson, S. (2003) LASIK vs LASEK vs PRK: advantages and indications. *Semin Ophthalmol*. 18: 2-10.

Anderson, N.J., Edelhauser, H.F., Sharara, N., Thompson, K.P., Rubinfeld, R.S., Devaney, D.M., L'hernault, N. and Grossniklaus, H.E., (2002). Histologic and ultrastructural findings in human corneas after successful laser in situ keratomileusis. *Arch Ophthalmol*, *120*(3), pp.288-293.

Andresen, J.L., Ledet, T., Hager, H., Josephsen, K. and Ehlers, N., (2000). The influence of corneal stromal matrix proteins on the migration of human corneal fibroblasts. *Exp Eye Res., 71*(1), pp.33-43.

Azar, D. T. and Farah, S. G. (1998) Laser in situ keratomileusis versus photorefractive keratectomy: an update on indications and safety. *Ophthalmology*. 105: 1357-1358.

Bansal, A. K. and Veenashree, M. P. (2001) Laser refractive surgery: technological advance and tissue response. *Biosci Rep*. 21: 491-512.

Basu, S., Hertsenberg, A.J., Funderburgh, M.L., Burrow, M.K., Mann, M.M., Du, Y., Lathrop, K.L., Syed-Picard, F.N., Adams, S.M., Birk, D.E. and Funderburgh, J.L., (2014). Human limbal biopsy–derived stromal stem cells prevent corneal scarring. *Sci Transl Med*, 6(266), pp.266ra172-266ra172.

Board-Davies E, Moses R, Sloan A, Stephens, P. and Davies L C. (2015), Oral Mucosal Lamina Propria-Progenitor Cells Exert Antibacterial Properties via the Secretion of Osteoprotegerin and Haptoglobin. *Stem Cell Transl Med*, 4: 1283-1293.

Bodner L, Dayan D, Oberman M, Hirshberg A, Tal H (1992). Healing of experimental wounds in sialadenectomized rat. *J Clin Periodontol* 19:345-347.

Borcherding, M. S., Blacik, L. J., Sittig, R. A., Bizzell, J. W., Breen, M. and Weinstein, H. G. (1975) Proteoglycans and collagen fibre organization in human corneoscleral tissue. *Exp Eye Res*. 21: 59-70.

Brown E, McKee T, DiTomaso E, Pluen A, Seed B, Boucher Y, Jain R K. (2003) Dynamic imaging of collagen and its modulation in tumors *in vivo* using second harmonic generation. *Nat. Med.* **9**, 796–800

Buznyk, O., Pasyechnikova, N., Islam, M.M., Iakymenko, S., Fagerholm, P. and Griffith, M., (2015). Bioengineered corneas grafted as alternatives to human donor corneas in three high risk patients. *Clin Transl Sci*, *8*(5), pp.558-562.

Campagnola P J, Loew L M (2003) Second-harmonic imaging microscopy for visualizing biomolecular arrays in cells, tissues and organisms *Nat Biotechnol*, 21: 1356–1360

Carrington, L. M., Albon, J., Anderson, I., Kamma, C. and Boulton, M. (2006) Differential regulation of key stages in early corneal wound healing by TGF-beta isoforms and their inhibitors. *Invest Ophthalmol Vis Sci*. 47: 1886-1894.

Carrington, L. M. and Boulton, M. (2005) Hepatocyte growth factor and keratinocyte growth factor regulation of epithelial and stromal corneal wound healing. *J Cataract Refract Surg*. 31: 412-423.

Chakravarti, S., Magnuson, T., Lass, J. H., Jepsen, K. J., LaMantia, C. and Carroll, H. (1998) Lumican regulates collagen fibril assembly: skin fragility and corneal opacity in the absence of lumican. *J Cell Biol*. 141: 1277-1286.

Chaurasia, S.S., Kaur, H., de Medeiros, F.W., Smith, S.D. and Wilson, S.E., 2009. Dynamics of the expression of intermediate filaments vimentin and desmin during myofibroblast differentiation after corneal injury. *Exp Eye Res*, *89*(2), pp.133-139.

EChen, J., Ahmad, R., Li, W., Swain, M., & Li, Q. (2015). Biomechanics of oral mucosa. *J R Soc Interface*, *12*(109), 20150325.

Chuck, R.S., Quiros, P.A., Perez, A.C. and McDonnell, P.J., 2000. Corneal sensation after laser in situ keratomileusis1. *J Cataract Refract Surg*, *26*(3), pp.337-339.

Cintron, C., Covington, H. I. and Kublin, C. L. (1990) Morphologic analyses of proteoglycans in rabbit corneal scars. *Invest Ophthalmol Vis Sci*. 31: 1789-1798.

Cintron, C. and Kublin, C.L., 1977. Regeneration of corneal tissue. *Dev Biol*, *61*(2), pp.346-357.

Cintron, C., Hong, B.S. and Kublin, C.L., 1981. Quantitative analysis of collagen from normal developing corneas and corneal scars. *Curr Eye Res*, *1*(1), pp.1-8.

Clark, R. A. (1993) Biology of dermal wound repair. *Dermatol Clin*. 11: 647-666.

Cogan, D. G. and Kinsey, V. E. (1942) Physiologic studies on the cornea. *Science*. 95: 607-608.

Connon, C. J. and Meek, K. M. (2003) Organization of corneal collagen fibrils during the healing of trephined wounds in rabbits. *Wound Repair Regen*. 11: 71–78.

Cox, G., Kable, E., Jones, A., Fraser, I., Manconi, F. and Gorrell, M.D., 2003. 3-dimensional imaging of collagen using second harmonic generation. *J Struct Biol*, *141*(1), pp.53-62.

Cox, J. L., Farrell, R. A., Hart, R. W. and Langham, M. E. (1970) The transparency of the mammalian cornea. *J Physiol*. 210: 601-616

Crawford, J.B., Aldave, A.J., McLeod, S., Howes, E. and Schwartz, D., 2003. Histopathological analysis of the cornea after laser in situ keratomileusis. *Arch Ophthalmol*, *121*(6), pp.896-898.

Christens-Barry, W.A., Green, W.J., Connolly, P.J., Farrell, R.A. and Mccally, R.L., 1996. Spatial mapping of polarized light transmission in the central rabbit cornea. *Exp Eye Res 62*(6), pp.651-662.

Darby I, Skalli O, Gabbiani G. (1990) Alpha-smooth muscle actin is transiently expressed by myofibroblasts during experimental wound healing. *Lab Invest*; 63: 21–9

Darzynkiewicz, Z., Galkowski, D. and Zhao, H. (2008) Analysis of apoptosis by cytometry using TUNEL assay. *Methods*. 44: 250-254.

Davies L C, Locke M, Webb R D J, Roberts J T, Langley M, Thomas D W. Archer C W, and Stephens P (2010) A Multipotent Neural Crest-Derived Progenitor Cell Population Is Resident Within the Oral Mucosa Lamina Propria *Stem Cell Dev* 19:6, 819-830

Davies L C, Lönnies H, Locke M, Sundberg B, Rosendahl K, Götherström C, Le Blanc K, and Stephens P (2012).Oral Mucosal Progenitor Cells Are Potently Immunosuppressive in a Dose-Independent Manner. *Stem Cell Dev,* 21:9: 1478-148

Davison P F, Galbavy E J; (1986) Connective tissue remodeling in corneal and scleral wounds. *Invest. Ophthalmol. Vis. Sci.*;27(10):1478-1484.

Dawson, D. G., Randleman, J. B., Grossniklaus, H. E., O'Brien, T. P., Dubovy S. R., Schmack, I., Stulting, R. D. and Edelhauser, H. F. (2008) Corneal ectasia after excimer laser keratorefractive surgery: histopathology, ultrastructure and pathophysiology. *Ophthalmology*. 115: 2181–2191.

Daxer, A., Misof, K., Grabner, B., Ettl, A. and Fratzl, P. (1998) Collagen fibrils in the human corneal stroma: structure and aging. *Invest Ophthalmol Vis Sci*. 39: 644-648.

Daxer, A. and Fratzl, P. (1997) Collagen fibril orientation in the human corneal stroma and its implications in keratoconus. *Invest Ophthalmol Vis Sci*. 38: 121–129.

Deering, M.F., 2005, July. A photon accurate model of the human eye. In *ACM T Graphic* (Vol. 24, No. 3, pp. 649-658). ACM.

DelMonte, D.W. and Kim, T., (2011). Anatomy and physiology of the cornea. *J Cataract Refract Surg*, *37*(3), pp.588-598.

Doutch, J., Quantock, A. J., Smith, V. A. and Meek, K. M. (2008) Light transmission in the human cornea as a function of position across the ocular surface: theoretical and experimental aspects. *Biophys J*. 95: 5092-5099.

Du, Y., Funderburgh, M. L., Mann, M. M., SundarRaj, N. and Funderburgh, J. L. (2005) Multipotent stem cells in human corneal stroma. *Stem Cells*. 23: 1266-1275.

Dua, H. S., Faraj, L. A., Said, D. G., Gray, T. and Lowe, J. (2013) Human corneal anatomy redefined: a novel pre-Descemet's layer (Dua's layer). *Ophthalmology*. 120:1778-1785.

Dua, H.S., Gomes, J.A. and Singh, A., (1994). Corneal epithelial wound healing. *The Brit J Ophthalmol*, *78*(5), p.401.

Dua, H.S., Miri, A., Alomar, T., Yeung, A.M. and Said, D.G., 2009. The role of limbal stem cells in corneal epithelial maintenance: testing the dogma. *Ophthalmology*, *116*(5), pp.856-863.

Elsheikh, A., Alhasso, D. and Rama P. (2008) Biomechanical properties of human and porcine corneas. *Exp Eye Res*. 86: 783-790.

Enoch, S., Moseley, R., Stephens, P. and Thomas, D.W., (2008). The oral mucosa: a model of wound healing with reduced scarring. *Oral Surg*, *1*(1), pp.11-21.

Enoch, S., Wall, I., Peake, M., Davies, L., Farrier, J., Giles, P., Baird, D., Kipling, D., Price, P., Moseley, R. and Thomas, D., (2009). Increased oral fibroblast lifespan is telomerase-independent. *J Dent Res*, *88*(10), pp.916-921.

Eraslan, M. and Toker, E., 2009. Mechanisms of corneal wound healing and its modulation following refractive surgery. *Marmara Med J*, 22(2); pp.169-178

Faber, C., Scherfig, E., Prause, J. U. and Sørensen, K. E. (2008) Corneal thickness in pigs measured by ultrasound pachymetry in vivo. *Scand. J Lab Anim Sci*. 35: 39-43.

Fagerholm, P., Hamberg-Nyström, H. and Tengroth, B. (1994) Wound healing and myopic regression following photorefractive keratectomy. *Acta Ophthalmol*. 72: 229-234.

Falabella, A. and Kirsner, R. (2005). Wound healing, Basic and Clinical Dermatology. Boca Raton: Talyor & Francis.

Farrell, R. A. and McCally, R. L. (2000) Corneal transparency. In: Albert, D. M. and Jakobiec, F. A. [ed.] *Principles and Practice of Ophthalmology*. Philadelphia: WB Saunders: PA, pp. 629–643.

Fini, M. E. (1999) Keratocyte and Fibroblast Phenotypes in the Repairing Cornea. *Prog Retin Eye Res*. 18: 529-551.

Fini, M. E., Yue, B. Y. and Sugar, J. (1992) Collagenolytic/gelatinolytic metalloproteinases in normal and keratoconus corneas. *Curr Eye Res*. 11: 849-862.

Fleisch, L. and Austin, J.C., (1978). A histologic study of the response of masticatory and lining mucosa to mechanical loading in the vervet monkey. *J Prosthet Dent*, *39*(2), pp.211-216.

Foreman, D. M., Pancholi, S., Jarvis-Evans, J., McLeod, D. and Boulton, M. E. (1996) A simple organ culture model for assessing the effects of growth factors on corneal reepithelialization. *Exp Eye Res*. 62: 555-564.

Forrester, J.V., Dick, A.D., McMenamin, P. and Lee, W., 1996. The eye. *Basic Sciences in Practice*.

Franěk F, Šorm F (1970) The character of homology between the N-terminal variable amino acid sequence of porcine and human immunoglobulin λ chains*, Biochim Biophys Acta - Protein Structure*, 221(3):593-603

Freund, D. E., McCally, R. L. and Farrell, R. A. (1986) Effects of fibril orientations on light scattering in the cornea. *J Opt Soc Am A*. 3: 1970-1982.

Freund, D. E., McCally, R. L. and Farrell, R. A. (1991) Light scattering tests of structure in normal and swollen rabbit corneas. *Johns Hopkins APL Tech Dig*. 12: 137–143.

Funderburgh, J. L., Corpuz, L. M., Roth, M. R., Funderburgh, M. L., Tasheva, E. S. and Conrad, G. W. (1997) Mimecan, the 25-kDa corneal keratan sulfate proteoglycan, is a product of the gene producing osteoglycin. *J Biol Chem*. 272: 28089-28095.

Funderburgh, J. L., Mann, M. M. and Funderburgh, M. L. (2003) Keratocyte phenotype mediates proteoglycan structure: a role for fibroblasts in corneal fibrosis. *J Biol Chem*. 278: 45629–45637.

Gabbiani, G. (2003), The myofibroblast in wound healing and fibrocontractive diseases. *J. Pathol*., 200: 500-503.

Gandhi, N. S. and Mancera, R. L. (2008) The structure of glycosaminoglycans and their interactions with proteins. *Chem Biol Drug Des*. 72: 455-482.

Gao, J., Gelber-Schwalb, T. A., Addeo, J. V. and Stern, M. E. (1997) Apoptosis in the rabbit cornea after photorefractive keratectomy. *Cornea*. 16: 200-208.

Gardner, S.J., White, N., Albon, J., Knupp, C., Kamma-Lorger, C.S. and Meek, K.M., 2015. Measuring the refractive index of bovine corneal stromal cells using quantitative phase imaging. *Biophys J*, *109*(8), pp.1592-1599

Georgiou, E., Theodossiou, T., Hovhannisyan, V., Politopoulos, K., Rapti, G.S. and Yova, D., 2000. Second and third optical harmonic generation in type I collagen, by nanosecond laser irradiation, over a broad spectral region. *Opt Commun, 176*(1-3), pp.253-260.

Gipson, I.K., 1993. Corneal wound healing and fibronectin. *Int Ophthalmol Clin.*, *33*, pp.149-163.

Girgis, R., Morris, D. S., Kotagiri, A. and Ramaesh, K. (2007) Bilateral corneal scarring after LASIK and PRK in a patient with propensity to keloid scar formation. *Eye*. 21: 96-97.

Glim J E, Everts V, Niessen F B, Ulrich M M, Beelen R H.J (2014) Extracellular matrix components of oral mucosa differ from skin and resemble that of foetal skin, *Arch Oral Biol* 59(10):1048-1055

Griffith, M., Osborne, R., Munger, R., Xiong, X., Doillon, C.J., Laycock, N.L., Hakim, M., Song, Y. and Watsky, M.A., (1999). Functional human corneal equivalents constructed from cell lines. *Science*, *286*(5447), pp.2169-2172.

Han M, Giese G, and Bille J (2005). Second harmonic generation imaging of collagen fibrils in cornea and sclera, *Opt Express* 13, 5791-5797

Hahnel, C., Somodi, S., Weiss, D.G. and Guthoff, R.F., 2000. The keratocyte network of human cornea: a three-dimensional study using confocal laser scanning fluorescence microscopy. *Cornea*, *19*(2), pp.185-193.

Hart, R. W. and Farrell, R. A. (1969) Light scattering in the cornea. *J Opt Soc Am*. 59:766-774.

Hashemi, H., Fotouhi, A., Yekta, A., Pakzad, R., Ostadimoghaddam, H. and Khabazkhoob, M., 2018. Global and regional estimates of prevalence of refractive errors: systematic review and meta-analysis. *J Curr Ophthalmol*, *30*(1), pp.3-22.

Hayashi, S., Osawa, T. and Tohyama, K., 2002. Comparative observations on corneas, with special reference to Bowman's layer and Descemet's membrane in mammals and amphibians. *J Morphol*, *254*(3), pp.247-258.

Hayes, S., Boote, C., Lewis, J., Sheppard, J., Abahussin, M., Quantock, A. J., Purslow, C., Vortruba, M. and Meek, K. M. (2007a) Comparative study of fibrillar collagen arrangement in the corneas of primates and other mammals. *Anat Rec*. 290: 1542-1550.

Hayes, S., White, T., Boote, C., Kamma-Lorger, C.S., Bell, J., Sorenson, T., Terrill, N., Shebanova, O. and Meek, K.M., (2017). The structural response of the cornea to changes in stromal hydration. *J R Soc Interface*, 14(131).

Heickell, A. G., Vesaluoma, M. H., Tervo, T. M., Vannas, A. and Krootila, K. (2004) Late traumatic dislocation of laser in situ keratomileusis flaps. *J Cataract Refract Surg*. 30: 253-256.

Helena, M. C., Baerveldt, F., Kim, W. J. and Wilson, S. E. (1998) Keratocyte apoptosis after corneal surgery. *Invest Ophthalmol Vis Sci*. 39: 276-283.

Hertsenberg, A.J. and Funderburgh, J.L., (2015). Generation of corneal keratocytes from human embryonic stem cells. In *Embryonic Stem Cell Protocols* (pp. 285-294). Humana Press, New York, NY.

Hirano, K., Kobayashi, M., Kobayashi, K., Hoshino, T. and Awaya, S. (1989) Experimental formation of 100 nm periodic fibrils in the mouse corneal stroma and trabecular meshwork. *Invest Ophthalmol Vis Sci*. 30: 869-874.

Hogan, M., Alvarado, J. and Weddell, J. (1971). *Histology of the human eye*. Philadelphia: Saunders.

Huang, Y. and Meek, K.M., 1999. Swelling studies on the cornea and sclera: the effects of pH and ionic strength. *Biophys J*, *77*(3), pp.1655-1665.

Hull, D. S., Green, K. and Laughter, L. (1984) Cornea endothelial rose Bengal photosensitization. Effect on permeability, sodium flux, and ultrastructure. *Invest Ophthalmol Vis Sci*. 25: 455-460.

Hutson JM, Niall M, Evans D, Fowler R (1979). Effect of salivary glands on wound contraction in mice. *Nature* 279:793-795.

Ihanamäki, T., Pelliniemi, L.J. and Vuorio, E., 2004. Collagens and collagen-related matrix components in the human and mouse eye. *Prog Retin Eye Res*, *23*(4), pp.403-434.

Irwin, C.R., Picardo, M., Ellis, I., Sloan, P., Grey, A., McGurk, M. and Schor, S.L., 1994. Inter-and intra-site heterogeneity in the expression of fetal-like phenotypic characteristics by gingival fibroblasts: potential significance for wound healing. *J Cell Sci*, *107*(5), pp.1333-1346.

Iskander, N. G., Peters, N. T., Anderson Penno, E. and Gimbel, H. V. (2001) Late traumatic flap dislocation after laser in situ keratomileusis. *J Cataract Refract Surg*. 27:1111-1114.

Ishizaki M, Wakamatsu K, Matsunami T, Yamanaka N, Saiga T, Shimizu Y, Zhu G, Kao W (1994) Dynamics of the Expression of Cytoskeleton Components and Adherens Molecules by Fibroblastic Cells in Alkali-burned and Lacerated Corneas, *Exp Eye Res*, 59(5); 537-549

Ivarsen, A., Laurberg, T. and Møller-Pedersen, T. (2003) Characterisation of corneal fibrotic wound repair at the LASIK flap margin. *Brit J Ophthalmol*. 87: 1272-1278.

Jain, S. and Azar, D.T., 1994. Extracellular matrix and growth factors in corneal wound healing. *Curr Opin Ophthalmol*, *5*(4), pp.3-12.

Jester, J.V., 2008, April. Corneal crystallins and the development of cellular transparency. In *Semin Cell Dev Biol* (Vol. 19, No. 2, pp. 82-93). Academic Press.

Jester, J. V., Brown, D., Pappa, A. and Vasiliou, V. (2012) Myofibroblast differentiation modulates keratocyte crystallin protein expression, concentration, and cellular light scattering. *Invest Ophthalmol Vis Sci*. 53: 770-778.

Jester, J. V., Budge, A., Fisher, S. and Huang, J. (2005) Corneal keratocytes: phenotypic and species differences in abundant protein expression and in vitro light-scattering. *Invest Ophthalmol Vis Sci*. 46: 2369–2378.

Jester, J.V. and Ho-Chang, J., 2003. Modulation of cultured corneal keratocyte phenotype by growth factors/cytokines control in vitro contractility and extracellular matrix contraction. *Exp Eye Res*, *77*(5), pp.581-592.

Jester, J. V., Moller-Pedersen, T., Huang, J., Sax, C. M., Kays, W. T., Cavangh, H. D., Petroll, W. M. and Piatigorsky, J. J. (1999b) The cellular basis of corneal transparency: evidence for 'corneal crystallins'. *Cell Sci*. 112: 613-622.

Jester, J. V., Petroll, W. M., Barry, P. A. and Cavanagh, H. D. (1995) Expression of alpha-smooth muscle (alpha-SM) actin during corneal stromal wound healing. *Invest Ophthalmol Vis Sci*. 36: 809-819.

Jester, J. V., Petroll, W. M. and Cavanagh, H. D. (1999a) Corneal stromal wound healing in refractive surgery: the role of myofibroblasts. *Prog Retin Eye Res*. 18: 311–356.

Jester, J. V., Rodrigues, M. M. and Herman, I. M. (1987) Characterization of avascular corneal wound healing fibroblasts. New insights into the myofibroblast. *Am J Pathol*. 127: 140-148.

Kamma-Lorger, C. S., Boote, C., Hayes, S., Albon, J., Boulton, M. E. and Meek, K. M. (2009) Collagen ultrastructural changes during stromal wound healing in organ cultured bovine corneas. *Exp Eye Res*. 88: 953-959.

Kao, W.W.Y., Funderburgh, J.L., Xia, Y., Liu, C.Y. and Conrad, G.W., 2006. Focus on molecules: lumican. *Exp Eye Res*, *82*(1), p.3.

Kaufman, P. and Alm, A. (2002). *Adlers physiology of the eye*. 10th ed. St. Louis, Mo.: Mosby.

Kaur, H., Chaurasia, S.S., Agrawal, V. and Wilson, S.E., 2009. Expression of PDGF receptor-α in corneal myofibroblasts in situ. *Exp Eye Res*, *89*(3), pp.432-434.

Kezirian, G.M. and Stonecipher, K.G., 2004. Comparison of the IntraLase femtosecond laser and mechanical keratomes for laser in situ keratomileusis. *J Cataract Refract Surg*, *30*(4), pp.804-811.

Knorz, M. L., Wiesinger, B., Liermann, A., Seiberth, V. and Liesenhoff, H. (1998) Laser in situ keratomileusis for moderate and high myopia and myopic astigmatism. *Ophthalmology*. 105: 932–940.

Koch, M., Foley, J. E., Hahn, R., Zhou, P., Burgeson, R. E., Gerecke, D. R. and Gordon, M. K. (2001) Alpha 1(Xx) collagen, a new member of the collagen subfamily, fibril associated collagens with interrupted triple helices. *J Biol Chem*. 276: 23120-23126.

Komai, Y. and Ushiki, T. (1991) The three-dimensional organisation of collagen fibrils in the human cornea and sclera. *Invest Ophthalmol Vis Sci*. 32: 2244–2258.

Krachmer, J., Mannis, M. and Holland, E. (2011). *Cornea*. [St. Louis, Mo.]: Mosby/Elsevier.

Landau, D., Levy, J., Solomon, A., Lifshitz, T., Orucov, F., Strassman, E. and Frucht- Pery, J. (2006) Traumatic corneal flap dislocation one to six years after LASIK in nine eyes with a favorable outcome. *J Refract Surg*. 22: 884-889.

Lee, R. E., Davison, P. F. and Cintron, C. (1982) The healing of linear nonperforating wounds in rabbit corneas of different ages. *Invest Ophthalmol Vis Sci*. 23: 660-665.

Lee H.G, Eun H.C. (1999) Differences between fibroblasts cultured from oral mucosa and normal skin: implication to wound healing *J Dermatol Sci*, 21, pp. 176-182

Lemley, H.L., Chodosh, J., Wolf, T.C., Bogie, C.P. and Hawkins, T.C., 2000. Partial dislocation of laser in situ keratomileusis flap by air bag injury. *J Refract Surg*, *16*(3), pp.373-374.

Leonard, D. W. and Meek, K. M. (1997) Refractive indices of the collagen fibrils and extrafibrillar material of the corneal stroma. *Biophys J*. 72: 1382-1387.

Li, W., Vergnes, J. P., Cornuet, P. K. and Hassell, J. R. (1992) cDNA clone to chick corneal chondroitin/dermatan sulfate proteoglycan reveals identity to decorin. *Arch Biochem Biophys*. 296: 190-197.

Littlechild, S. L., Brummer, G., Zhang, Y. and Conrad, G. W. (2012) Fibrinogen, riboflavin, and UVA to immobilize a corneal flap--conditions for tissue adhesion. *Invest Ophthalmol Vis Sci*. 53: 4011-4020.

Liu C, Paul B, Tandon R, Lee E, Fong K, Mavrikakis I, Herold J, Thorp S, Brittain P, Francis I, Ferrett C, Hull C, Lloyd A, Green D, Franklin V, Tighe B, Fukuda M & Hamada S (2005) The Osteo-Odonto-Keratoprosthesis (OOKP), *Semin Ophthalmol*, 20:2, 113-128

Ljubimov, A.V. and Saghizadeh, M., 2015. Progress in corneal wound healing. *Prog Retin Eye Res*, *49*, pp.17-45.

Locke M, Davies L C, Stephens P, (2016) Oral mucosal progenitor cell clones resist in vitro myogenic differentiation. *Arch Oral Biol* 7: 100-110

Lu, L., Reinach, P. S. and Kao, W. W. (2001) Corneal epithelial wound healing. *Exp Biol Med*. 226: 653-664.

Mak K., Manji A., Gallant-Behm C., Wiebe C., Hart D.A., Larjav. H, et al. (2009). Scarless healing of oral mucosa is characterized by faster resolution of inflammation and control of myofibroblast action compared to skin wounds in the red Duroc pig model *J Dermatol Sci*, 56, pp. 168-180

Mantry, S. and Shah, S., 2004. Surgical management of presbyopia. *Contact Lens Anterio, 27*(4), pp.171-175.

Massof, R.W. and Chang, F.W., 1972. A revision of the rat schematic eye. *Vision Res 12*(5), pp.793-796.

Masur, S. K., Dewal, H. S., Dinh, T. T., Erenburg, I. and Petridou, S. (1996) Myofibroblasts differentiate from fibroblasts when plated at low density. *Proc Natl Acad Sci*. 93: 4219 4223.

Maurice, D. M. (1957) The structure and transparency of the corneal stroma. *J Physiol*. 136: 263–286.

Maurice, D. M. (1984) The cornea and sclera. In: Davson, H. [ed.] *The Eye*. Orlando: Academic Press, pp. 1-158.

Meek, K. M. (2009) Corneal collagen - its role in maintaining corneal shape and transparency. *Biophys Rev*. 1: 83-93.

Meek, K. M., Blamires, T., Elliott, G. F., Gyi, T. J. and Nave, C. (1987) The organisation of collagen fibrils in the human corneal stroma: a synchrotron X-ray diffraction study. *Curr Eye Res*. 6: 841-846.

Meek, K. M. and Boote, C. (2004) The organization of collagen in the corneal stroma. *Exp Eye Res*. 78: 503-512.

Meek, K. M. and Boote, C. (2009) The use of X-ray scattering techniques to quantify the orientation and distribution of collagen in the corneal stroma. *Prog Retin Eye Res*. 28: 369-392.

Meek, K. M., Chapman, J. A. and Hardcastle, R. A. (1979) The staining pattern of collagen fibrils. Improved correlation with sequence data. *J Biol Chem*. 254: 10710-10714.

Meek, K. M., Dennis, S. and Khan, S. (2003a) Changes in the refractive index of the stroma and its extrafibrillar matrix when the cornea swells. *Biophys J*. 85: 2205-2212.

Meek, K. M., Elliott, G. F., Sayers, Z., Whitburn, S. B. and Koch, M. H. (1981) Interpretation of the meridional X-ray diffraction pattern from collagen fibrils in corneal stroma. *J Mol Biol*. 149: 477-488.

Meek, K. M. and Leonard, D. W. (1993) Ultrastructure of the corneal stroma: a comparative study. *Biophys J*. 64: 273-280.

Meek, K. M., Leonard, D. W., Connon, C. J., Dennis, S. and Khan, S. (2003b) Transparency, swelling and scarring in the corneal stroma. *Eye*. 17: 927-936.

Melki, S. A., Talamo, J. H., Demetriades, A. M., Jabbur, N. S., Essepian, J. P., O'Brien, T. P. and Azar, D. T. (2000) Late traumatic dislocation of laser in situ keratomileusis corneal flaps. *Ophthalmology*. 107: 2136-2139.

Meran, S., Thomas, D., Stephens, P., Martin, J., Bowen, T., Phillips, A. and Steadman, R., (2007). Involvement of hyaluronan in regulation of fibroblast phenotype. *J Biol Chem*, *282*(35), pp.25687-25697.

Mi, S., Dooley, E. P., Albon, J., Boulton, M. E., Meek, K. M. and Kamma-Lorger, C. S. (2011) Adhesion of laser in situ keratomileusis-like flaps in the cornea: Effects of crosslinking, stromal fibroblasts, and cytokine treatment. *J Cataract Refract Surg*. 37:166-172.

Mohan, R.R., Hutcheon, A.E., Choi, R., Hong, J., Lee, J., Mohan, R.R., Ambrósio Jr, R., Oie, Y. and Nishida, K., 2016. Corneal regenerative medicine. *Regen Ther,* pp.40-45.

Mohan R R, Hutcheon A E.K, Choi R, Hong J, Lee J, Mohan R R, Ambrósio R, Zieske J D, Wilson S E, (2003) Apoptosis, necrosis, proliferation, and myofibroblast generation in the stroma following LASIK and PRK, *Exp Eye Res* 76: 71-87

Mohan, R. R., Liang, Q., Kim, W. J., Helena, M. C., Baerveldt, F. and Wilson, S. E. (1997) Apoptosis in the cornea: further characterization of Fas/Fas ligand system. *Exp Eye Res*. 65: 575-589.

Mohan, R. R., Mohan, R. R. and Wilson, S. E. (2001) Discoidin domain receptor (DDR) 1 and 2: collagen-activated tyrosine kinase receptors in the cornea. *Exp Eye Res*. 72: 87-92.

Møller-Pedersen, T., 2004. Keratocyte reflectivity and corneal haze. *Exp Eye Res*, *78*(3), pp.553-560.

Møller-Pedersen, T., Cavanagh, H. D., Petroll, W. M. and Jester, J. V. (2000) Stromal wound healing explains refractive instability and haze development after photorefractive keratectomy: a 1-year confocal microscopic study. *Ophthalmology*. 107:1235-1245.

Møller-Pedersen T, Voge M, Li H F, Petroll W M, Cavanagh H D, Jester, J V. (1997) Quantification of Stromal Thinning, Epithelial Thickness, and Corneal Haze after Photorefractive Keratectomy Using In Vivo Confocal Microscopy *Ophthalmology* 104(3);360-368

Montés-Micó, R., Rodríguez-Galietero, A. and Alió, J.L., 2007. Femtosecond laser versus mechanical keratome LASIK for myopia. *Ophthalmology*, *114*(1), pp.62-68.

Moshirfar, M., Churgin, D.S. and Hsu, M., (2011). Femtosecond laser-assisted cataract surgery: a current review. *Middle East Afr J Ophthalmol*, *18*(4), p.285.

Moshirfar, M., Gardiner, J.P., Schliesser, J.A., Espandar, L., Feiz, V., Mifflin, M.D. and Chang, J.C., 2010. Laser in situ keratomileusis flap complications using mechanical microkeratome versus femtosecond laser: retrospective comparison. *J Cataract Refract Surg*, *36*(11), pp.1925-1933.

Morgan, I.G., Ohno-Matsui, K. and Saw, S.M., 2012. Myopia. *The Lancet*, *379*(9827), pp.1739-1748.

Morgan, S. R., Dooley, E. P., Hocking, P. M., Inglehearn, C. F., Ali, M., Sorensen, T.L., Meek, K. M., Boote, C. (2013) An x-ray scattering study into the structural basis of corneal refractive function in an avian model. *Biophys J*. 104: 2586-2594.

Müller, L. J., Pels, L. and Vrensen, G. F. (1995) Novel aspects of the ultrastructural organization of human corneal keratocytes. *Invest Ophthalmol Vis Sci*. 36: 2557-2567.

Müller, L. J., Pels, E. and Vrensen, G. F. (2001) The effects of organ-culture on the density of keratocytes and collagen fibers in human corneas. *Cornea*. 20: 86-95.

Nakamura T, Inatomi T, Sotozono C, et al (2004). Transplantation of cultivated autologous oral mucosal epithelial cells in patients with severe ocular surface disorders. *Brit J Ophthalmol*; 88:1280-1284

Netto, M.V., Mohan, R.R., Medeiros, F.W., Dupps, W.J., Sinha, S., Krueger, R.R., Stapleton, W.M., Rayborn, M., Suto, C. and Wilson, S.E., (2007). Femtosecond laser and microkeratome corneal flaps: comparison of stromal wound healing and inflammation. *J Refract Surg*, *23*(7), pp.667-676.

Newton, R. H. and Meek, K. M. (1998) The integration of the corneal and limbal fibrils in the human eye. *Biophys J*. 75: 2508-2512.

Nishida, K., Yamato, M., Hayashida, Y., Watanabe, K., Yamamoto, K., Adachi, E., Nagai, S., Kikuchi, A., Maeda, N., Watanabe, H. and Okano, T., (2004). Corneal reconstruction with tissue-engineered cell sheets composed of autologous oral mucosal epithelium. *N Engl J Med*, *351*(12), pp.1187-1196.

Nishida, T., Ueda, A., Fukuda, M., Mishima, H., Yasumoto, K. and Otori, T. (1988) Interactions of extracellular collagen and corneal fibroblasts: morphologic and biochemical changes of rabbit corneal cells cultured in a collagen matrix. *In Vitro Cell Dev Biol*. 24: 1009-1014.

Ohki T, Yamato M, Murakami D, et al (2006). Treatment of oesophageal ulcerations using endoscopic transplantation of tissue-engineered autologous oral mucosal epithelial cell sheets in a canine model *Gut*; 55:1704-1710.

Pallikaris, I. G., Kymionis, G. D. and Astyrakakis, N. I. (2001) Corneal ectasia induced by laser in situ keratomileusis. *J Cataract Refract Surg*. 27: 1796-1802.

Pallikaris, I. G., Papatzanaki, M. E., Stathi, E. Z., Frenschock, O. and Georgiadis, A. (1990) Laser in situ keratomileusis. *Lasers Surg Med*. 10: 463-468.

Pallikaris, I.G., Papatzanaki, M.E., Siganos, D.S. and Tsilimbaris, M.K., (1991). A corneal flap technique for laser in situ keratomileusis: human studies. *Arch Ophthalmol*, *109*(12), pp.1699-1702.

Pallikaris, I. G. and Siganos, D. S. (1994) Excimer laser in situ keratomileusis and photorefractive keratectomy for correction of high myopia. *J Refract Corneal Surg*. 10: 498–510.

Patel, C.K., Hanson, R., McDonald, B. and Cox, N., (2001). Late dislocation of a LASIK flap caused by a fingernail. *Arch Ophthalmol*, *119*(3), pp.447-449.

Patel, S.V., McLaren, J.W., Hodge, D.O. and Bourne, W.M., 2001. Normal human keratocyte density and corneal thickness measurement by using confocal microscopy in vivo. *Invest Ophthalmol Vis Sci*, *42*(2), pp.333-339.

Pellegrini, G., Traverso, C.E., Franzi, A.T., Zingirian, M., Cancedda, R. and De Luca, M., (1997). Long-term restoration of damaged corneal surfaces with autologous cultivated corneal epithelium. *The Lancet*, *349*(9057), pp.990-993.

Pei, Y., Reins, R. Y. and McDermott, A. M. (2006) Aldehyde dehydrogenase (ALDH) 3A1 expression by the human keratocyte and its repair phenotypes. *Exp Eye Res*. 83:1063-1073.

Pérez-Santonja, J. J., Linna, T. U., Tervo, K. M., Sakla, H. F., Alió y Sanz, J. L., Tervo, T. M. (1998) Corneal wound healing after laser in situ keratomileusis in rabbits. *J Refract Surg*. 14: 602-609

Perez-Santonja, J.J., Sakla, H.F. and Alió, J.L., 1998. Contrast sensitivity after laser in situ keratomileusis. *J Cataract Refract Surg*, *24*(2), pp.183-189.

Petersen, H. and Seiler, T., (1999). Intraoperative and postoperative complications after laser in situ keratomileusis (LASIK). *Der Ophthalmologe*, *96*(4), pp.240-247.

Petroll, W.M., Cavanagh, H.D. and Jester, J.V., (1993). Three-dimensional imaging of corneal cells using in vivo confocal microscopy. *J Microsc*, *170*(3), pp.213-219

Petroll, W.M., Cavanagh, H.D. and Jester, J.V., (2004). Dynamic three-dimensional visualization of collagen matrix remodeling and cytoskeletal organization in living corneal fibroblasts. *Scanning,* 26(1), pp.1-10

Piatigorsky, J. (2000) Review: A case for corneal crystallins. *J Ocul Pharmacol Ther*. 16: 173-180.

Poole, C.A., Brookes, N.H. and Clover, G.M., (1993). Keratocyte networks visualised in the living cornea using vital dyes. *J Cell Sci*, *106*(2), pp.685-691.

Radner, W., Zehetmayer, M., Aufreiter, R. and Mallinger, R. (1998) Interlacing and cross-angle distribution of collagen lamellae in the human cornea. *Cornea*. 17: 537-543

Raiskup, F., Hoyer, A. and Spoerl, E. (2009) Permanent corneal haze after riboflavin-UVA-induced cross-linking in keratoconus. *J Refract Surg*. 25: S824-828.

Randleman, J. B., Woodward, M., Lynn, M. J. and Stulting, R. D. (2008) Risk assessment for ectasia after corneal refractive surgery. *Ophthalmology*. 115: 37–50.

Rawe, I.M., Meek, K.M., Leonard, D.W., Takahashi, T. and Cintron, C., (1994). Structure of corneal scar tissue: an X-ray diffraction study. *Biophys J*, *67*(4), pp.1743-1748.

Read, S.A., Collins, M.J. and Carney, L.G., 2007. A review of astigmatism and its possible genesis. *Clin Exp Optom*, *90*(1), pp.5-19.

Robert, L., Legeais, J. M., Robert, A. M. and Renard, G. (2001) Corneal collagens. *Pathol Biol*. 49: 353-363.

Rosen, E.S., 2000. LASIK mania. *J Cataract Refract Surg*, *26*(3), p.303.

Saika, S., Shiraishi, A., Liu, C. Y., Funderburgh, J. L., Kao, C. W., Converse, R. L. and Kao, W. W. (2000) Role of lumican in the corneal epithelium during wound healing. *J Biol Chem*. 275: 2607-2612.

Sanchez, I., Martin, R., Ussa, F. and Fernandez-Bueno, I., (2011). The parameters of the porcine eyeball. *Graefe's Arch Clin Exp Ophthalmol*, 249(4), pp.475-482.

Saude, T. (1993) *Occular anatomy and physiology*. Oxford: Blackwell Scientific Publications.

Schmack, I., Dawson, D. G., McCarey, B. E., Waring, G. O. 3rd, Grossniklaus, H. E. and Edelhauser, H. F. (2005) Cohesive tensile strength of human LASIK wounds with histologic, ultrastructural, and clinical correlations. *J Refract Surg.* 21: 433-445.

Shannon D.B., McKeown S.T., Lundy F.T., Irwin C.R. (2006) Phenotypic differences between oral and skin fibroblasts in wound contraction and growth factor expression *Wound Repair Regen*, 14, pp. 172-178

Shaw, L. M. and Olsen, B. R. (1991) FACIT collagens: diverse molecular bridges in extracellular matrices. *Trends Biochem Sci*. 16: 191-194.

Singerman, L. J. and Coscas, G. (1998) Current techniques in ophthalmic laser surgery. Boston: Butterworth-Heinemann.

Sloan P (1991). Current concepts of the role of fibroblasts and extracellular matrix in wound healing and their relevance to oral implantology *J Dent*, 19, pp. 107-109

Smolin, G., Foster, C.S., Azar, D.T. and Dohlman, C.H. eds., (2005). *Smolin and Thoft's the cornea: scientific foundations and clinical practice*. Lippincott Williams & Wilkins.

Steele, C. (1999) Corneal wound healing: a review. *Optometry Today*. 24: 28-34.

Stephens P (1995) An In-Vitro Comparison of the Contractile Ability of Oral and Dermal Fibroblasts *J Dental Res* 74(3), p.862

Stephens, P., Davies, K.J., Al-Khateeb, T., Shepherd, J.P. and Thomas, D.W., (1996). A comparison of the ability of intra-oral and extra-oral fibroblasts to stimulate extracellular matrix reorganization in a model of wound contraction. *J Dent Res*, *75*(6), pp.1358-1364.

Stephens, P., Davies, K.J., Occleston, N., Pleass, R.D., Kon, C., Daniels, J., Khaw, P.T. and Thomas, D.W., (2001). Skin and oral fibroblasts exhibit phenotypic differences in extracellular matrix reorganization and matrix metalloproteinase activity. *Brit J Dermatol*, *144*(2), pp.229-237.

Stephens, P., Hiscox, S., Cook, H., Jiang, W.G., Zhiquiang, W. and Thomas, D.W., (2001). Phenotypic variation in the production of bioactive hepatocyte growth factor/scatter factor by oral mucosal and skin fibroblasts. *Wound Repair Regen*, *9*(1), pp.34-43.

Stephens, P. and Davies, L.C., 2015. Oral Mucosal Progenitor Cells. In *Stem Cell Biology and Tissue Engineering in Dental Sciences* (pp. 297-306). Academic Press.

Stiemke, M.M., Edelhauser, H.F. and Geroski, D.H., (1991). The developing corneal endothelium: correlation of morphology, hydration and Na/K ATPase pump site density. *Curr Eye Res*, *10*(2), pp.145-156.

Strupler, M., Pena, A.M., Hernest, M., Tharaux, P.L., Martin, J.L., Beaurepaire, E. and Schanne-Klein, M.C., (2007). Second harmonic imaging and scoring of collagen in fibrotic tissues. *Opt Express*, 15(7), pp.4054-4065.

Summerlin W T, Miller G E, Harris J E, Good R A (1973) The Organ-Cultured Cornea: An in vitro Study. *Invest. Ophthalmol. Vis. Sci.*;12(3):176-180

Syed-Picard, F.N., Du, Y., Lathrop, K.L., Mann, M.M., Funderburgh, M.L. and Funderburgh, J.L., (2015). Dental pulp stem cells: a new cellular resource for corneal stromal regeneration. *Stem Cell Transl Med*, *4*(3), pp.276-285.

Szpaderska A.M., Zuckerman J.D, DiPietro L.A (2003) Differential injury responses in oral mucosal and cutaneous wounds *J Dent Res*, 82, pp. 621-626

Taliana, L., Evans, M.D., Dimitrijevich, S.D. and Steele, J.G., (2000). Vitronectin or Fibronectin Is Required for Corneal Fibroblast–Seeded Collagen Gel Contraction. *Invest Ophthalmol Vis Sci*, *41*(1), pp.103-109.

Tan, D.T., Dart, J.K., Holland, E.J. and Kinoshita, S., (2012). Corneal transplantation. *The Lancet*, *379*(9827), pp.1749-1761.

Taneri, S., Zieske, J.D. and Azar, D.T., (2004). Evolution, techniques, clinical outcomes, and pathophysiology of LASEK: review of the literature. *Surv Ophthalmol*, *49*(6), pp.576-602.

Thomas B, McIntosh D, Fildes T, Smith L, Hargrave F, Islam M, Thompson T, Layfield R, Scott D, Shaw B, Burrell C L, Gonzalez S, Taylor S (2017) Second-harmonic generation imaging of collagen in ancient bone. *Bone Reports* 7: 137-144

Thomasy, S.M., Raghunathan, V.K., Winkler, M., Reilly, C.M., Sadeli, A.R., Russell, P., Jester, J.V. and Murphy, C.J., (2014). Elastic modulus and collagen organization of the rabbit cornea: epithelium to endothelium. *Acta biomater*, *10*(2), pp.785-791.

Toda, I., Asano-Kato, N., Komai-Hori, Y. and Tsubota, K., (2001). Dry eye after laser in situ keratomileusis. *Am J Ophthalmol*, *132*(1), pp.1-7.

Torricelli A .M, Wilson, S E. (2014) Cellular and extracellular matrix modulation of corneal stromal opacity, *Exp Eye Res*, 129: 151-160

Tsai C, Hata K, Torii S et al. (1995) Contraction potency of hypertrophic scar-derived fibroblasts in a connective tissue model: in vitro analysis of wound contraction. *Ann Plast Surg*; 35: 638–46

Upadhyay, S., 2015. Myopia, Hyperopia and Astigmatism: A Complete Review with View of Differentiation. *Int J Sci Res*.

van der Want, H.J., Pels, E., Schuchard, Y., Olesen, B. and Sperling, S., (1983). Electron microscopy of cultured human corneas: osmotic hydration and the use of a dextran fraction (dextran T 500) in organ culture. *Arch Ophthalmol*, *101*(12), pp.1920-1926

Van Horn, D. L., Doughman, D. J., Harris, J. E., Miller, G. E., Lindstrom, R. and Good, R. A. (1975) Ultrastructure of human organ-cultured cornea. II. Stroma and epithelium. *Arch Ophthalmol*. 93: 275-277.

Vargas-Fragoso, V. and Alió, J.L., 2017. Corneal compensation of presbyopia: PresbyLASIK: an updated review. *Eye and Vision*, *4*(1), p.11.

Warner, N., 2016. Update on myopia. *Current Opin Ophthalmol*, *27*(5), pp.402-406.

Wang, J.F., Olson, M.E., Reno, C.R., Kulyk, W., Wright, J.B. and Hart, D.A., (2000). Molecular and cell biology of skin wound healing in a pig model. *Connect Tissue Res*, *41*(3), pp.195-211

Widera, D., Zander, C., Heidbreder, M., Kasperek, Y., Noll, T., Seitz, O., Saldamli, B., Sudhoff, H., Sader, R., Kaltschmidt, C. and Kaltschmidt, B., (2009). Adult palatum as a novel source of neural crest-related stem cells. *Stem Cells*, *27*(8), pp.1899-1910.

William Mohler, Andrew C. Millard, Paul J. Campagnola, (2003) Second harmonic generation imaging of endogenous structural proteins, *Methods*, 29(1):97-101

Wilson, S. E. (2002) Analysis of the keratocyte apoptosis, keratocyte proliferation, and myofibroblast transformation responses after photorefractive keratectomy and laser in situ keratomileusis. *Trans Am Ophthalmol Soc*. 100: 411-433.

Wilson, S. E., He, Y. G., Weng, J., Li, Q., McDowall, A. W., Vital, M. and Chwang, E. L. (1996) Epithelial injury induces keratocyte apoptosis: hypothesized role for the interleukin-1 system in the modulation of corneal tissue organization and wound healing. *Exp Eye Res*. 62: 325-327.

Wilson, S. E. and Hong, J. W. (2000) Bowman's layer structure and function: critical or dispensable to corneal function? A hypothesis. *Cornea*. 19: 417-420.

Wilson, S. E., Liu, J. J. and Mohan, R. R. (1999) Stromal-epithelial interactions in the cornea. *Prog Retin Eye Res*. 18: 293-309.

Wilson, S. E., Mohan, R. R., Mohan, R. R., Ambrósio, R. Jr, Hong, J. and Lee, J. (2001) The corneal wound healing response: cytokine-mediated interaction of the epithelium, stroma, and inflammatory cells. *Prog Retin Eye Res*. 20: 625-637.

Wong, J.W., Gallant-Behm, C., Wiebe, C., Mak, K., Hart, D.A., Larjava, H. and Häkkinen, L., 2009. Wound healing in oral mucosa results in reduced scar formation as compared with skin: evidence from the red Duroc pig model and humans. *Wound Repair Regen,* 17(5), pp.717-729.

Woodhead-Galloway, J., 1980. Structure of the collagen fibril: some variations on a theme of tetragonally packed dimers. *Proc R Soc Lond B Biol Sci*, pp.275-297.

Yin, G.H.W., McAlinden, C., Pieri, E., Giulardi, C., Holweck, G. and Hoffart, L., 2016. Surgical treatment of presbyopia with central presbyopic keratomileusis: One-year results. *J Cataract Refract Surg*, *42*(10), pp.1415-1423.

Zerbe, B.L., Belin, M.W., Ciolino, J.B. and Boston Type 1 Keratoprosthesis Study Group, 2006. Results from the multicenter Boston type 1 keratoprosthesis study. *Ophthalmology*, *113*(10), pp.1779-1784.

Zieske, J D (2001) Extracellular matrix and wound healing *Curr. Op. in Ophthalmology*.; 12(4):237-241

Zieske, J. D., Guimarães, S. R. and Hutcheon, A. E. (2001) Kinetics of keratocyte proliferation in response to epithelial debridement. *Exp Eye Res*. 72: 33-39.

Zieske, J.D. and Wilson, S.E., 2003. Apoptosis, necrosis, proliferation, and myofibroblast generation in the stroma following LASIK and PRK. *Exp Eye Res*, *76*(1), pp.71-87.

Appendix

Preparation of Phosphate Buffer Solution (PBS)

Materials

7.4pH Phosphate Buffer Saline Tablets (1282-1680, Fisher Scientific, UK)
dH2O (as required)
1L dewar

Solution Preparation

1. Dissolve one tablet per 100ml of dH_2O in a 1L dewar.

Preparation of Stock Antibiotic solution

Materials

500 mg Streptomycin Sulphate (S1400000, Sigma, UK)
500 mg Kanamycin Sulphate from Streptomyces Kanamycetious (K4000, Sigma, UK
300 mg Penicillin G (P3032, Sigma, UK)
730 mg L-Glutamine (G8540, Sigma, UK)
50 ml ddH2O

Solution Preparation

1. Weigh out and dissolve all powders into the ddH_20
2. Filter into 10 ml aliquots using a 0.2 µm filter in sterile conditions.

Preparation of 1% Agar/1% Gelatine Solution

Materials

Agar Powder (A1296, Sigma, UK)
Gelatine Powder (G2500, Sigma, UK)
ddH_2O
300ml Dewar
60 ml Sterile Pots.

Solution Preparation

1.Weigh out 2g of agar and 2g of gelatine powder
2.Place in a 300ml Dewar
3.Add 200ml ddH2O
4.Stir continuously until completely dissolved.
5.Place in individual pots, leave to set overnight and then store in fridge.

Preparation of Dulbecco's Modified Eagles Medium (DMEM)

Materials

500ml bottle DMEM - High glucose, Pyruvate, no glutamine 500mL (21969035, Thermofisher, UK)
70% IMS Spray
Fungizone® antimycotic solution (11520496, Thermofisher, UK)
Stock antibiotic solution (see separate SOP)
Syringe
0.2µl Filters

Solution Preparation

1.The 500ml bottle of DMEM media must be prepared inside the class II culture cabinet. Spray the outside of unopened/factory sealed DMEM bottle with 70% IMS to sterilise. Introduce into the cabinet.
2.Spray the outside of previously prepared antibiotic stock solution (5ml) and Fungizone® antimycotic solution (5ml) and introduce to the class II cabinet.
3.Filter the antibiotic solution and Fungizone® into the DMEM solution using a syringe with a 0.2µm filter attached.
4.This can be prepared in advance and stored in the fridge until day of use.

Preparation of 7.4% Sodium Bicarbonate ($NaHCO_3$) Solution

Materials

$NaHCO_3$ Powder (S5761, Sigma, UK)
300ml Dewar
ddH_2O

Solution Preparation

1. Weigh out 22.2g of $NaHCO_3$
2.Place the $NaHCO_3$ into a 300ml dewar.
3. Add 300mls of ddH_2O and stir continuously until dissolved.

4. Can be stored at room temperature.

Preparation of 1% Agar/1% Gelatine Support Matrix

Materials

70% IMS
1%Agar/1%Gelatine (see previous SOP)
500ml DMEM (11520496, Thermofisher, UK)
7.4% NaHCO3 Solution (see previous SOP)
Antibiotic stock solution (see previous SOP)
Fungizone® Antimycotic solution (11520496, Thermofisher, UK)
Stripettes
2ml syringes
Sterile pots
0.2µm syringe filters

Solution Preparation

1.The preparation of this support matrix is to take place in the sterile conditions of a class II cabinet.
2.To turn the 1%agar/1%gelatine mixture into a solution, heat in a microwave on low power for 20 seconds at a time until melted. Then spray the surface with 70% IMS and introduce into the class II cabinet.
3.Spray the surface of 500ml DMEM bottle, 7.4% $NaHCO_3$ flask, antibiotic stock solution, Fungizone®, 10 ml stripette, 2ml syringes, sterile pots and 0.2µm filters with 70% IMS and introduce them into the class II cabinet.
4.Using the syringes with the filters attached, filter the following solutions and quantities into the agar/gelatine solution;

20ml DMEM media

10ml 7.4% $NaHCO_3$

2ml Stock Antibiotic solution

2ml Fungizone® solution

5.Decant the final solution into sterile pots, label appropriately and seal.
6.Store the solution in the fridge until needed.

Preparation of 0.2M Sodium Cacodylate buffer

Materials

Sodium Cacodylate
Calcium Chloride Dihydrate
dH_20
1M Hycrochloric Acid (HCL)

Solution Preparation

1.Transfer open pan balance to fume hood and, wearing gloves, weigh 4.28g sodium cacodylate powder into a beaker.
2.Clear up any spillage of powder immediately with damp tissue.
3.Add (Calcium Chloride Dihydrate) $CaCl_2.2H_2O$ for 3mM
4.Add 50ml distilled water.
5.Transfer to pH meter and correct pH to 7.2 with 1M HCl
6.Make up to 100ml with dH20.

Preparation of 2.5% glutaraldehyde/0.1M sodium cacodylate

Materials

0.2M sodium cacodylate buffer
stock 25% glutaraldehyde
dH_20

Solution Preparation

1.Add 5ml stock 25% glutaraldehyde to 25ml Sodium Cacodylate
2.Add 20ml dH_20

***TUNEL solutions (all solutions and chemicals, unless otherwise stated, are from the Click-iT™ Plus TUNEL Assay (C10617, Invitrogen, UK)**

Preparation of Click-iT™ TUNEL Reaction Buffer

Materials

Click-iT™ TUNEL Reaction Buffer
Deionised Water

Solution Preparation

1.Transfer 500µl of Click-iTTM TUNEL Reaction Buffer into 4.5ml of deionised water
2.Rinse the original vial with some of the Click-iTTM TUNEL Reaction Buffer solution to ensure all of the 10X concentration
3.Dilute 1:10 with deionised water for storage at 2-8˚C

Preparation of 1X Click-iT™ Plus TUNEL Supermix

Materials

Click-iT™ TUNEL Reaction Buffer
Copper Protectant
Alexafluor™ 488 Picolyl Azide

Solution Preparation

1.To 2630µl Click-iT™ TUNEL Reaction Buffer add 67µl Copper Protectant and 3.7 µl Alexa Fluor™ picolyl azide
2.Store at -20 ˚C

Preparation of 100X stock Click-iT™ TUNEL Reaction Buffer Additive

Materials

Click-iT™ TUNEL Reaction Buffer Additive
Deionised water

Solution Preparation

1.Add 2ml of deionised water into vial containing Click-iT™ TUNEL Reaction Buffer Additive (400mg)
2.Mix until fully dissolved
3.Aliquot and store at -20 ˚C

Preparation of 1X Proteinase K Solution

Materials

Proteinase K
PBS (see previous SOP)

Solution Preparation

1.Dilute Proteinase K 1:25 in PBS
2.Aliquot and store at -20 ˚C

Preparation of Terminal deoxynucleotidyl transferase (TdT) reaction mixture

Materials

TdT Reaction Buffer
EdUTP
TdT Enzyme

Solution Preparation

1.For 10 sections, to 470µl of TdT Reaction Buffer add 10 µl of EdUTP and 20 µl of TdT Enzyme
2.Do not store as a prepared solution

,

Preparation of Click-iT™ Plus TUNEL Reaction Cocktail

Materials

1X Click-iT™ Plus TUNEL Supermix
10X Click-iT™ TUNEL Reaction Buffer

Solution Preparation

1.For 10 sections, to 450µl of 1X Click-iT™ Plus TUNEL Supermix add 50µl of 10XClick-iT™ TUNEL Reaction Buffer
2.Use within 15minutes of preparation.
3.Do not store prepared solution